



Compendium on ElectroMagnetic Compatibility

Compendium on ElectroMagnetic Compatibility

JAN SROKA

WARSAW UNIVERSITY OF TECHNOLOGY
WARSAW



**Politechnika
Warszawska**

Unia Europejska
Europejski Fundusz Społeczny



This book was created with support of the funding with Project NERW – Knowledge, Education, Development and Cooperation. (<https://www.nerw.pw.edu.pl/>)

Realizacja podręcznika została sfinansowana w projekcie „NERW PW. Nauka-Edukacja-Rozwój-Współpraca” współfinansowanego ze środków Unii Europejskiej w ramach Europejskiego Funduszu Społecznego. (<https://www.nerw.pw.edu.pl/>)

This book was produced with Pressbooks (<https://pressbooks.com>) and rendered with Prince.

Contents

1. Preface	1
2. Low frequency current and voltage disturbances	26
3. Radio frequency electromagnetic disturbances	41
4. Propagation of disturbances	71
5. Protection from disturbances	115
Bibliography	143

1. Preface

Electromagnetic environment

Perception and consequences of embedding in the environment

All subjects, underneath human beings and all objects on the Earth are embedded in the electromagnetic environment. The Earth static magnetic and electric fields are example of it.

In Fig.1.1 spectrum of the module of the vertical component of the electric field $|E_v|$ in the frequency range from 30 MHz to 1 GHz in one of the the premises at the Technical University of Warsaw is shown. The blue plot represents intentional signals. By 100 MHz radio FM broadcasts are visible, by 200 MHz TV channels, above 900 MHz signals of the cellular telephony. Moreover services like: emergency medical service, police, fire service are also present. All these signals are useful for functioning of the society but for someone or something incidental they can be disturbing. The red plot is captured by switched on drilling hand tool. Sparks on the commutator of the motor increases significantly level of spectrum in the wide frequency range. It is waste product by operating the tool which is evidently the disturbance and not at all desirable.

It is impossible to remove, compensate or fly away from the electromagnetic environment. Human beings and its artefacts are forced to live and to operate in it without spoiling it excessively, being at the same time immune enough for performance as intended in the presence of it.

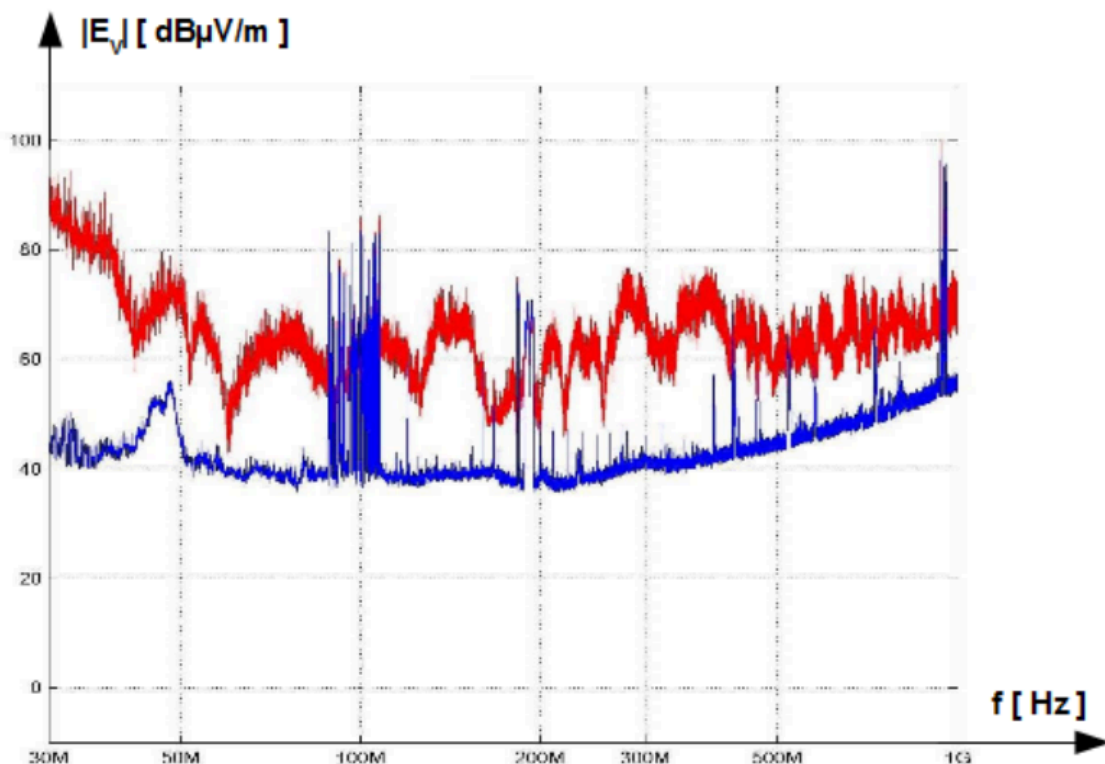


Figure 1.1. The module of the vertical component of the electric field $|E_v|$. Spectrum of useful signals – blue plot, by operating hand drilling tool – red plot.

Obviously there is interaction between the environment and items embedded in it. Human being can be influenced by the electromagnetic environment through the impact on the health and through undesired theft of electronically processed data.

Cellular telephones are example of the impact of the electromagnetic environment on the human being health. In the 90th of the 20th century, when the first generation of the cellular telephones became the mass consumer good, many customers observed anxious symptoms after long calls. They observed redness and warming up of the head region next to the phone, they filled physical and psycho tiredness. Already then the results of experiments with monkeys were known. They behaved abnormally when temperature of their brains was increased by 1 deg. Very rapidly it was proved that temperature of human brain increases much more extensively by the cellular phone call. Exemplary numerical simulation of energy absorption by cellular phone call is shown in Fig.1.2.



Figure 1.2: Simulation of electromagnetic energy absorbed by cellular telephone call.

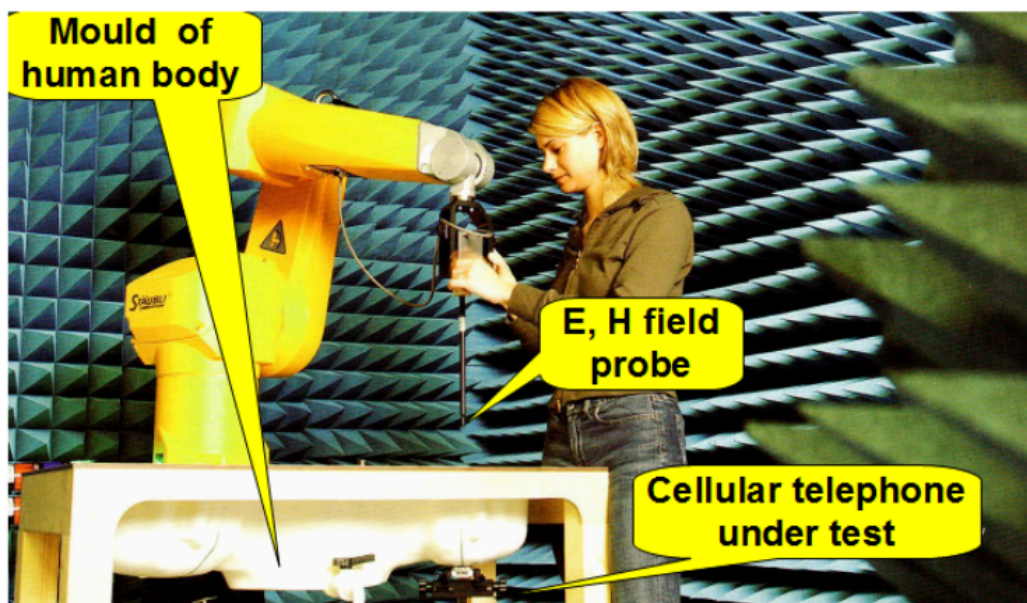


Figure 1.3: Set up for SAR measurement of the cellular telephone.

The method for quantification of ability of cellular telephones for warming up the brain tissue was worked out. Specific Absorption Rate SAR which is energy absorbed by the human brain per unit mass was chosen as the quantification parameter. It is measured in W/m^3 . In Fig.1.3 the set up for SAR measurement by cellular phone call is shown. It is built in the anechoic chamber laid up with the pyramid absorption material. It consists of mould of the half of human body filled with solution with electric and magnetic properties similar to human brain. Beneath the phone under test is placed. The robot moves the arm with isotropic electric and magnetic near field probes. Measured distribution of both fields in the volume of the brain are recalculated to SAR. All phones available on the market must contain in the manual the value of its SAR parameter.

The phenomenon described above is direct thermal effect of the phones. Long term influence of the cellular telephones on human being is still under investigation. The answer on this question is unknown.

I wonder if someone realizes that content of the PC monitor emits to the environment. The same happens by scanning or printing something. Processed data are contained in the electromagnetic disturbance leaked out to the surroundings. It is sufficient to place appropriate antenna and receiver and the data can be reconstructed.

Even without antenna the data can be stolen. Emitted data are present in all metal objects in the vicinity. It is enough to mount the current measurement probe on the metal leg of a table placed next to the source of leaked data in order to reconstruct them.

Banks, insurance companies, authorities, secret services, armies spends a lot of money to avoid the thefts of electronically processed data of their customers or citizens. Topics concerning safe data processing are collected under keyword Transient ElectroMagnetic Pulse Emanation Standard TEMPEST.

European regulation relating to electromagnetic compatibility {#EU regulation}

Interaction between electromagnetic environment and items embedded in it is called electromagnetic compatibility EMC.

The laws of the Member States of the European Union relating to electromagnetic compatibility are harmonized according to the so called EMC Directive [EMCD].

The first sentence in chapter 1 of this Directive sounds: "This Directive regulates electromagnetic compatibility of equipment". It means that EMC in concept of the Directive is limited to equipment. The human being is left out of the scope of it. The same line is adopted in these lecture notes.

Some other definitions from the first chapter of the Directive [EMCD] :

- *electromagnetic environment* means all electromagnetic phenomena observable in the given location,
- *electromagnetic compatibility* means the ability of equipment to function satisfactorily in its electromagnetic environment without introducing intolerable electromagnetic disturbances to other equipment in that environment,
- *electromagnetic disturbance* means any electromagnetic phenomenon which may degrade the performance of equipment; an electromagnetic disturbance may be electromagnetic noise, an unwanted signal or a change in the propagation medium itself,
- *immunity* means the ability of equipment to perform as intended without degradation in the presence of an electromagnetic disturbance.

Though the EMC Directive is limited to equipments, electromagnetic environment according to it covers also natural phenomena in addition to disturbances generated by equipments.

Stipulating that an equipment lives when it is energized, the statement: "live and let live" is good paraphrase of definition of the EMC in the Directive [EMCD]. It is essential and sole legal requirement of the Directive.

The relationship between standardization and legislation at European level has been developed in accordance with the so-called 'New Approach' to technical harmonization and standards. This is cardinal rule regulating the EU market.

According to the New Approach:

- the Countries of the European Union adopts legislation (EU Directives) that defines essential requirements – in relation to safety and other aspects of public interest – which should be satisfied by products and services being sold in the Single Market,
- the European Commission issues standardization requests (Mandates) to the European Standardization Organizations: CEN *Comité Européen de Normalisation* European Committee for Standardization, CENELEC *Comité Européen de Normalisation Electrotechnique* European Committee for Electrotechnical Standardization, and ETSI European Telecommunications Standards Institute, which are responsible for preparing technical standards and specifications that facilitate compliance with these essential requirements,
- public authorities of EU countries must recognize that all products manufactured (and services provided) in accordance with harmonized standards are presumed to conform to the essential requirements as defined by the relevant EU legislation,
- European Standards remain voluntary and there is no legal obligation to apply them. Any manufacturer (or service provider) who chooses not to follow a harmonized standard is obliged to prove that his products (or services) conform to the essential requirements.

European Standards remain voluntary but as stated in Chapter 3 of the Directive [EMCD] "Equipment which is in conformity with harmonised standards shall be presumed to be in conformity with the essential requirements" of the Directive.

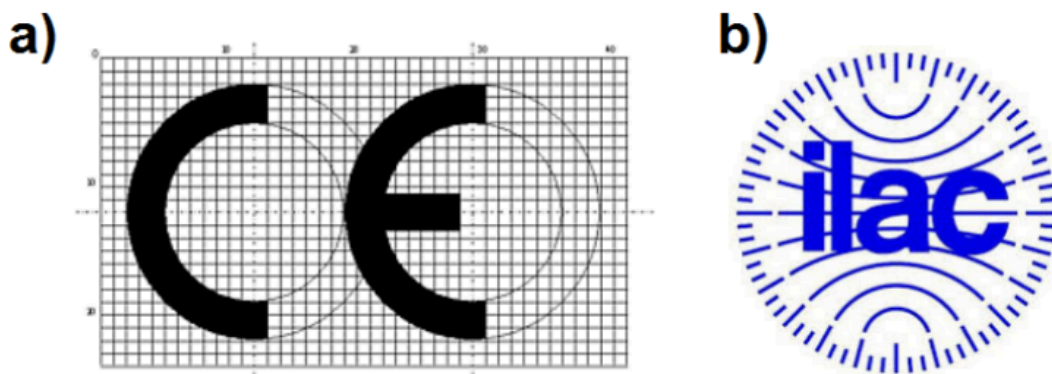


Figure 1.4: CE marking a), ILAC label b).

For placing the product on the market the authorized representative of the manufacturer must sign the declaration of conformity. It must be attached to the product. Moreover marking such as in Fig.1.4 a) must be affixed on the product in visible place. CE is abbreviation of the term in French CONFORMITÉ EUROPÉENNE. The authorized representative bears legal responsibility for any violation of the essential requirements concerning the product. The authorized representative means any natural or legal person established within the Union who has written mandate from a manufacturer to act on his behalf.

Implications of the New Approach relating to EMC is establishing plenty of independent accredited laboratories and notified bodies offering services in conformity assessment procedure. EMC testing according to European Standards is the main part of this assessment.

Manufacturer can perform EMC testing with own facility but contracting it to independent accredited laboratory has following benefits:

- liberation from suspicions of lack of objectivity and impartiality,
- test equipment calibrated with traceability,
- educated engineer staff competent to define scope of applicable harmonized standards and to go professionally through the testing program,
- test performance according to valid, not obsolete editions of the harmonized standards,
- accredited test report as the trace that the tested product (DUT Device Under Test, EUT Equipment Under Test) is in conformity with harmonised standards.

As mentioned before, conformity with harmonised standards is enough to presume that the product is in conformity with the essential requirements of the Directive [EMCD].

Each Member Country designates accrediting and notifying authority. In Poland it is PCA Polskie Centrum Akredytacji *Polish Center for Accreditation*. In the home page of the PCA a list of all accredited laboratories with their scope of accreditation can be found. Notified bodies are additionally notified the European Commission and other Member States.

Directive [EMCD] provides also institution called Market Surveillance Authority of the Member States. In Poland it is Urząd Komunikacji Elektronicznej UKE *Office of Electronic Communication*.

If the apparatus presents the risk, the Surveillance Authority shell carry out an evaluation. Thereafter shell force the relevant economic operator to take all appropriate corrective actions to bring the apparatus into compliance, to withdraw the apparatus from the market, or to recall it within the reasonable period. If the relevant economic operator does not take adequate corrective actions, the Market Surveillance Authority shell take appropriate provisional measures to prohibit or restrict the being made available, to withdraw it or to recall it. The Surveillance Authority can impose financial penalty.

Accrediting and notifying authorities from many countries around the World, significantly exceeding European Union are associated in the International Laboratory Accreditation Cooperation ILAC. Agreement of ILAC Countries guaranties mutual recognition of the test results performed in the accredited laboratories. For the EU Countries it is tremendous simplification and costs reduction of the conformity assessment procedure. This procedure can be performed only in one EU Country and is recognized elsewhere in EU. The label shown in Fig.1.4 b), placed at the front page of the accredited test report is the seal confirming this.

dB, or not dB, that is the question

Floating decibels

Definitions of floating decibel are as follows

$$N \text{ dB (of power)} \equiv 10 \log_{10} \left(\frac{P_2}{P_1} \right) \quad (1.1)$$

$$N \text{ dB (of voltage)} \equiv 20 \log_{10} \left(\frac{U_2}{U_1} \right) \quad (1.2)$$

$$N \text{ dB (of current)} \equiv 20 \log_{10} \left(\frac{I_2}{I_1} \right) \quad (1.3)$$

$$N \text{ dB (of electric field strength)} \equiv 20 \log_{10} \left(\frac{E_2}{E_1} \right) \quad (1.4)$$

$$N \text{ dB (of magnetic field strength)} \equiv 20 \log_{10} \left(\frac{H_2}{H_1} \right) \quad (1.5)$$

N is a number. The adjective “floating” means that both values in numerator as well as in denominator can be arbitrary. They are not fixed. Definitions (1.4) and (1.5) concerns vectors. Therefore only one component of electric field respectively magnetic field, e.g. horizontal or vertical component is meant in them.

Inverse calculation is as follows

$$\frac{P_2}{P_1} = 10^{\frac{N \text{ dB}}{10}} \quad (1.6)$$

$$\frac{U_2}{U_1} = 10^{\frac{N \text{ dB}}{20}} \quad (1.7)$$

$$\frac{I_2}{I_1} = 10^{\frac{N \text{ dB}}{20}} \quad (1.8)$$

$$\frac{E_2}{E_1} = 10^{\frac{N \text{ dB}}{20}} \quad (1.9)$$

$$\frac{H_2}{H_1} = 10^{\frac{N \text{ dB}}{20}} \quad (1.10)$$

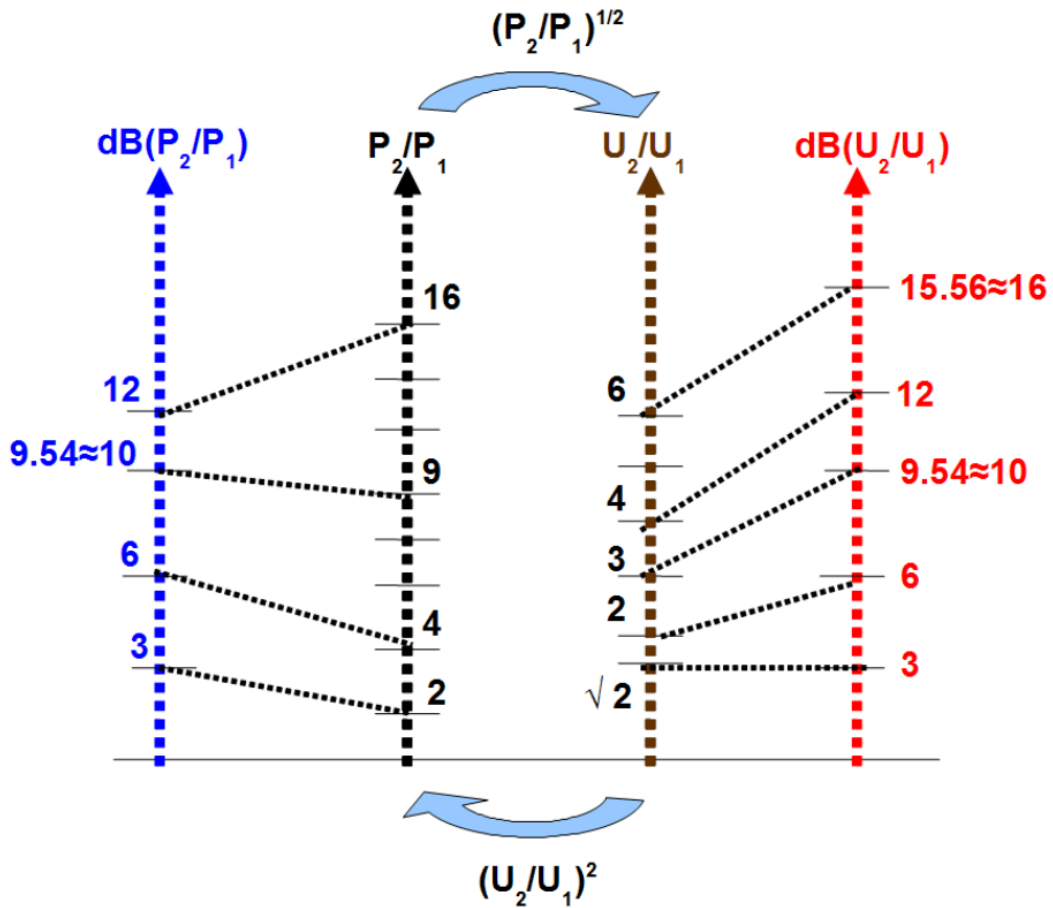


Figure 1.5: dB-Linear recalculation.

It is clear that 10-tuple change of power means change about 10dB , Eq.1.1. It must be also clear that 10-tuple change of voltage, current or field strength means change about 20dB , Eqs.: 1.2, 1.3, 1.4, 1.5.

Moreover it is advisory to remember some other selected relations between linear and dB scale. They are shown in Fig.1.5. Ratio 2 and 3 in linear scale of voltage (brown axis) corresponds respectively with 6dB and 9.54dB , Eq.1.2 which is almost equal to 10dB (red axis). The same concerns definitions (Eq.: 1.3), (1.4), (1.5).

Exception is power due to multiplier 10 before \log Def.(Eq.1.1). Ratio 2 and 9 in linear scale of power (black axis) corresponds respectively with 3dB and 9.54dB , Eq.1.1 which is almost 10dB (blue axis).

Usually explanation in parentheses behind dB symbol is omitted. It is redundant due to clever use of multiplier 10 by power and 20 by remaining definitions of dB .

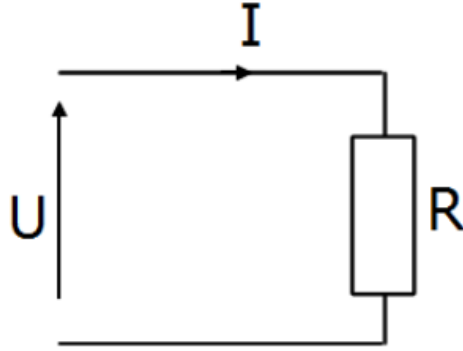


Figure 1.6: Voltage and current relations for resistance R .

For any one-port as shown in Fig.1.6 relation between power, voltage and current is as follows

$$P_1 = \frac{U_1^2}{R} = RI_1^2$$

$$P_2 = \frac{U_2^2}{R} = RI_2^2 \quad (1.12)$$

where R is resistance of the one-port.

Any change of power by the ratio P_2/P_1 is coupled with following changes of voltage and current

$$N \text{ dB} = 10 \log_{10} \left(\frac{P_2}{P_1} \right) = 10 \log_{10} \left(\frac{U_2}{U_1} \right)^2 = 20 \log_{10} \left(\frac{U_2}{U_1} \right)$$

$$N \text{ dB} = 10 \log_{10} \left(\frac{P_2}{P_1} \right) = 10 \log_{10} \left(\frac{I_2}{I_1} \right)^2 = 20 \log_{10} \left(\frac{I_2}{I_1} \right) \quad (1.14)$$

Conclusions from Eqs.(1.14) can be generalized. Any change of power about $N \text{ dB}$ causes change of voltage, current or field strength also about $N \text{ dB}$.

It can be interpreted in Fig.1.5. Let's say that voltage is increased about 3dB (red axis). It means that it is increased by ratio $\sqrt{2}$ Eq.1.7, (brown axis). By jumping from voltage axis (brown axis) to power axis (black axis) operator "power 2" must be applied, due to Eq.1.12. $\sqrt{2}$ in brown axis is coupled with 2 on black axis. Finally it is coupled with 3dB on blue axis, Eq.1.1.

An example in opposite direction. Let's say that power is increased about 12dB (blue axis). It means that it is increased by ratio 16 (black axis), Eq.1.6. By jumping from power axis (blue axis) to voltage axis (brown axis) operator "square root of 2" must be applied, due to Eq.1.12. 16 in black axis is coupled with 4 on brown axis. Finally it is coupled with 12dB Eq.1.1 on red axis.

Bound decibels

Despite floating decibels very often decibels with fixed value in denominator are used. Most commonly decibels are bound to

$$N \text{ dB}[mW] \equiv 10 \log_{10} \left(\frac{P}{1mW} \right) \quad (1.15)$$

$$N \text{ dB}[\mu V] \equiv 20 \log_{10} \left(\frac{U}{1\mu V} \right) \quad (1.16)$$

$$N \text{ dB}[\mu A] \equiv 20 \log_{10} \left(\frac{I}{1 \mu A} \right) \quad (1.17)$$

$$N \text{ dB}[\mu V/m] \equiv 20 \log_{10} \left(\frac{E}{1 \frac{\mu V}{m}} \right) \quad (1.18)$$

$$N \text{ dB}[\mu A/m] \equiv 20 \log_{10} \left(\frac{H}{1 \frac{\mu A}{m}} \right) \quad (1.19)$$

Equivalently $\text{dB}[m]$ is often used in definition (1.15). Moreover the square brackets can be omitted. Do not be astonished meeting notations like dBm , $\text{dB}\mu V$, $\text{dB}\mu V/m$.

The denominator is the reference value. Number N says about how many dB is the value in question (in numerator) bigger or smaller than the reference value in denominator.

In another way one can say, that decibel is bound the reference value in denominator.

Inverse calculation is as follows

$$P [mW] = 10^{\frac{N \text{ dBmW}}{10}} \quad (1.20)$$

$$U [\mu V] = 10^{\frac{N \mu V}{20}} \quad (1.21)$$

$$I [\mu A] = 10^{\frac{N \mu A}{20}} \quad (1.22)$$

$$E [\mu V/m] = 10^{\frac{N \mu V/m}{20}} \quad (1.23)$$

$$H [\mu A/m] = 10^{\frac{N \mu A/m}{20}} \quad (1.24)$$

There is still another group of bound decibels such as dB_i , $\text{dB}_{\lambda/2}$, dB_d and dB_c . In the first one the reference is the isotropic antenna. The second and the third are equivalent and concerns the dipole antenna. dB_c concerns content of the harmonics in the RF signal for which the main harmonic i.e. carrier signal is the reference. This group of bound decibels will be presented in the later part of the course.

Good exercise for surfing in the decibel world is calculation of relation between power in dBm and voltage in $\text{dB}\mu V$ for the one-port as shown in Fig.1.6.

Voltage – power relation yields

$$U^2 = R \cdot P \quad (1.25)$$

Nothing will change if the left hand side will be divided by $(1\mu V)^2$ and multiplied by $(1\mu V)^2$ i.e. by $10^{-12} V^2$ and the right hand side will be divided by $1mW$ and multiplied by $1mW$ i.e. by $10^{-3} W$

$$U^2 \cdot \frac{10^{-12} V^2}{(1\mu V)^2} = R \cdot P \cdot \frac{10^{-3} W}{1mW} \quad (1.26)$$

Rearranging yields

$$\left(\frac{U}{1\mu V} \right)^2 = \frac{R}{1\Omega} \cdot \frac{P}{1mW} \cdot 10^9 \quad (1.27)$$

Logarithmising both side of equality with 10-tuple logarithm to base 10 yields

$$20 \log \left(\frac{U}{1\mu V} \right) = 10 \log \left(\frac{R}{1\Omega} \right) + 90 + 10 \log \left(\frac{P}{1mW} \right) \quad (1.28)$$

Finally for resistance $R = 50\Omega$

$$U_{\text{dB}\mu V} \approx 107 + P_{\text{dBmW}} \quad (1.29)$$

Electrical dimension

Physical dimensions of a radiating structure such as antenna are not important in determining the ability of that structure to transmit or receive electromagnetic energy. Electrical dimension, meant as ratio of physical dimensions of the structure to the wavelength λ feeding it or induced in it are more significant in determining this ability.

Similarly, by transporting energy or transmitting signal with a line, physical length of the line does not rule presence of wave propagation along it. Again electrical length, meant as physical length of the line related to the wavelength λ of the transported energy or transmitted signal is relevant in respect of it.

In [Clayton] the criterion for electrically small circuit is defined. Circuit is electrically small if its largest dimension is smaller than one-tenth of a wavelength accompanied with signal or energy processed with the circuit. In such case distributed nature of the electromagnetic field can be ignored and lumped circuit models are an adequate representation of the electromagnetic phenomena. This criterion includes also electrically short line which can be represented with the lumped circuit, unlike electrically long line which must be represented with distributed parameters.

This criterion is applied in everyday engineer life. Nowadays oscilloscopes have optional setting of the input resistance 50Ω or $1M\Omega$. If the cable in the measurement path is electrically short then it doesn't matter which setting is chosen. However if the cable in the measurement path is electrically long it must be viewed as distributed line in which the wave is propagating. In such a case distortion-free measurement of the signal is assured only by setting 50Ω input resistance. Usually cable in the measurement path is coaxial one with 50Ω characteristic impedance. Its 50Ω termination at the oscilloscope input enables to avoid mismatching.

In Table 1.1 wavelength in vacuum for different frequencies are gathered. It is beneficial to learn by hard one row of that table $f = 300MHz \Rightarrow \lambda_0 = 1m$. It is good reference for estimating the wavelength by other frequencies.

Frequency f	Wavelength λ_0
50 Hz	6000 km
3 kHz	100 km
30 kHz	10 km
300 kHz	1 km
3 MHz	100 m
30 MHz	10 m
300 MHz	1 m
3 GHz	10 cm
30 GHz	1 cm
300 GHz	1 mm

Table 1.1: Frequencies of sinusoidal waves and their corresponding wavelength in free space in vacuum.

[[Dlugosc falii]]{#Dlugosc falii label="Dlugosc falii"}

The velocity of propagation in free space in vacuum is

$$v_0 = \frac{1}{\sqrt{\epsilon_0 \mu_0}} \approx 3 \cdot 10^8 m/s \quad (1.30)$$

where $\epsilon_0 \approx 8.854 \cdot 10^{-12} \text{ F/m}$, $\mu_0 \approx 4\pi \cdot 10^{-7} \text{ H/m}$.

In other media with relative parameters μ_r , ϵ_r not equal to 1, it is

$$v = \frac{1}{\sqrt{\epsilon\mu}} = \frac{v_0}{\sqrt{\epsilon_r\mu_r}} \quad (1.31)$$

For example, a wave propagation in Teflon ($\epsilon_r = 2.1$, $\mu_r = 1$) has a velocity of propagation of $v = 0.69 \cdot v_0$. Accordingly, the wavelength in Teflon is shortened by factor 0.69.

If the frequency band of the signal measured with the oscilloscope goes up to 100MHz and cable in the measurement path is 50Ω Teflon cable, then the wavelength in the cable is 2.07m . Available coaxial cables have length of 0.5m , 1.0m or more. It is obvious that in such case they are electrically long and oscilloscope setting must be practically always 50Ω .

In standard [EN-4-20] another definition of electrical dimension is introduced. The context of it is the size estimation of the device which can be measured in the Gigahertz Transverse Electromagnetic GTEM cell. Device is electrically small if its largest dimension is smaller than one wavelength at the highest frequency for which the measurement should be done.

Both definitions introduced in [Clayton] and in [EN-4-20] are only rules of thumb and as such can better or worse estimate reality depending on situation.

Power (impedance) matching {#impedance maching}

Considered is the circuit in Fig.1.7 a). Let us assume the internal source resistance as parameter $R_S = \text{const}$ and variable load resistance $R_L = \text{var}$.

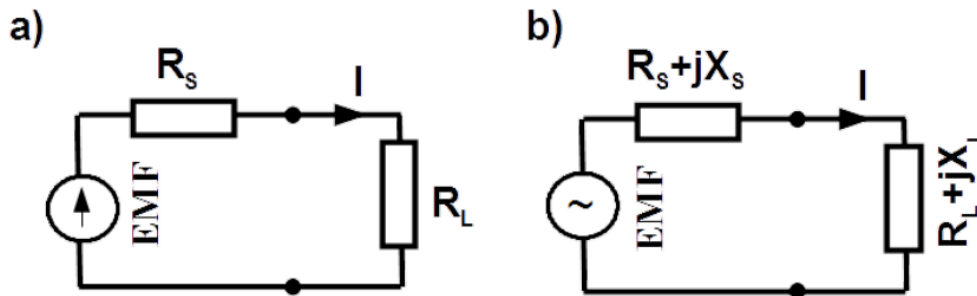


Figure 1.7: DC a) and AC b) circuits for matching consideration.

Power delivered from the source to the circuit in Fig. 1.7 a) is $P(R_L) = EMF \cdot I = \frac{EMF^2}{R_S + R_L}$

Power dissipated in the load is

$$P_L(R_L) = R_L \cdot I^2 = \frac{R_L \cdot EMF^2}{(R_S + R_L)^2} \quad (1.33)$$

Power losses in the source are

$$P_S(R_L) = R_S \cdot I^2 = \frac{R_S \cdot EMF^2}{(R_S + R_L)^2}$$

The source has unlimited capability but it delivers power as demanded by the load. In order to figure out how big is maximal demanded power, extremum condition on variable $P_L(R_L)$ in Eq. (1.33) must be imposed. The answer is $R_S = R_L$. This is called power or impedance matching condition.

By matching, the load absorbs maximal power from the source

$$P_{L_{max}} = \frac{EMF^2}{2R_S} \quad (1.35)$$

The same amount of power is dissipated in the internal source resistance R_S .

Budget of power can be explained with incident and reflected power. The source sends incident power $P_{L_{max}}$ to the load. If the load is ready to absorb the whole amount of delivered power i.e. matching condition is fulfilled, then it does it. Otherwise part of the incident power is reflected from the load and travels back to the source. The net power dissipated in the load is equal to the incident power decreased about the reflected power. The same happens to the power delivered from the source.

Let us introduce variable k as quotient of the load and the source resistance $k = R_L/R_S$. Moreover let us define variable: power dissipated in the load related to the maximal power that can be absorbed in the load, see Eq. (1.35)

$$p_L(k) = \frac{P_L(k)}{P_{L_{max}}} = \frac{4k}{(1+k)^2}$$

along with variable: power losses in the source related to the maximal power that can be absorbed in the load, see Eq. (1.35)

$$p_S(k) = \frac{P_S(k)}{P_{L_{max}}} = \frac{4}{(1+k)^2}$$

Finally let us define efficiency as the ratio of power dissipated in the load and delivered from the source

$$\eta(k) = \frac{P_L(k)}{P} = \frac{k}{(1+k)}$$

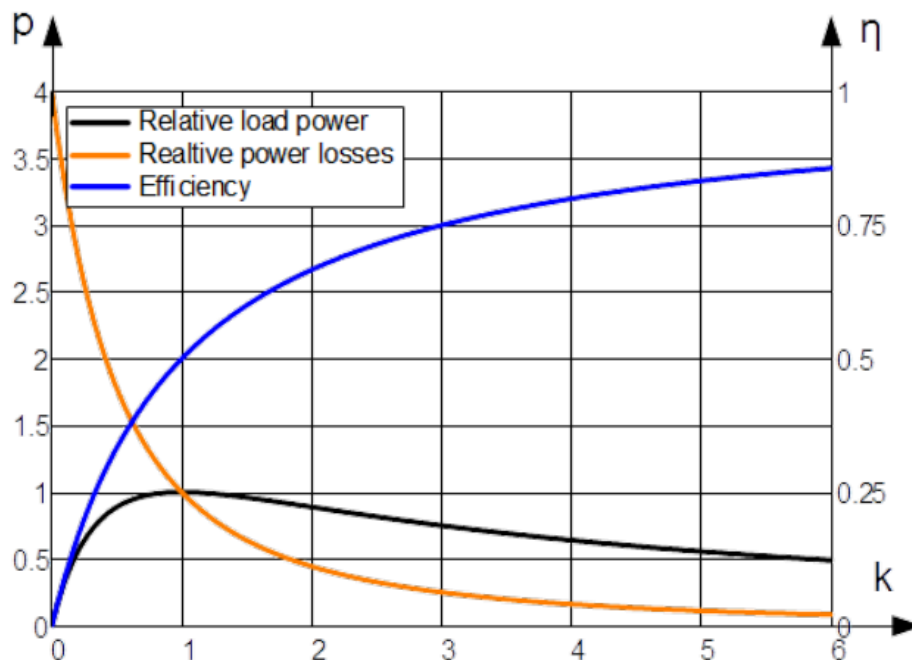


Figure 1.8: Relative power and efficiency versus coefficient k .

$p_L(k)$, $p_S(k)$ and $\eta(k)$ are presented in Fig.1.8. In the distinctive point, by matching ($k = 1$) both relative powers are equal 1. The efficiency in that point is equal 0.5.

Power electro engineers are accustomed with coefficient $k \gg 1$. They cannot design generators which deliver maximal power to the load with 50 % of internal losses. They try to operate in the region by which efficiency η is approaching 1. Indeed, delivered power is smaller there than maximal P_{Lmax} but in the same time losses are suppressed, so that efficiency is big.

On the contrary, electronic engineers pursuit of matching point ($k = 1$). Never mind that they have to provide twice as much power as they require. Matching for them is indispensable. They operate in the frequency range in which lines for transmitting signal or power must be regarded as distributed lines. Due to frequency dependence of the input impedance of a transmission lines, the line which is open circuited at the end can have input impedance close to zero. RF signal generators and amplifiers are not design to sustain the short circuit.

Matching condition for the AC circuit shown in Fig. 1.7 b) can be explained in two steps:

- imaginary part of impedance Z_S must be equal to the conjugate of the imaginary part of Z_L ($jX_S = -jX_L$).
- real parts of Z_S and Z_L (resistances R_S and R_L) must be equal one to another. This results from the same consideration as for the DC circuit.

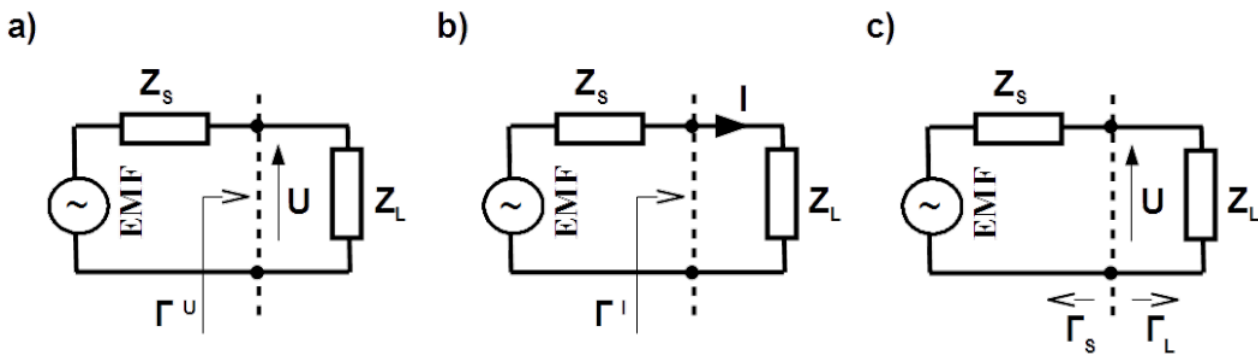


Figure 1.9: Reflection on the two-port: voltage a), current b), in both directions.

Voltage U across the load in Fig. 1.9 a) can be expressed with the Ohm's and the Kirchhoff's circuit laws

$$U = \frac{Z_L}{Z_S + Z_L} \text{EMF} = U_i + U_r \quad (1.39)$$

Similar as for power this voltage can be split into incident and reflected component: U_i and U_r respectively. The first is meant as voltage that would be received by the load in case of matching to the source impedance ($Z_L = Z_S^*$). It will be $U_i = \text{EMF}/2$. In order to fulfill Eq.(1.39) reflected voltage

yields
$$U_r = \frac{Z_L - Z_S}{Z_L + Z_S} \cdot \frac{\text{EMF}}{2}$$

U_r is the voltage reflected by the load in case of mismatching and sent back to the source.

Voltage reflection coefficient is defined as quotient of reflected and incident voltage ($\Gamma^U = U_r/U_i$).

$$\Gamma^U = \frac{Z_L - Z_S}{Z_L + Z_S} \quad Z_L = \frac{1 + \Gamma^U}{1 - \Gamma^U} \quad (1.41)$$

With rearrangement the load impedance can be derived.

Analogue the current reflection coefficient can be derived for the circuit in Fig.1.9 b).

$$I = \frac{\text{EMF}}{Z_L + Z_S} = I_i + I_r \quad (1.42)$$

The incident current will be $I_i = \mathbf{EMF}/2\mathbf{Z}_S$. In order to fulfill Eq.(1.42) reflected current yields

$$I_r = -\frac{\mathbf{Z}_L - \mathbf{Z}_S}{\mathbf{Z}_L + \mathbf{Z}_S} \cdot \frac{\mathbf{EMF}}{2\mathbf{Z}_S}$$

Current reflection coefficient is defined as quotient of reflected and incident current ($\Gamma^I = I_r/I_i$).

$$\Gamma^I = -\frac{\mathbf{Z}_L - \mathbf{Z}_S}{\mathbf{Z}_L + \mathbf{Z}_S} \quad \Gamma^U = -\Gamma^I \quad (1.44)$$

Γ^I is rarely used. Lack of upper case in symbol means the voltage coefficient.

Reflection coefficient is always related to some impedance. Up to now reference was the source impedance \mathbf{Z}_S . Generally it can be arbitrary impedance \mathbf{Z}_0 causing reflection in both directions: toward the source $\Gamma_S = (\mathbf{Z}_S - \mathbf{Z}_0)/(\mathbf{Z}_S + \mathbf{Z}_0)$ and toward the load $\Gamma_L = (\mathbf{Z}_L - \mathbf{Z}_0)/(\mathbf{Z}_L + \mathbf{Z}_0)$ as shown in Fig. 1.9 c). Majority of measurement instruments are referred to resistance $\mathbf{Z}_0 = 50 \Omega$.

Very easily following relation between reflection coefficients can be derived

$$\frac{\mathbf{Z}_S}{\mathbf{Z}_L} = \frac{1 + \Gamma_S}{1 + \Gamma_L} \cdot \frac{1 - \Gamma_L}{1 - \Gamma_S}$$

Finally

$$U = \frac{\mathbf{EMF}}{1 + \frac{\mathbf{Z}_S}{\mathbf{Z}_L}} = \frac{(1 - \Gamma_S)(1 + \Gamma_L)}{1 - \Gamma_S\Gamma_L} \cdot \frac{\mathbf{EMF}}{2} \quad (1.46)$$

This voltage looks much more friendly in dependence on impedances, see Eq.(1.39). Derivation of it in dependence on reflection coefficients seems to be scholastic exercise but it is not the case. Mind that in RF technique direct measurement of impedances and resistances unlike reflection coefficients is not possible.

Attenuation (transmission) vs. voltage division factor

Insertion loss L_i of a two-port illustrated in Fig. 1.10 as Device Under Test (DUT) is ratio of voltages across the load impedance \mathbf{Z}_L , which terminates the DUT in two situations, when:

- the load \mathbf{Z}_L is connected directly to the source, U in Fig. 1.10 a),
- between the load and the source the DUT is inserted, U_2 in Fig. 1.10 b).

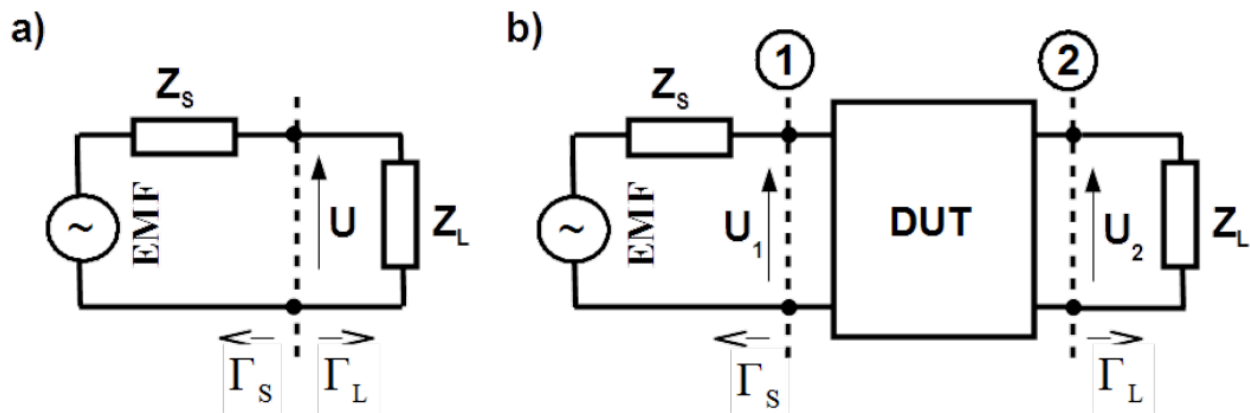


Figure 1.10: Illustration of insertion and voltage loss of a DUT.

Insertion loss $L_i = U/U_2$ depends on the source \mathbf{Z}_S and the load \mathbf{Z}_L impedance.

Attenuation of a DUT is insertion loss under matching regime at the source and the load ($\mathbf{Z}_S = \mathbf{Z}_L = \mathbf{Z}_0$)². Transmission is inverse of the attenuation.

For reciprocal DUTs e.g. passive, linear DUTs attenuation \mathbf{A}_{12} from port 2 to 1 (source applied to port 1, see Fig. 1.10 b)) and in opposite direction \mathbf{A}_{21} (source applied to port 2) are the same

$$\mathbf{A}_{12} = \mathbf{A}_{21} \quad (1.47)$$

Memorise that attenuation is referred to the source and load impedance equal to \mathbf{Z}_0 .

Voltage loss \mathbf{L}_v of a two-port illustrated in Fig. 1.10 b) as Device Under Test (DUT) is ratio of input voltage \mathbf{U}_1 and output voltage \mathbf{U}_2 .

Voltage loss $\mathbf{L}_v = \mathbf{U}_1/\mathbf{U}_2$ depends only on the load \mathbf{Z}_L impedance.

Voltage division factor of a DUT is voltage loss under matching regime at the load ($\mathbf{Z}_L = \mathbf{Z}_0$)

$$\mathbf{VDF} = \mathbf{L}_v|_{\Gamma_L=0} \quad (1.48)$$

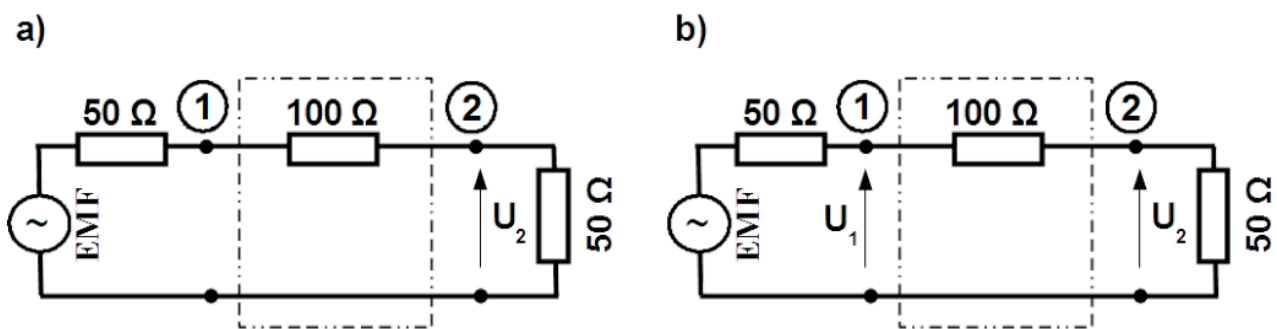


Figure 1.11: Data for calculus illustration of attenuation and voltage division factor.

Let us calculate attenuation of the two-port shown in Fig. 1.11 a), referred to 50Ω resistance. Since $\mathbf{U} = \mathbf{EMF}/2$ and $\mathbf{U}_2 = \mathbf{EMF}/4$ hence $\mathbf{A}_{12} = 2$ i.e. ($6dB$).

In Fig. 1.11 b) $\mathbf{U}_2 = \mathbf{U}_1/3$ then $\mathbf{VDF} = 3$ i.e. ($10dB$).

Memorise that attenuation and voltage division factor are different quantities. Apply them consciously, do not confound them!

Let us exercise once more calculation of attenuation referred to 50Ω resistance, illustrating simultaneously the reciprocity principle. The considered two-port has topology with 100Ω serial resistance and 1Ω resistance parallel to the port 2, as shown in Fig. 1.12.

In both cases voltage across the load without insertion of the two-port $\mathbf{U} = \mathbf{EMF}/2$.

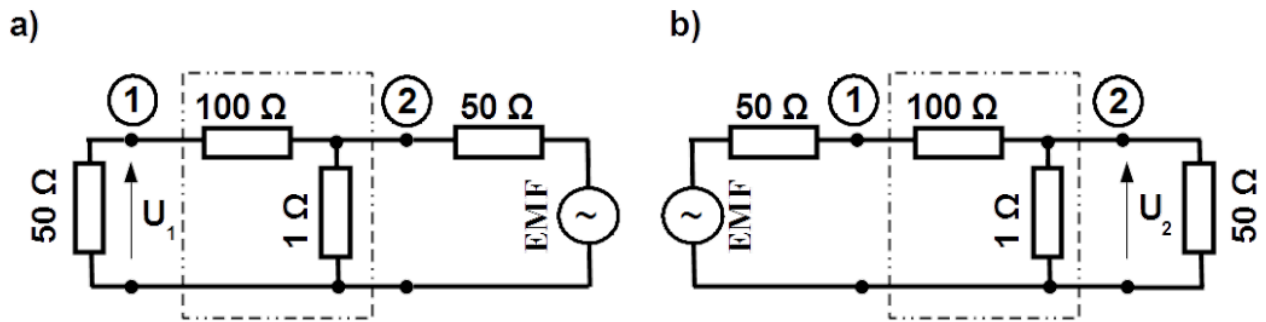


Figure 1.12: Data for calculus illustration of reciprocity principle of linear passive two-port by means of attenuation ($A_{12} = A_{21}$); circuit for calculation of A_{12} a), circuit for calculation of A_{21} b).

U_1 by calculation of A_{12} in the circuit in Fig. 1.12 a) is as follows

$$U_1 = \frac{EMF}{50\Omega + \frac{150\Omega^2}{151\Omega}} \cdot \frac{150\Omega^2}{151\Omega} \cdot \frac{50\Omega}{150\Omega} = \frac{EMF}{154} \quad \text{Finally} \quad A_{12} = U/U_1 = 77 \quad .$$

U_2 by calculation of A_{21} in the circuit in Fig. 1.12 b) is as follows

$$U_2 = \frac{EMF}{150\Omega + \frac{50\Omega^2}{51\Omega}} \cdot \frac{50\Omega^2}{51\Omega} = \frac{EMF}{154} \quad A_{21} = U/U_2 = 77 = A_{12} \quad , \quad \text{quod} \quad \text{erat}$$

demonstrandum (q.e.d.)!

What actually R,L,C one-ports are?

In this section examples of frequency characteristics of the passive assembly component RLC are gathered. The aim of it is to evoke strong and everlasting impression that depending on the frequency, even such simple components exhibits any electric properties but that for what they are designed.

Wire wound resistor

In Fig.1.13 impedance of resistor with rated resistance 216Ω made of resistive wire in Through Hole Technology *THD* is shown. It is measured in the frequency range from 9 kHz to 300 MHz. Actually it is resistance only up to 100 kHz. Its module is equal to rated value and phase is almost equal to zero. From that frequency on inductive character appears. Module and phase rises. Between 20 MHz and 30 MHz there is parallel resonance. Above that frequency module decreases, phase as well reaching -90° i.e. resistor becomes capacitor.

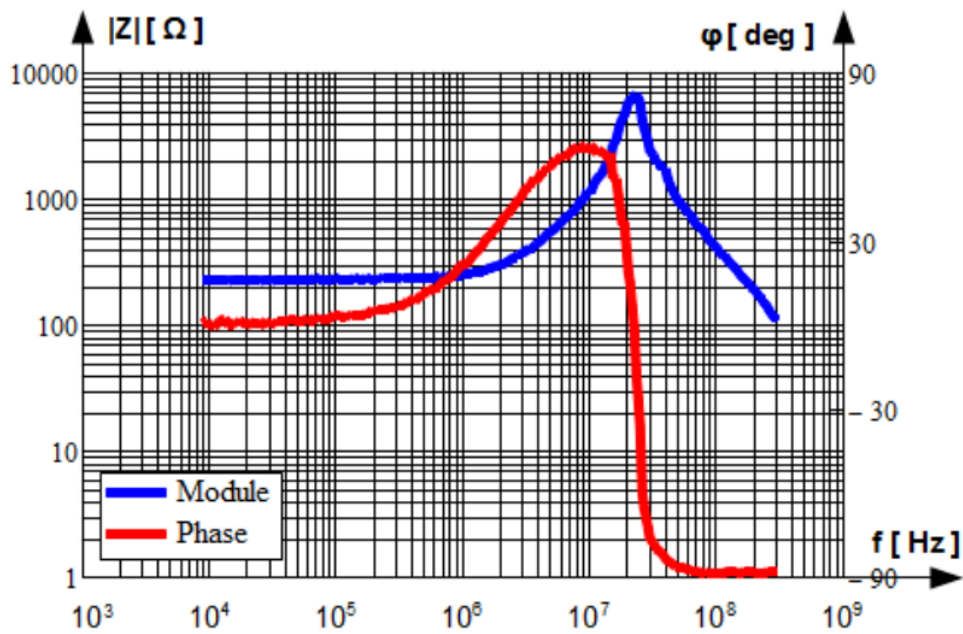


Figure 1.13: Frequency dependent impedance of the wire wound resistor.

Such plots are clear by focusing on building technology of the resistor. It is shown in Fig.1.14. Wire with circular cross-section wound on the cylindrical former exhibits inductance in addition to resistance. Therefore serial branch $R_{Cu}(f)L$. Resistance is frequency dependent due to skin effect. There exist also capacitance between turns of wire. Actually there is matrix of all two turns combinations. One capacitance C shown in Fig.1.14 is simplified model. Two inductances L_L represents inductances of the resistor leads. They are negligible small in comparison to the inductance L of the wound wire.

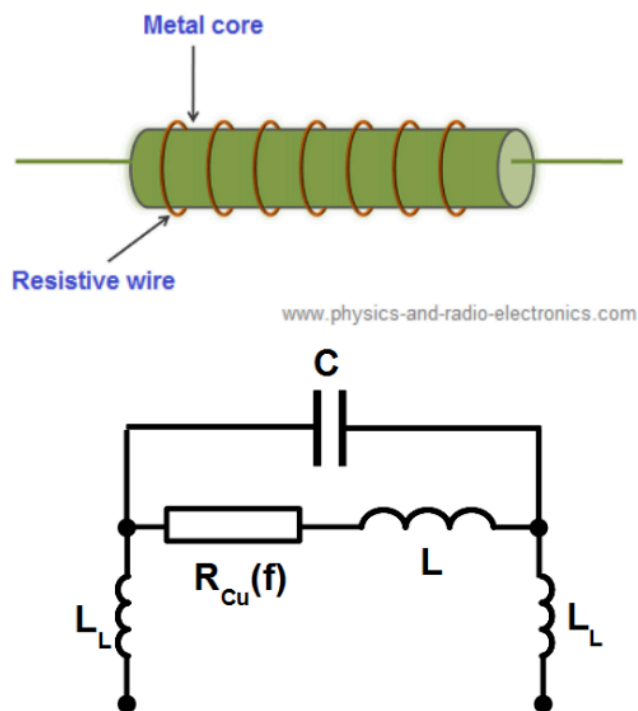


Figure 1.14: Wire wound resistor.

Metal film resistor

In Fig.1.15 impedance of the THD metal film resistor with rated resistance $200\ \Omega$ is shown. Impedance of this resistor does not exhibit inductive but capacitive character by increasing frequency. This suggests serial resonance by frequency significantly far above 300MHz . Explanation lays also in building technology.

Resistance is build with metal oxide sheet etched on the ceramic substrate. Etching due to geometry i.e. rectangular cross-section with width much bigger than height is low inductive, practically non inductive. The metal sheet is encapsulated on both ends in metal caps which serves as the junction between the sheet and the leads. Caps due to relatively big layer oriented parallel one to another build flat condenser which is represented with capacitance C parallel to resistance R in the equivalent circuit in Fig.1.16. Resonance frequency of the serial branch $2L_L C$ which is $f_0 = 1/\sqrt{2L_L C}$ is much above 300MHz due to small values of leads inductances L_L . Influence of the skin effect on the resistance of the metal sheet can be neglected due to rectangular cross-section with width much bigger than height.

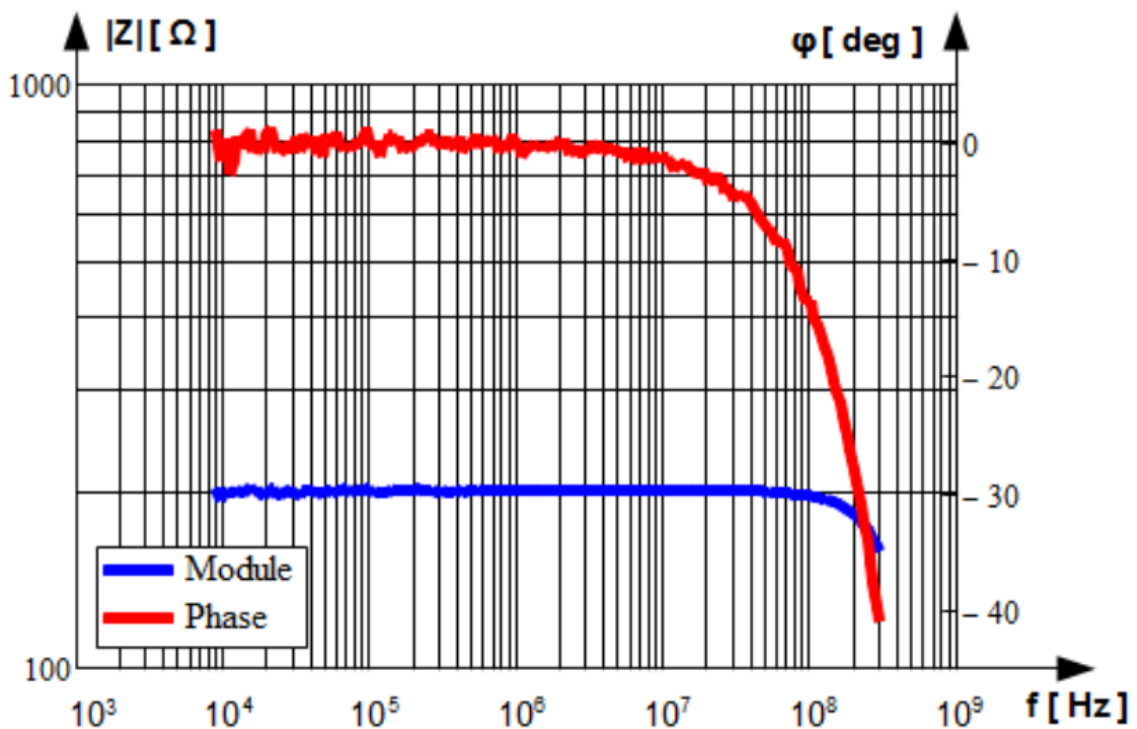
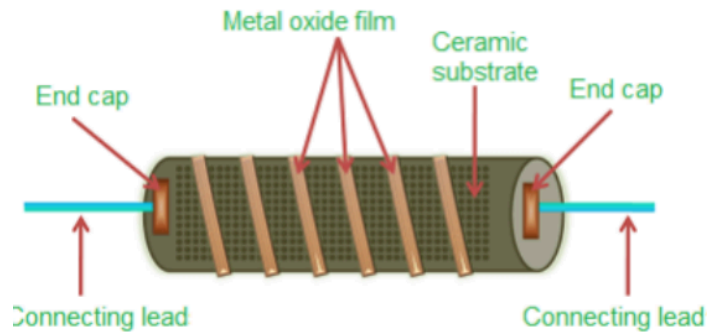


Figure 1.15: Impedance of the metal film resistor.



www.physics-and-radio-electronics.com

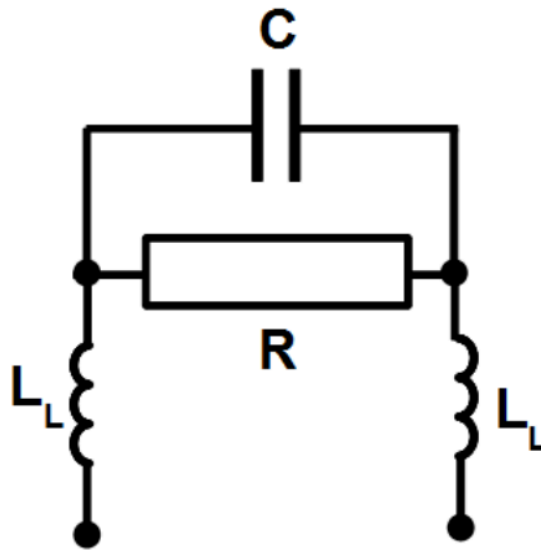


Figure 1.16: The metal film resistor.

Film capacitor

In Fig.1.17 impedance of a THD metal film condenser with rated capacitance 10 nF is shown. Again plot suggests serial resonance between capacitance C for what this one-pole is built and the leads inductances L_L . The resonance frequency falls upon much smaller frequency than in the case of the film resistor, in this case between 5 MHz and 6 MHz , because capacitance is significantly bigger.

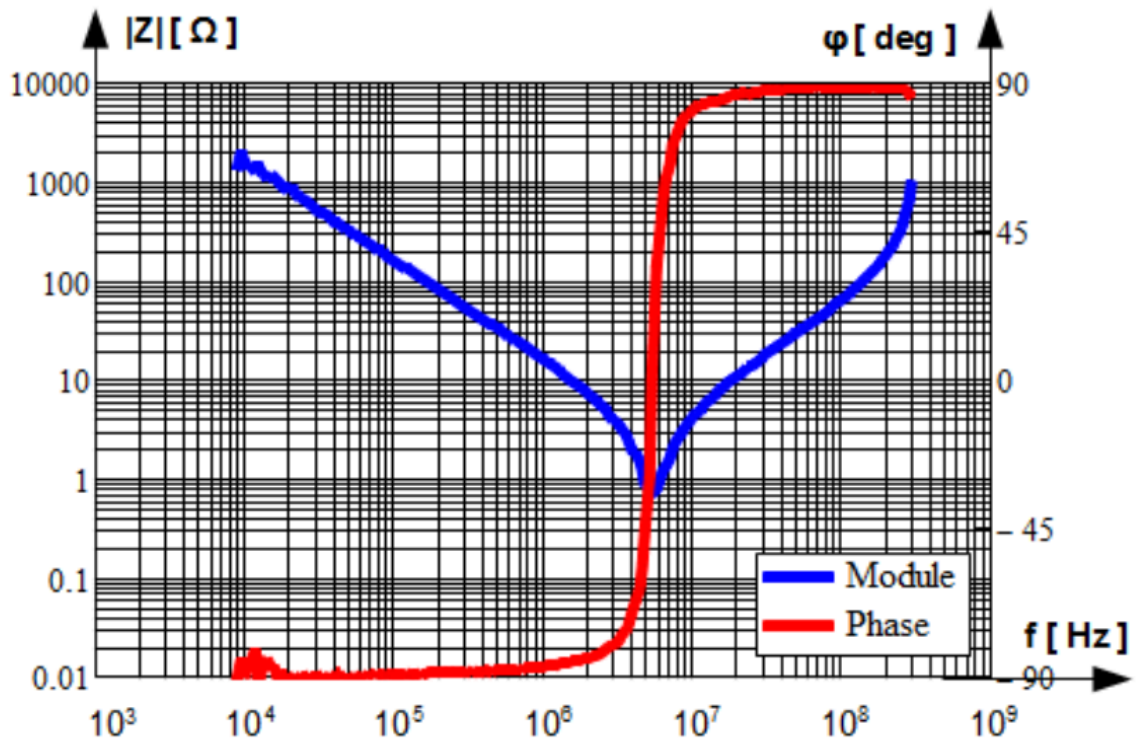


Figure 1.17: Impedance of the film capacitor.

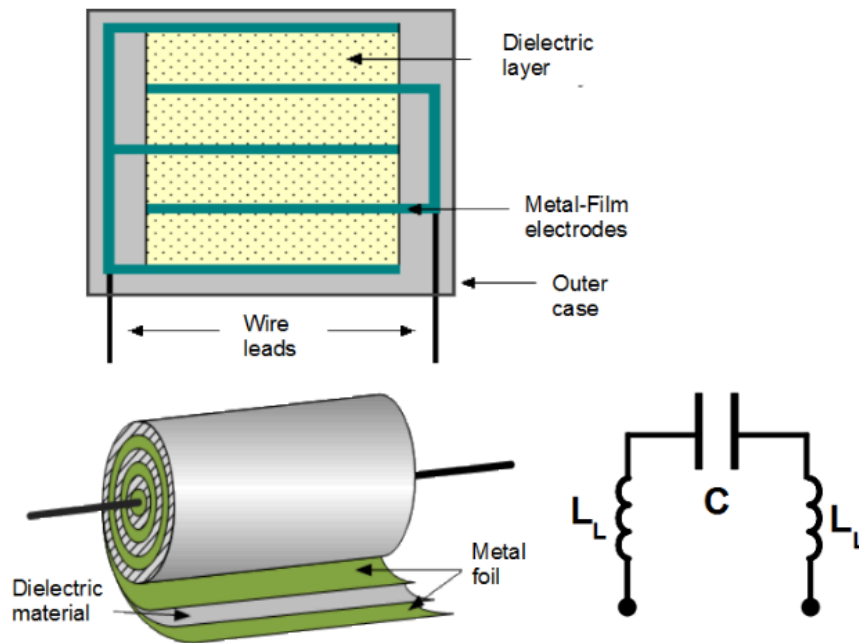


Figure 1.18: The film capacitor.

High frequency choke

In Fig.1.19 impedance of a high frequency choke built with 4 mm diameter laboratory cable wound on the MnZn toroidal core is shown. The core material exhibits frequency dependent inductance $L(f)$ and frequency dependent losses $R(f)$. In the low frequency range material is lossless and inductance is constant. Impedance rises with the slope 20 dB/dec. However by frequency about 2 MHz fall of inductance accompanied with rise of losses reveals. Capacitance between turns causes parallel resonance with the choke inductance $L(f)$ by 10 MHz. Resistances representing losses in the core material $R(f)$ and conducting losses in the turns $R_{Cu}(f)$ suppresses resulting resistance by the resonance. Above the parallel resonance the circuit has capacitive character. Another serial resonance between capacitance C and leads inductances L_L is observed above 200 MHz.

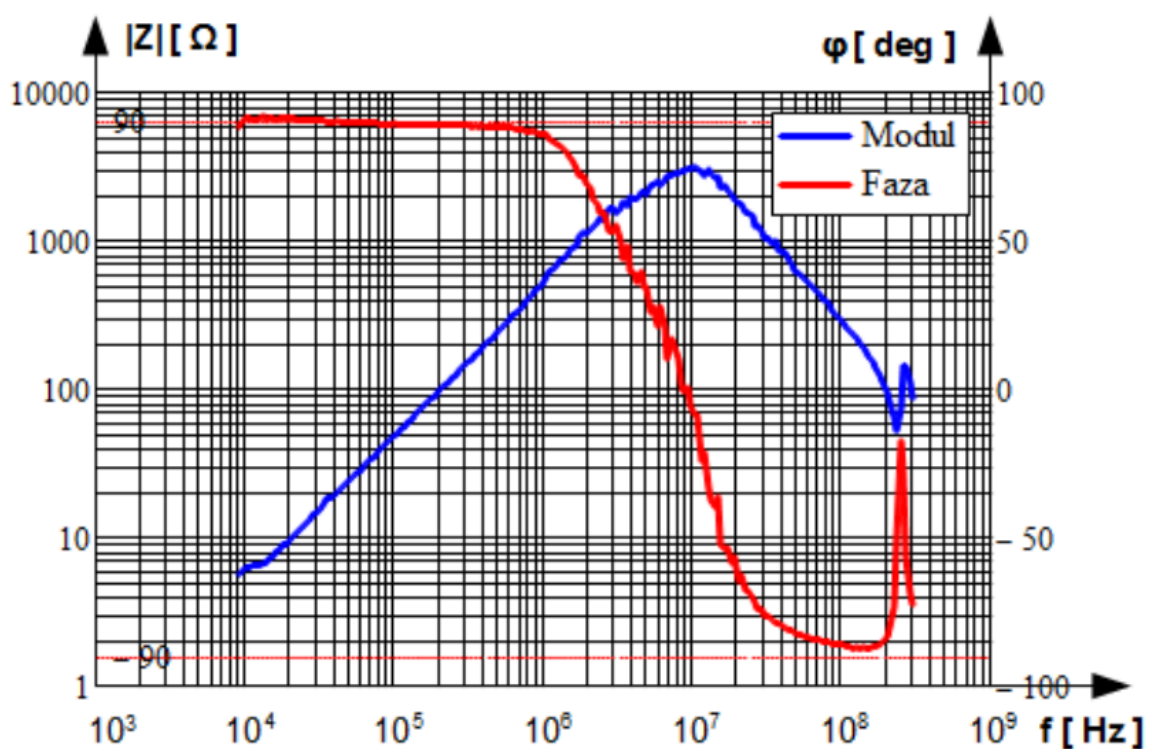


Figure 1.19: Impedance of the HF choke.

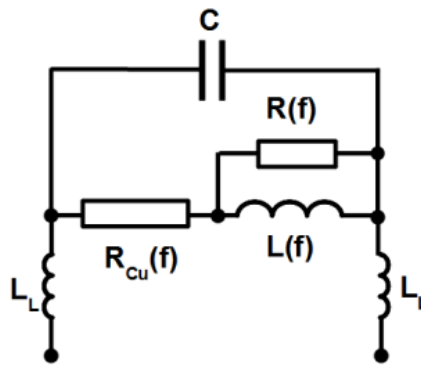


Figure 1.20: The high frequency choke.

In bush of the pulse parameters

Pulses are usually captured in the time domain with the single shot oscilloscopes. Nowadays the oscilloscopes have ability to activate cursors for direct measuring of arbitrary instantaneous value of the pulse and the instant. This enables to cope with the pulse parameters. Unfortunately there is really bush by their definitions. The terms are used very often without reflection what they really are? Devoting some time for that section helps to avoid misunderstanding in discussions and to prevent from drawing ill conclusions.

Measurable pulse parameters

The primary measurable pulse parameter is the pulse peak defined as the first maximum of the wave shape. Remaining parameters i.e. the pulse rise time and the pulse width can be derived from it.

The pulse rise time is the time elapsed between two instants for which instantaneous values of the pulse gets predefined part of the pulse peak. In most cases 90% and 10% of the peak value are used. It is called then $t_r = t_{90\%-10\%}$ as shown in Fig.1.21. In some cases $t_{90\%-30\%}$ is applied. Less frequently $t_{80\%-20\%}$ is used.

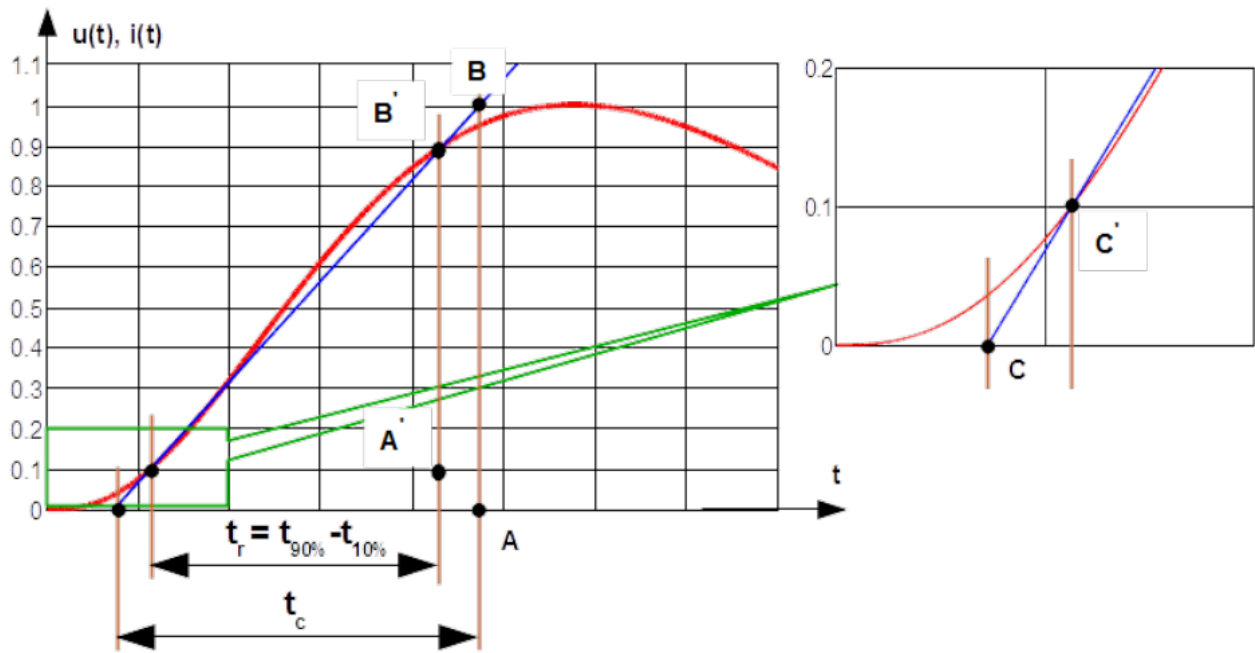


Figure 1.21: Illustration of the pulse rise time t_r and the pulse crest (front) time t_c .

The pulse width is the time elapsed between instants for which instantaneous values of the pulse gets predefined part of the pulse peak on rising slope and on falling slope of the pulse tail. In common use is $t_w = t_{50\%}$ as shown in Fig.1.22.

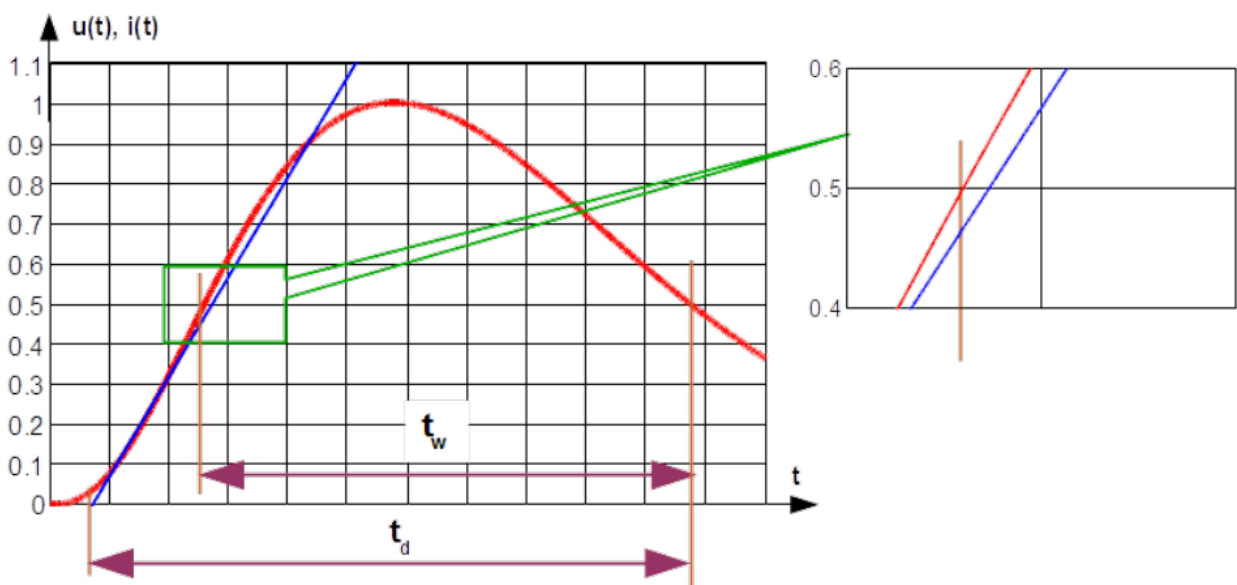


Figure 1.22: Illustration of the pulse width t_w and the pulse duration t_d .

Calculable pulse parameters

From the measurable parameters other parameters can be calculated.

For calculating the pulse crest (front) time t_c the secant passing through the points constituting the rise time must be built. See blue line in Fig.1.21 which crosses the pulse by 90% and 10% of its peak value. The pulse crest (front) time is the time elapsed between two instants for which the secant reaches the peak value and crosses the time axis.

Relation between lengths of sides of similar triangles $AB/CA = A'B'/C'A'$, particularly $1/t_c = (0.9 - 0.1)/t_r$ in case shown in Fig.1.21 yields

$$t_c = \begin{cases} 1.25 \cdot t_r & \text{for } t_r = t_{\{90\%-10\%\}} \\ 1.67 \cdot t_r & \text{for } t_r = t_{\{90\%-30\%\}} \text{ or } t_r = t_{\{80\%-20\%\}} \end{cases} \quad (1.51)$$

The same secant is used for calculation of the pulse duration t_d . The pulse duration is the time elapsed between instants on the tail when the pulse decreases to 50% of the the peak value and the instant when secant crosses the time axis. See Fig.1.22. Sometime the pulse duration is used interchangeably with the pulse width, causing ambiguity.

Fourier transformations

Fourier series is a way to decompose any periodic function $c(t)$ into the weighted sum of a (possibly infinite) set of simple oscillating functions, namely sines and cosines

$$c(t) = a_0 + \sum_{n=1}^{\infty} [A_n \cos(n\omega_1 t) + B_n \sin(n\omega_1 t)] \quad (1.52)$$

The first term in series, $n = 1$ is called fundamental harmonic and ω_1 angular fundamental frequency. It is related with fundamental frequency f_1 and fundamental period T_1 as follows

$$\omega_1 = \frac{2\pi}{T_1} = 2\pi f_1 \quad (1.53)$$

Frequency of n-th harmonic is n-tuple of fundamental frequency.

Coefficients of the Fourier series are as follows

$$a_0 = \frac{1}{T_1} \int_0^{T_1} c(t) dt \quad (1.54)$$

$$A_n = \frac{2}{T_1} \int_0^{T_1} c(t) \cdot \cos(n\omega_1 t) dt \quad (1.55)$$

$$B_n = \frac{2}{T_1} \int_0^{T_1} c(t) \cdot \sin(n\omega_1 t) dt \quad (1.56)$$

It should be noted that a_0 in Eq.(1.54) is average value of function $c(t)$. Function with $a_0 = 0$ is called alternated.

More convenient representation of the Fourier series is series of sines functions with phase angle ψ_n dependent on number n of harmonic

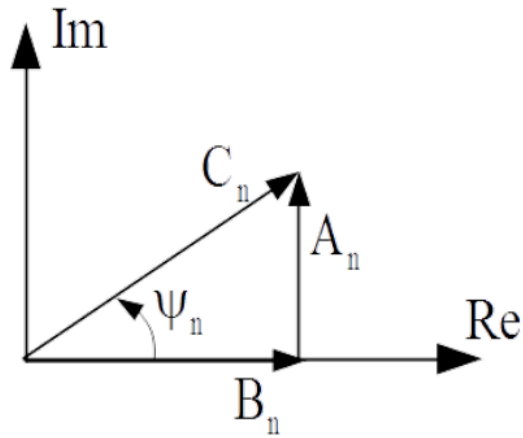


Figure 1.23: Fourier terms in complex plane.

$$c(t) = c_0 + \text{Im} \left[|C_n| e^{j(n\omega_1 t + \psi_n)} \right] = c_0 + \sum_{n=1}^{\infty} |C_n| \sin(n\omega_1 t + \psi_n) \quad (1.57)$$

$$c_0 = a_0 \quad (1.58)$$

$$|C_n| = \sqrt{A_n^2 + B_n^2} \quad (1.59)$$

$$\psi_n = \arctan\left(\frac{A_n}{B_n}\right) \quad (1.60)$$

In Fig.1.24 an example of periodic function with constant component and harmonics $n = 1$, $n = 2$, $n = 3$ is shown. Period T of this function is identical with period T_1 of fundamental harmonic. It is general rule. Constant component is proportional to area below plot $c(t)$ (black curve in Fig.1.24 a). This area above time axis has positive sign (red colour in Fig.1.24 a) and negative below time axis (green colour Fig.1.24 a).

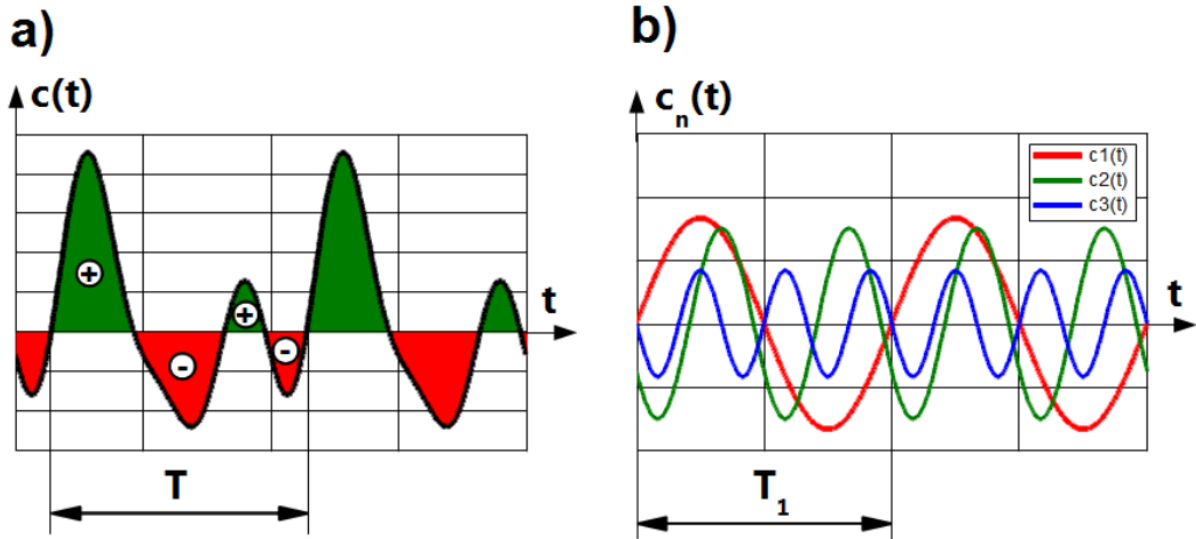


Figure 1.24: Arbitrary periodic function.

Spectral density per frequency unit of a single event $u(t)$ is represented with the Fourier integral as follows

$$u(f) = \int_{-\infty}^{\infty} u(t) e^{-j2\pi ft} dt \quad (1.61)$$

-
1. It means serial resonance of the source and the load impedance by which the current is maximal and there is no reactive power commuting between the source and the load.↵
 2. Usually reference impedance is resistance ($Z_0 = 50\Omega$).↵
 3. More frequently the term front time is used. Here the term crest time rationalizes assigning index "c" in symbol t_c . Symbol t_f is dedicated to fall time.↵

2. Low frequency current and voltage disturbances

Definition of electromagnetic disturbance, named shortly disturbance in these lecture notes is inserted in sub chapter [EU regulation]. Another relevant definition is *interference* which is unwanted impact of the electromagnetic disturbance on other arrangements energized electrically. Disturbance is cause and interference is effect.

Disturbance can be for instance sparking on the commutator of the brush motor in the hair dryer or drilling machine, that can *interfere* radio receiver or garage door opener.

There are two kind of origins (of sources) of the electromagnetic disturbance: Man and Nature. Man-made disturbance can be either side effect of operation of arrangement or can be intentional.

It is commonly known that AC/AC inverters widespread in power electronic are source of nasty radio frequency disturbances which are unwanted side effect of their operation.

Purpose of intentional sources of disturbances can be peaceful or military.

Two examples of intentional, peaceful sources of disturbances:

1. electro erosion machine tool is equipped with high voltage source which generates intentionally electric arc to form parts by removing metal chips from a workpiece, but electromagnetic field accompanying the arc can interfere other arrangements in the surroundings,
2. mobile telephone communicates with radio signal which is intentional and useful for someone who wants to talk on the mobile phone but this radio signal can be disastrous for an aircraft especially by takeoff and landing.

Unfortunately Man uses also electromagnetic energy intentionally as a weapon. High power microwaves or Nuclear Electromagnetic Pulse are example of that. They are called “humanitarian” weapons.

Disturbances can be classified in respect to different features:

- *frequency* – low frequency (e.g. voltage flicker in public electricity network), radio frequency (e.g. glow discharge in a gas-discharge lamp),
- *frequency band* – narrowband (e.g. radiation of microprocessor by its operating frequency or harmonics of it), wideband (e.g. radio frequency RF propagation from the switched mode power supply SMPS¹),
- *inherent energy* – low energy (e.g. electrostatic discharge), high energy (e.g. lightning electromagnetic pulse LEMP),
- *dwell time* – transient event (e.g. commutation notches) or continuous event (e.g. power frequency magnetic field in the vicinity of house electrical installation).

Current harmonics

Rectifier is inherent module in the front end of majority of electronic devices. It is essential source of current harmonics. An example is discussed below.

In Fig.2.1 a) two-pulse rectifier is shown. From the instant t_1 on, instantaneous rectified voltage is bigger than condenser voltage. Condenser is charged with the current drawn from the AC source. Charging stops in the instant t_2 when instantaneous rectified voltage becomes smaller than condenser voltage. Condenser begins to discharge with the time constant RC . Current is not drawn anymore from the AC source. Discharge lasts till the instant t_3 which is the end of charging-discharging period. The AC current is drawn

in the short time interval $t_2 - t_1$ by the peak value of the AC voltage. The bigger time constant RC the shorter is the current impulse drawn from the AC source.

In Fig.2.1 c) on the right, current for such rectifier measured in the time domain is shown. Such current in the frequency domain is characterized with very big content of odd harmonics. In this case the 3^{rd} , 5^{th} , 7^{th} and 9^{th} are bigger than 80% of the main harmonic, see the left of Fig.2.1. The frequency range of interest is up to 40-th harmonic e.i. up to 2 kHz by 50 Hz supply network.

For measurements of current harmonics the AC source with practically zero internal impedance must be used. Voltage at the AC input of rectifier shown in the frequency and time domain in Fig.2.1 b) is practically free of harmonics. It means that origin of measured current harmonics is solely rectifier but not interaction of the rectifier and AC source impedance.

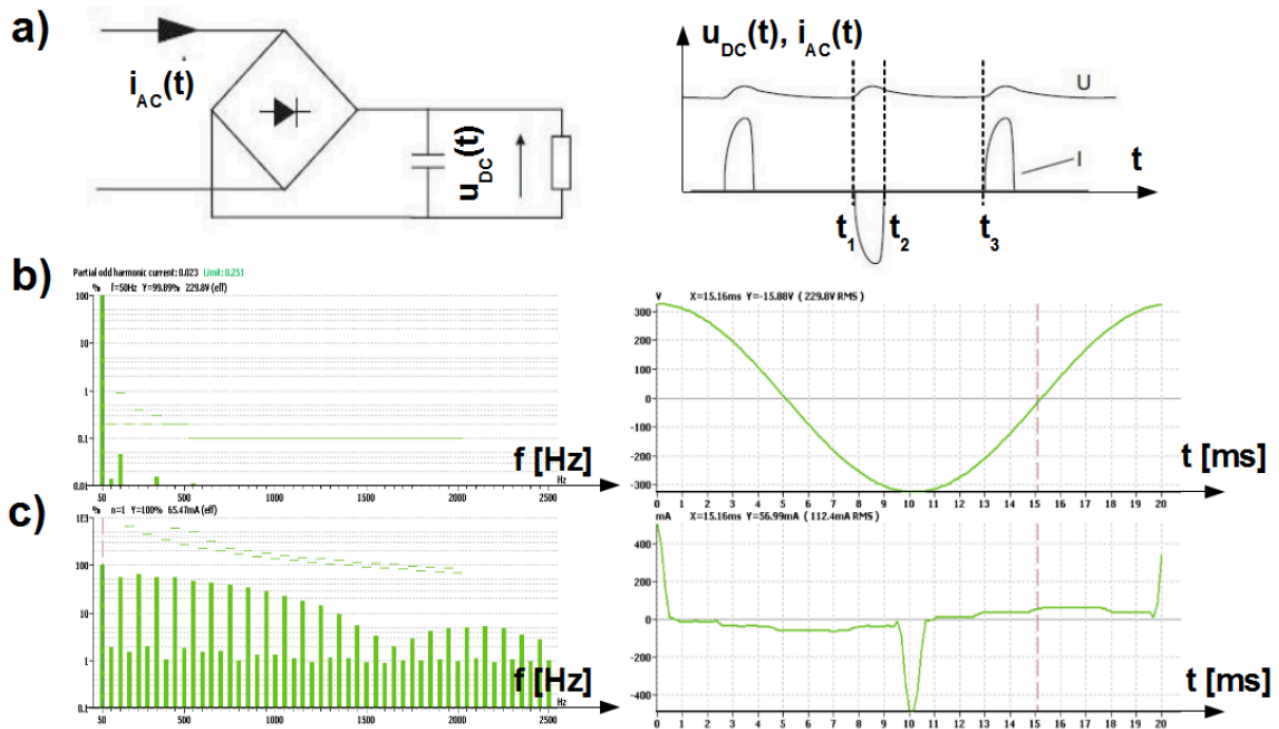


Figure 2.1: Example of current harmonics generated by two-pulse rectifier.

Flicker

If the light flux captured by eye changes, retina sends signal with optic nerve to the brain, see Fig.2.2. Feedback of the brain is to activate muscles of iris in order to adjust pupil size to the flux. Single flux change is not remarkable by the Man. However repetitive changes of the light flux, called light flicker, shadow flicker or just flicker can cause physiological discomfort, physical and psycho tiredness by healthy people up to inducing epileptic seizures by people who suffer from photosensitive epilepsy. Scale of impact depends on repetition rate and depth of the flux changes.

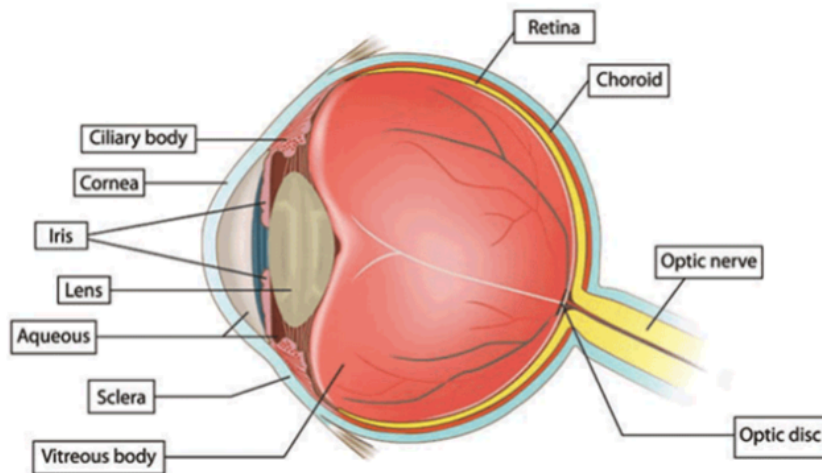


Figure 2.2: Anatomy of eye according to [Eye].

There are different origins of flicker. One of them is the wind turbine. Shadow flicker occurs when the sun is low in the sky and a wind turbine creates a shadow on a building Fig.2.3. As the turbine blades pass in front of the sun, a shadow moves across the landscape, appearing to flicker on and off as the turbine rotates. The location of the turbine shadow varies by time of day and season and usually only falls on a single building for a few minutes of a day. Shadows that fall on a home may be disruptive. Shadow flicker has been a concern in Northern Europe where the high latitude and low sun angle exacerbate the effect [Shadow; flicker].

The intermittent shadows can also experience a car driver driving along a tree lined street or in a road tunnel lighted with lamps mounted with spacing.



Figure 2.3: Wind turbine causing a flickering shadow on buildings during certain periods of the day. American Wind Energy Assoc. [Shadow; flicker].

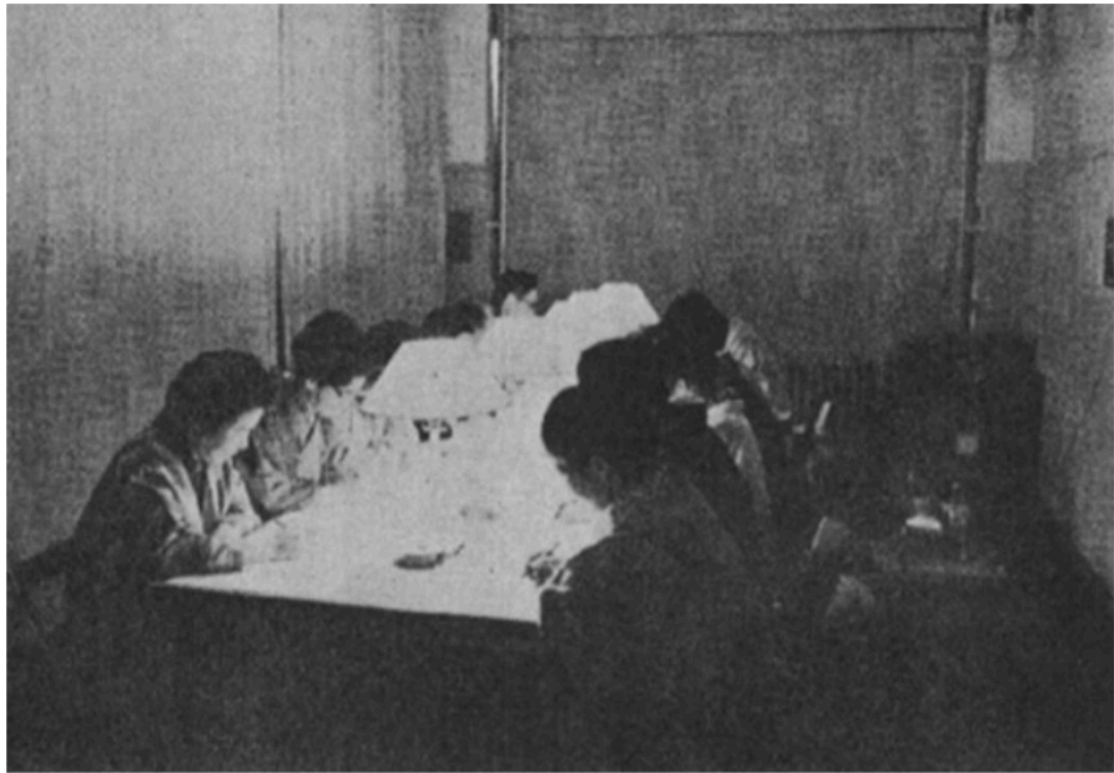


Figure 2.4: The proband group exposed to flicker stress.

The concern of this lecture notes is flicker caused by light flux changes due to power delivered to the electric lighting. This power is proportional to the Root Mean Square RMS value of supply voltage therefore flicker is equalized with changes of the RMS voltage.

In rural areas by long distances to the transformer, low voltage public electricity networks is weak. It has relatively big impedance. If in such area one consumer switches ON/OFF for instance electrical welding machine, his neighbors sens it as repetitive changes of the RMS of supply voltage, actually flicker.

In 80th of 20th century many experiments were done on different groups of people exposed to the flicker of the electric light. 60 \bar{W} incandescent bulbs were used as a flickering light source. Picture of probants by such experiment is shown in Fig Fig.1.4. It was agreed for 10 *min* observation time.

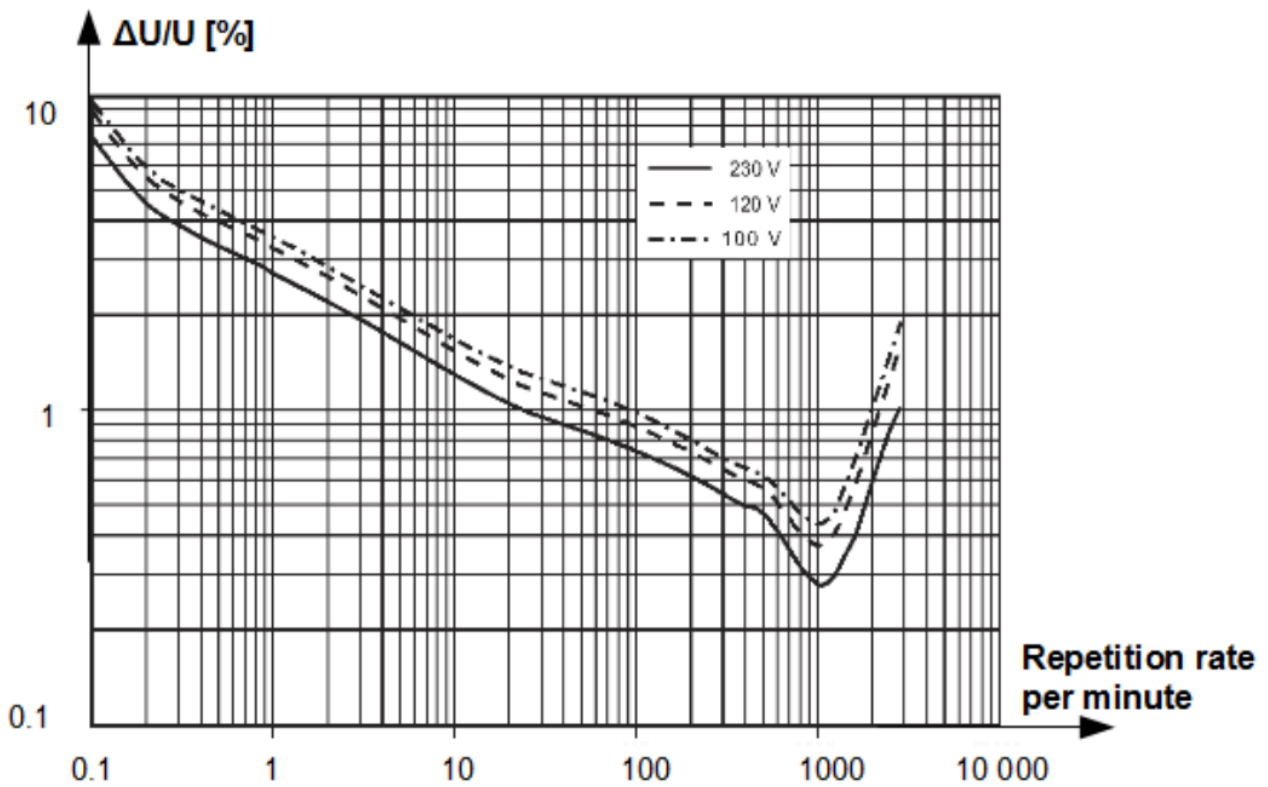


Figure 2.5: Threshold curves of the short time flicker factors P_{st} .

Result of that experiments are curves of the short time flicker factors P_{st} shown in Fig.1.5. There are three curves for 100 V, 120 V and 230 V rated voltage. Value $P_{st} = 1$ is assigned to them. The region below is tolerable, above is considered as disruptive. Remarkable is that this phenomenon has extremely low frequency. Plots ends by 50 Hz. Moreover very small relative changes of the RMS voltage are critical. Most sensitive region is by 1000 changes per minute i.e. by 16.6 Hz by which changes below 0.3% are already critical (by 230 V rated voltage).

In addition to the short time flicker factor P_{st} , the long time flicker factor P_{lt} is defined. It is indispensable because there are processes which last for a longer time e.g. washing machine programs which can last up to two hours. During that time current consumption goes up and down due to sequence of different operations: water drawing, heating, tumbling, drying, water pumping down etc.. P_{lt} is defined as follows

$$P_{lt} = \left[\frac{\sum_{i=1}^N P_{st_i}^3}{N} \right]^{\frac{1}{3}} \quad (2.1)$$

where P_{st_i} is the short time flicker factor observed in the i -th 10 min time segment and N is the number of observed time segments.

Characteristic of main's voltage

Origin of phenomena described before: current harmonics and flicker are arrangements supplied by the public electricity network. These disturbances are emitted from the arrangement to the environment, to the public electricity network. Interaction is mutual. Disturbances in the public electricity network can influence the arrangements supplied from it. The standard [EN-50160] is devoted to characterizing the quality

of the main's voltage. The main features of this quality are: flicker, harmonics, unbalance, commutation notches, dips, interruptions and variations. Flicker, unlike remaining features do not need any additional informations.

The quality of voltage is characterized in so called supply terminal which is point in a public supply network designated as such and contractually fixed, at which electrical energy is exchanged between contractual partners [EN-50160] i.e. at the input of energy meter by the consumer.

Harmonics

Voltage total harmonic distortion THD_U defined as quotient of root of sum of squares RSS of all harmonics to fundamental harmonic U_1 is used as distortion measure

$$THD_U = \frac{\sqrt{\sum_{n=1}^{40} U_n^2}}{U_1} \quad (2.5)$$

Sometimes THD is split to odd harmonic distortion OHD

$$OHD_U = \frac{\sqrt{\sum_{n=1}^{19} U_{2n+1}^2}}{U_1} \quad (2.5)$$

and even harmonic distortion EHD

$$EHD_U = \frac{\sqrt{\sum_{n=1}^{20} U_{2n}^2}}{U_1} \quad (2.5)$$

Understandably THD is geometric sum of OHD and EHD

$$THD_U = \sqrt{OHD_U^2 + EHD_U^2} \quad (2.5)$$

In Fig.1.6 decapitated sinus voltage with $THD = 12\%$ is shown. Remarkable is dominant contribution of OHD. EHD is practically negligible. Moreover RMS value of this voltage is only slightly increased by distortion $U_{RMS} \approx 1.007 \cdot U_{1RMS}$.

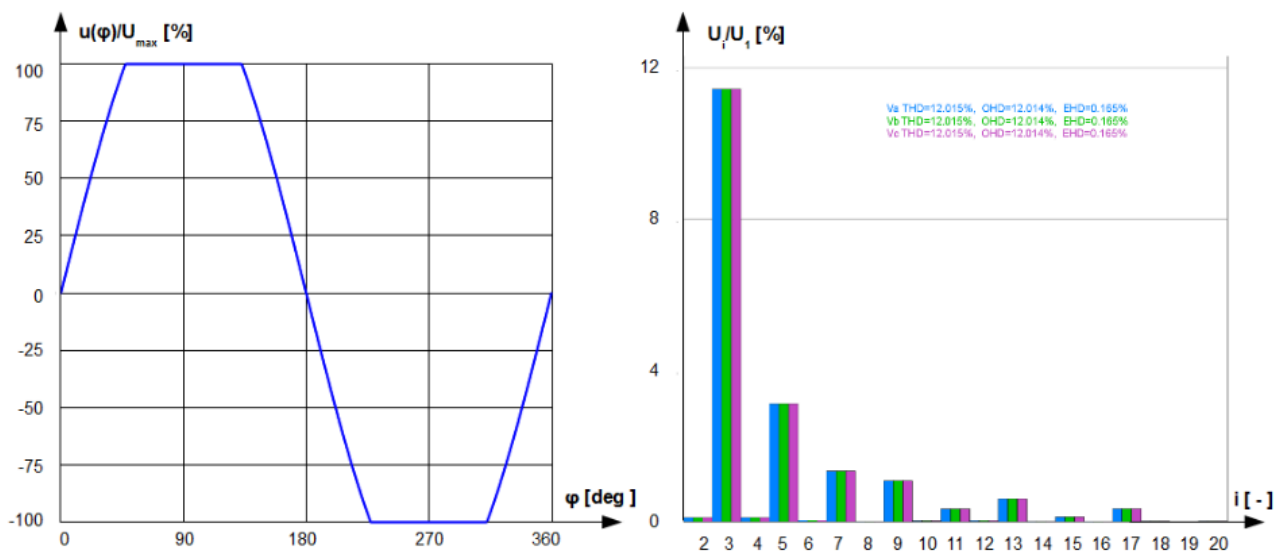
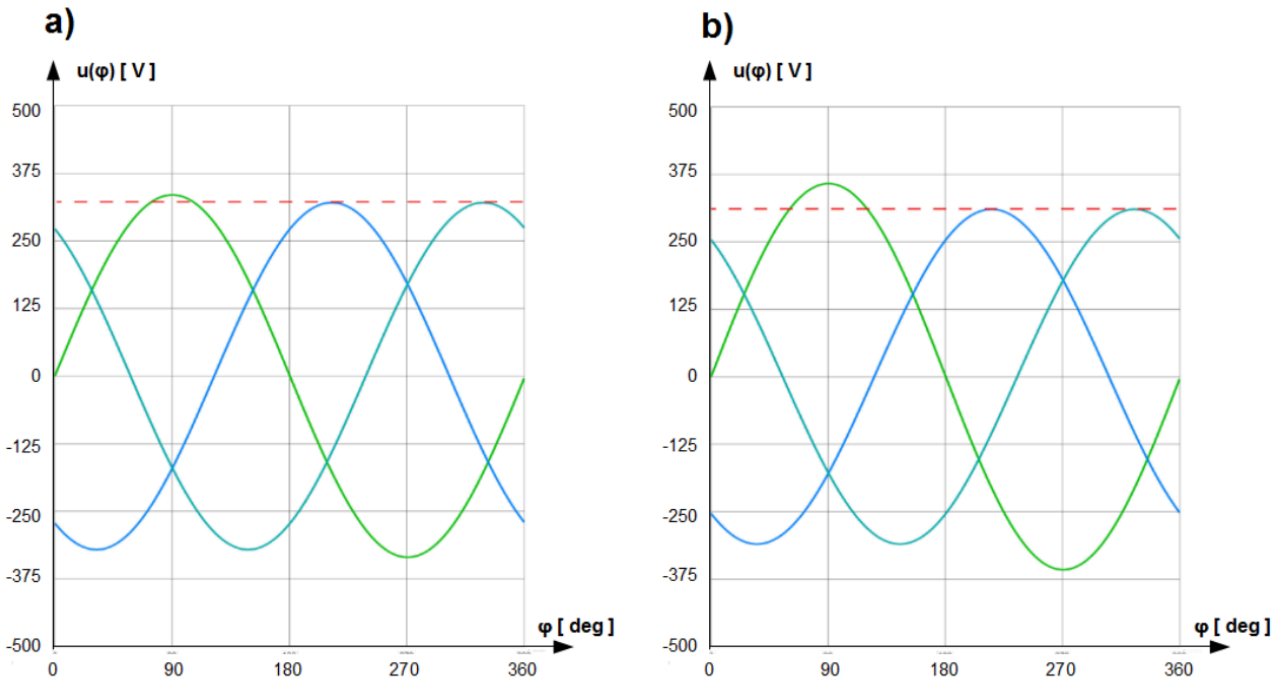


Figure 2.6: Decapitated sine voltage in the time domain and its harmonics by $THD = 12\%$.

Unbalance

Any three phase unbalanced voltage system can be decomposed into: plus, minus and zero component as shown in Fig.1.7.



Phasors of positive components rotate counterclockwise in sequence: U_{A_P} , U_{B_P} , U_{C_P} on the complex plane

$$U_{A_P} = |U_P| e^{j\omega t} \quad (2.6)$$

$$U_{B_P} = |U_P| e^{-j120^\circ} e^{j\omega t} \quad (2.7)$$

$$U_{C_P} = |U_P| e^{j120^\circ} e^{j\omega t} \quad (2.8)$$

Phasors of negative components rotate counterclockwise in sequence: U_{A_N} , U_{C_N} , U_{B_N} on the complex plane

$$U_{A_N} = |U_N| e^{j\omega t} \quad (2.9)$$

$$U_{B_N} = |U_N| e^{j120^\circ} e^{j\omega t} \quad (2.10)$$

$$U_{C_N} = |U_N| e^{-j120^\circ} e^{j\omega t} \quad (2.11)$$

Phasors of zero components rotate on the complex plane without phase shift

$$U_{A_0} = U_{B_0} = U_{C_0} = |U_0| e^{j\omega t} \quad (2.12)$$

Voltage unsymmetry factor VUF_N of the negative component defined as

$$VUF_N = \frac{|U_N|}{|U_P|} \quad (2.13)$$

and voltage unsymmetry factor of the zero component VUF_0 defined as

$$VUF_0 = \frac{|U_0|}{|U_P|} \quad (2.14)$$

are unsymmetry measures.

In Fig.1.8 a) and b) three phase unsymmetrical voltage system with $VUF_N = 3\%$ and $VUF_N = 10\%$ respectively, free of zero component ($VUF_0 = 0\%$) are shown.

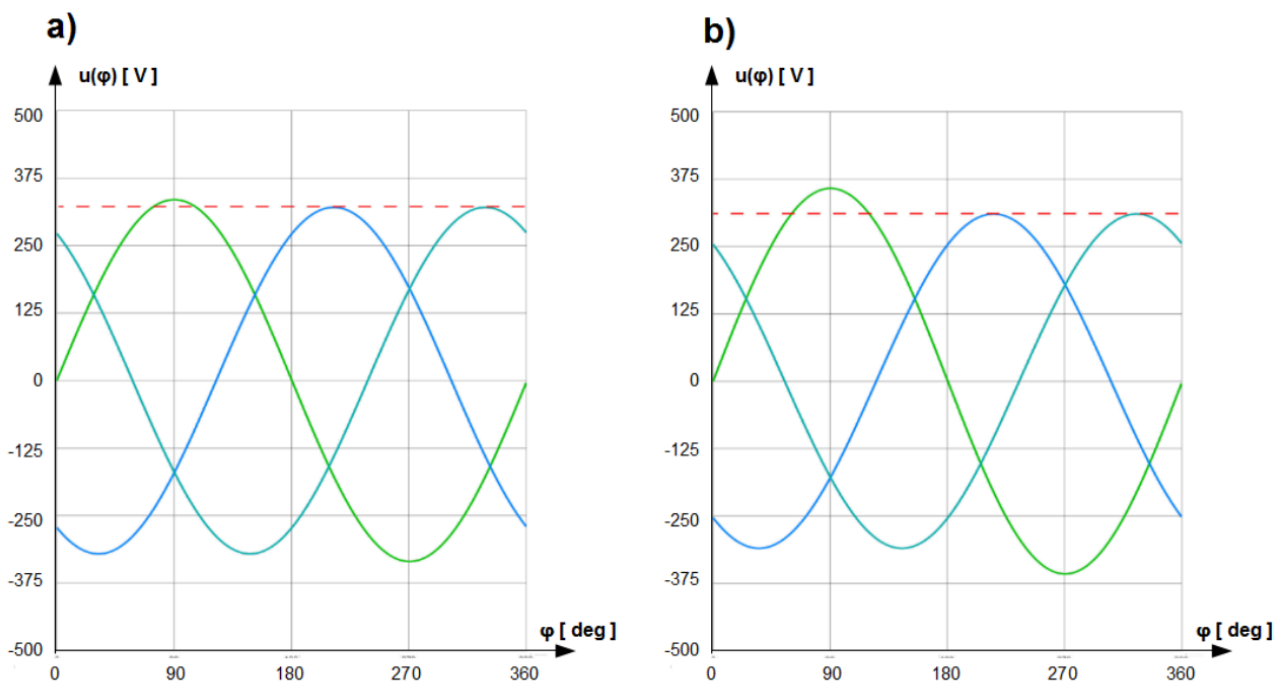


Figure 2.8: Unsymmetrical three phase voltage system with: a) $VUF_N = 3\%$ and b) $VUF_N = 10\%$.

Dips and interruptions

Dips of interest depends on whether loads in the arrangement are supplied with line to neutral or line to line voltage. In Fig.1.9 a) line to neutral voltage U_A is reduced. The residual voltage $U_{A'}$ is shown as dashed arrow.

In Fig.1.9 b) line to line voltage U_{BC} is reduced. The residual voltage $U_{B'C}$ is shown as dashed arrow. This dip has impact also on U_{AB} voltage which becomes $U_{AB'}$ (dashed arrow).

Dwell time of dips is expressed in fold of a period. Additionally dip with $0V$ residual voltage and half of a period dwell time is of interest due to risk of saturation of chokes in the front end of the appliances.

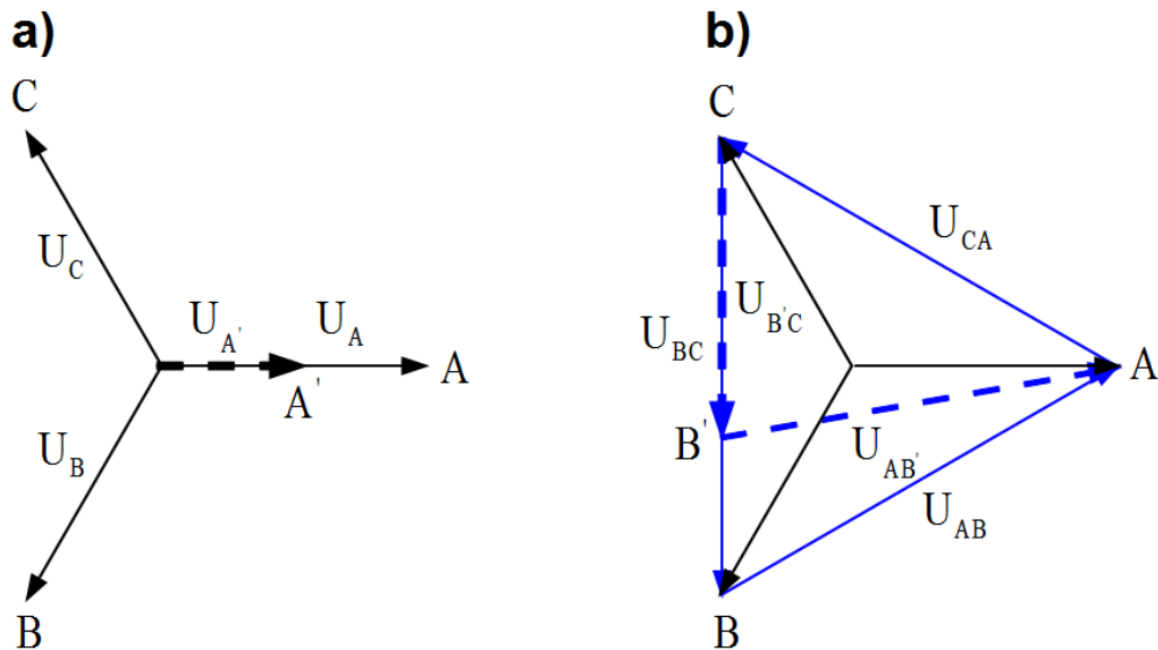


Figure 2.9: Dip of voltage Line to Neutral a), Line to Line b).

Two features distinguish voltage interruption from dip: it is longer phenomenon, measured in seconds and the rest voltage is $0V$ in all lines simultaneously.

Commutation notches

Output inverter in the frequency drive is composed of three columns with pair of valves (IGBTs in Fig.1.10) 1-4, 3-6, 5-2 or recently valves built in Silicon Carbon Technology SiC. They are operated in such sequence that never valves from the same column should be closed. For example if in one instant valves 1-6 are closed (blue dashed line), in the next 5-4. It will surely be the case if commutation (state transition of the valve) would have unchangeable rise and fall time. Unfortunately duration of commutation can vary randomly. As a cause valve for instance 1 will be not yet totally opened while valve 4 will be already partly closed. On the AC side of the drive such situation looks like a short circuit for a short instance of the time, fraction of milliseconds. For other consumers it can be sensed as short time dip in supply voltage as shown in Fig.1.10. This phenomenon is called commutation notch.

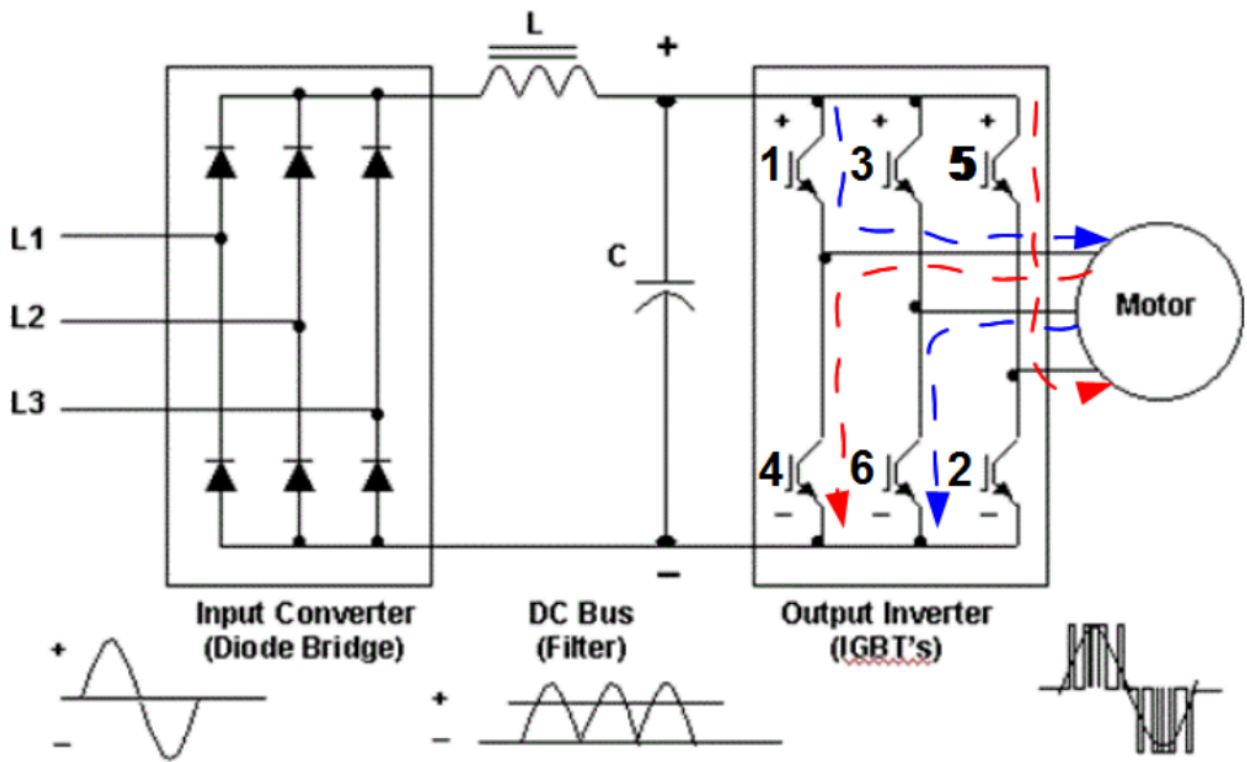


Figure 2.10: Frequency drive for controlled propulsion of asynchronous motor.

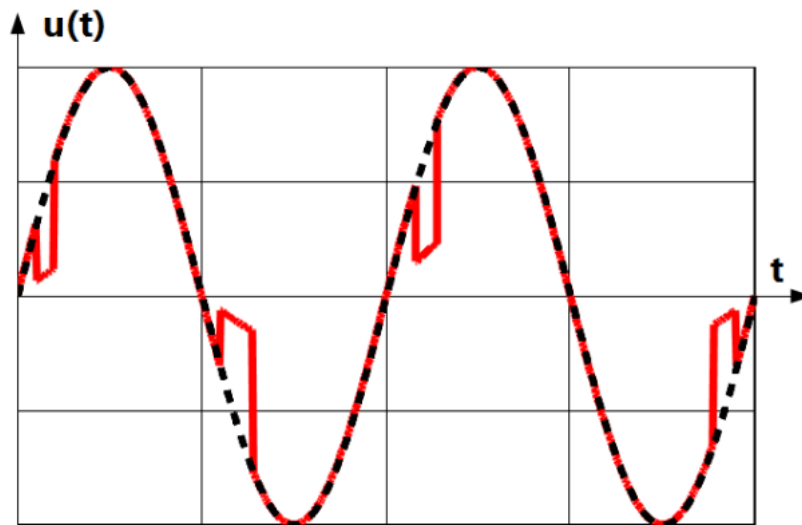


Figure 2.11: Commutation notches in supply voltage.

Solar storm {#Solar storm}

There is continuous eruption of plasma from the Sun's surface. A stream of it released from the upper atmosphere of the Sun builds so called solar wind. Plasma embedded within the solar wind is the interplanetary magnetic field called also magnetic cloud. If the material carried by the solar wind reached a planet's surface, its radiation would do severe damage to any life that might exist. Earth's magnetic field

serves as a shield, redirecting the material around the planet so that it streams beyond it. If the stream is constant in time, interplanetary magnetic cloud and Earth's magnetosphere are in equilibrium.

However the Sun's activity shifts over the course of its 11-year cycle with radiation levels, and ejected material changing over time. These alterations affect the properties of the solar wind, including its magnetic field. This phenomenon is called solar storm.

Time dependent magnetic field of the interplanetary magnetic cloud stretches out the Earth's magnetosphere so that it is smoothed inward on the sun-side and stretched out on the night side, see Fig. 1.12. The duration of the main phase of the storm is typically 2 – 8 hours. The recovery phase may last as short as 8 hours or as long as 7 days.

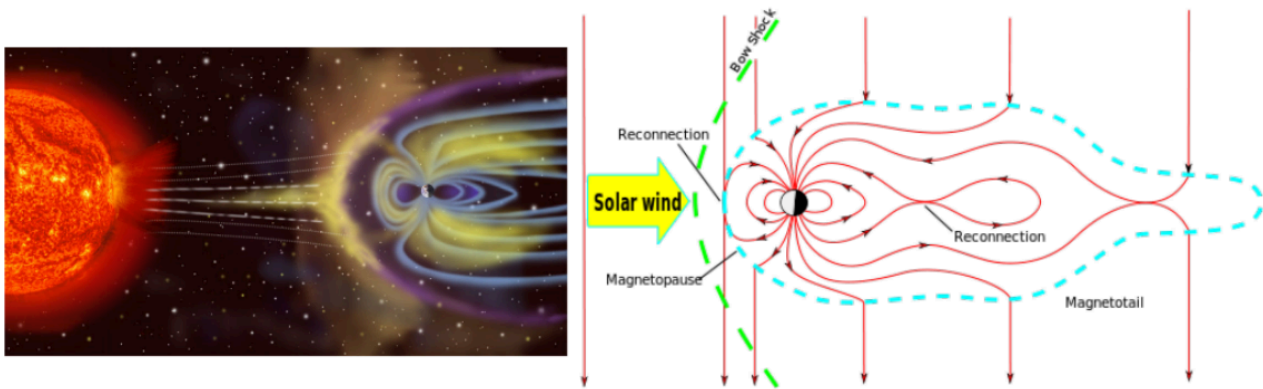


Figure 2.12: Depiction of solar wind particles interacting with the Earth's magnetosphere.

Aurora phenomenon observable usually in the polar circles can be observed by solar storm in much smaller latitudes eg. in Australia, see Fig. 1.13. But there are more severe influences of the solar storm on our civilization.

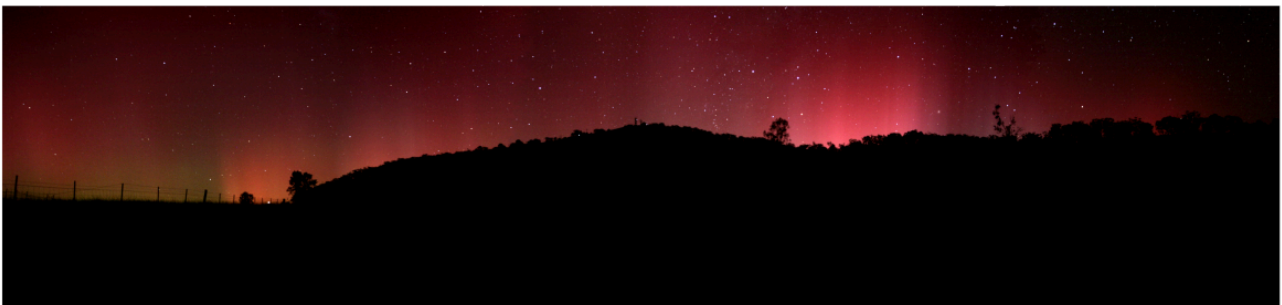


Figure 2.13: Aurora panorama in Australia.

According to Faraday's law [Hammond] changes of magnetic flux generates electromotive force EMF in any metal structure comprising the flux

$$EMF = -\frac{d\phi(t)}{dt} = -\mu_0 \frac{d\left(\int_S \vec{H}(t) \cdot d\vec{S}\right)}{dt} \quad (2.15)$$

where S is area which flux is crossing.

The EMF caused by the solar storm is not measurable if the size of building or even town is considered. It is simply too small, but it can be destructive for any huge metal installation like railway track, pipeline or high voltage transmission power line, see Fig. 1.14. It can for instance destroy anticorrosion system of a pipeline.

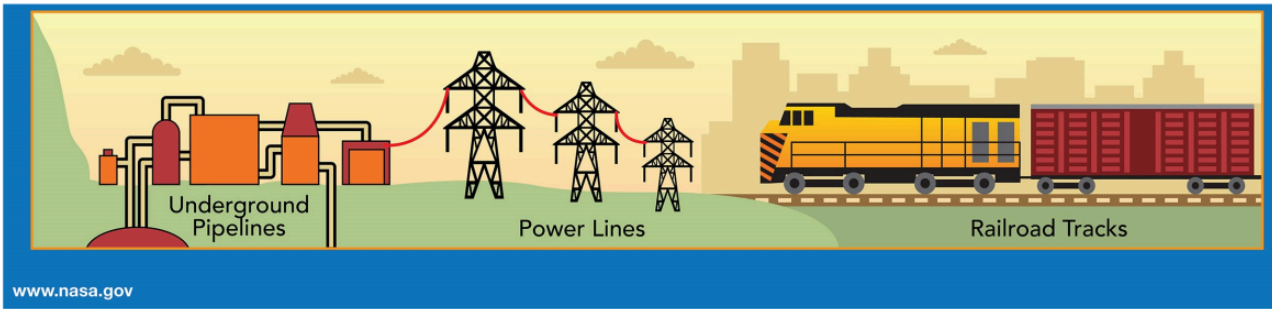


Figure 2.14: Metal distributed structures potentially hazarded with induced electromotive force by solar storm, [NASA].

In the North America are operated transcontinental high voltage power transmission lines traced along the parallels of latitude, connecting the east with the west coast. Distances between transformer stations are something like 50 km-100 km. The high voltage pillars have the height of about 30 m. The surface which Earth's magnetic field is crossing is huge. The star points of the transformers in substations are grounded. This establishes a mesh in which Geomagnetically Induced Current GIC driven by the solar storm EMF can run, see blue line in Fig. 1.15.

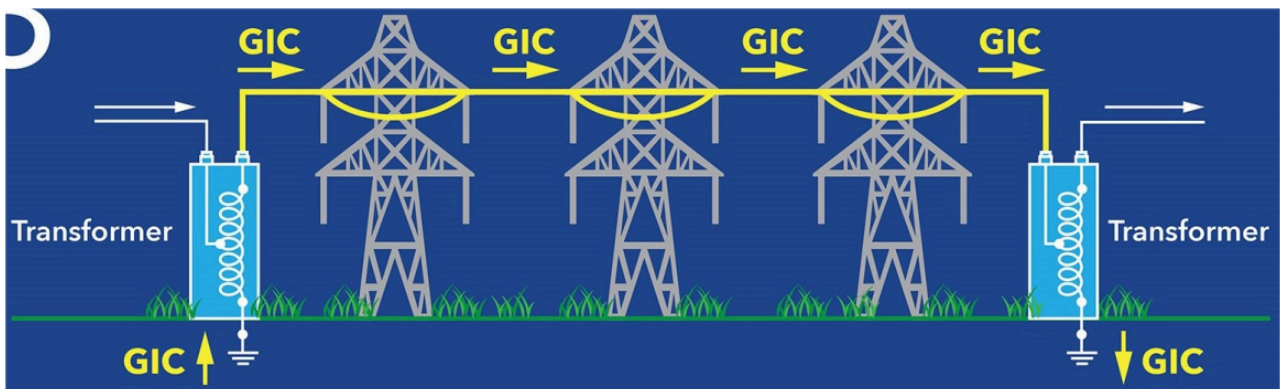


Figure 2.15: Geomagnetically induced current GIC in High Voltage Power Transmission Line, [NASA].

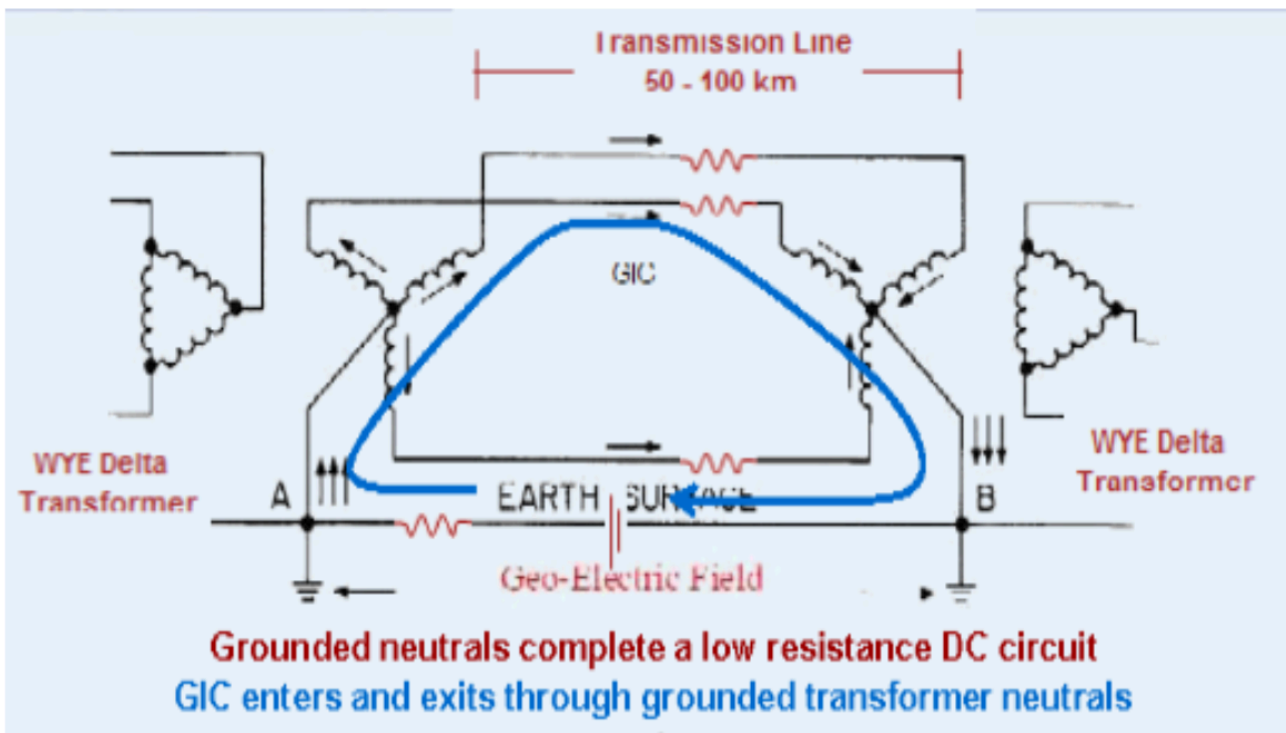


Figure 2.16: Geomagnetically Induced Current GIC in High Voltage Power Transmission Line, [NASA].

The EMF generated by the solar storm is nearly direct compared to power frequency. Therefore it can be represented as the DC bias overlapped with ordinary operation voltage, see Fig. 1.17. DC bias voltage shifts operating point on the $B(H)$ curve² of the transformer core in the substation. In consequence the core saturates for short time segments of the power period. It is mirrored with peaks in transformer current appearing periodically, see Fig. 1.17 causing coils and cores to heat up. In extreme cases, this heat can disable or destroy them, even inducing a chain reaction that can overload transformers and lead to fire of the substation.

Isolating the star point in the substation would make the transmission line much less susceptible to damage due to geomagnetically induced current. However, a transformer that is subjected to this will act as an unbalanced load to the generator, causing negative component current, see Chapter 1.3.2 in the stator and consequently rotor heating.

The solar storm in province Quebec in Canada in March 1989 caused power blackout for nine hours. Picture of the transformer winding destroyed by this disaster is shown in Fig. 1.18.

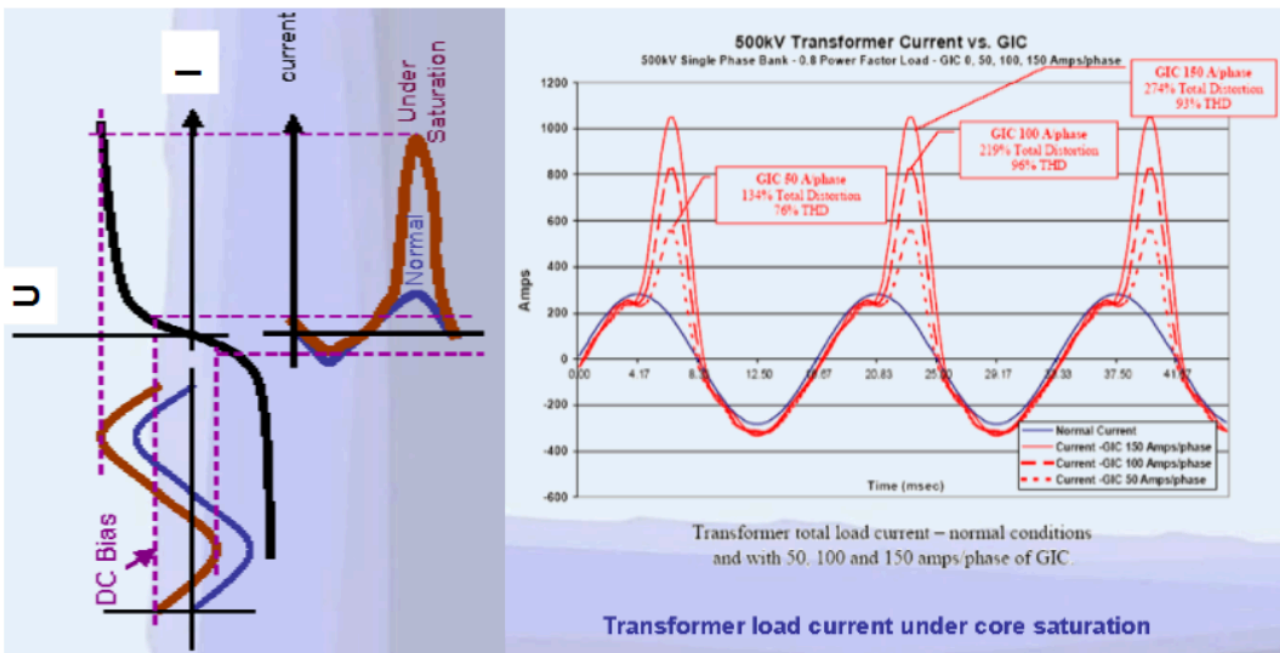


Figure 2.17: Illustration of transformer saturation due to GIC.

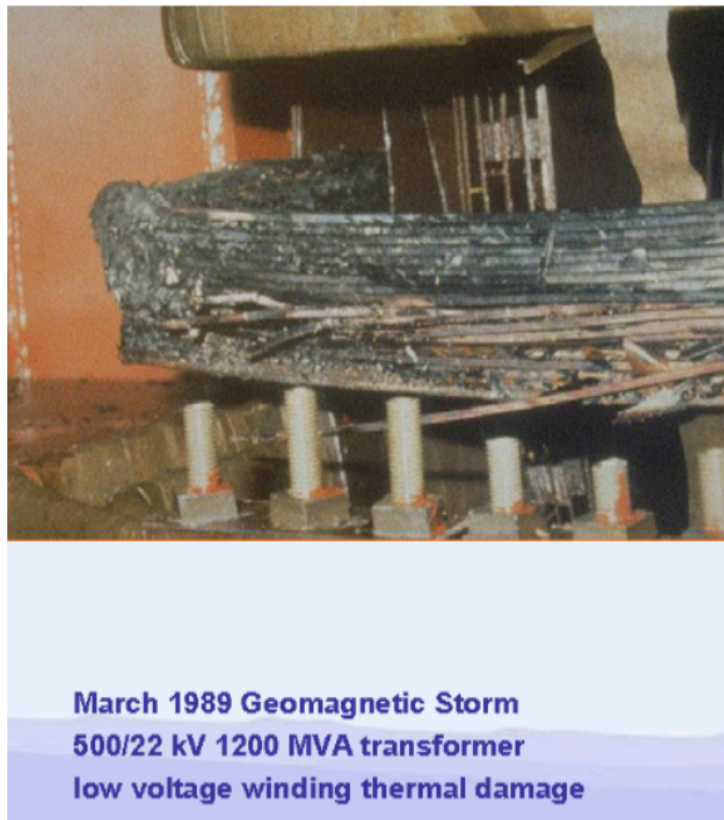


Figure 2.18: Transformer winding destroyed due to GIC in Quebec, March 1989.

The European grid consists mainly of shorter transmission circuits, which are less vulnerable to damage.

1. Distinction between narrow and wide band is not absolute but related to the resolution bandwidth RBW of the measurement receiver. Disturbance of the SMPS operating with 16 kHz repetition frequency is narrow band if measured with $RBW = 9kHz$ (by conducted emission) and in the same time wide band if measured with $RBW = 120kHz$ (by radiated emission).↵
2. $B(H)$ curve is identical with $U(I)$ curve of the coil wound on the core material. It has just another scale.↵
3. Discharge via metallic carriage with isolating wheels called also furniture discharge is much slower. It was in the past in the scope of ANSI standard but it is no more the case.↵
4. Ionosphere is expanded from about 50 km to 1000 km above the Earth's surface.↵

3. Radio frequency electromagnetic disturbances

Long-term disturbances

Electric discharge in gases

Electrons in metal are free to move around within it. Some of these electrons will have sufficient velocity to escape from the surface of the material. However, when they leave, they produce an electric field which pulls them back to the surface. If an external electric field is present with sufficient field strength, it can overcome the force that normally returns the electron to the surface. The electrons are therefore, removed from the surface and set free.

As electrons finally bombard the anode, the material of anode is heated and may vaporise. In general, either the anode or cathode may vaporise first, depending on the rates at which heat is delivered to and removed from the two contacts. Vaporized metal forms plasma between the electrodes [Ott] which displaces ions as current's carrier. Transition from ions' to plasma's current takes place in time less than a nanosecond [Ott].

The field strength required for initiation of this phenomenon is approximately $500kV/m$ according to [Ott] and $10GV/m$ according to [Clayton]. In Fig.3.2 it is represented with the line with $100MV/m$ (black continuous line on the left, with black dashed line continuation on the right).

Such big field strength can be generated by small distance of electrodes. Therefore this phenomenon is called short arc. By transition from ions' to plasma's current voltage across electrodes drops significantly. To sustain arc minimum arcing voltage and current is required.

After the short arc is initiated the voltage across as well as current through the contact must exceed minimum arcing (sustaining) values. They are dependent on electrodes' material, as gathered in Tab.3.1, [Ott].

Table 3.1: Minimal parameters for sustaining metal-vapor discharge. (* 69% gold, 25% silver, 6% platinum)

Material	Minimum arcing voltage [V]	Minimum arcing current [mA]
Silver	12	400
Gold	15	400
Gold alloy*	9	400
Palladium	16	800
Platinum	17.5	700

Short arc can occur even in vacuum, since it does not require the presence of gas. Therefore another name metal-vapor arc. The short arc forms the basis for instance by cutting metals in electro erosion machine tools or in arc welding tools.

If distance between electrodes is too big for initiating short arc discharge, then discharge follows other way which is common also for natural lightning by thunderstorm. Namely, three discharge regimes can be distinguished: dark, glow and long arc. This phenomenon is illustrated in Fig. 3.1 as voltage versus current. Consciously lacks scale of voltage axis in Fig. 3.1 because its quantification depends on type of gas, electrodes' distance and electrodes' shape.

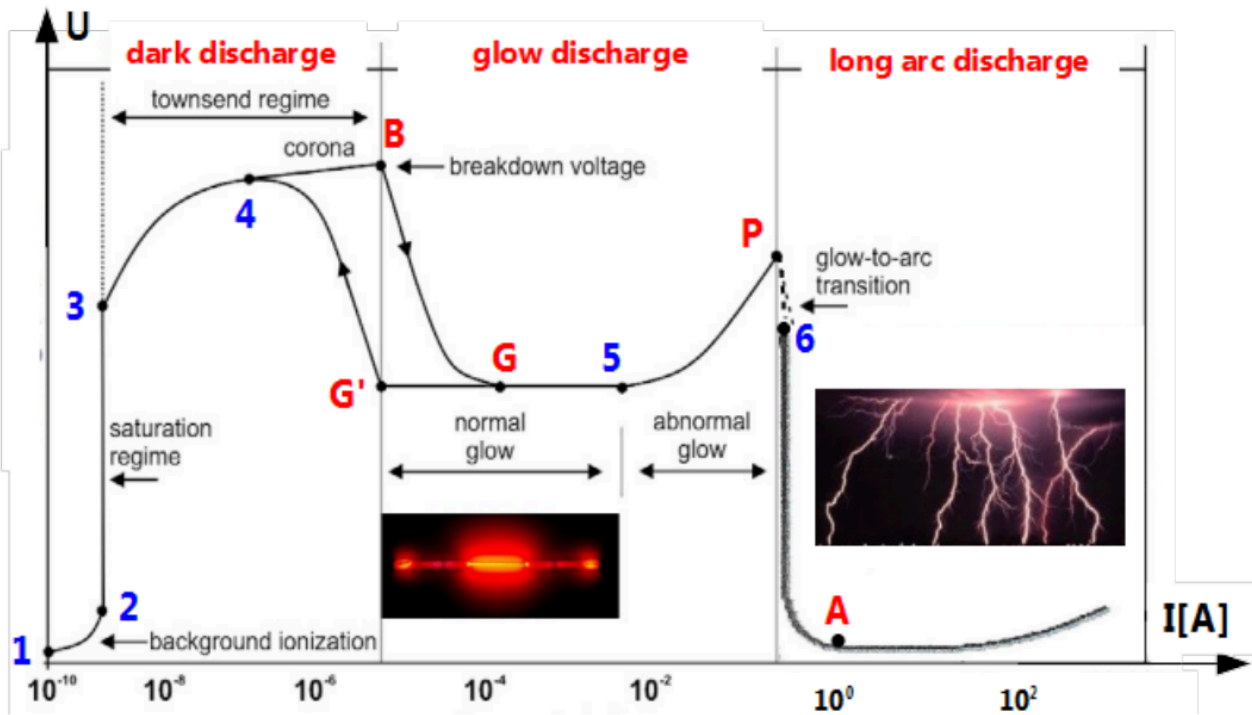


Figure 3.1: Regimes of discharge in gas.

In the region from 1 to 2 the background ionisation due to cosmic rays or other sources of ionising radiation takes place. There exist small amount of free electrons and positively charged atoms in gas. Applied voltage accelerates ions. Number of ions does not increase. Some of them, but not all reaches attracting electrode. In point 3 stream of ions reaching attracting electrode saturates. Range between point 3 and 4 means passage to avalanche process. Energy of free electrons is enough for liberating other electrons from electrically neutral atoms by striking them. In consequence number of free electrons and positively charged atoms increases. This is accompanied with emission of electromagnetic energy in form of radio-frequency electromagnetic waves. This is not self sustained process called partial discharge or Ramsauer-Townsend discharge named for its discoverers. Its intensity is proportional to energy of electrons i.e. to the applied voltage. It can cause buzzing on radio receivers. Between 4 and B emission of electromagnetic energy shifts to visible light. It is called corona discharge which can be observed by high voltage overhead power lines. The same nature has St. Elmo's fire observable by sailors on top of masts by thunderstorms.

There is hysteresis between 4 and G. By increased voltage passage follows points 4, B and G, by decreased G, G' and 4. Between G and 5 the gas ionization becomes self-sustained.

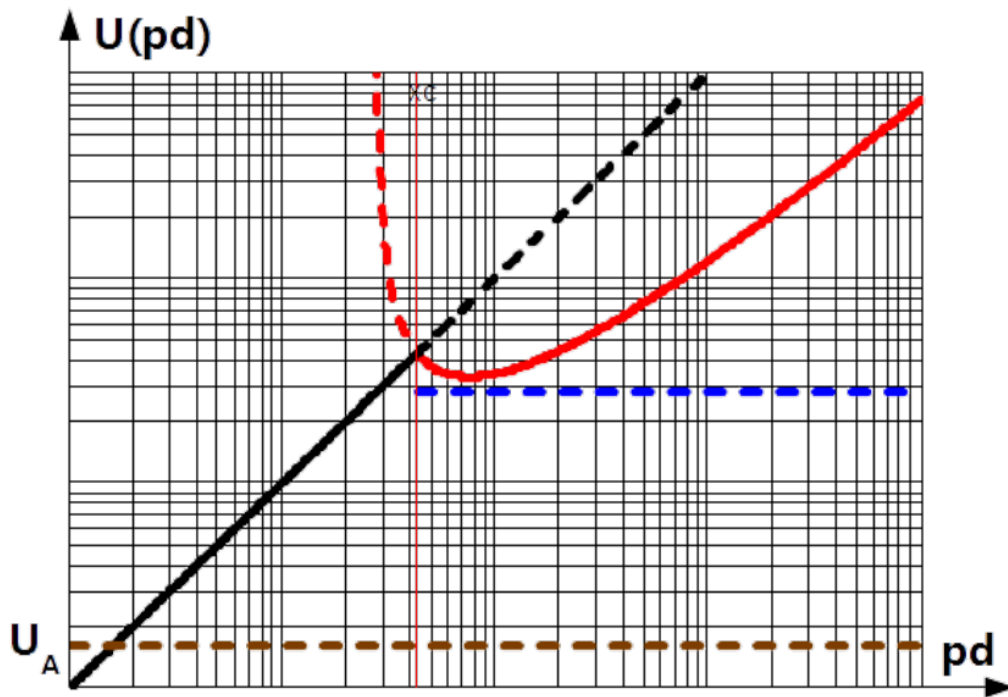


Figure 3.2: Variation of voltage threshold for different discharge regimes in gas.

By B amount of ions is such that gas isolation ability ends. Gas starts to glow. This is called breakdown. Paschen found that the breakdown voltage U_B is dependent on the product of electrode separations d and pressure p as

$$U_B(p \cdot d) = \frac{K_1 \cdot p \cdot d}{K_2 + \ln(p \cdot d)} \quad (3.16)$$

where K_1 and K_2 are constants that depend on gas. $\ln(p \cdot d)$ is normalised with product of units in which pressure and distance are expressed.

The Paschen curve is shown in Fig.3.2 for air in standard atmospheric pressure as red dashed curve on the left side and solid red curve continuation on the right. Air pressure p and distance d are taken in Atm and m respectively. $K_1 = 43.6 \cdot 10^6 / (Atm \cdot m)$ and $K_2 = 12.8$ are applied in Fig.3.2. Minimal breakdown voltage in air by standard atmospheric pressure is approximately $U_B^{min} \approx 320V$ and occurs at electrodes' separation $d^{min} \approx 7.6\mu m$.

Jumping to the self-sustained glow discharge situated on the right to point G is possible, provide the current available from the external circuit exceeds minimum glow discharge sustaining current I_G . Voltage across electrodes drops to

$$U_G(d) = 280 + 1000 \cdot d \quad (3.17)$$

$U_G(d)$ is presented with blue dashed curve in Fig. 3.2.

Voltage drop by transition from B to G is relatively small. In air by atmospheric pressure the breakdown voltage is of order $U_B = 320V$ and glow voltage of order $U_G = 280V$. Minimum glow sustaining current is quite variable. Its representative range is $I_G \approx 1 - 100mA$ [Clayton] Glow regime is utilised in operation of electrical gas lighting equipment.

The voltage across the electrodes $U_G(d)$ for currents between G and 5 is primarily determined by the dark region between the cathode and the beginning of the glow region, so called the cathode fall region. As the current increases, the dimension of the glow region increases toward anode, but the voltage across the

gap remains $U_G(d)$. In consequence the fall region shrinks and by crossing the threshold field strength for short arc initiation the arcing process starts. State is reached where the heating causes vaporization of the contact metal (point P) resulting in a rapid drop in contact voltage, which marks the beginning of the arc discharge region where in the volume of ionised gas channels filled with plasma are initiated, point A [Clayton].

In long arc regime building of channel is completed. Plasma can freely flow between electrodes building conducting bridge. Plasma regime is accompanied with intensive emission of whole spectrum of visible light.

It must be reemphasized that, in order to sustain a glow / arc discharge, the voltage across and current through the contact that are available from the external circuit must exceed U_G , I_G and U_A , I_A respectively. They are the most left points on the plot in Fig. 3.2.

Actually, plasma current is initiated by long arc discharge identically as by short arc discharge. As it is explained before, voltage fall between electrodes is only in dark, not illuminating segments. In addition by increased current glowing region expands and dark segments shrinks. It means that field strength in dark regions increases leading to heating electrode materials, vapourisation and formation of plasma.

Signals with Amplitude Modulation

Electronic nowadays is predominately digital. It uses variety of modulations for signal transmission. However experience shows, that electronic is mostly susceptible on amplitude modulation AM. That's why application of AM by most radio frequency EMC immunity tests should be not amazing. Therefore approach to this theme here.

Two waves are combined in AM. One is modulating signal $u_m(t) = mA \cos(2\pi f_m t)$ in which message is coded and carrier $u_c(t) = A \cos(2\pi f_0 t)$ responsible for message transportation. m is called modulation depth or modulation index.

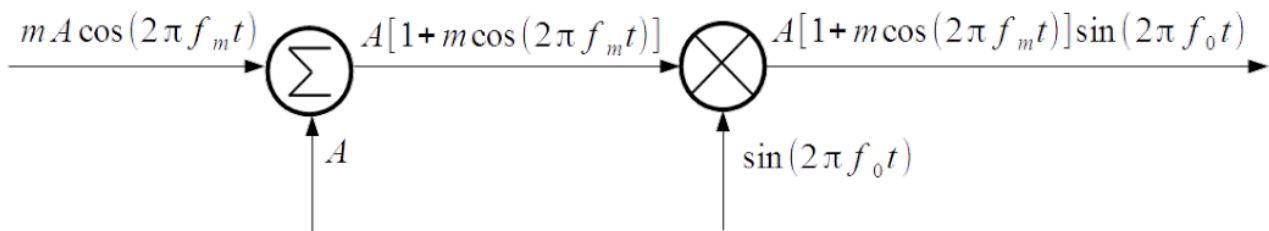


Figure 3.3: Functional block diagram of Double Sideband – Full Carrier DSB-FC amplitude modulation.

The simplest way of AM, in fact applied in EMC immunity tests is called Double Sideband – Full Carrier DSB-FC. Its principle is explained in Fig.3.3. The modulating signal $u_m(t)$ and amplitude of carrier A are conveyed to the adder. Sum of both signals along with carrier signal are conveyed to multiplier (mixer). Modulated signal at the output of mixer yields

$$\begin{aligned}
 u(t) &= A \sin(2\pi f_0 t) + mA \cos(2\pi f_m t) \sin(2\pi f_0 t) = \\
 &= \frac{m}{2} A \sin[2\pi(f_0 - f_m)t] + A \sin(2\pi f_0 t) + \frac{m}{2} A \sin[2\pi(f_0 + f_m)t]
 \end{aligned} \tag{3.18}$$

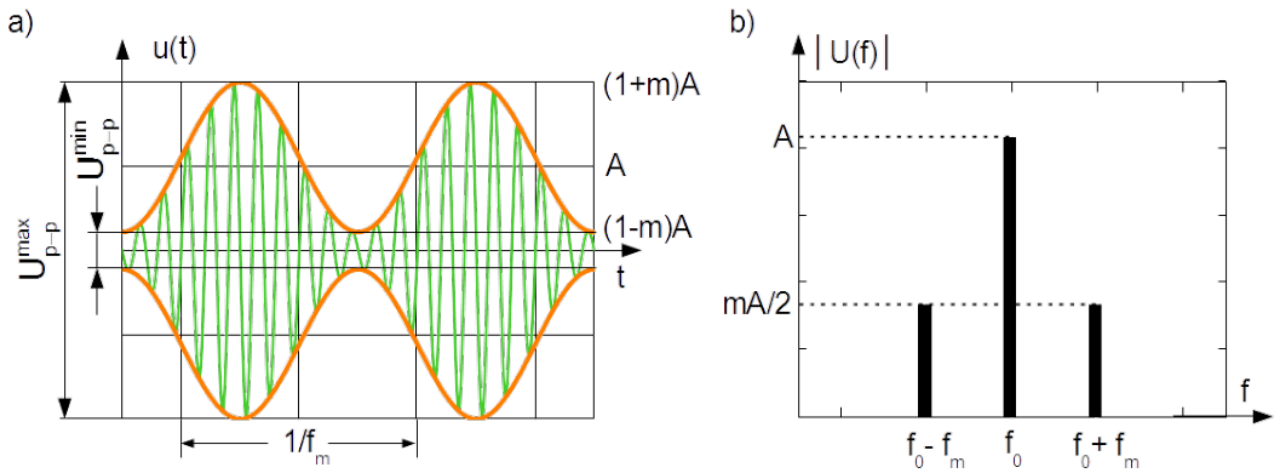


Figure 3.4: Amplitude modulation with DSB-FC: in the time domain a), in the frequency domain b).

It can be interpreted as the modulated signal (green line in Fig.3.4a)) had been superposition of the pure carrier and carrier with amplitude alternated according to modulating signal, see middle part of Eq.(3.18). Envelope of the instantaneous amplitude of the modulated signal is brown line in Fig.3.4a). In the frequency domain the DSB-FC is represented with three spectral lines, see the right part of Eq.(3.18) and Fig.3.4b).

Obviously RMS of AM DSB-FC signal yields

$$U_{RMS} = \frac{A}{\sqrt{2}} \sqrt{1 + \frac{m^2}{2}} \quad (3.19)$$

and consequently power relation of modulated signal $P_m + P_c$ and carrier signal P_c

$$\frac{P_m + P_c}{P_c} = 1 + \frac{m^2}{2} \quad (3.20)$$

Maximal instantaneous amplitude of the modulated signal is bigger than amplitude of carrier signal by $(1 + m)$ or about $(1 + m)dB$ in floating dB. Minimal instantaneous amplitude of the modulated signal is smaller than amplitude of carrier signal by $(1 - m)$ or about $(1 - m)dB$ in floating dB.

Maximal instantaneous power of the modulated signal is bigger than power of carrier signal by $(1 + m)^2$ or about $(1 + m)dB$ in floating dB. Minimal instantaneous power of the modulated signal is smaller than power of carrier signal by $(1 - m)^2$ or about $(1 - m)dB$ in floating dB.

Modulation depth can be easily calculated from the maximal and minimal peak-to-peak spans U_{p-p}^{max} and U_{p-p}^{min} taken from the signal observed in the time domain as shown in Fig.3.4a)

$$\frac{U_{p-p}^{max}}{U_{p-p}^{min}} = \frac{1+m}{1-m} \Rightarrow m = \frac{U_{p-p}^{max} - U_{p-p}^{min}}{U_{p-p}^{max} + U_{p-p}^{min}} \quad (3.21)$$

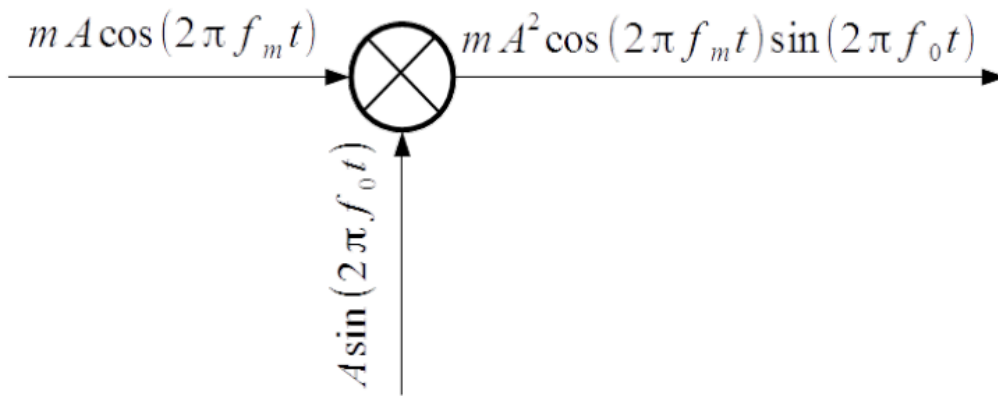


Figure 3.5: Functional block diagram of Double Sideband – Suppressed Carrier DSB-SC amplitude modulation.

Principle of Double Sideband – Suppressed Carrier DSB-SC is explained in Fig.3.5. The modulating signal $u_m(t)$ and carrier signal $u_c(t)$ are conveyed to multiplier. Modulated signal at the output of it yields

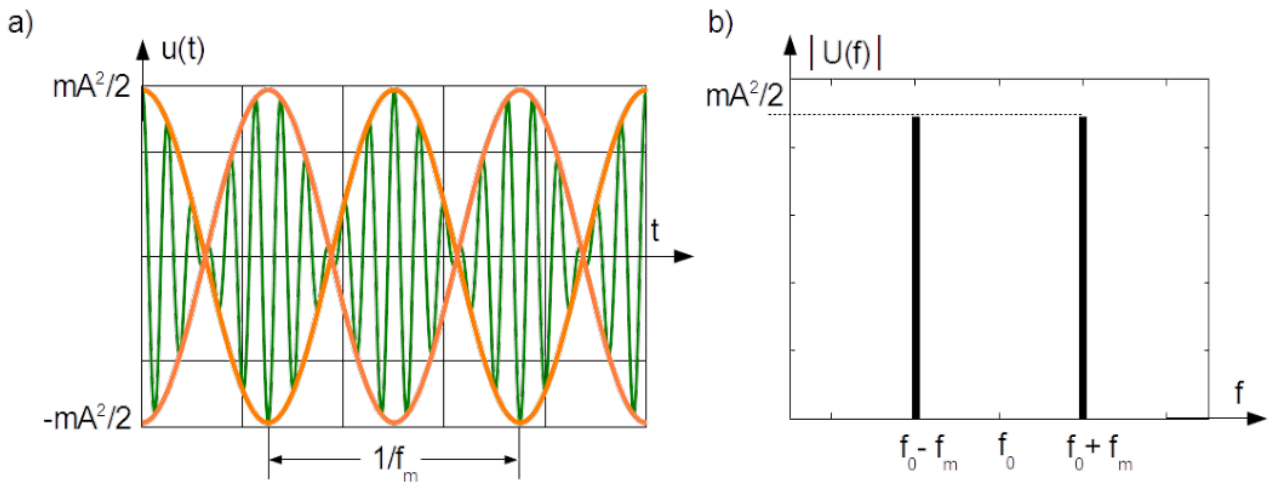


Figure 3.6: Amplitude modulation with DSB-SC: in the time domain a), in the frequency domain b).

$$\begin{aligned}
 u(t) &= mA^2 \cos(2\pi f_m t) \sin(2\pi f_0 t) = \\
 &= \frac{mA^2}{2} \sin[2\pi(f_0 - f_m)t] + \frac{mA^2}{2} \sin[2\pi(f_0 + f_m)t]
 \end{aligned}
 \tag{3.22}$$

It can be interpreted as the carrier signal (green line in Fig.3.6a) would have amplitude alternated according to modulating signal, see middle part of Eq.(3.22). Envelope of the instantaneous amplitude of the modulated signal is brown line in Fig.3.6a). In the frequency domain the DSB-SC is represented with two spectral lines, see the right part of Eq.(3.22b) and Fig.3.6b).

There is another amplitude modulation called Single Sideband – Suppressed Carrier SSB-SC. It is realized similarly to DSB-SC with only one difference. Namely low pass or high pass filter is mounted behind the mixer in Fig.3.5. It suppresses either upper or lower spectral line by frequency $f_0 + f_m$ or $f_0 - f_m$ respectively.

Sequence of toggled DC voltage

In today's electronic there are two important branches based on toggling DC voltage. In power electronic, semiconductor valves operating in ON/OFF state are core of appliances such as: AC/AC inverters described in Chapter 3.1, switched mode power supplies SMPS, DC/DC converters, power factor correctors PFC. They are beneficial due to smaller losses and weight and they guarantee flexible, rigid and robust energy sources. In digital, binary electronic logical state 0 and 1 are realized with VOLTAGE/VOLTAGE-LOSS state of the gates.

It is of primary interest to know frequency representation of toggled DC voltage in order to estimate hazards due to side effects of operation of electronic devices.

Rectangular waveform

Neglecting the rise and fall time of pulses leads to simplification of toggling which in the time domain is represented with the rectangular waveform as shown in Fig. 3.7 a). Instant $t = 0$ in Fig. 3.7 a) coincides with the half of the pulse width t_w , therefore coefficients b_n in the Fourier series expansion disappears.

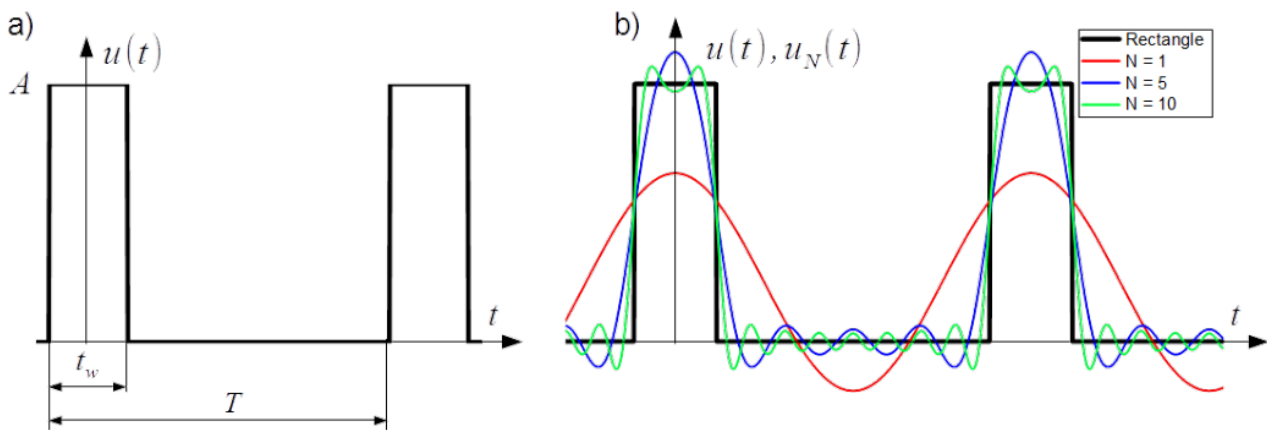


Figure 3.7: Rectangular waveform with the duty cycle of 0.23 in the time domain a) and its selected Fourier expansions b).

Coefficient $a_0 = At_w/T$ is average value of the waveform. Remaining expansion coefficients a_n are as follows

$$a_n = \frac{2A}{T} \int_{-\frac{t_w}{2}}^{\frac{t_w}{2}} \cos(n\omega t) dt = 2A \frac{t_w}{T} \frac{\sin\left(n\pi \frac{t_w}{T}\right)}{n\pi \frac{t_w}{T}} \quad (3.23)$$

The pulse width expressed as a ration of the period t_w/T , present in Eq.(3.23) is called duty cycle.

Fourier expansion of the rectangular waveform is as follows

$$u(t) = A \frac{t_w}{T} + 2A \frac{t_w}{T} \sum_{n=1}^{\infty} \left[\frac{\sin\left(n\pi \frac{t_w}{T}\right)}{n\pi \frac{t_w}{T}} \cos(2\pi n f_1 t) \right] \quad (3.24)$$

Selected Fourier expansions for $n = 1$, $n = 1, 2, \dots, 5$ and $n = 1, 2, \dots, 10$ of the rectangle waveform from Fig. 3.7 a) are presented in Fig. 3.7 b).

Coefficients a_n are values of continuous function $a(f)$ by spot frequencies $f_n = n f_1$, where $f_1 = 1/T$ is fundamental harmonic of the waveform

$$a(f) = 2A \frac{t_w}{T} \frac{\sin(\pi t_w f)}{\pi t_w f} \quad (3.25)$$

Eqs. from (3.23) to (3.25) encompasses term $\sin x/x$ which is called cardinal sine function *sinc* and is typical by frequency representation of pulses.

$$\text{sinc}(x) = \frac{\sin x}{x} \quad (3.26)$$

Function *sinc* shown in Fig.3.8 is continuous, symmetric, periodic function with period 2π and value 1 by argument equal to zero, $\text{sinc}(0) = 1$. It decays to 0 by x approaching plus and minus infinity

$$\lim_{x \rightarrow \pm\infty} [\text{sinc}(x)] = 0$$

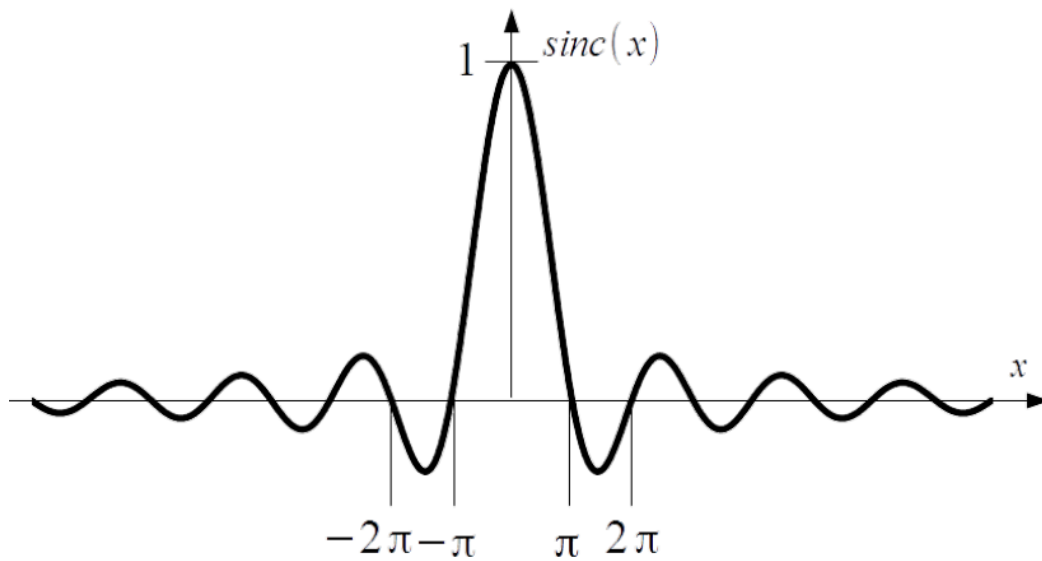


Figure 3.8: Cardinal sine function.

In respect of the harmonics, the lowest frequency of function Eq.(3.25) which must be considered is f_1 . Absolute function imposed on $a(f)$ of the waveform from Fig.3.7a) in the frequency range from f_1 to infinity is represented with black continuous curve in Fig. 3.9a). It is the envelope of absolute values of the Fourier coefficients $|a_n|$ for variability of the duty cycles [@Schnorren]. Its downward extrapolation is represented with black dashed line. Notable is its value by $f = 0$, $a(0) = 2A \frac{t_w}{T}$. It is double value of the a_0 of the Fourier expansion. Distinctive are zero cross frequencies which falls by multiple of inverse of the pulse width $1/t_w$. Notable is the number of harmonics between consecutive zero crossing. It oscillates by reciprocal of the duty cycle. It is four or five for duty cycle equal to 0.23 as shown in Fig. 3.7 and Fig. 3.9.

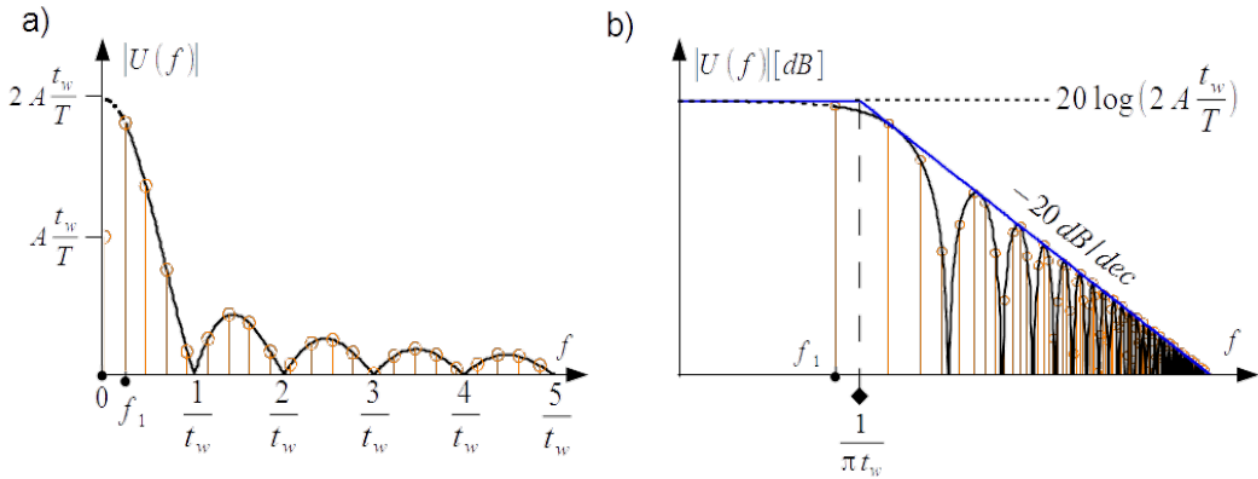


Figure 3.9: Frequency spectrum of the waveform from Fig. 3.7a) in linear scale a) and in double logarithmic scale b).

Very practical is representation of the frequency spectrum from Fig. 3.9a) in the double logarithmic scale as shown in Fig. 3.9b). The envelope is as follows

$$|U(f)|[dB] = 20 \log \left(2A \frac{t_w}{T} \right) + 20 \log \left| \frac{\sin(\pi t_w f)}{\pi t_w f} \right| \quad (3.27)$$

For upper bound of the spectrum, $|\text{sinc}(\pi t_w f)|$ is set to one by low frequencies and $|\sin(\pi t_w f)|$ is set to one by high frequencies yielding

$$|U_p(f)| = \begin{cases} 20 \log \left(2A \frac{t_w}{T} \right) & \text{for } f < \frac{1}{\pi t_w} \\ 20 \log \left(2A \frac{t_w}{T} \right) - 20 \log(\pi t_w f) & \text{for } f > \frac{1}{\pi t_w} \end{cases} \quad (3.33)$$

$\frac{1}{\pi t_w}$ \end{array} \right.. \label{Bounds}\tag{3.33}" title="|U_p(f)| = \left\{ \begin{array} {l} 20 \log \left(2A \frac{t_w}{T} \right) & \text{for } f < \frac{1}{\pi t_w} \\ 20 \log \left(2A \frac{t_w}{T} \right) - 20 \log(\pi t_w f) & \text{for } f > \frac{1}{\pi t_w} \end{array} \right. \label{Bounds}\tag{3.33}" class="latex mathjax">

In consequence the upper bound is composed of two segments of the straight line, horizontal by low frequencies and declined with the slope -20dB/decade by high frequencies, see blue line in Fig.3.9b).

The corner frequency depends on the pulse width $1/(\pi t_w)$.

Rectangular modulation, radar pulsing

Trapezoidal waveform

Considered is the case with equal rise and fall time $t_r = t_f$. Assumption of $t_w = t_{50\%}$ simplifies

expression for coefficient $a_0 = A \frac{t_w}{T}$ which is trapeze area divided by the period T i.e. it is average value of the waveform.

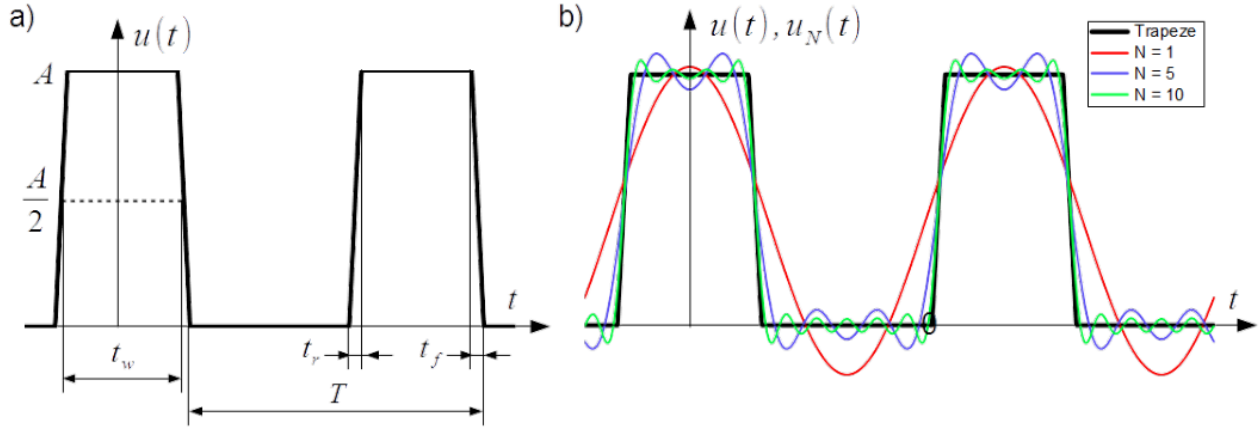


Figure 3.10: Trapezoidal waveform with the duty cycle of 0.42 in the time domain a) and its selected Fourier expansions b).

Instant $t = 0$ in Fig. 3.10 a) coincides with the half of the pulse width t_w , therefore coefficients b_n in the Fourier series expansion disappears. Remaining expansion coefficients a_n are as follows

$$\begin{aligned}
 a_n &= \frac{2A}{T} \left\{ \int_{-\frac{t_w}{2}-t_r}^{-\frac{t_w}{2}} \left[\frac{1}{t_r} \left(t + t_r + \frac{t_w}{2} \right) \cos(n\omega t) \right] dt + \right. \\
 &+ \int_{-\frac{t_w}{2}}^{\frac{t_w}{2}} \cos(n\omega t) dt + \\
 &\left. + \int_{\frac{t_w}{2}}^{\frac{t_w}{2}+t_r} \left[\frac{1}{t_r} \left(-t + t_r + \frac{t_w}{2} \right) \cos(n\omega t) \right] dt \right\} = \\
 &= 2A \frac{t_w}{T} \frac{\sin\left(n\pi \frac{t_w}{T}\right)}{n\pi \frac{t_w}{T}} \frac{\sin\left(n\pi \frac{t_r}{T}\right)}{n\pi \frac{t_r}{T}} \quad (3.29)
 \end{aligned}$$

The 50% pulse width expressed as a ration of the period t_w/T , present in Eq.(3.29) is also called duty cycle.

Fourier expansion of the trapezoidal waveform is as follows

$$u(t) = A \frac{t_w}{T} + 2A \frac{t_w}{T} \sum_{n=1}^{\infty} \left[\frac{\sin\left(n\pi \frac{t_w}{T}\right)}{n\pi \frac{t_w}{T}} \frac{\sin\left(n\pi \frac{t_r}{T}\right)}{n\pi \frac{t_r}{T}} \cos(2\pi n f_1 t) \right] \quad (3.30)$$

Selected Fourier expansions for $n = 1$, $n = 1, 2, \dots, 5$ and $n = 1, 2, \dots, 10$ of the trapezoidal waveform from Fig. 3.10 a) are presented in Fig. 3.10 b).

Coefficients a_n are values of continuous function $a(f)$ by spot frequencies $f_n = n f_1$, where $f_1 = 1/T$ is fundamental harmonic of the waveform

$$a(f) = 2A \frac{t_w}{T} \frac{\sin(\pi t_w f)}{\pi t_w f} \frac{\sin(\pi t_r f)}{\pi t_r f} \quad (3.31)$$

Eq.(3.31) encompasses product of two *sinc* functions $\text{sinc}(\pi t_w f)$ and $\text{sinc}(\pi t_r f)$.

In respect of the harmonics, the lowest frequency of function Eq.(3.31) which must be considered is f_1 . Absolute function imposed on $a(f)$ of the waveform from Fig.3.10a) in the frequency range from f_1 to

infinity is represented with black continuous curve in Fig. 3.11a). It is the envelope of absolute values of the Fourier coefficients $|a_n|$ for variability of the duty cycles. Its downward extrapolation is represented with black dashed line. Notable is its value by $f = 0$, $a(0) = 2A \frac{t_w}{T}$. It is double value of the a_0 of the Fourier expansion.

Very practical is representation of the frequency spectrum from Fig. 3.11a) in the double logarithmic scale as shown in Fig. 3.11b). The envelope is as follows

$$|U(f)|[dB] = 20 \log \left(2A \frac{t_w}{T} \right) + 20 \log \left| \frac{\text{sinc}(\pi t_w f)}{\pi t_w f} \right| + 20 \log \left| \frac{\text{sinc}(\pi t_r f)}{\pi t_r f} \right| \quad (3.32)$$

For upper bound of the spectrum, $|\text{sinc}(\pi t_w f)|$ and $|\text{sinc}(\pi t_r f)|$ are set to one by low frequencies, and $|\sin(\pi t_w f)|$ and $|\sin(\pi t_r f)|$ are set to one by high frequencies. In the intermediate frequencies $|\text{sinc}(\pi t_r f)|$ is set to one and $|\sin(\pi t_w f)|$ is set to one yielding

Formula does not parse $\frac{1}{\pi t_r}$ title="|U_p(f)|= \left\{ \begin{array}{l} 20 \log \left(2A \frac{t_w}{T} \right) \text{ for } f < \frac{1}{\pi t_w} \\ -20 \log \left(\left(2A \frac{t_w}{T} \right) \left(\pi t_w f \right) \right) \text{ for } \frac{1}{\pi t_w} < f < \frac{1}{\pi t_r} \\ -20 \log \left(\left(2A \frac{t_w}{T} \right) \left(\pi t_w f \right) \right) - 20 \log \left(\left(\pi t_r f \right) \right) \text{ for } f > \frac{1}{\pi t_r} \end{array} \right\}
 \end{array}
 $\right.$
 $\text{\label{Bounds}\tag{3.33} \$}$

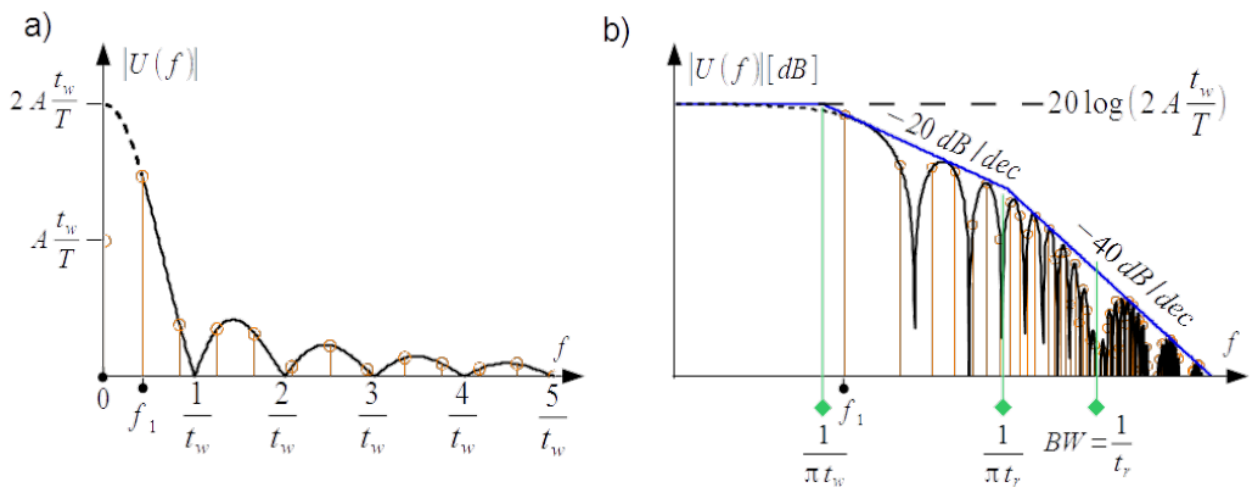


Figure 3.11: Frequency spectrum from Fig. 3.10 b) in double logarithmic scale.

In consequence the upper bound is composed of three segments of the straight line, horizontal by low frequencies, declined with the slope -20dB/decade by intermediate frequencies and declined with the slope -40dB/decade by high frequencies, see blue line in Fig.3.11b). The corner frequencies depends on the pulse width $1/(\pi t_w)$ and the pulse rise time $1/(\pi t_r)$.

Zero cross frequencies marked in and Fig. 3.11a) falls by multiple of inverse of the pulse width $1/t_w$ in the low and intermediate frequencies because term $|\text{sinc}(\pi t_r f)|$ is negligible. The number of harmonics between consecutive zero crossing in that range oscillates by reciprocal of the duty cycle. It is two or three for duty cycle equal to 0.417 as shown in Fig. 3.10 and Fig. 3.11.

The frequency bandwidth BW of the trapezoidal waveform defined as follows

$$BW = \frac{1}{t_r} \quad (3.34)$$

is marked in Fig. 3.11b). It seems to be very conservative, but if the pulse width approaches the rise time, such bandwidth ensures removal of the spectral lines which approximately are only 27 dB below the fundamental harmonic.

Damped oscillatory waveform

Very often happens, that toggled DC voltage is followed with ringing (overshoot/undershoot) due to parasitic inductances and capacitances, for instance in power cable connecting motor with the inverter or in PCB signal path. Analysis of the series RLC circuit supplied with rectangularly switched ON and OFF electromotive force, as shown in Fig.3.12 gives good insight into how this phenomenon is mirrored in the frequency domain.

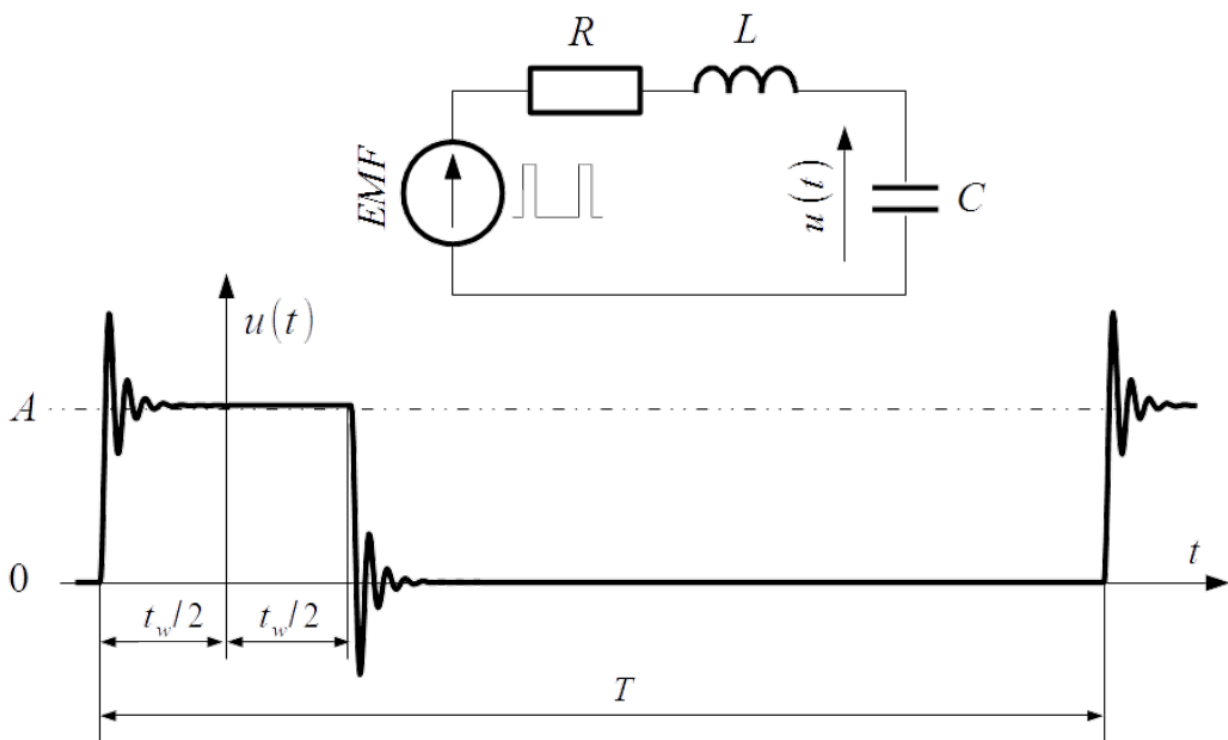


Figure 3.12: Ringing (undershoot/overshoot) in series RLC circuit supplied with rectangularly switched ON and OFF electromotive force.

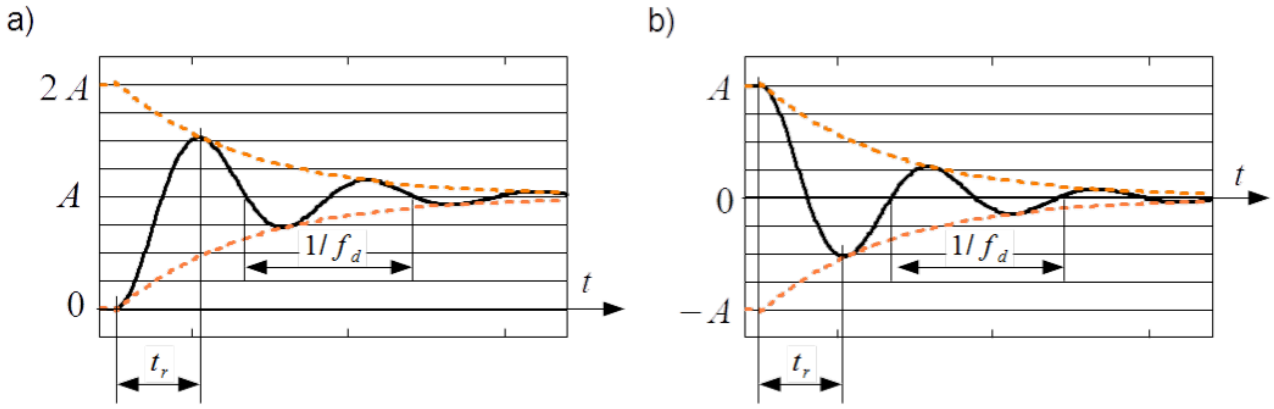


Figure 3.13: Piece of period from Fig.3.12, damped oscillatory by: EMF ON a), EMF OFF b).

Pattern of damped oscillatory in the period shown in Fig.3.12 is as follows

$$u(t) = \begin{cases} A - Ke^{-\alpha(t + \frac{t_w}{2})} \sin\left[2\pi f_r(t + \frac{t_w}{2}) + \varphi\right] & \text{for } \frac{-t_w}{2} < t < \frac{t_w}{2} \\ Ke^{-\alpha(t - \frac{t_w}{2})} \sin\left[2\pi f_r(t - \frac{t_w}{2}) + \varphi\right] & \text{for } \frac{t_w}{2} < t < T - \frac{t_w}{2} \end{cases} \quad (3.35)$$

where A is amplitude of the EMF, t_w is pulse width and T pulse period as shown in Fig.3.12.

The RLC circuit has resonance frequency f_0 . By this frequency its impedance is shrunk to resistance R . Damping coefficient α depends on resistance R and inductance L .

$$f_0 = \frac{1}{2\pi} \sqrt{LC} \quad ; \quad \alpha = \frac{R}{2L} \quad (3.36)$$

Damped oscillatory frequency f_d is combined with resonance frequency f_0 and damping coefficient α . After excitation (step change of EMF in this case) extinguishes, the circuit exhibits damped oscillations with frequency f_d , see Fig.3.13. That's why f_d is called also natural frequency. In that figure the rise time t_r defined as time interval between transient initiation and peak value of the first overshoot is shown.

K depends on amplitude A , resonance frequency f_0 and natural frequency f_d . φ is the phase angle of damped oscillations.

$$f_d = \frac{1}{2\pi} \sqrt{4\pi^2 f_0^2 - \alpha^2} \quad ; \quad K = \frac{f_0}{f_d} A \quad ; \quad \varphi = \arctan\left(\frac{2\pi f_d}{\alpha}\right) \quad (3.37)$$

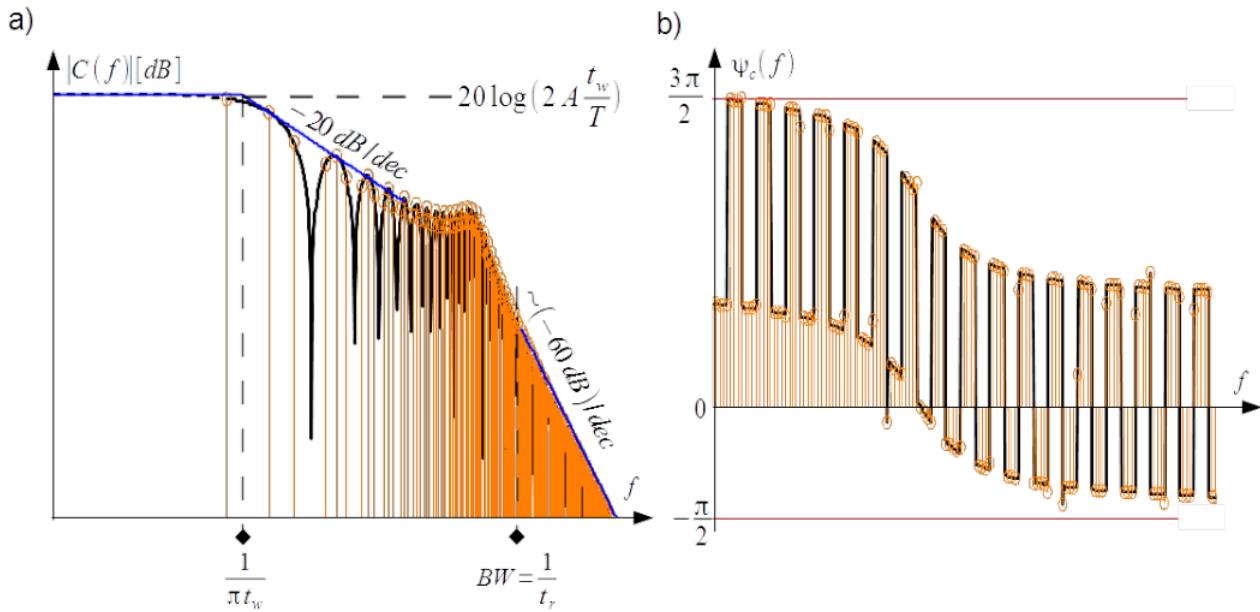


Figure 3.14: Frequency spectrum of damped oscillatory from Fig.3.12: magnitude a), phase angle b).

Damped oscillatory as shown in Fig.3.12 is overlapping of three time sequences: rectangle with amplitude A by EMF ON in the time interval $[-t_w/2, t_w/2]$ and zero by EMF OFF in the time interval $[t_w/2, T - t_w/2]$, up ringing in the time interval $[-t_w/2, t_w/2]$, see Fig.3.13a) and down ringing in the time interval $[t_w/2, T - t_w/2]$ see Fig.3.13b). Therefore coefficients of the Fourier expansion Eq.([an]) and Eq.([bn]) are sums of three integrals. Its complex representation with $C(f)$ as magnitude and phase angle is shown in Fig.3.14.

Upper bound of the spectrum, blue line in Fig.3.14a) are in the lower frequency range the same as for rectangle toggling, i.e. segment of the straight horizontal line up to the corner frequency depending on the pulse width $1/(\pi t_w)$ and line decreased with the slope -20dB/decade above the corner frequency, compare Fig.3.9b).

Remarkable in the spectrum is resonant region in a narrow frequency band. Quality factor and bandwidth of this region depends on f_0 and α . Maximum in this region is by ringing frequency f_r . In the case presented here ringing frequency f_r is about forty times bigger than corner frequency and quality of resonance is moderate, therefore maximum of resonance is significantly below the horizontal upper bound. If corner frequency and f_r are closer one to another and resonance has big quality, the resonant region can exceed the upper bound.

Above the resonant region upper bound decays with the slope approximately $\sim (-60\text{dB/decade})$. Bandwidth frequency defined as usual $BW = 1/t_r$ is situated on this slope.

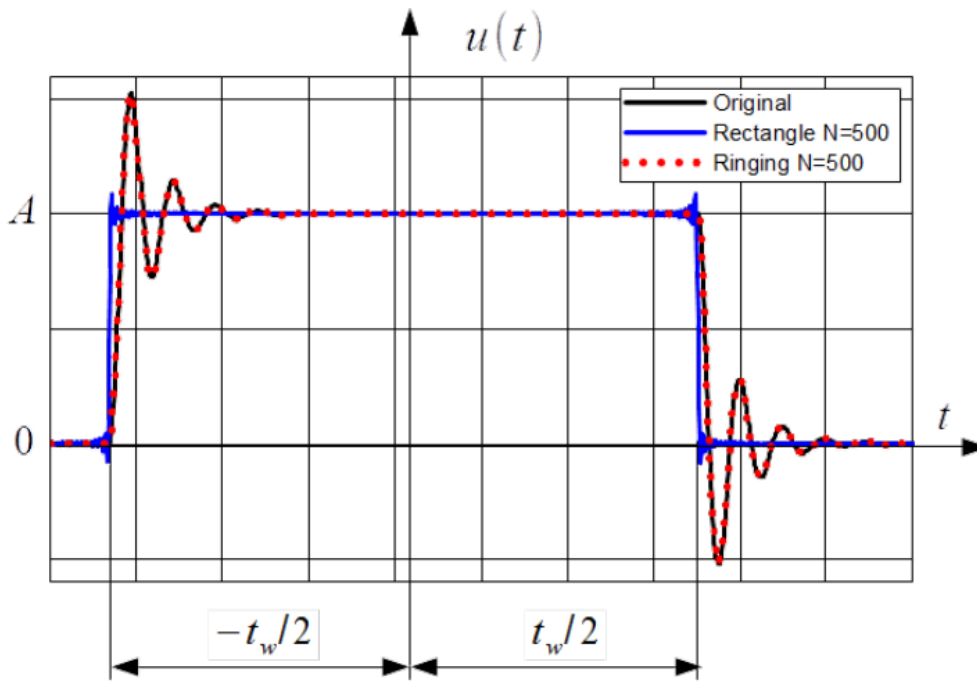


Figure 3.15: Reconstruction of damped oscillatory from the frequency domain to the time domain.

In Fig.3.15 reconstruction of ringing from the frequency domain into the time domain with $N = 500$ harmonics (red dotted line) together with the original (black line) ringing is shown. Added is reconstruction of the rectangle (blue line).

Single events – pulses

Spectral density of triangle pulse

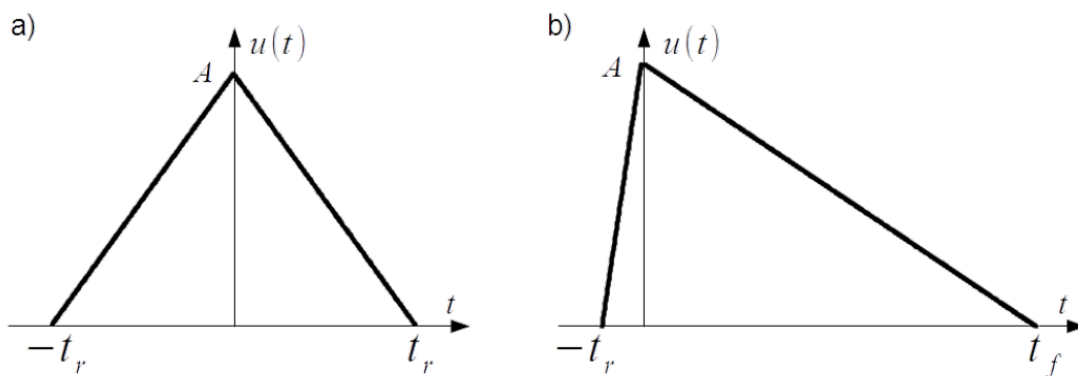


Figure 3.16: Triangle pulse with equal rise and fall time $t_r = t_f$, a) and with bigger fall time $t_f > t_r$, b).

The Fourier integral of the triangle pulse with equal rise and fall time $t_r = t_f$, as shown in Fig.3.16a) according to Eq.(Fourier_int) yields

$$u(f) = At_r \text{sinc}^2(\pi t_r f) \quad (3.38)$$

This spectrum density is a real function with value equal to the pulse area At_r by zero frequency and has zero minima by multiples of the inverse of the pulse rise time $1/t_r$ as shown in Fig.3.17a).

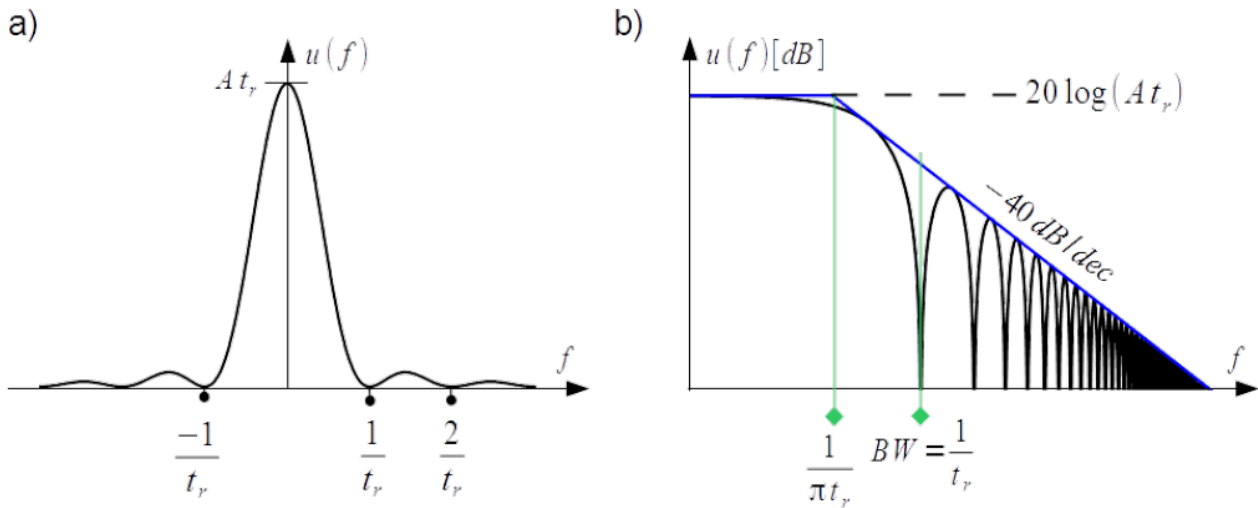


Figure 3.17: Spectrum density of triangle pulse with equal rise and fall time in linear scale a) and in double logarithmic scale b).

The upper boundary of the spectrum density represented in double logarithmic scale is composed of horizontal line $20 \log(At_r)$, a slope -40 dB/decade and the corner frequency by $f = 1/(\pi t_r)$, see Fig.3.17b).

$$u_p(f) = \begin{cases} 20 \log(At_r) & \text{for } f < \frac{1}{\pi t_r} \\ 20 \log(At_r) - 40 \log(\pi t_r f) & \text{for } f > \frac{1}{\pi t_r} \end{cases} \quad (3.39)$$

$\frac{1}{\pi t_r}$ \end{array} \right. \label{Bounds_triangle} \tag{3.39}'' title="u_p(f) = \left\{ \begin{array} {l} 20 \log(At_r) \ \& \ \mbox{ for } f < \frac{1}{\pi t_r} \ \} \ 20 \log(At_r) - 40 \log(\pi t_r f) \ \& \ \mbox{ for } f > \frac{1}{\pi t_r} \ \end{array} \right. \label{Bounds_triangle} \tag{3.39}'' class="latex mathjax">

Bandwidth estimation in the same way as for the trapezoidal wave form $BW = 1/t_r$ Eq.(3.4), ensures removal of the spectral lines which are approximately 27 dB below the value of spectral density by zero frequency.

The Fourier integral of the triangle pulse with different rise and fall time $t_r \neq t_f$, as shown in Fig.3.16b) is complex function

$$\begin{aligned} \text{Re}[u(f)] &= \frac{A}{2\pi^2 f^2} \left[\frac{1}{t_r} \sin^2(\pi f t_r) + \frac{1}{t_f} \sin^2(\pi f t_f) \right] = \\ &= \frac{At_r t_f}{2} \left[\frac{1}{t_f} \text{sinc}^2(\pi f t_r) + \frac{1}{t_r} \text{sinc}^2(\pi f t_f) \right] \\ \text{Im}[u(f)] &= \frac{A}{2\pi^2 f^2} \left[\frac{-1}{t_r} \sin(\pi f t_r) \cos(\pi f t_r) + \frac{1}{t_f} \sin(\pi f t_f) \cos(\pi f t_f) \right] \end{aligned} \quad (3.42)$$

It is depicted in Fig.3.18a) in single logarithmic scale in order to accentuate spectrum by high frequencies. This spectrum density is equal to area of the pulse $A(t_r + t_f)/2$ by zero frequency since $\text{sinc}^2(0) = 1$.

The upper boundary of the absolute value of the spectrum density represented in double logarithmic

scale can be established only by very low and very high frequencies. By very low frequencies imaginary part can be neglected and the real part builds horizontal line $20 \log[A(t_r + t_f)/2]$ as for zero frequency. It ends by corner frequency $1/(\pi t_f)$. By very high frequencies which starts by another corner frequency $1/(\pi t_r)$ again imaginary part can be neglected and functions $\sin^2(\pi f t_r)$ and $\sin^2(\pi f t_f)$ in the real part can be replaced with 1. In consequence the upper bound decays with the slope -40dB/decade , see Fig.3.18b).

$$|u_p(f)| = \begin{cases} 20 \log\left(A \frac{t_r+t_f}{2}\right) & \text{for } f < \frac{1}{\pi t_f} \\ 20 \log\left[\frac{A}{2\pi^2} \left(\frac{1}{t_r} + \frac{1}{t_f}\right)\right] - 40 \log(f) & \text{for } f > \frac{1}{\pi t_r} \end{cases} \quad (3.43)$$

$\frac{1}{\pi t_r}$ \end{array} \right. \label{Bounds_triangle_trf}\tag{3.43}" title="|u_p(f)|= \left\{ \begin{array}{l} 20 \log\left(A \frac{t_r + t_f}{2} \right) \text{ for } f < \frac{1}{\pi t_f} \\ 20 \log\left[\frac{A}{2\pi^2} \left(\frac{1}{t_r} + \frac{1}{t_f} \right) \right] - 40 \log(f) \text{ for } f > \frac{1}{\pi t_r} \end{array} \right. \right. \label{Bounds_triangle_trf}\tag{3.43}" class="latex mathjax">

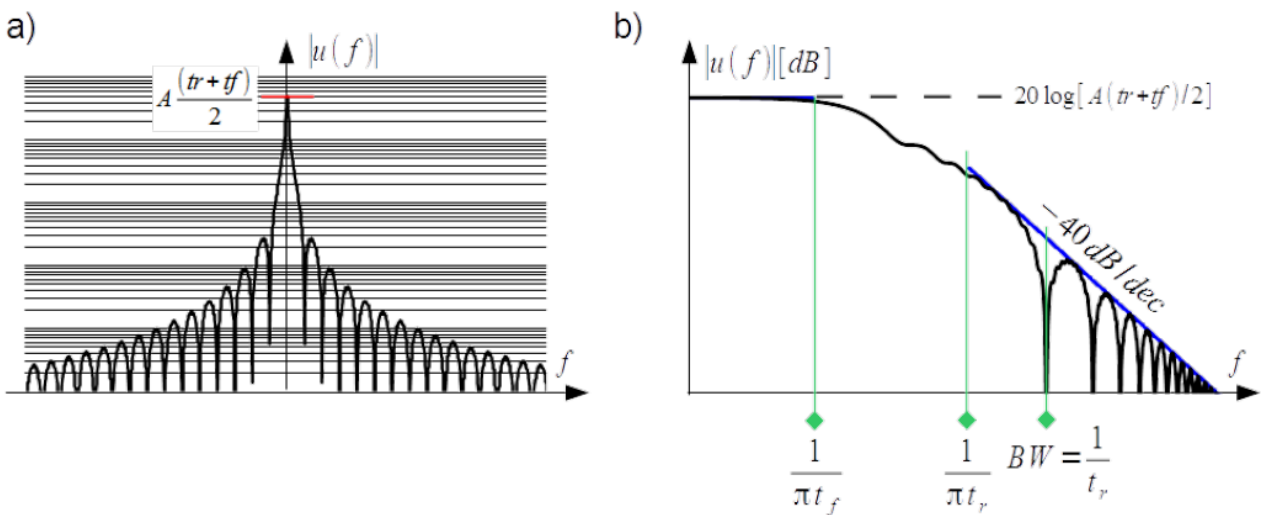


Figure 3.18: Spectrum density of triangle pulse with different rise and fall time in single logarithmic scale a) and in double logarithmic scale b).

Bandwidth estimation in the same way as for the trapezoidal wave form $BW = 1/t_r$ Eq.(3.4), is more conservative than for triangle pulse with equal rise and fall time.

Discharge of static electricity

When two objects rub against each other, some charge (electrons) is transferred from material of one object to material of the other. When these two objects are separated thereafter, this charge may not return to the original one. If the two objects were originally neutral, they are now charged, one positively and the other negatively.

This method of generating static electricity is referred to as the triboelectric effect. Some materials readily absorb electrons while others tend to give them up easily. The triboelectric series is a listing of materials in order of their affinity for giving up electrons [Ott].

Table 3.2 is a typical triboelectric series. The materials at the top of the table easily give up electrons and

therefore acquire a positive charge. The materials at the bottom of the table easily absorb electrons and therefore acquire a negative charge [1].

Table 3.2: Triboelectric series

Triboelectric series

3.	Air	19.	Sealing wax
3.	Human skin	20.	Hard rubber
3.	Asbestos	21.	Mylar
4.	Rabbit fur	22.	Epoxy glass
5.	Glass	23.	Nickel, copper
6.	Human hair	24.	Brass, silver
7.	Mica	25.	Gold, platinum
8.	Nylon	26.	Polystyrene foam
9.	Wool	27.	Acrylic rayon
10.	Fur	28.	Orlon
11.	Lead	29.	Polyester
12.	Silk	30.	Celluloid
13.	Aluminium	31.	Polyurethane foam
14.	Paper	32.	Polyethylene
15.	Cotton	33.	Polypropylene
16.	Wood	34.	PVC
17.	Steel	35.	Silicon
18.	Amber	36.	Teflon

Amount of energy collected by triboelectric effect depends not only on the ordering of the materials in the series but also on the surface cleanliness, amount of rubbing, surface area in contact, smoothness of surface, the speed of separation and relative humidity [1]. By friction between the blades of the rotor of a helicopter or airfoil of airplane, between isolating wheels and ground floor voltage of static electricity can reach hundreds of kV.

The concern of this lecture notes is human discharge of static electricity which, depending on low/high relative humidity can reach the level of [1]:

- 35 kV / 1.5 kV by walking across carpet,
- 12 kV / 0.25 kV by walking on vinyl floor,
- 6 kV / 0.1 kV worker moving at bench,
- 20 kV / 1.2 kV picking up common polyethylene bag,
- 18 kV / 1.5 kV sitting on chair padded with polyurethane foam.

Different types of human discharge are described in chapter 13 of [2], which is contribution of Mr. Heinrich Ryser in the joint publication authored by Mrs. Frank Dittmann, Martin Kahmann.

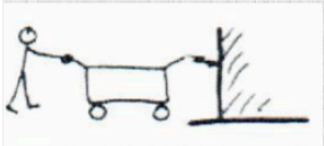
a)		Static voltage Peak current Rise time	4 kV 1 A ca. 1 ns
b)		Static voltage Peak current Rise time	4 kV 5 A ca. 1 ns
c)		Static voltage Peak current Rise time	4 kV 20 A ca. 1 ns
d)		Static voltage Peak current Rise time	4 kV 70 A ca. 5 ns

Figure 3.19: Different arts of human discharge of static electricity: a) with finger, b) with fist, c) with pointed metal object kept in hand, d) via metallic carriage with isolating wheels.

Analysis of Fig.3.19 indicates the human discharge with pointed metal object like: tweezers, key, screw driver or ball pen kept in hand, as most severe discharge. Therefore only this discharge is in scope of standards IEC 61000-4-2 and EN 61000-4-2³.

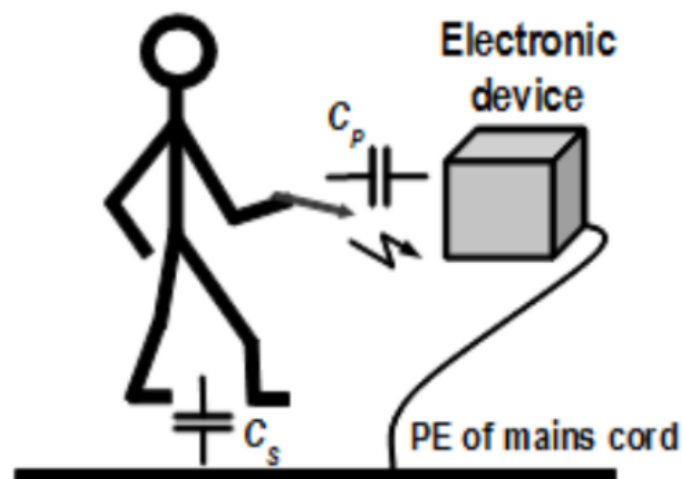


Figure 3.20: Illustration of human-metal discharge.

Charged person, standing on the floor can be represented with the charged capacitance C_P of the soles against the ground and the body resistance. If the person is keeping pointed object in hand and approaches grounded electronic equipment [JB_JSr_TEMC], then electric field strength in small capacitance C_P ,

which by movement of hand is decreased anyway, can exceed value of arc initiation and arc discharge is started. This is the first, fast-varying component of the discharge. The loop is closed and energy stored in capacitance C_S can be dissipated in resistance of human body due to current streaming through the person, arc in capacitance C_P , earthing wire in the mains cord and ground. This is the second, slow-varying component of the discharge.

Both components of pulse wave of the human-metal discharge current are shown in Fig.3.21 according to [JB_JSr_TEMC]. The rise time of the fast component is ca. $800ps$. According to Eq.(3.4) it means bandwidth of the ESD up to $1.25GHz$. This is the fastest phenomenon in the time domain, discussed in this lecture note and in the same time the widest in the frequency domain.

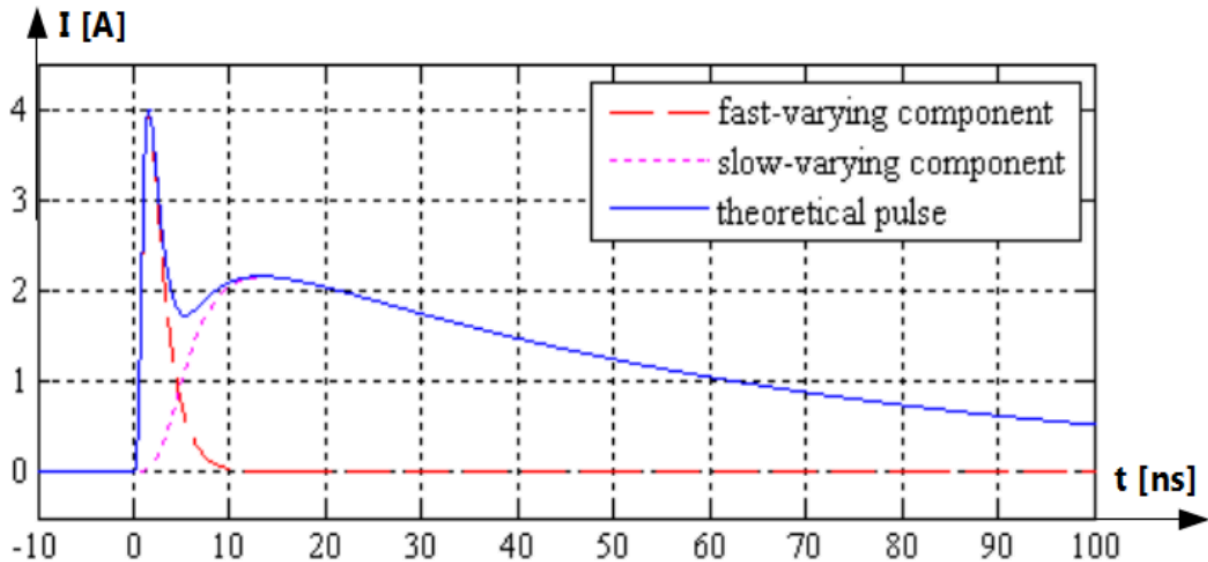


Figure 3.21: Pulse wave of the human-metal discharge current.

For the sake of completeness module of transient electric field strength $|E(t)|$ of human metal discharge at 5 kV charge voltage and a distance of 10 cm is illustrated in Fig.3.22, according to [EN-4-2]. The plot is inserted in order to emphasise that although magnetic field and current by discharge of static electricity have pulse form, yet electric field and voltage passes from one to another static state.

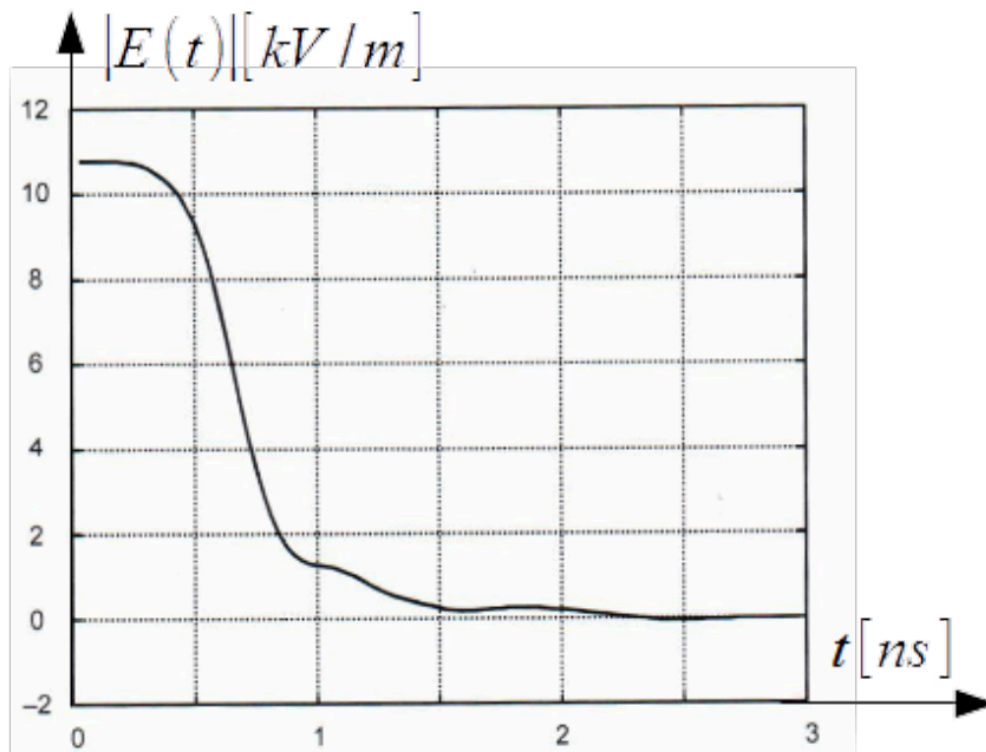


Figure 3.22: Exemplary module of electric field strength by human-metal discharge, according to [EN-4-2].

Electric fast transients BURST

For explanation of BURST we must return to the chapter 3.1.1. Electric fast transients are generated by opening a mechanical switch in the circuit with inductance. An example is shown in Fig.3.23. Inductance L with serial resistance R_L can represent a choke or motor with conducting losses of winding. In parallel is condenser C covering capacitances between turns. Actually plot of voltage threshold for different discharge regimes in Fig.3.23 is identical as in Fig.3.2 but displayed versus time. It is justified assuming uniform movement of the switch contacts $d = v \cdot t$. Gas pressure is constant anyway.

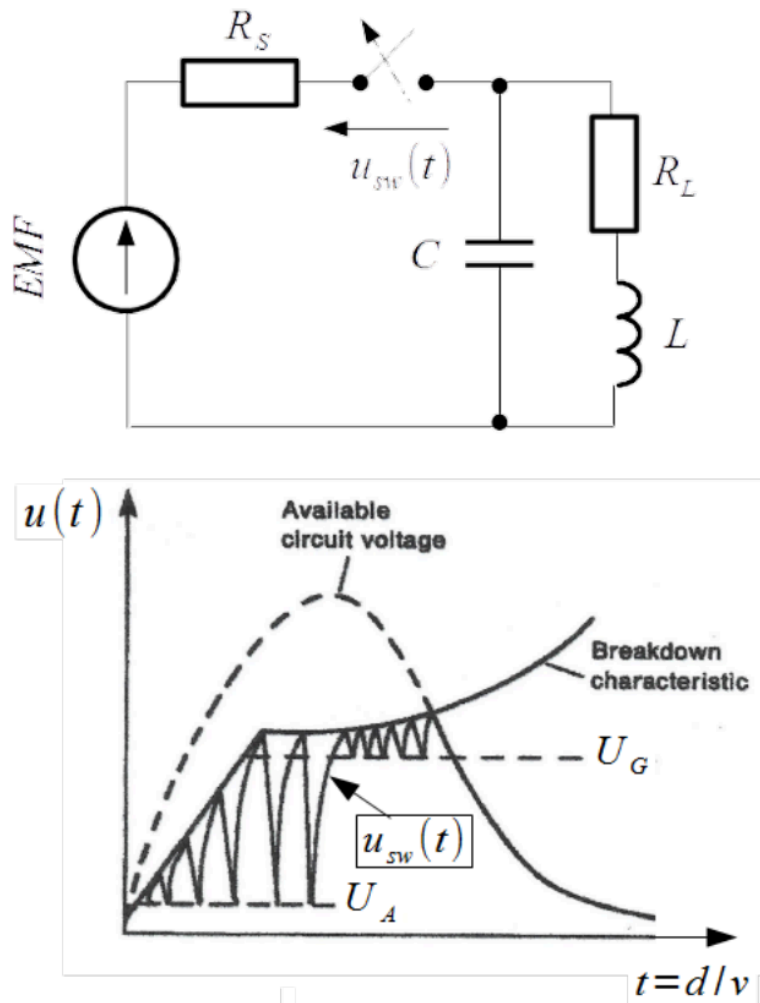


Figure 3.23: BURST generation by breaking inductive load [Clayton].

If not any side effect accompanies the opening then the voltage across switch contacts $u_{sw}(t)$ would follow the curve named "available circuit voltage" in Fig.3.23. However shortly after breaking the circuit the field strength between contacts reaches the threshold for short arc initiation. Arc bridges the circuit and voltage across contacts drops rapidly to voltage U_A required for sustaining the arc. Energy stored in capacitance C is dissipated in source resistance R_S . Current through the contacts is usually smaller than minimal sustaining current I_A and arc extinguishes. Voltage across contacts rises up till the field strength between contacts reaches again the threshold for short arc initiation. The next rapid voltage drop on the contacts happens. The repetitive ignition and extinction of arc can continue even in the time after the threshold voltage passes to the Paschen curve (Breakdown characteristic in Fig.3.23), provide voltage across and current through contacts are sufficient for arcing. It means that long arc are generated. Two of them are illustrated in Fig.3.23. Thereafter conditions required for arcing are not fulfilled but fulfilled are conditions for glow discharge. Voltage across contacts drops to voltage U_G required for sustaining the glow discharge. Current through the contacts is usually smaller than minimal sustaining current I_G and glow discharge stops. Voltage across contacts rises up till it reaches again the Paschen curve. The next rapid voltage drop on the contacts happens. These are called miniature burst because jumps between maximal (Paschen curve) and minimal voltage U_G are much smaller. The voltage drops by arcing initiation is as fast as few nanoseconds

of lightning strike driven in earthing resistance Z_E^B causes surge of voltage across and current driven in the impedance of the PEN . This surge appears automatically in the live conductors of the mains in the whole building. It must be emphasized that voltage and current surge is also present in the earthing impedance of the transformer Z_E^T .

Moreover there exists other possible circuit meshes. One of them consists of the earthing impedance of the building Z_E^B , the segment of the PEN conductor between building input and the transformer and then either PEN conductor in the supply line of the house 1 and the earthing impedance Z_E^1 of the house 1 or the PEN conductor in the supply line of the house 2 and the earthing impedance Z_E^2 of the house 2. It means that current driven through the external lightning protection system of the building to earth as shown in Fig.3.24 is sensed as the surge by all customers supplied from the same transformer.

The surge is also sensed everywhere in IT installation due to the fact, that shields of the IT cables are connected to the PE i.e. to the star point in the supply transformer. As already mentioned, the star point of the transformer is also stressed with the surge.

It happen very often that supply mains and IT installation builds loops **case 3**. Current driven through the external lightning protection system to earth is accompanied with magnetic field. Flux of magnetic field induces voltage surges in them.

Strikes in the medium voltage overhead lines or traveling waves in it can easily get through supply transformer and appear in the building's mains as a surge.

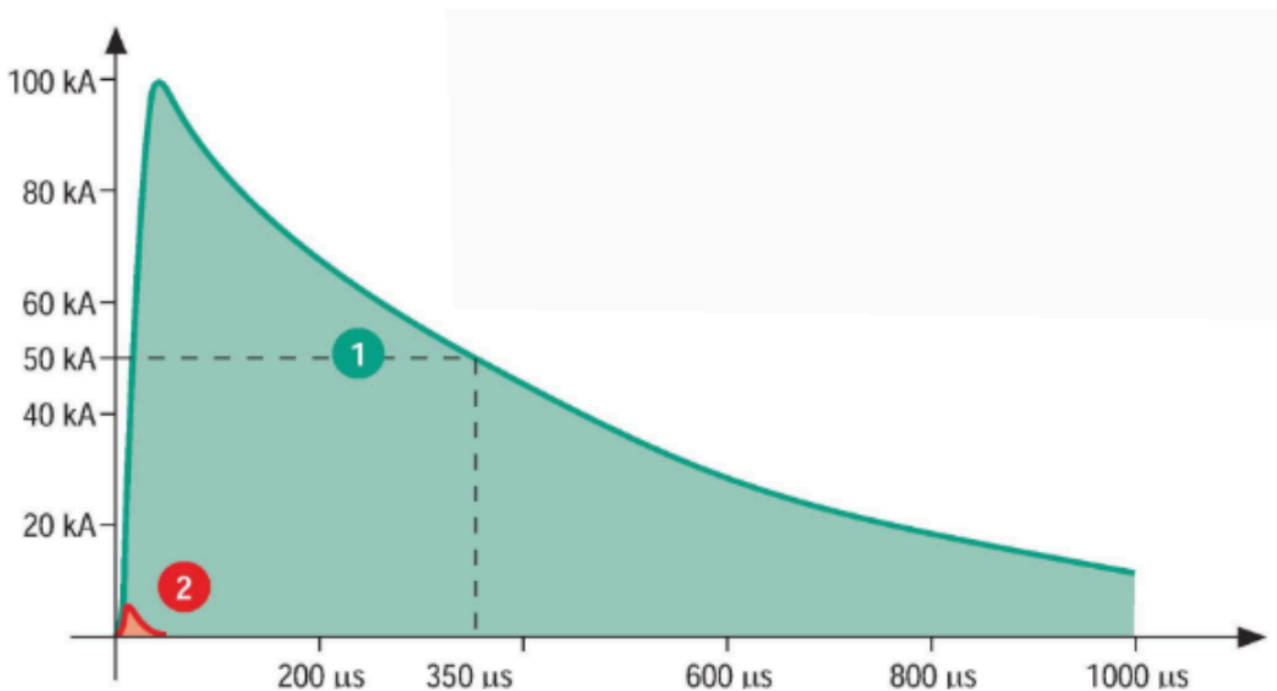


Figure 3.25: Standardized current of direct strike (1) and surge (2).

Current by direct strike is a random event. Its parameters like crest (front) time, duration and peak value have statistical distribution. Obviously the same concerns the current surge. These pulses are standardized for objectivity in technical applications. Standardized current pulse by direct strike is defined in the standard [EN-61643-11] as shown with the **plot 1** in Fig.3.25. It is assumed that this current is independent on the load through which it is driven. In other words that energy of the source of this pulse is unlimited.

For comparison, in the same figure standardized current surge defined in the standard [EN-4-5] is plotted **plot 2**. It is assumed that energy of the source of that pulse is limited and the current 2 shown

in Fig.3.25 is the short circuit current i.e. current by zero load. Additionally for completeness open circuit voltage of the surge pulse is defined in the standard [EN-4-5]. Parameters of the direct strike current and surges are gathered in Tab.3.3. In this table the symbol t_f is assigned to the crest time t_c as defined in Fig. [t_r], in order to be in line with the nomenclature of the standard [EN-4-5].

Table 3.3: Parameters of direct strike vs. surge.

	Direct strike		
	Short circuit current	Open circuit voltage	
Front (crest) time t_f [μs]	10	8	3.2
Pulse duration t_d [μs]	350	20	50
Peak value	100 [kA]	2 [kA]	4 [kV]

[LEMP_tab]

In Figs. 3.26 and 3.27 standardized surge current and voltage waveforms, according to [EN-4-5] are shown. They are normalized with the peak value.

It should be noticed that by the short circuit current surge, the rise time $t_r = t_{90\%} - t_{10\%}$ is applied. In consequence relation between the rise and the front (crest) time is as follows

$$t_f = \frac{100\%}{90\% - 10\%} \cdot t_r = 1.25 \cdot t_r, \text{ see Fig.[t_r] and Eq.([t_c]).}$$

For a change by the open circuit voltage surge, the rise time $t_r = t_{90\%} - t_{30\%}$ is applied. In consequence relation between the rise and the front (crest) time is as follows

$$t_f = \frac{100\%}{90\% - 30\%} \cdot t_r \approx 1.67 \cdot t_r, \text{ see Fig.[t_r] and Eq.([t_c]).}$$

As to pulse duration by the short circuit current surge, the pulse width t_w is multiplied with empirical factor $t_d = 1.18 \cdot t_w$ but by the open circuit voltage surge, the time duration is identical with the pulse width $t_d = t_w$. All these definitions are historically conditioned.

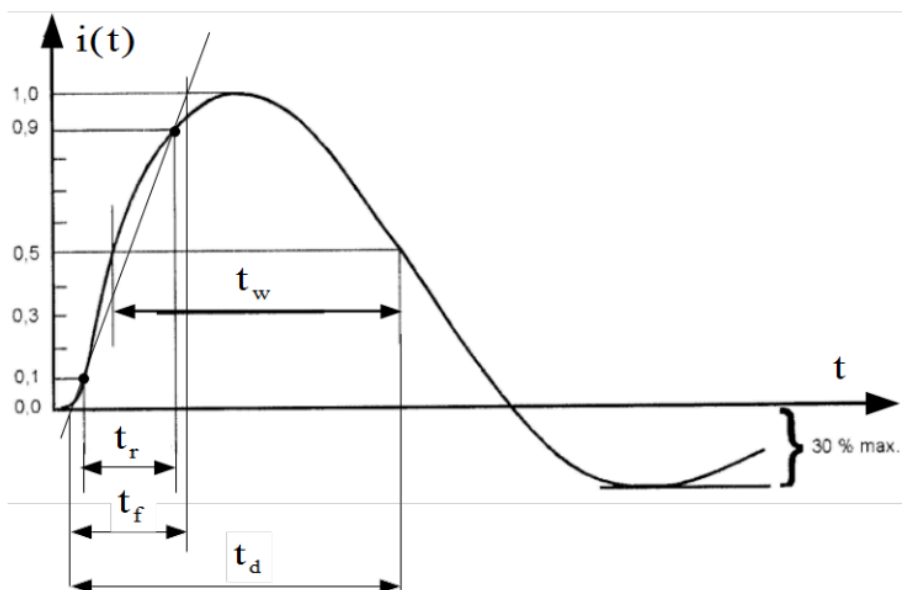


Figure 3.26: Standardized and normalized short circuit surge current, according to [EN-4-5].

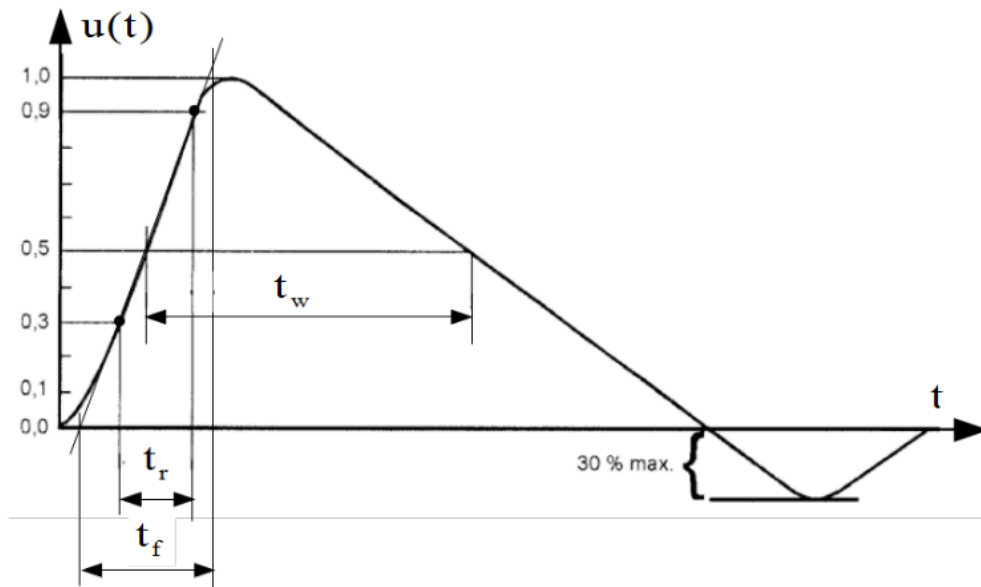


Figure 3.27: Standardized and normalized open circuit surge voltage, according to [EN-4-5].

Pay attention to ringing in voltage and current surge, less than 30% as shown in Figs. 3.26 and 3.27. It must be like that because surges are coupled with the direct strike, **plot 1** in Fig.3.25 with derive operator.

It can be learned from Tab. 3.3 that the ratio of peak open-circuit output voltage to peak short-circuit current by surge is equal to 2Ω . Except unit it has nothing to do with impedance, but nevertheless it is called an effective source impedance in the standard [EN-4-5].

Nuclear/High-altitude ElectroMagnetic Pulse

After the first experiences with the atomic weapon during the Second World War, the Nuclear Powers started investigation on “humanitarian nuclear weapon” which should be harmless for the human being but paralyzing commandment, logistics and operation of military troops.

Interests were focused on thermonuclear explosions at very high altitude above the Earth in order to avoid the destructive effect of the blast wave and thermal effect. It was expected that ionizing radiations i.e.: α , β , γ and neutron radiation by such explosions as well as plasma shell are able to act indirectly on the Earth’s surface in a form of electromagnetic pulse. Thus the term Nuclear ElectroMagnetic Pulse NEMP used for indicating this kind of explosions. The outcome of the NEMP on the Earth’s surface is named High-altitude ElectroMagnetic Pulse HEMP.

The International Electrotechnical Commission described and standardized the HEMP phenomenon in the document [IEC-2-9]. Three components of the HEMP namely: E1, E2 and E3 are distinguished there. They are illustrated in Fig.3.28 in the time domain in the double logarithmic scale.

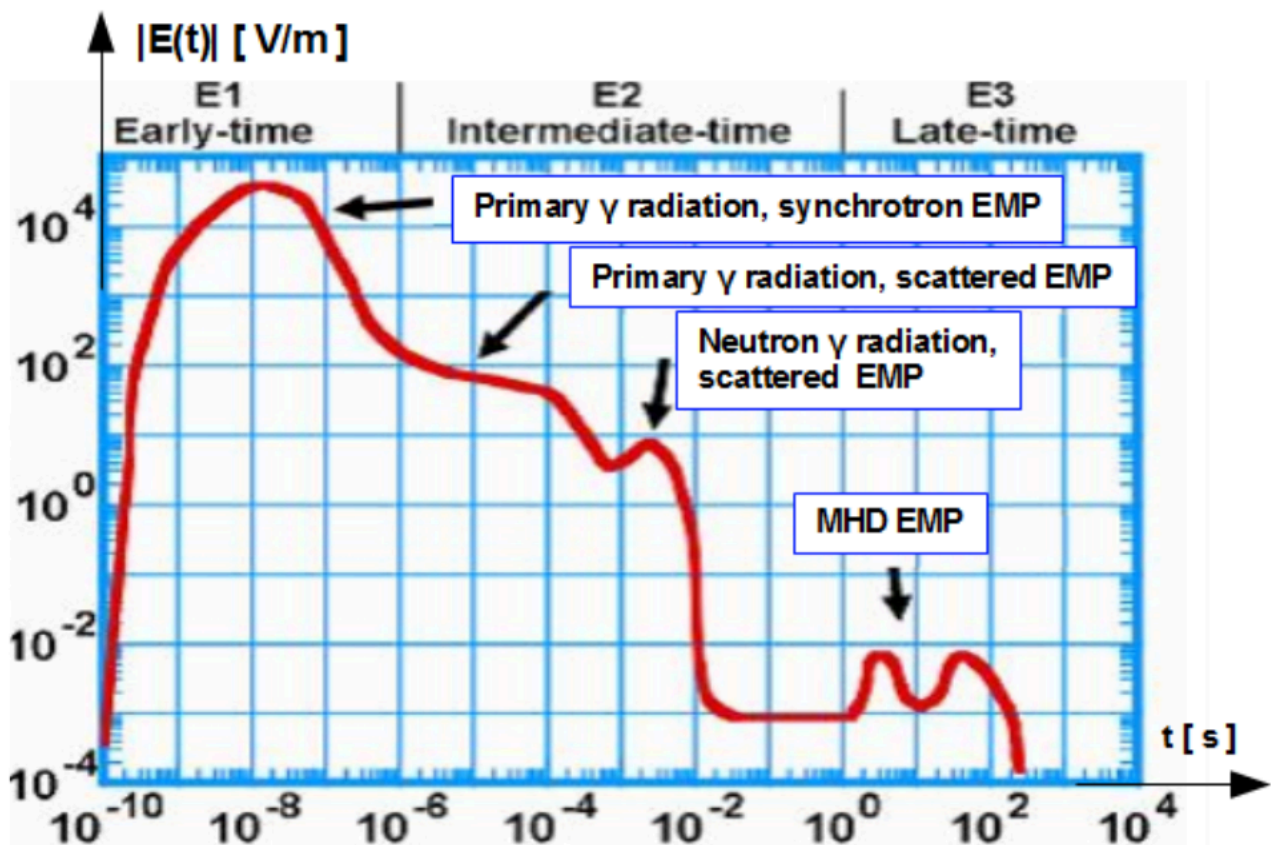


Figure 3.28: Three component of the HEMP acc. to [IEC-2-9].

E1 the early time

By thermonuclear explosion at the altitude of several hundreds of kilometers above surface of the Earth i.e. in the ionosphere,⁴ the primary γ rays propagate toward the Earth, as shown in Fig.3.29. Elastic collision of γ rays with electrons is ruled with the Compton effect i.e. electrons are accelerated by γ rays. As momentum conservation rules this process, the scattered γ rays have much smaller frequency shifted to non-ionizing range. Electrons travel generally in downward direction with relativistic speed of more than 90% of the light speed.

At height between 20 km and 40 km above the Earth's surface the Earth's magnetic field comes into play. Magnetic field with induction \vec{B} exerts a force on electrons moving with the linear speed of \vec{v} . It is ruled with the Lorentz formula $\vec{F}_B = e \cdot \vec{v} \times \vec{B}$ where e is the charge of electron. By perpendicular orientation of \vec{v} and \vec{B} one to another, force \vec{F}_B would be centripetal and trajectory would be a circle. By other angles the force \vec{F}_B has also shifting component and the trajectory of electron is helical as shown in Fig.3.30. By the mid latitude electron rotate with the radius of about 85m .

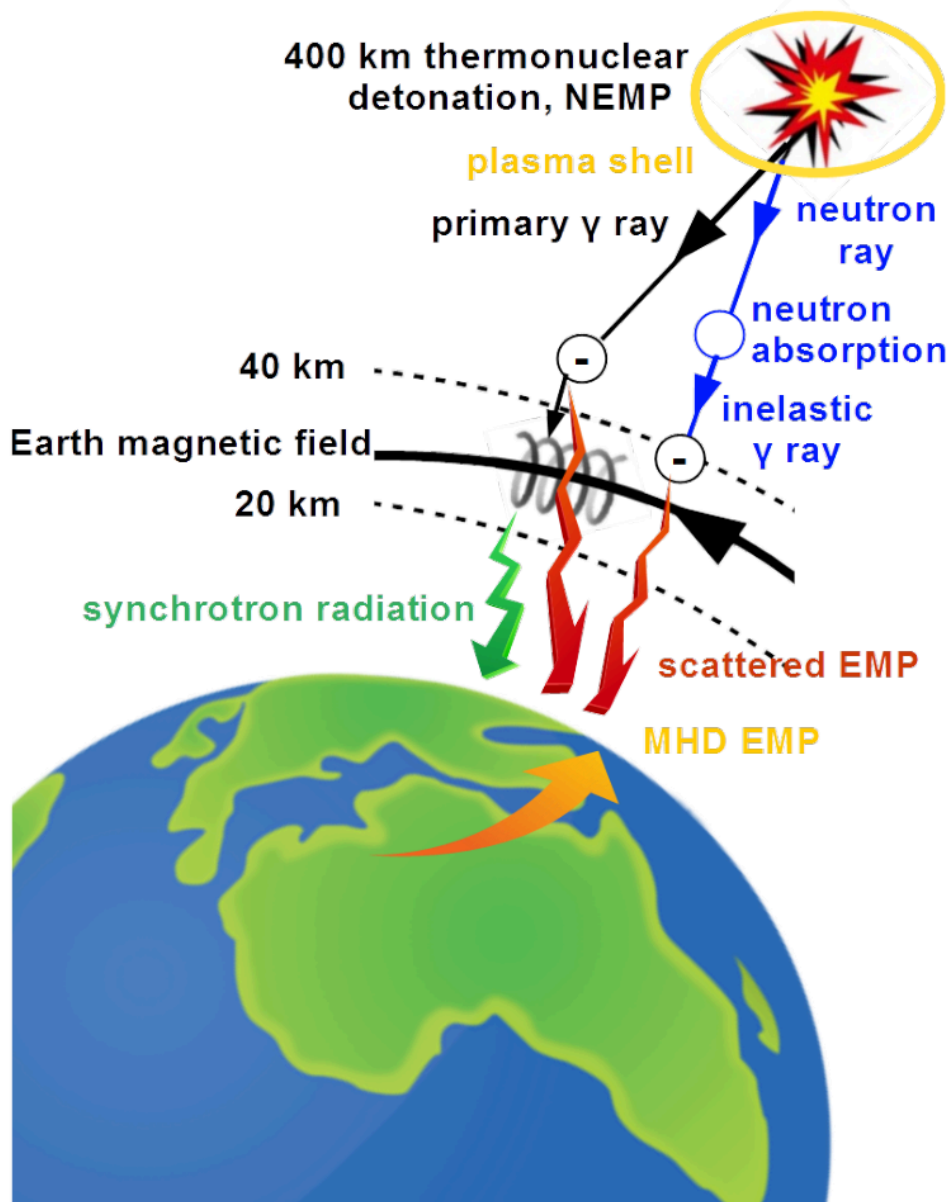


Figure 3.29: Illustration of NEMP propagating toward the Earth by high altitude nuclear explosion.

This movement of electrons with linear speed comparable with the light speed and deflected due to angular acceleration is accompanied with the synchrotron electromagnetic radiation like in the synchrotron. This is non ionizing electromagnetic pulse propagating with the speed of light. Standardized E1 pulse has $(1.8 - 2.3)ns$ rise time and $(23 \pm 5)ns$ half width. I.e. that energy of E1 is concentrated between DC and $1/(\pi \cdot 20ns) \approx 16MHz$ and pulse bandwidth reaches $BW = 1/(3.05ns) \approx 488MHz$. Standardized pulse peak value is $50kV/m$. Bigger field strength are non realistic due to strongly ionized air. By pure circular movement of electron the field strength of the synchrotron pulse is biggest.

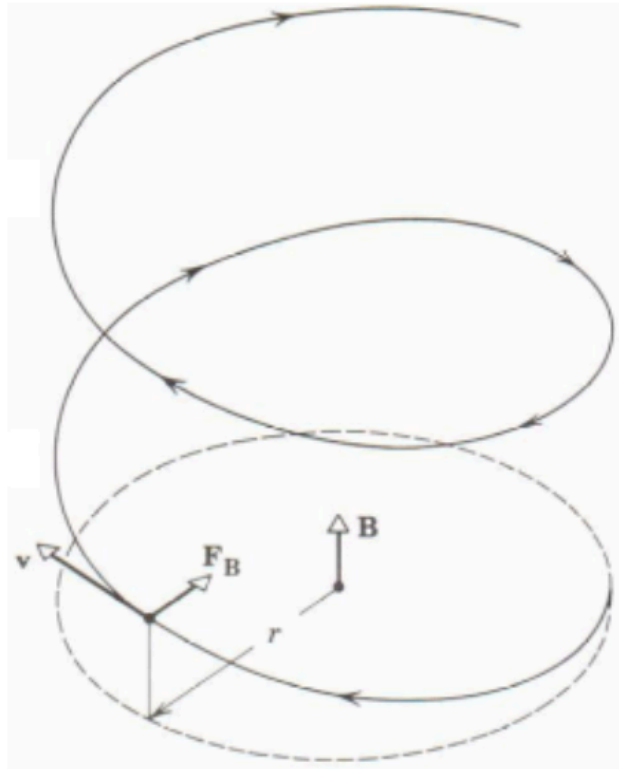


Figure 3.30: Helix trajectory of a charge moving in the Earth magnetic field, [Halliday].

E2 the intermediate time

Scattered γ rays, described above is one component of the E2 EMP. Another comes from neutron radiation. Neutrons are not able to ionize an atom directly. They can be absorbed by the stable atom. This collision is called inelastic one. By collision atom becomes unstable and is likely to emit the scattered EMP.

E2 has many similarities to thunderstorm lightning, described in chapter 3.3.4 but it is weaker.

E3 the late time

By thermonuclear explosion so called plasma shell around the source of explosion is built. It is also called plasma ball, light ball or magnetic bubble. It is volume with highly energized plasma which exhibits diamagnetical property. Obviously this bubble deforms the Earth's magnetic field like solar wind described in chapter 3.4. Moreover the plasma shell spreading toward the Earth comes to the region where it interacts with the Earth's magnetic field like in the MagnetoHydroDynamic MHD Generator. The Earth's magnetic field deflects charges of plasma. Positive in one direction, negative in opposite. This evokes strong electric field in the atmosphere oriented horizontally. It is the cause of geomagnetically induced currents in long high voltage power transmission lines and other installations like pipe lines or railroad tracks, as described in chapter 3.4. E3 lasts for about 100 s. It is much shorter than solar storm but it is more intensive.

In 1962 the USA carried out the program of the high altitude nuclear explosions named the Operation Fishbowl. It was launched in July with the 1.44 megaton bomb detonated at the height of 400 km above the Johnston Atoll at mid-Pacific Ocean. This experiment had the name the Starfish Prime. Electrical damage in Hawaii, about 1445 km away from detonation point were reported. The EMP in Hawaii was relatively weak, about 5.6 kV/m . Later calculations showed that if the Starfish Prime had been detonated over the northern continental US, the magnitude of the EMP would have been much larger, 22 kV/m to 30 kV/m due to greater strength of the Earth magnetic field over the US as well as its different orientation at bigger latitudes.

In the same time Soviet Union performed three high altitude nuclear explosions over Kazakhstan. This

program was called Soviet Project K Nuclear Tests. These weapons had only 300 kilotons but at the detonation place the Earth magnetic field is stronger than over the mid-Pacific Ocean. The damage caused by the resulting EMP was much greater than by the Starfish One. The third test called K-3, known also as Test 184 blew fuses and fired all overvoltage protectors in the telephone lines in the radius of 570km beneath the detonation point. There were also problems with ceramic insulators on the overhead electric power lines. Current induced in the long underground power line caused a fire in the power plant in the city of Karaganda.

Relevance of the frequency bandwidth BW

In the sections above the frequency bandwidth expressed with the formula $BW = 1/t_r$ is introduced. In [Clayton] it is asserted that by removal of spectral components above BW , the time domain reconstruction of the waveform is marginally distorted from the original one.

This estimate can be interpreted as minimal bandwidth of the low-pass filter which ensures practically undistorted pulse on the filter output. In other words, such filter is transparent for the waveform.

In definition of BW in [Clayton] the rise time $t_r = t_{100\%-0\%}$ of an ideal pulse is meant. Therefore real pulses verified with the rise time $t_{90\%-10\%}$ must be multiplied by factor 1.25 according to Eq.([t_c]) and Fig.([t_r]) in order to become the crest (front) time t_c which is better estimate of the $t_r = t_{100\%-0\%}$. It is done so by the ESD, HEMP and BURST pulses in Tab.3.4.

Table 3.4: Time – frequency relation by selected phenomena.

Phenomenon	Crest (front) time [ns]	Bandwidth [MHz]
ESD	3.000	1'000.000
HEMP, E1	3.125	320.000
BURST	6.250	160.000
SURGE, open circuit voltage	1'200.000	<0.834
SURGE, short circuit current	8'000.000	0.125
LEMP, direct current strike	10'000.000	0.100

Mind that oscilloscope is nothing else but low-pass filter. Therefore this definition of the bandwidth gives the hint for choice of the analogue bandwidth of the oscilloscope necessary for trusty recording of the series of pulses or single pulse.

4. Propagation of disturbances

There are four ways for disturbance to pass from the source to the victim, via:

- galvanic coupling,
- capacitive (electric) coupling,
- inductive (magnetic) coupling,
- wave coupling.

The first three accompany transmission of power or signals via conductors. It can proceed unsymmetrically or symmetrically.

Unsymmetrical transmission comes about when return conductor is common for more circuits and nonzero current as an overlay of currents of all circuits drives in the common return path. Three examples are shown in Fig.4.1. The return path can be identical with feeding lines or can differ with them.

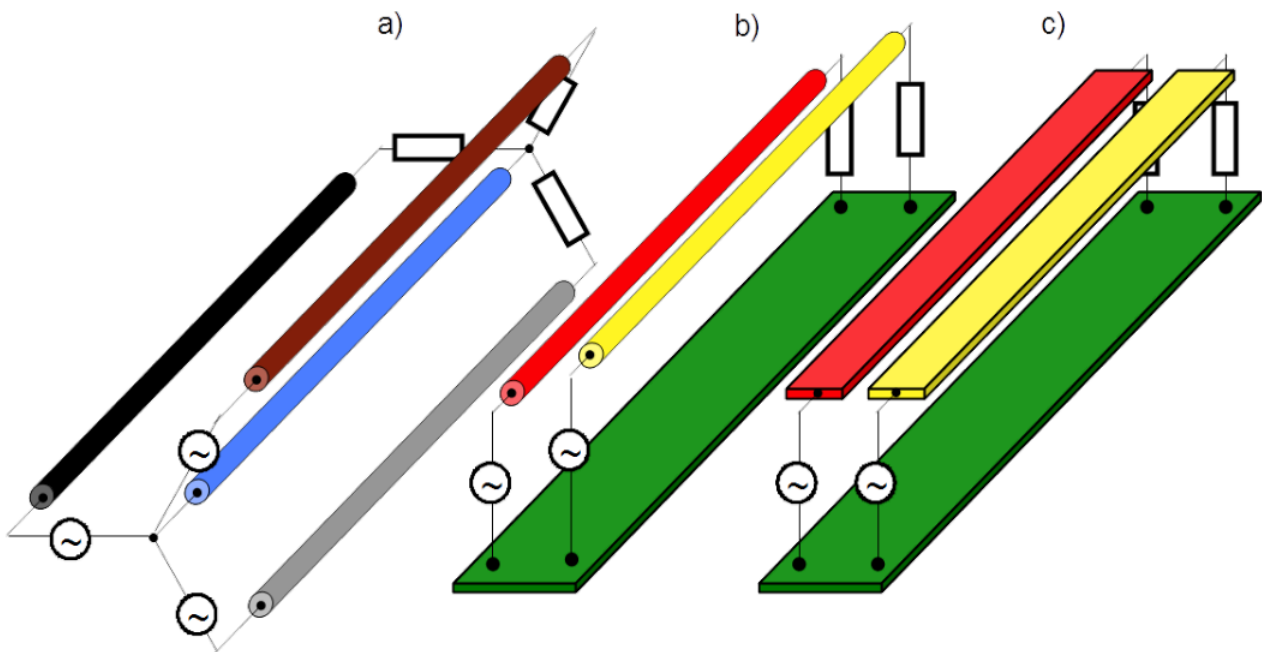


Figure 4.1: Three examples of unsymmetrical lines.

Symmetrical transmission is carried with a pair of identical conductors isolated from the surrounding. Examples are shown in Fig.4.2. There is always better or worse conducting layer beneath (striped plane) which builds the ground reference.

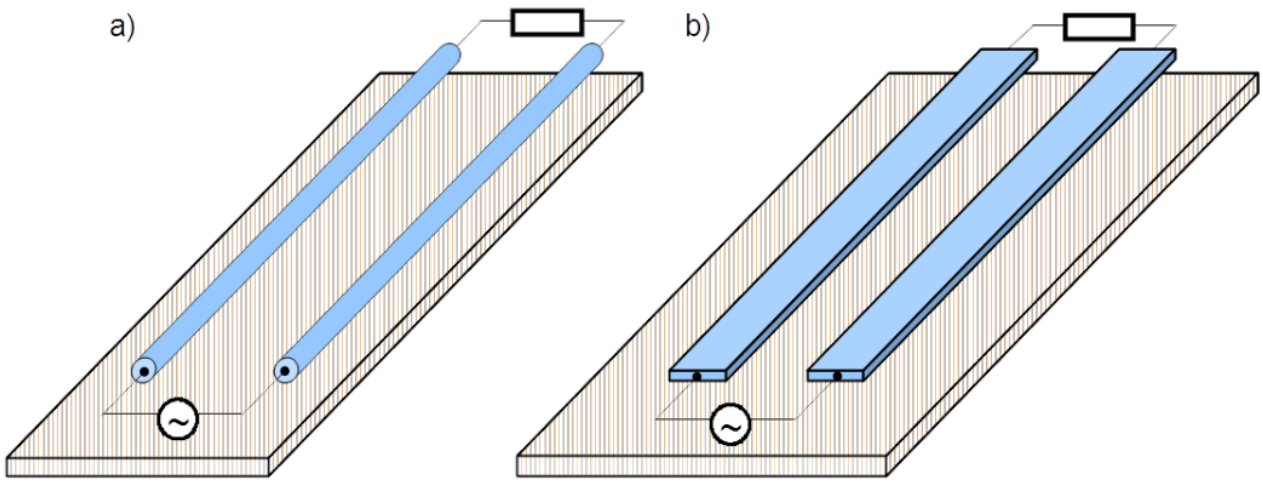


Figure 4.2: Two examples of symmetrical lines.

Unsymmetrical transmission is potentially accompanied with galvanic, capacitive and inductive coupling. Symmetrical transmission only with capacitive and inductive. They must be considered simultaneously. Here the phenomena will be presented separately in order to catch its essence. Such approach is violation of circuit theory, provide only one type of coupling is dominant, remaining negligible. It is case dependent.

Examples of unsymmetrical and symmetrical transmission

An example of unsymmetrical transmission is cabling of a sensor as shown in Fig.4.3 in which supply circuit V_{cc+} and signal circuit have the same return path GND .

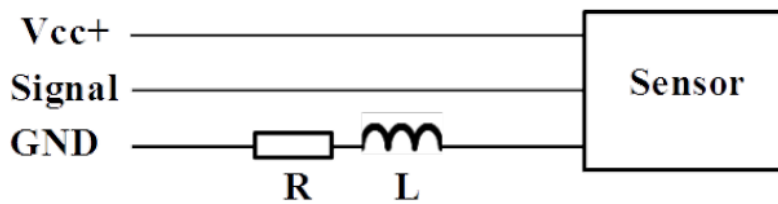


Figure 4.3: An example of galvanic coupling.

Another example is electrical installation in vehicles which very often is single ended. Return path is vehicle's chassis.

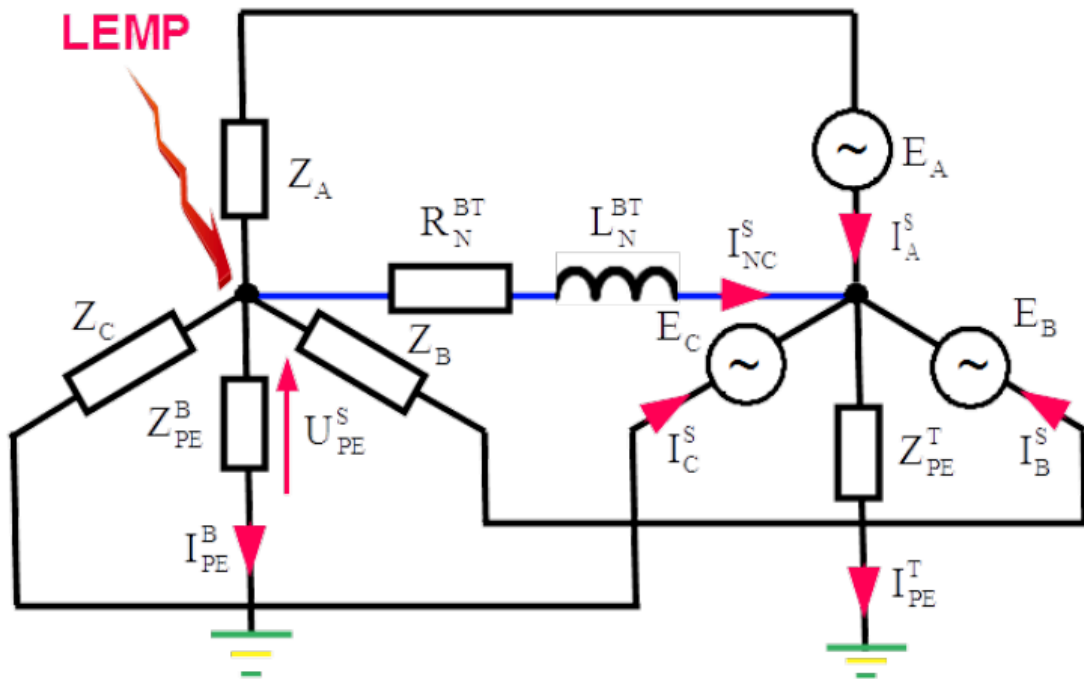


Figure 4.4: Surge due to galvanic coupling in TN-C mains supply system, by direct strike in the external lightning protection system of the building.

Mind that three phase supply system shown in Fig.4.1a) with Neutral (blue line) as return path is an example of unsymmetrical transmission as soon as current is driven in the neutral line. One case common for house installation is presented below.

Low voltage AC power is delivered to a house as shown in Fig.[Lemp_1] in chapter [Thunderstorm]. Regulations forces to carry out the supply line between the transformer and the building input as the TN-C system [IEC-60364-1]. It is four line supply system in which the Neutral line N acts just as well as the Protective Earth line PE , therefore it is called PEN line.

In Fig.4.4 electric circuit of the transformer with Line to Neutral EMF: E_A , E_B and E_C feeding the building with the four line system L_1 , L_2 , L_3 and PEN is shown. Z_A , Z_B and Z_C represents impedances of the whole building installation seen from the feeding point of the building. Z_{PE}^B and Z_{PE}^T are earthing impedances of the star point of the building and the transformer respectively. By direct strike of the lightning electromagnetic pulse $LEMP$ in the external lightning protection system of the building the current is driven to the star point of the building where it is split as shown with the red arrows in Fig.4.4. The biggest part of the current drives to the Earth through earthing impedance of the building Z_{PE}^B but due to the fact that between the building and the transformer there is common PEN line, part of the current is driven as the surge in the whole installation inside the building and between the building and the transformer.

Usually there are more customers supplied from one transformer, as shown in Fig.[Lemp_1]. Due to galvanic connection of all of them with the star point of the transformer, all customers experiences the surge with different degree.

More resistive against surges would be the TN-S system [IEC-60364-1]. It is five line supply system which has separate the Neutral N and the Protective Earth PE line.

Example of symmetrical transmission can be:

- power or signal cables of house installation layouted in the walls, ceilings or floors,

- cables layouted on the mounting plate in the control cabinet of a system,
- signal paths on the printed circuit board.

Galvanic coupling

Galvanic coupling is illustrated in Fig.4.5 with very simple situation. There is a circuit composed of two meshes. In mesh 1 there is a source of power or a signal with electromotive force EMF_1 and internal resistance R_{S1} and load R_{L1} . The second with EMF_2 and R_{L2} . Intension is to deliver electric power or signal from EMF_1 to R_{L1} and from EMF_2 to R_{L2} . However for some reason the two meshes have common return path represented with R_{GND} and L_{GND} which build the impedance

$$Z_{GND} = R_{GND} + j\omega L_{GND} \quad .$$

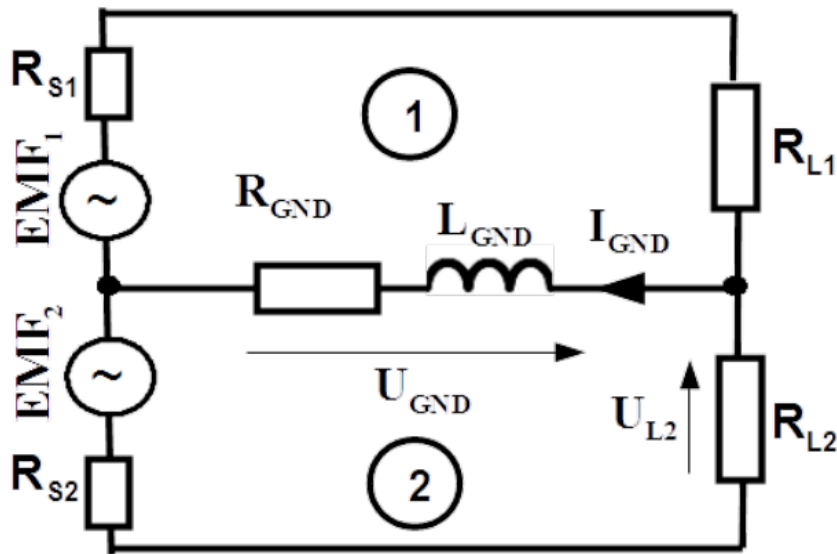


Figure 4.5: Explanation of galvanic coupling.

Each loop has self-inductance. It is composed of external inductance depending on wires layout and consequently on the area of the loop they build. Internal inductance of wires from which the loops are built also contribute to the total inductance. Obviously inductance must be assigned to the mesh but it is justified to extract the internal inductance of the common return path L_{GND} as shown in Fig.4.5 because it is the attribute of the return path. External inductances of both meshes and internal inductances of feeding wires are disregarded as declared earlier.

Voltage U_{GND} across the common return path represented with impedance Z_{GND} is as follows

$$U_{GND} = - \frac{\frac{EMF_1}{R_{S1}+R_{L1}} + \frac{EMF_2}{R_{S2}+R_{L2}}}{\frac{1}{R_{S1}+R_{L1}} + \frac{1}{R_{S2}+R_{L2}} + \frac{1}{Z_{GND}}} \quad (4.1)$$

Voltage U_{L2} across the load resistance R_{L2} in mesh 2 is as follows

$$U_{L2} = \frac{R_{L2}}{R_{S2} + R_{L2}} (EMF_2 - U_{GND}) \quad (4.2)$$

Electromotive force EMF_1 contributes to the voltage U_{L2} across the load of mesh 2 as follows

$$U_{L2}^{EMF_1} = - \frac{R_{L2} \cdot EMF_1}{(R_{S1} + R_{L1})(R_{S2} + R_{L2}) \left(\frac{1}{R_{S1} + R_{L1}} + \frac{1}{R_{S2} + R_{L2}} + \frac{1}{Z_{GND}} \right)} \quad (4.3)$$

The common return path causes unintentional contribution of EMF_1 to voltage across R_{L2} and vice versa, via galvanic coupling.

Obviously, coupled voltage $U_{L2}^{EMF_1}$ would disappear by zero voltage U_{GND} across the common return path. It can happen in two cases:

- by zero impedance of the return path $Z_{GND} = 0\Omega$. That is unrealistic to achieve.
- by total symmetry of the meshes i.e. if electromotive forces have the same amplitude and opposite phases. Moreover impedances of both paths are the same. In most cases it does not have sense by energy as well signal transmission.

Moreover perfect galvanic decoupling will happen with replacement of electromotive forces EMF_1 and EMF_2 with current sources. By power transportation it is hardly to imagine but transmission of current signals is used very often for that reason.

Intensity of galvanic coupling rises with increased impedance of the return path. By Z_{GND} tending to infinity, I_{GND} tends to zero and coupled voltage U_{L2} approaches maximum expressed with the formula below

$$U_{L2MAX}^{EMF_1} = \lim_{Z_{GND} \rightarrow \infty} U_{L2}^{EMF_1} = \frac{R_{L2} \cdot EMF_1}{R_{S1} + R_{S2} + R_{L1} + R_{L2}} \quad (4.4)$$

As galvanic coupling rises with increased internal impedance Z_{GND} of the common return path it is valuable to investigate frequency dependence of impedance Z_{GND} . This impedance depends on the shape of the cross section of the conductor. Considered are two cases for: round wire and rectangle cross section.

Internal impedance of round wire

Considered is idealized case of infinitely long strait wire with circular cross-section with radius r placed in free space in order to neglect proximity effects. Segment of such wire with length l is shown in Fig.4.6a).

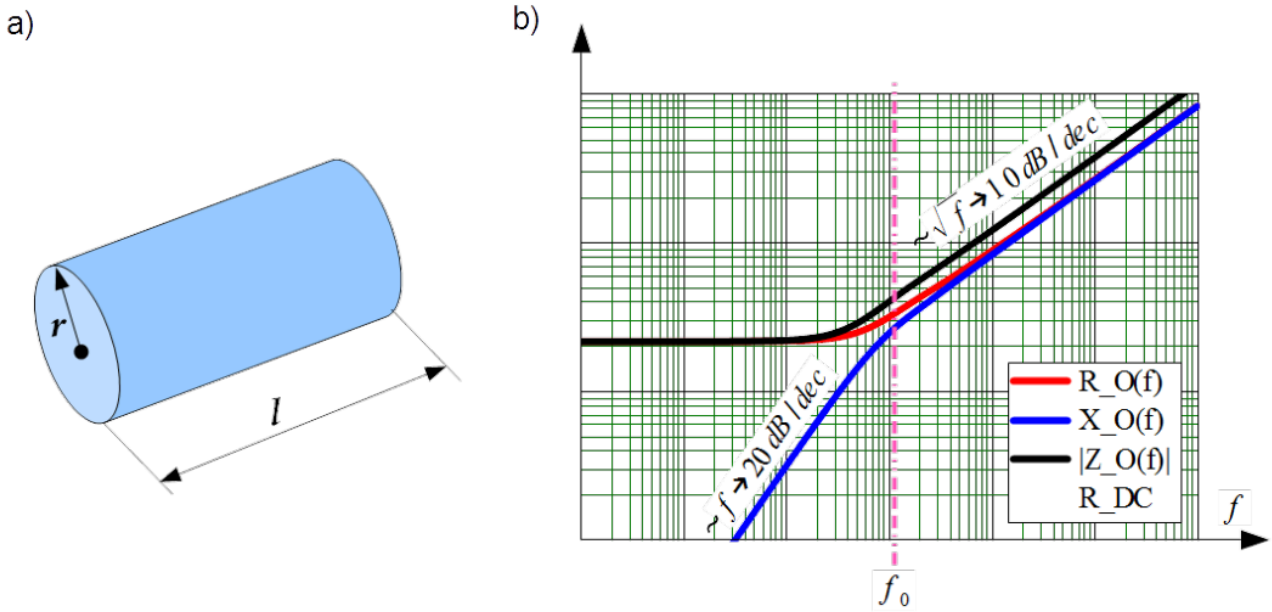


Figure 4.6: Frequency dependence of round wire impedance per unit length.

Impedance of such wire per unit length yields

$$Z(f) = \frac{k(f) J_0[k(f)r]}{2\pi r \sigma J_1[k(f)r]} \quad (4.5)$$

where $J_0[k(f)r]$ and $J_1[k(f)r]$ are Bessel's functions of zero and first order, σ and μ is conductivity and magnetic permeability of wire material respectively and $k(f)$ is the wave number in the wire material

$$k(f) = \frac{1-j}{\delta(f)} \quad (4.6)$$

$\delta(f)$ is called the skin depth

$$\delta(f) = \sqrt{\frac{2}{\omega \mu \sigma}} \quad (4.7)$$

which expresses depth in which current density is e times smaller than on the surface of the wire, where e is Euler's number. To be precise it is valid for plane wave facing infinite conducting medium oriented perpendicularly to the direction of the wave propagation.

By low frequencies the real part of impedance $Z(f)$, Eq.(4.5) is nothing else but DC resistance of the round wire

$$R_{LF} = \frac{1}{\pi \sigma r^2} \quad (4.8)$$

By high frequencies the real part of impedance $Z(f)$, Eq.(4.5) can be solved as if the current flowed uniformly through a layer of thickness equal to skin depth δ . The effective cross-sectional area for driving the current would be then approximately equal to skin depth δ times the conductor's circumference

$2r - \delta \approx 2r$. Thus HF resistance of round wire is approximately equal to DC resistance of a hollow tube with wall thickness $2r - \delta \approx 2r$ carrying direct current

$$R_{HF}(f) = \frac{1}{\pi \sigma [2r - \delta(f)] \delta(f)} \approx \frac{1}{2\pi \sigma r \delta(f)} \quad (4.9)$$

Static and low frequency inductance of the round wire, accompanying uniformly flowed current is independent on wire radius r [Clayton]

$$L_{DC} = \frac{\mu}{8\pi} \quad (4.18)$$

Thus the imaginary part of impedance $Z(f)$, Eq.(4.5) i.e. reactance $X_{LF}(f)$ in low frequencies depends linearly on frequency

$$X_{LF}(f) = 2\pi f L_{DC} \quad (4.11)$$

By high frequencies reactance and resistance are equal $X_{HF}(f) = R_{HF}(f)$. It can be explained with the plane electromagnetic wave penetrating good conducting medium. The wave impedance has then equal real and imaginary part.

Frequency dependence of the internal impedance of the round wire in double logarithmic scale is illustrated in Fig.4.6b). Breaking frequency f_0 marked there, which is border between low and high frequency regions can be established equating LF resistance and reactance

$$f_0 = \frac{4}{\pi\mu\sigma r^2} \quad (4.12)$$

Mind that low frequency reactance is proportional to frequency, therefore it is straight line with the slope $20dB/dec$, compare Eq.(4.11). The HF resistance and reactance are reciprocally proportional to the skin depth $\delta(f)$, see Eq.(4.9) therefore they increase proportionally to the square root of frequency. In other words they have slopes $10dB/dec$. Module of high frequency impedance $|Z_{GND}(f)|$ is by factor $\sqrt{2}$ bigger than HF resistance or reactance, because they are equal one to another. In double logarithmic scale it is bigger about $3dB$.

Eq.(4.12) gives the hint how to keep impedance of the round wire small up to relatively high frequencies. The trick consists in keeping the radius r of wire relatively small. It is done in so called HF litz-wire in which wire is composed of bundle of individually isolated strands, as shown in Fig.4.7.

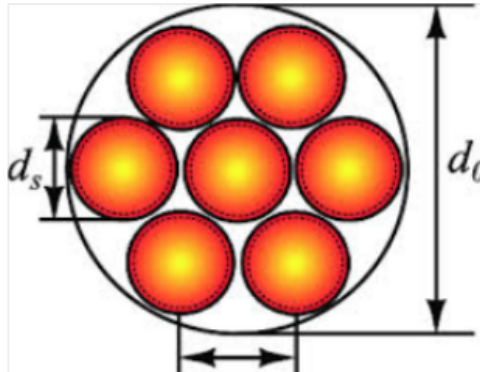


Figure 4.6: High frequency litz-wire built of seven isolated strands.

In such wire, in spite of the cross-section equal to sum of cross-sections of individual strands, the breaking frequency Eq.(4.12) is correlated with individual strand¹.

Internal impedance of conductor with rectangular cross section

Considered is idealized case of infinitely long straight conductor with rectangular cross section with width w and thickness t placed in free space in order to neglect proximity effects. Segment of such wire with length l is shown in Fig.4.8a).

Unlike by round wire no analytical formula exist for such conductor.

The low frequency resistance yields

$$R_{LF} = \frac{1}{\sigma w t} \tag{4.13}$$

By high frequencies resistance can be solved as by round wire i.e. as if the current flowed uniformly through a layer of thickness equal to skin depth δ . The effective cross-sectional area for driving the current would be then approximately equal to skin depth δ times the conductor's circumference $2(w + t)$. Thus HF resistance of round wire is approximately equal to DC resistance of a hollow rectangular tube with wall thickness δ carrying direct current [Clayton_MTL]

$$R_{HF}(f) = \frac{1}{2\sigma\delta(f)(w + t)} \tag{4.14}$$

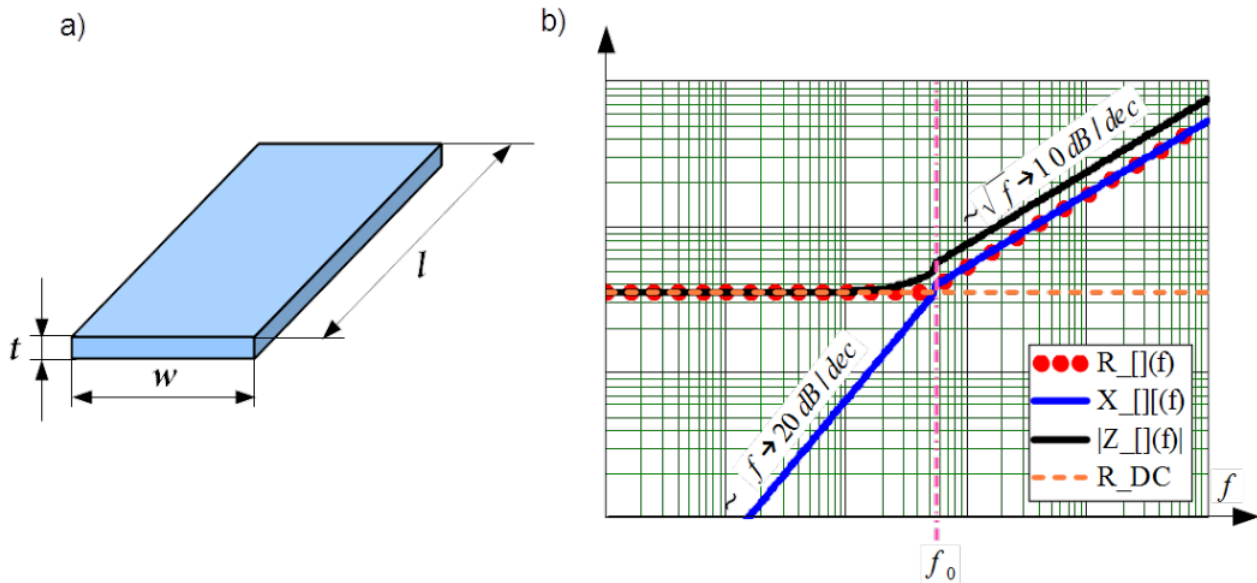


Figure 4.8: Frequency dependence of impedance of conductor with rectangular cross section.

Prime to derivation of static and low frequency inductance of the conductor, distribution of magnetic field inside the conductor must be considered. If in the whole cross section uniformly distributed current I is driven, then circulation of magnetic field along the rectangular circumference shown with dashed line in Fig.4.9 yields

$$2 \cdot H_x(y) \cdot 2x + 2 \cdot H_y(x) \cdot 2y = \frac{I}{wt} \cdot 4xy \tag{4.16}$$

$$H_x(y) = \frac{I}{wt} \cdot y \tag{4.16}$$

This is valid only if $H_x(y)$ is constant along the whole length of horizontal sides and contribution of circulation along vertical sides can be neglected. These rough simplification are justified provide $w \gg t$.

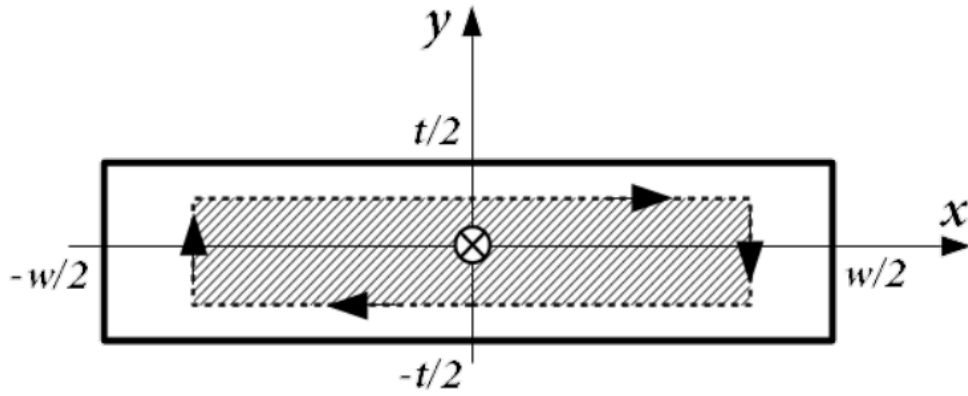


Figure 4.9: $\vec{H}(x, y)$ circulation inside the conductor with rectangular cross section.

Internal inductance can be directly computed from energy relation by equating magnetic energy stored inside the conductor expressed with magnetic field strength $\vec{H}(x, y)$ to the same energy expressed with the internal inductance L_{DC}

$$\frac{1}{2}L_{DC}I^2 = \frac{\mu}{2} \int_S |H(x, y)|^2 dS = \frac{\mu}{2} \cdot \frac{I^2}{w^2 t^2} \int_{-w/2}^{w/2} dy \int_{-t/2}^{t/2} x^2 dx \quad (4.17)$$

Finally

$$L_{DC} = \frac{\mu}{12} \cdot tw \quad (4.18)$$

Breaking frequency f_0 can be established as by the round wire with equating LF resistance and reactance

$$f_0 = \frac{6}{\pi \mu \sigma t^2} \quad (4.19)$$

Frequency dependence of the internal impedance of conductor with rectangle cross section in double logarithmic scale is illustrated in Fig.4.8b). Qualitatively it is identical with behavior of the round wire shown in Fig.4.6b).

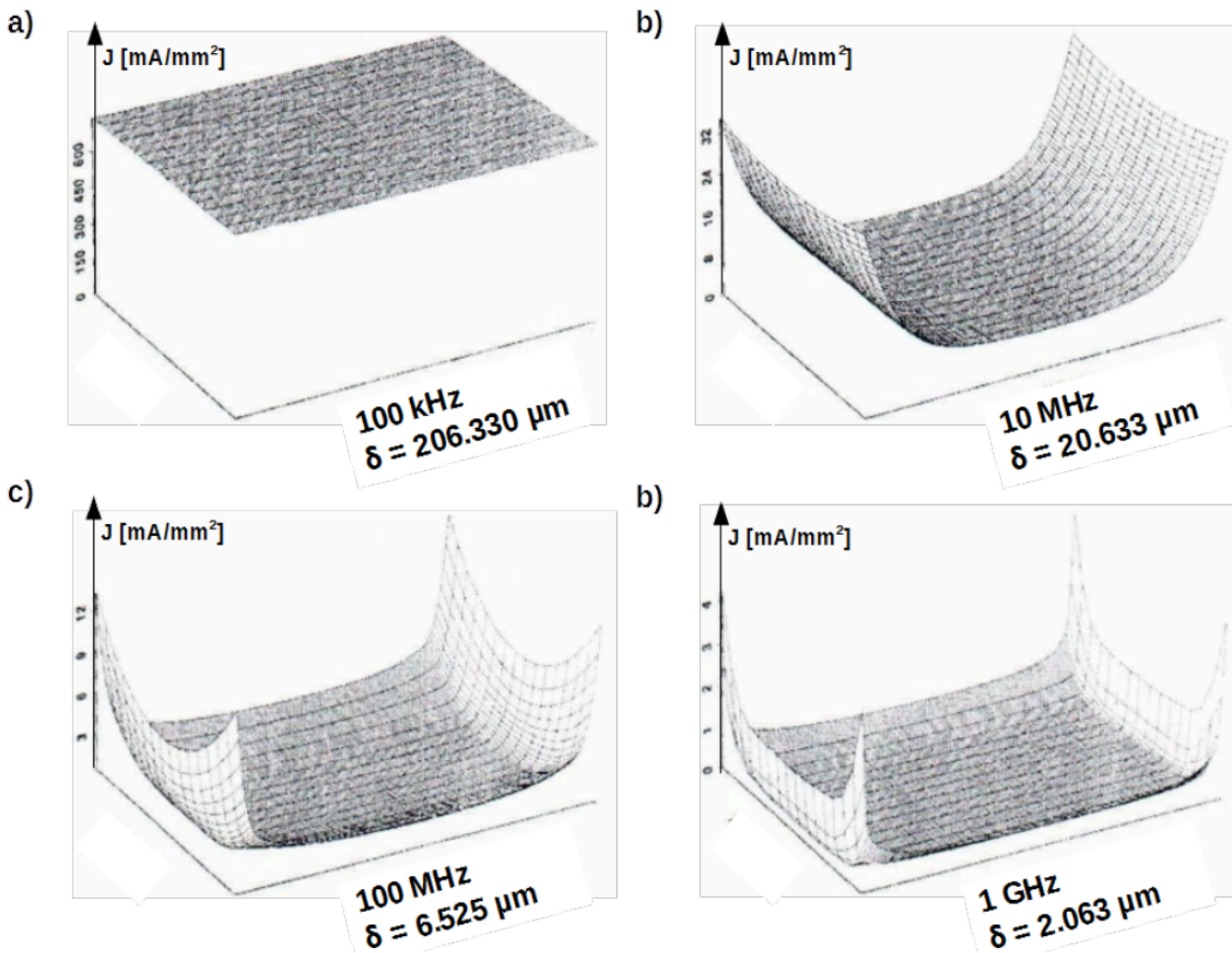


Figure 4.10: Distribution of current density in the rectangular conductor with width $w = 381\mu m$ and thickness $t = 35.56\mu m$.

An example of distribution of current density in the rectangular conductor in frequency dependence, sourced from [Clayton_MTL] is shown in Fig.4.10. Features notable in it are summarized below:

- current crowding toward the outer edge is remarkable only in direction for which the skin depth $\delta(f)$ is much smaller than the side of the rectangle,
- current which is the integral of current density $J(x, y)$ over the cross section surface is the smaller the bigger frequency is, because impedance of conductor rises,
- proportionality of the skin depth $\delta(f)$ to the square root of frequency \sqrt{f} can be confirmed.

Precedence of rectangular conductor over round wire

It is desired to compare impedance Z_{GND} of the common path for different shape of the cross section because as presented in previous sections it is shape dependent.

Breaking frequency is the upper bound of the frequency by which internal impedance is kept relatively deep i.e. impedance is only slightly bigger than DC resistance. Comparison of Eq.(4.12) and Eq.(4.19) shows unequivocally that f_0 is much bigger for conductor with rectangle cross section. Indeed in case of rectangle

cross section the number in numerator is bigger than by round wire, 6 instead of 4 but crucial is thickness in square in denominator which by $w \gg t$ is much smaller than square of radius r in case of round wire. By comparison of HF litz-wire and rectangle conductor the break frequencies can be similar but costs of HF litz-wire exceeds pretty costs of ordinary solid conductor.

This rationalises precedence of rectangular conductor over round wire. The wider conductor with rectangle cross section by unchanged thickness the smaller low frequency resistance R_{LF} . Therefore as shown in Fig.[Unsym_line]c) by double layers' PCBs the return path are as wide as practical and by multilayers' PCBs separate layer or even more layers are dedicated to the return paths.

Electric (capacitive) and magnetic (inductive) coupling

Capacitive coupling

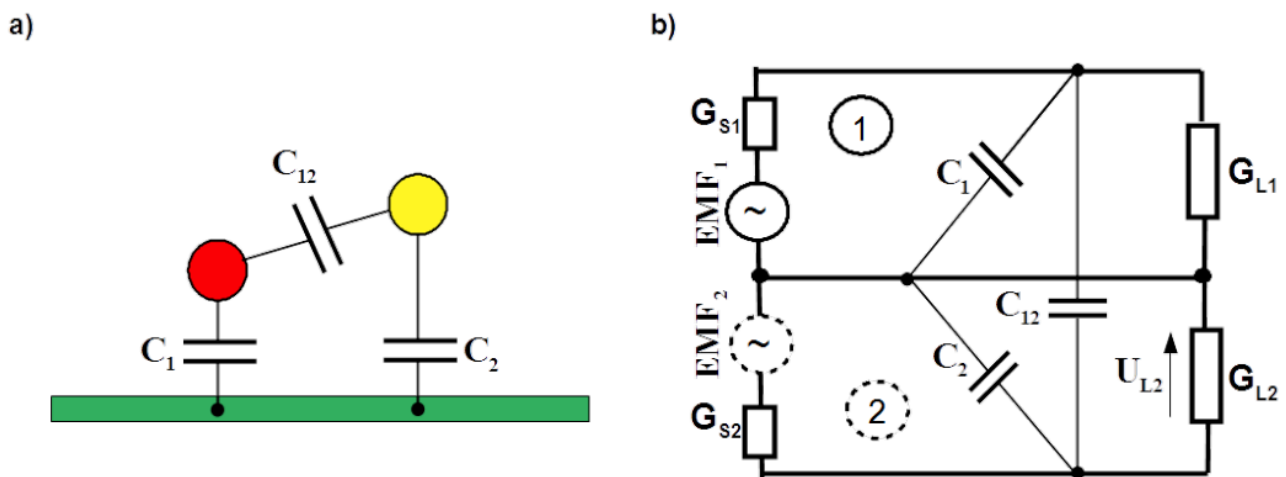


Figure 4.11: Illustration of capacitive coupling by unsymmetrical transmission: cross sectional view a), top view b).

Total voltage across load conductance G_{L2} yields

$$U_{L2_{total}} = \frac{G_{S2}(G_{L1} + G_{S1} + Y_1 + Y_{12}) \cdot EMF_2 + G_{S1}Y_{12} \cdot EMF_1}{(G_{L1} + G_{S1} + Y_1)(G_{L2} + G_{S2} + Y_2) + Y_{12}(G_{L1} + G_{L2} + G_{S1} + G_{S2} + Y_1 + Y_2)} \quad (4.20)$$

where $Y = j\omega C$ is admittance of a capacitor

Electromotive force EMF_1 contributes to the voltage U_{L2} across the load conductance G_{L2} of mesh 2 as follows

$$U_{L2} = \frac{G_{S1}Y_{12} \cdot EMF_1}{(G_{L1} + G_{S1} + Y_1)(G_{L2} + G_{S2} + Y_2) + Y_{12}(G_{L1} + G_{L2} + G_{S1} + G_{S2} + Y_1 + Y_2)} \quad (4.21)$$

Obviously, coupled voltage U_{L2} would be zero by zero mutual capacitance C_{12} , $Y_{12} = 0 \frac{1}{\Omega}$. That

is unrealistic. There exist always capacitance between two metallic objects as signal or power lines. Even replacement of electromotive forces EMF_1 and EMF_2 with current sources does not liberate from capacitive coupling.

Inductive coupling

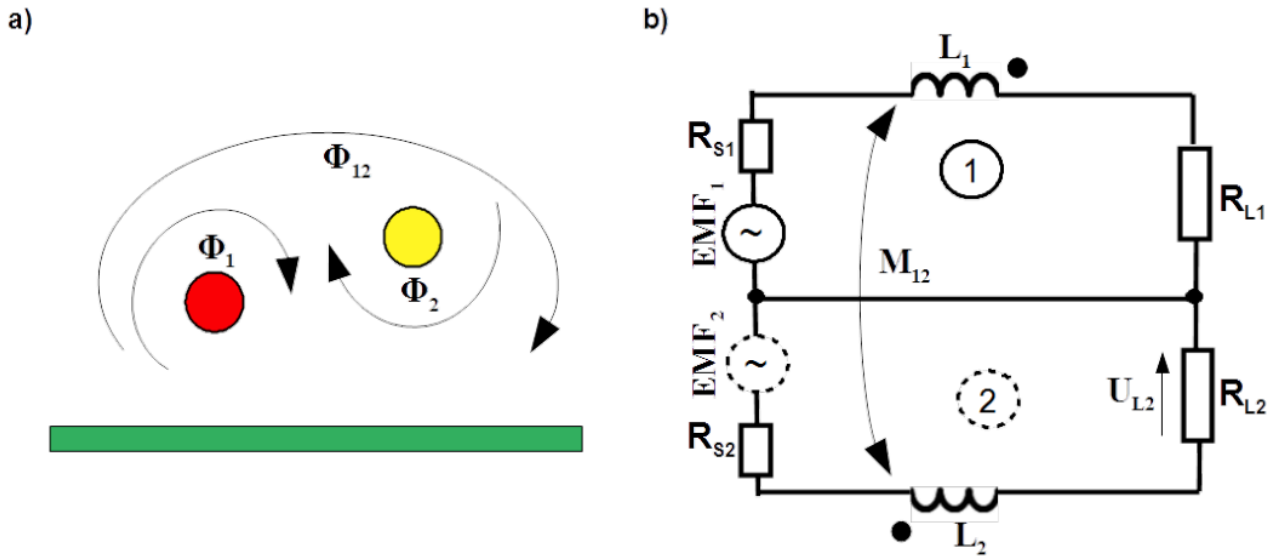


Figure 4.12: Illustration of inductive coupling by unsymmetrical transmission: cross sectional view a), top view b).

Total voltage across load resistance R_{L2} yields

$$U_{L2total} = \frac{R_{L2}}{R_{L2} + R_{S2} + Z_2 + Z_{12}} \left[EMF_2 - \frac{EMF_1}{\frac{1}{R_{L1} + R_{S1} + Z_1 + Z_{12}} + \frac{1}{R_{L2} + R_{S2} + Z_2 + Z_{12}} - \frac{1}{Z_{12}}} + \frac{EMF_2}{R_{L2} + R_{S2} + Z_2 + Z_{12}} \right] \quad (4.22)$$

where $Z_1 = j\omega L_1$ and $Z_2 = j\omega L_2$ are impedances of self inductances L_1 and L_2 respectively. $Z_{12} = j\omega M_{12}$ is impedance of a mutual inductance M_{12} . It depends on self inductances as follows $M_{12} = k\sqrt{L_1 L_2}$ where $0 < k < 1$ is coupling factor.

Electromotive force EMF_1 contributes to the voltage U_{L2} across the load resistance R_{L2} of mesh 2 as follows

$$U_{L2} = \frac{-\frac{R_{L2}}{R_{L2} + R_{S2} + Z_2 + Z_{12}} \cdot EMF_1}{\left[\frac{1}{R_{L1} + R_{S1} + Z_1 + Z_{12}} + \frac{1}{R_{L2} + R_{S2} + Z_2 + Z_{12}} - \frac{1}{Z_{12}} \right] (R_{L1} + R_{S1} + Z_1 + Z_{12})} \quad (4.23)$$

Obviously, coupled voltage U_{L2} would be zero by zeroised coupling factor k . Though it can be kept on very low level, it is never equal to zero.

Replacement of electromotive forces EMF_1 and EMF_2 with current sources liberate from inductive coupling.

Dependence of capacitance and external inductance on cross section's shape

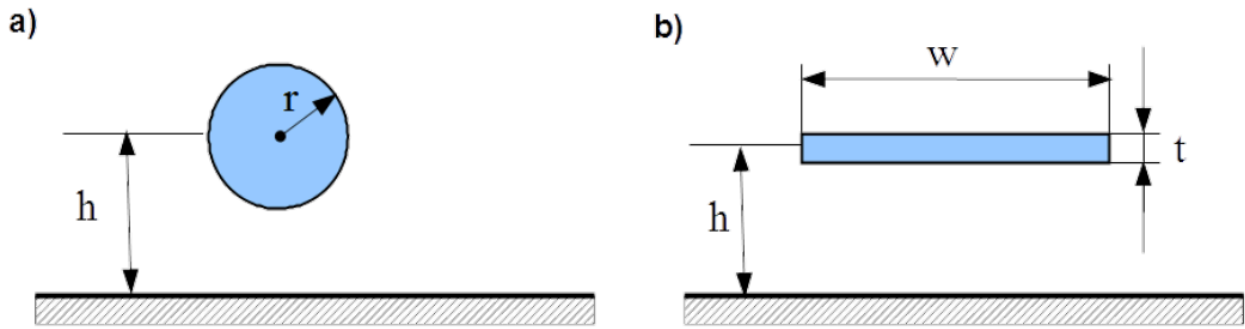


Figure 4.13: Illustration for consideration of capacitance and external inductance.

Capacitance per unit length of a infinitely long strait wire with circular cross section, layouted in air parallel to infinite conducting plane, as shown in Fig.4.13a) yields [Clayton]

$$C_{\circ} = \frac{2\pi\epsilon_0}{\text{ar cosh}\left(\frac{h}{r}\right)} \quad (4.24)$$

where $\text{ar cosh}(x) = \ln\left[\sqrt{x^2 - 1} + x\right] \approx \ln(2x)$ for $x \gg 1$. Therefore for a wire that is sufficiently far from the conducting plane, $h \gg r$ this simplifies to

$$C_{\circ} \approx \frac{2\pi\epsilon_0}{\ln\left(\frac{2h}{r}\right)} \quad \text{for } h \gg r \quad (4.25)$$

As explained in chapter [El size], wave propogates along a transmission line if it is electrically long. Velocity of propagation is the quantity that binds parameters μ and ϵ of the surrounding medium with per length parameters L and C of the transmission line. On one side it is given as in Eq.([v_propagation]), on the other side as $v = \frac{1}{\sqrt{LC}}$. Therefore by homogeneous surrounding of transmission line holds

$$LC = \mu\epsilon \quad (4.26)$$

This straightforwardly leads to formulas for external inductance of the round wire

$$L_{\circ}^{EXT} = \frac{\mu_0}{2\pi} \text{ar cosh}\left(\frac{h}{r}\right) \quad (4.27)$$

$$L_{\circ}^{EXT} \approx \frac{\mu_0}{2\pi} \ln\left(\frac{2h}{r}\right) \quad \text{for } h \gg r \quad (4.28)$$

There exist no general analytical formula for parameters of conductor with rectangular cross section. Cited here is approximate relation for the case shown in Fig.4.13b), according to [Clayton], assuming zero thickness of conductor

Formula does not parse

Formula does not parse

Capacitance of the round wire with 2.5mm^2 cross section area i.e. with radius $= 0.892\text{mm}$ layouted $h = 1\text{cm}$ above ground plane, according to Eq.(4.25) amounts to $C_{\circ} = 17.89\text{pF}/\text{m}$. Rectangular conductor with the same cross section area and longer size $w = 2\text{cm}$ has shorter size $t = 0.125\text{mm}$. According to Eq.(4.29) its capacitance is

Formula does not parse

Analogue is with external inductance. By the same geometry relations, according to Eq.(4.28) external inductance of the round wire amounts to $L_{\circ}^{EXT} = 0.622\mu\text{H}/\text{m}$ and by rectangular conductor is

Formula does not parse, according to Eq.(4.30).

In numerical example above capacitance/external inductance is smaller/ bigger for a round wire/ rectangular conductor. This example is realistic and the relation can be generalized. Rationale of it is rooted

in the Euclidean geometry. It is taught there, that from all plane figures, the circle has the smallest ratio of circumference to surface area.

Let us compare capacitances. The Gauss's flux theorem is a law relating the distribution of electric field to charges originating it. The electric flux through any hypothetical closed surface S is equal to the net electric charge Q within that closed surface **Formula does not parse**. For infinite straight conductor the electric flux can be calculated through the surface per unit length and therefore it is reduced to the integral along arbitrary closed loop enclosing the conductor.

Let us compare round wire and rectangular conductor with the same surface area, layouted on the same height h above the ground plane. For round wire the integration path is shorter than for rectangular conductor, due to ratio of circumference to area. Therefore if in both cases net charge is the same, electric field strength distributed around rectangular conductor is smaller.

Voltage across conductor and the ground plane is given by the line integral of electric field along arbitrary path between them $U = \int_l \vec{E} \cdot d\vec{l}$. Consequently it is smaller in case of rectangular conductor.

Capacitance is ratio of free charge on the conductor or the ground plane to voltage necessary for gathering this amount of charge $C = Q/U$. Conclusion is that, for gathering particular net charge less voltage is needed in case of rectangular conductor than of round wire. Finally, capacitance of rectangular conductor is bigger than of round wire.

Similarly can be proceeded by comparing external inductances. The Ampere's circular law relates the distribution of magnetic field strength to current causing it. The line integral of magnetic field strength \vec{H} along any hypothetical closed loop l is equal to the net current I enclosed in this loop

$$\oint_l \vec{H} \cdot d\vec{l} = \sum I$$

Let us compare round wire and rectangular conductor with the same surface area, layouted on the same height h above the ground plane. For round wire the integration path is shorter than for rectangular conductor, due to ratio of circumference to area. Therefore if in both cases enclosed net current is the same, magnetic field strength distributed around rectangular conductor is smaller.

Magnetic flux through any hypothetical surface built by the loop driving current I is given by **Formula does not parse**. For infinite loop composed of round wire or rectangular conductor, lead in infinity and the ground plane as return path, only flux per unit length makes sense. It is smaller in case of rectangular conductor due to smaller field strength. Inductance is ratio of magnetic flux to current necessary for generating it $L = \Phi/I$. It means that, by driving the same particular net current less flux is generated in case of rectangular conductor than of round wire. Finally, inductance of rectangular conductor is smaller than of round wire.

This statement can be rationalised alternatively starting with comparison of capacitances along with conclusion from Eq.(4.26).

Notice, that capacitance/external inductance of the round wire rises/decays slower with increased radius r than capacitance/external inductance of the rectangular conductor with its width w . In the first case the change is compressed because radius is argument of natural logarithm. In the second case, dependence on width w is direct.

Capacitive and inductive coupling by symmetrical transmission

Up to now only unsymmetrical transmission was covered. The only message concerning symmetrical transmission discussed here is the size of zone surrounding transmission line in which risk of capacitive or inductive coupling exist.

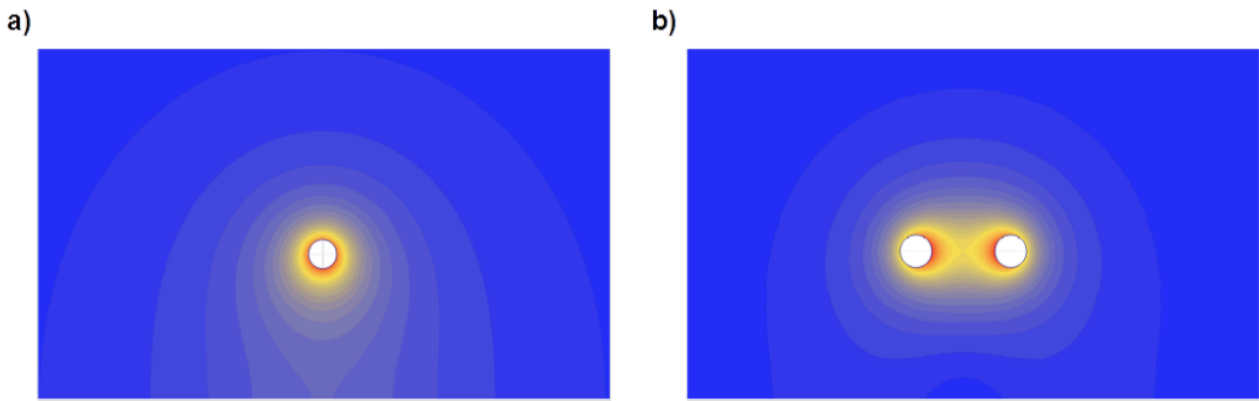


Figure 4.14: Module of electric field strength around unsymmetric a) and symmetric b) transmission line with round wire.

In Fig.4.14 distribution of module of electric field strength around unsymmetric and symmetric transmission line with round wire is illustrated. The same voltage is applied and spectrum of colours has the same scale in both cases.

Evidently the zone polluted with the electric field in case of symmetrical transmission is smaller. Module of electric field strength by symmetrical line decays stronger versus distance from the line in horizontal as well vertical direction. Rationale for it is the fact that space between feeding and return line in case of symmetrical transmission is much smaller than in case of unsymmetrical transmission. Fields outside the line cancel one another. As a consequence of it, zone with practically total cancellation of field is closer to the line in the case of symmetrical transmission.

The same can be concluded for unsymmetrical and symmetrical lines build of conductors with rectangular cross sections as shown in Fig.4.15.

In Fig.4.16 distribution of module of magnetic field strength around unsymmetric and symmetric transmission line with round wire is illustrated. The same current is driven and spectrum of colours has the same scale in both cases.

Evidently the zone polluted with the magnetic field in case of symmetrical transmission is smaller.

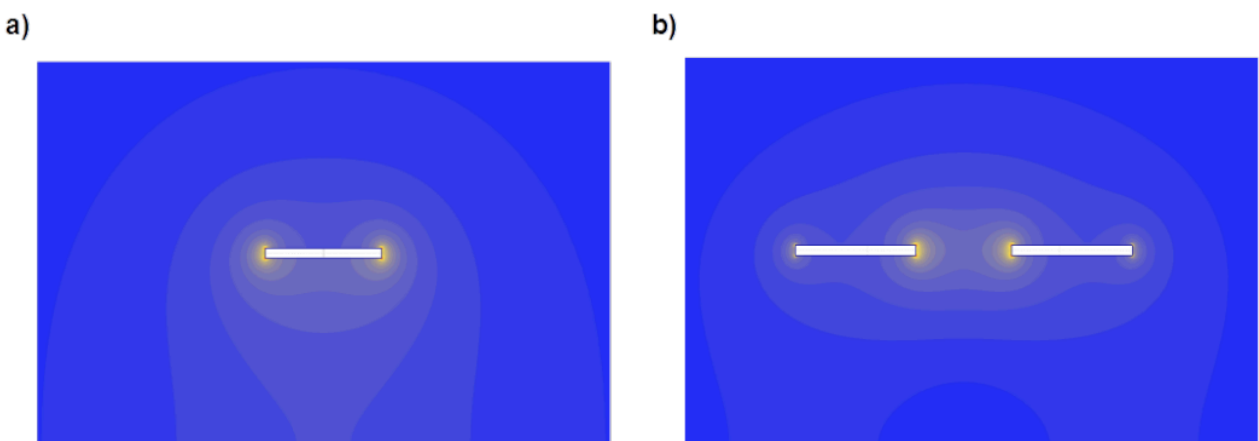


Figure 4.15: Module of electric field strength around unsymmetric a) and symmetric b) transmission line with conductor having rectangle cross section.

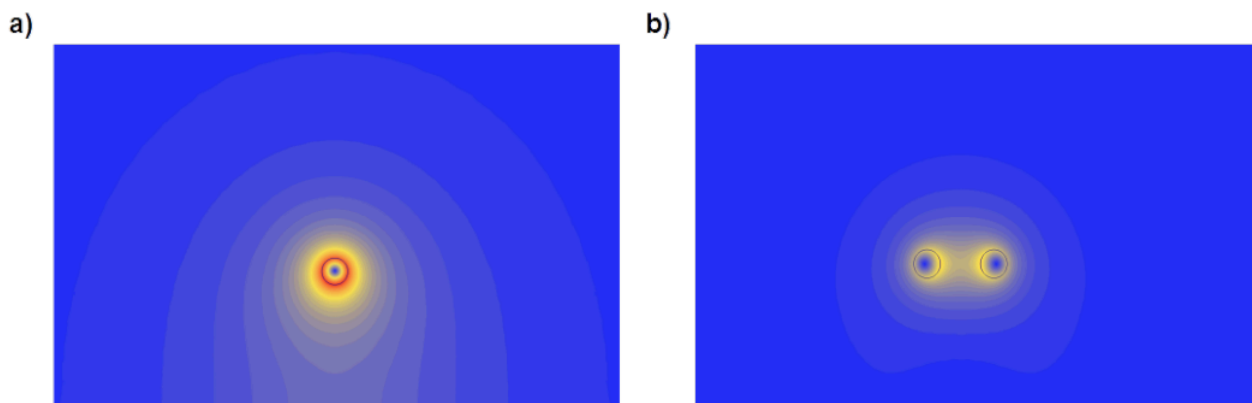


Figure 4.16: Module of magnetic field strength around unsymmetric a) and symmetric b) transmission line with round wire.

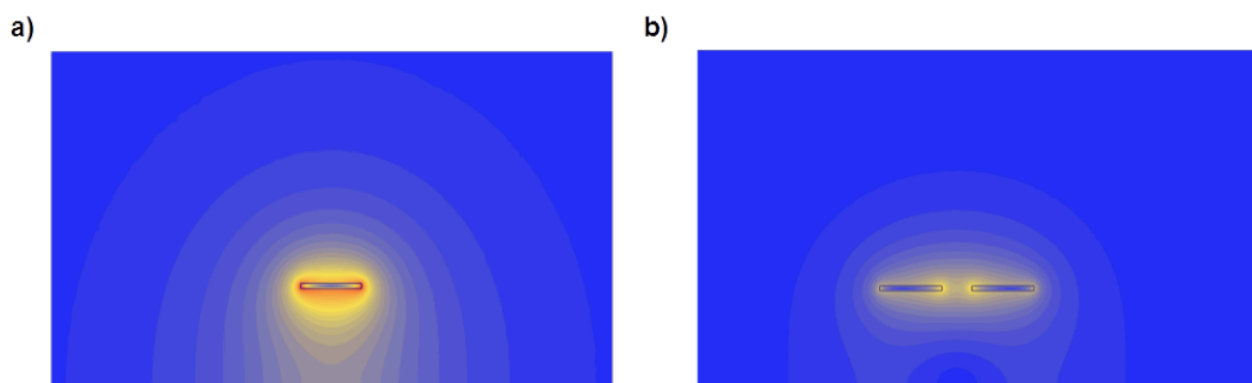


Figure 4.17: Module of magnetic field strength around unsymmetric a) and symmetric b) transmission line with conductor having rectangle cross section.

The same can be concluded for unsymmetrical and symmetrical lines build of conductors with rectangular cross sections as shown in Fig.4.17.

Transverse to longitudinal conversion

Equivalent scheme of symmetric transmission is shown in Fig.4.18. Energy or signal should be delivered from the source EMF with internal resistance R_S to the load R_L via symmetrical line. This line is layouted above the ground. Each line i.e. feeding: 1-3 and return: 2-4 has parasitic capacitance related to the ground. They are represented with capacitances C_{10} and C_{20} by the source and C_{35} and C_{45} by the load. There are also parasitic capacitances of one to another line. They are represented with capacitances C_{12} by the source and C_{34} by the load. Moreover each line builds inductance represented with L_{13} and L_{24} .

Symmetric transmission means that parasitic parameters are in equilibrium consisted in following

$$\begin{aligned} C_{10} &= C_{20} \\ \text{identities } C_{35} &= C_{45} \\ L_{13} &= L_{24} \end{aligned}$$

In such situation $U_{50} = 0$. Transmission line is perfectly balanced.

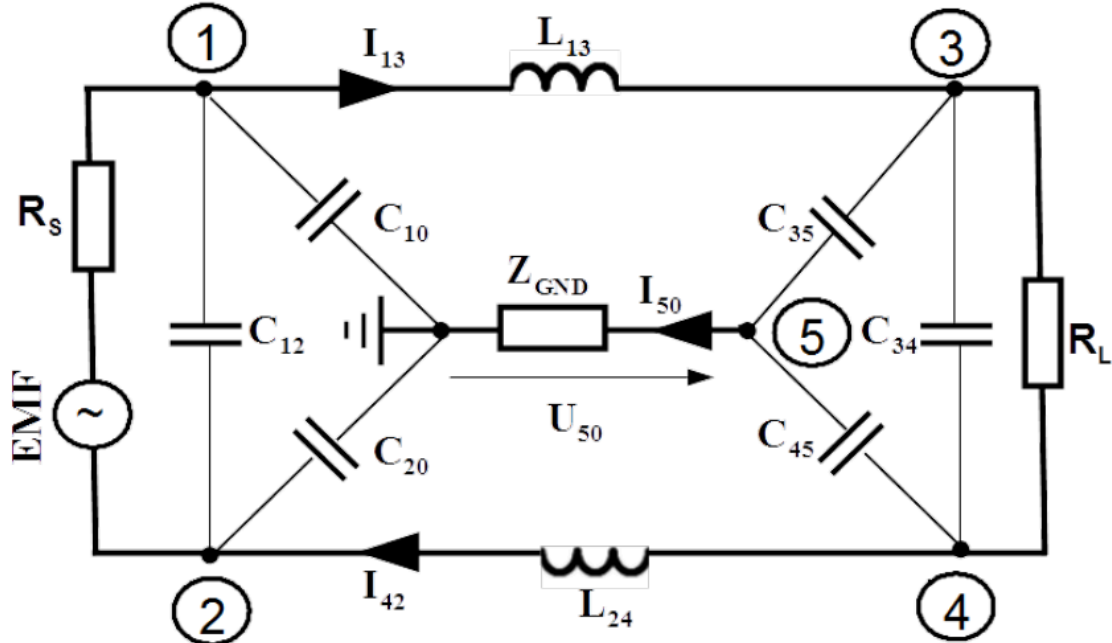


Figure 4.18: Symmetrical transmission over the ground plane, top view.

Electromotive force EMF , which is oriented crosswise to the direction of transmission generates voltage U_{50} along direction of transmission only if the circuit is out of balance.

Ratio of transverse electromotive force EMF to longitudinal voltage U_{50}

$$\begin{aligned} L_{TC} &= \frac{EMF}{U_{50}} \\ L_{TC(dB)} &= 20 \log\left(\frac{EMF}{U_{50}}\right) \end{aligned} \tag{4.35}$$

is called loss of transverse (to longitudinal) conversion, alternatively Transverse Conversion Loss TCL. It is used for rating deviation from the ideal balance by symmetrical transmission. By approaching perfect equilibrium, L_{TC} tends to infinity.

There are two reasons for transverse conversion to be undesired: deterioration of integrity of transmitted signal and enlargement of the zone around the line polluted with the electromagnetic field, similarly as by unsymmetrical transmission.

Decomposition of currents into common and differential mode

In this subsection currents in the transmission line shown in Fig.4.18 will be derived. For suppressing complexity of the formulas, source resistance R_s will be omitted.

Voltage U_{50} unequal to zero means current I_{50} driven through the ground impedance Z_{GND} . It can be calculated with the Thevenin's Theorem. Open circuit voltage U_{50}^{Th} by removing branch Z_{GND} yields

$$U_{50}^{Th} = \frac{Y_{13} [Y_{34}(Y_{35} + Y_{45}) + Y_{35}(Y_{24} + Y_{45})] \cdot EMF}{(Y_{13} + Y_{24}) [Y_{34}(Y_{35} + Y_{45}) + Y_{35}Y_{45}] + Y_{13}Y_{24}(Y_{35} + Y_{45})} - \frac{Y_{10} \cdot EMF}{Y_{10} + Y_{20}} \quad (4.36)$$

where $Y_{34} = \frac{R_L + \frac{1}{j\omega C_{34}}}{R_L \frac{1}{j\omega C_{34}}}$

For derivation of the Thevenin's impedance seen between poles 5-0, transposition of triangle 3-4-5 to the star with the star node 0' as shown in Fig.4.19 must be performed

$$Z_{30'} = \frac{Z_{34}Z_{35}}{Z_{34} + Z_{35} + Z_{45}}$$

$$Z_{40'} = \frac{Z_{34}Z_{45}}{Z_{34} + Z_{35} + Z_{45}}$$

$$Z_{50'} = \frac{Z_{35}Z_{45}}{Z_{34} + Z_{35} + Z_{45}}$$

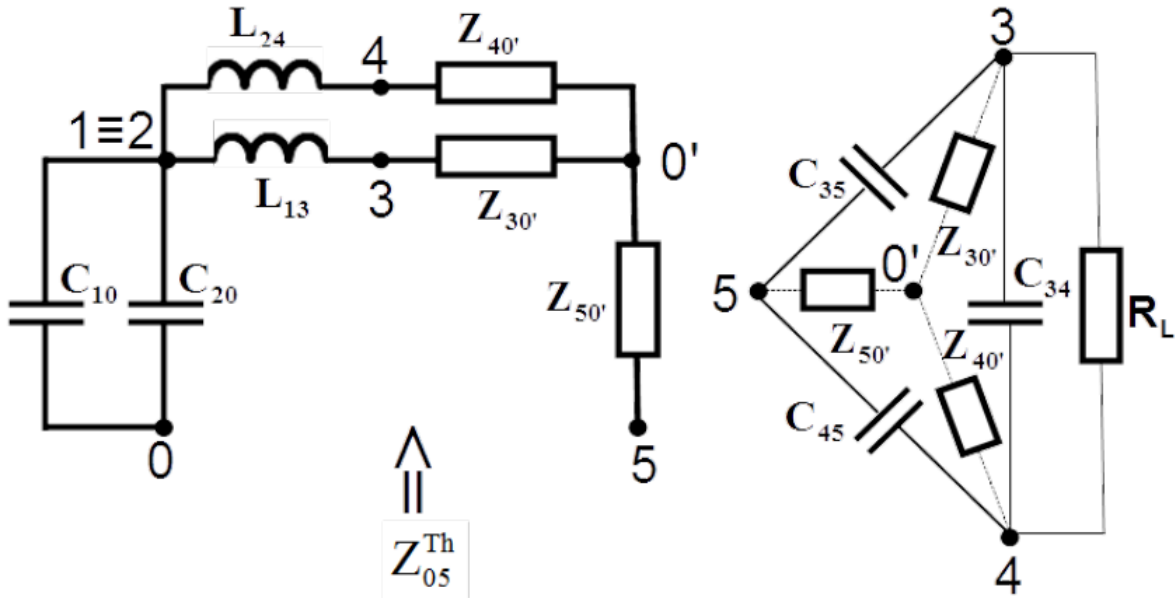


Figure 4.19: Circuit for calculation of the Thevenin's impedance seen between poles 0-5.

Current I_{50} driven through the ground impedance Z_{GND} is called common mode current I^{CM} . It yields

$$I^{CM} = I_{50} = \frac{U_{50}^{Th}}{Z_{50}^{Th} + Z_{GND}} \quad (4.38)$$

In node 0 it is split to current I_{13}^{CM} and I_{24}^{CM} driven in line 1-3 and 2-4 respectively. Ratio of currents I_{13}^{CM} and I_{24}^{CM} depends on relation between impedances of paths 0-1-3-5 and 0-2-4-5.

Along with the common mode component the differential mode current I^{DM} is driven in the feeding and return line.

It can be calculated after removing branch with the ground impedance Z_{GND}

$$I^{DM} = I_{50} = \frac{EMF}{Z_{13} + Z_{24} + \frac{(Z_{35} + Z_{45})Z_{34}}{Z_{35} + Z_{45} + Z_{34}}} \quad (4.39)$$

Finally actual currents in the transmission lines expressed with the common and differential components yields

$$I_{13} = I^{DM} + I_{13}^{CM}$$

$$I_{42} = I^{DM} - I_{24}^{CM}$$

Calculation of capacitances C_{10} , C_{20} and C_{12} as well C_{35} , C_{45} and C_{34} can be done only numerically because both triple of capacitors are linked. Any change of one of them causes changes of the rest.

The same concerns inductances. Notice that L_{13} is serial connection of two inductances because line 1-3 is part of the loop 1-3-5-0 and 1-3-4-2.

Wave coupling

Radiated waves

Idealized entities as elementary radiators

- *Isotropic antenna.* It is omni directional radiator. In other words it radiates the same power in all directions.
- *Electric (Hertzian) dipole.* Imagine electrically short, infinitesimally thin strait conducting segment carrying a current represented with the phasor \mathbf{I} that is assumed to be constant (as to magnitude and phase) at all points along the segment. If the segment length l tends to zero whereas the current \mathbf{I} infinitely grows so that the quantity $\mathbf{p} = l\mathbf{I}$ remains finite and constant, then this product constitutes magnitude of the vector called the dipole moment. Its direction is along the segment and the sense according to the current direction $\vec{\mathbf{1}}_l$

$$\vec{\mathbf{p}} = \lim_{l \rightarrow 0, I \rightarrow \infty} (l\mathbf{I}) \vec{\mathbf{1}}_l \quad (4.41)$$

- *Magnetic (Fitzgeraldian) dipole.* Imagine electrically small, infinitesimally thin ring with azimuthal current \mathbf{I} flowing in it which does not depend on the angle. If the ring radius a tends to zero whereas the current \mathbf{I} infinitely grows so that the product of the ring area and current $\mathbf{m} = \pi a^2 \mathbf{I}$ remains finite and constant, then this product constitutes magnitude of the vector called the dipole moment. Its direction is orthogonal to the plane of the ring and the sense results from the vector product of unit radius vector $\vec{\mathbf{1}}_r$ and unit current density vector $\vec{\mathbf{1}}_j$

$$\vec{\mathbf{m}} = \lim_{\pi a^2 \rightarrow 0, I \rightarrow \infty} (\pi a^2 \mathbf{I}) \vec{\mathbf{1}}_r \times \vec{\mathbf{1}}_j \quad (4.42)$$

All these entities are lossless. None of them exist in reality but they are useful in understanding the antenna theory including unintentional antennas such as cables connected to the EUT.

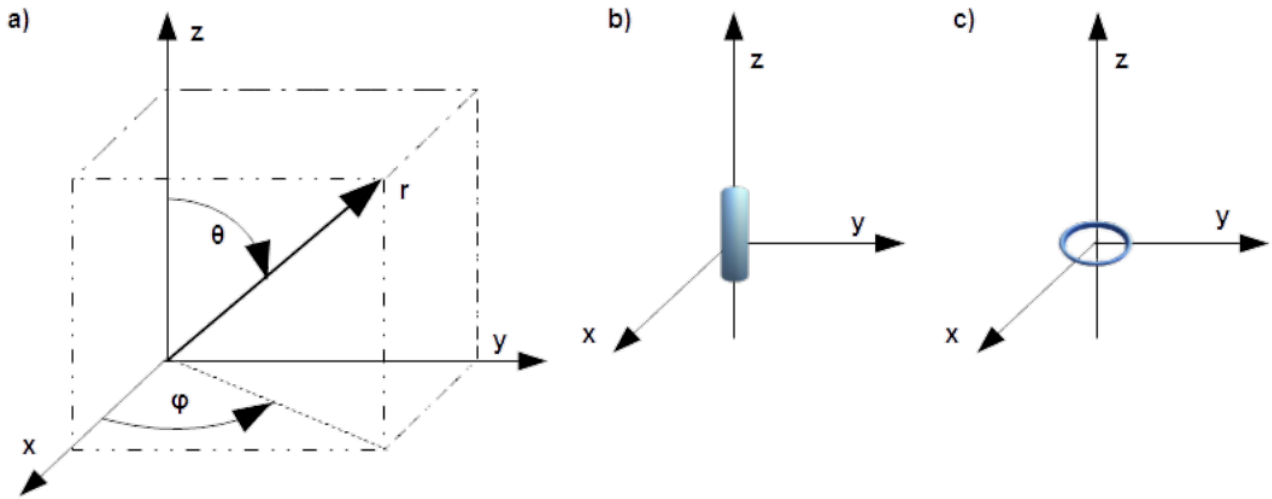


Figure 4.20: Cartesian orthogonal 3D system of coordinates a), electric dipole with only \mathbf{P}_z component of dipole moment b), magnetic dipole with only \mathbf{m}_z component of dipole moment.

The best way of describing the 3D fields generated by dipoles is the spherical system of co-ordinates in which the spacial position of the point under interest is described with three following numbers: r, θ, φ , as shown in Fig.4.20a). The radius r is distance from the origin of the co-ordinates system, θ elevation angle between the z axis and radius r , φ is the azimuthal angle between x axis and projection of the radius r on the $x0y$ plane.

Components of the electric field strength of the electric dipole oriented as shown in Fig.4.20b), according to [Clayton] are as follows

$$\mathbf{E}_r(r, \theta) = \frac{\mathbf{P}_z Z_0 \beta_0^2}{2\pi} \cos(\theta) \left(\frac{1}{\beta_0^2 r^2} - j \frac{1}{\beta_0^3 r^3} \right) e^{-j\beta_0 r} \quad (4.43)$$

$$\mathbf{E}_\theta(r, \theta) = \frac{\mathbf{P}_z Z_0 \beta_0^2}{4\pi} \sin(\theta) \left(j \frac{1}{\beta_0 r} + \frac{1}{\beta_0^2 r^2} - j \frac{1}{\beta_0^3 r^3} \right) e^{-j\beta_0 r} \quad (4.44)$$

$$\mathbf{E}_\varphi = 0 \quad (4.45)$$

and of magnetic field strength

$$\mathbf{H}_r = 0 \quad (4.46)$$

$$\mathbf{H}_\theta = 0 \quad (4.47)$$

$$\mathbf{H}_\varphi(r, \theta) = \frac{\mathbf{P}_z \beta_0^2}{4\pi} \sin(\theta) \left(j \frac{1}{\beta_0 r} + \frac{1}{\beta_0^2 r^2} \right) e^{-j\beta_0 r} \quad (4.48)$$

where Z_0 is the intrinsic impedance of the medium in which the dipole is placed. It depends on the magnetic and dielectric constants μ_0 and ϵ_0 of the medium as follows

$$Z_0 = \sqrt{\frac{\mu_0}{\epsilon_0}} \quad (4.49)$$

and β_0 is the phase constant of the wave expressed with the formula

$$\beta_0 = \omega \sqrt{\mu_0 \epsilon_0} = \frac{2\pi}{\lambda_0} \quad (4.50)$$

where ω is angular frequency of the propagated wave and λ_0 is the wave length.

Far away from the electric dipole, regardless of direction disappears dependence of electric field on the second and the third power of radius r , refer to Eqs. (4.43) and (4.44) and dependence of \mathbf{H}_φ component

of magnetic field on the second power of radius r , refer to Eq. (4.48). Solely summands reciprocally proportional to the distance r remains.

In the immediate vicinity of the electric dipole dominant is dependence of electric field on the third power of radius r , refer to Eqs. (4.43), (4.44). Zone within such solid is the near field zone. Magnetic field \mathbf{H}_φ does not exist in it because it does not possess summand with radius r in the third power. Emerges only electric field distributed as in static case. Therefore another name of the zone is the static zone.

Between the near field and the far field zone there is the buffer called the reactive zone.

Components of the electric field strength of the magnetic dipole oriented as shown in Fig.4.20c), according to [Clayton] are as follows

$$\mathbf{E}_r = 0 \quad (4.51)$$

$$\mathbf{E}_\theta = 0 \quad (4.52)$$

$$\mathbf{E}_\varphi(r, \theta) = -j \frac{\mathbf{m}_z \omega \mu_0 \beta_0^2}{4\pi} \sin(\theta) \left(j \frac{1}{\beta_0 r} + \frac{1}{\beta_0^2 r^2} \right) e^{-j\beta_0 r} \quad (4.53)$$

and of magnetic field strength

$$\mathbf{H}_r(r, \theta) = j \frac{\mathbf{m}_z \omega \mu_0 \beta_0^2}{2\pi Z_0} \cos(\theta) \left(\frac{1}{\beta_0^2 r^2} - j \frac{1}{\beta_0^3 r^3} \right) e^{-j\beta_0 r} \quad (4.54)$$

$$\mathbf{H}_\theta(r, \theta) = j \frac{\mathbf{m}_z \omega \mu_0 \beta_0^2}{4\pi Z_0} \sin(\theta) \left(j \frac{1}{\beta_0 r} + \frac{1}{\beta_0^2 r^2} - j \frac{1}{\beta_0^3 r^3} \right) e^{-j\beta_0 r} \quad (4.55)$$

$$\mathbf{H}_\varphi = 0 \quad (4.56)$$

Definition of the far, reactive and near field zones are valid also for the magnetic dipole.

Phasor of total strength of electric and magnetic field in the far field zone of electric dipole, oriented as in Fig. 4.20 b) dependent on locus of point yields

$$\mathbf{E}_\theta(r, \theta) = \frac{\mathbf{p}_z Z_0 \beta_0}{4\pi} \cdot \sin(\theta) \cdot \frac{e^{j\left(\frac{\pi}{2} - \beta_0 r\right)}}{r} \quad (4.57)$$

$$\mathbf{H}_\varphi(r, \theta) = \frac{\mathbf{p}_z \beta_0}{4\pi} \cdot \sin(\theta) \cdot \frac{e^{j\left(\frac{\pi}{2} - \beta_0 r\right)}}{r} \quad (4.58)$$

Phasor of total strength of electric and magnetic field in the far field zone of magnetic dipole, oriented as in Fig. 4.20 c) dependent on locus of point yields

$$\mathbf{E}_\varphi(\omega t, r, \theta) = \frac{\mathbf{m}_z \omega \mu_0 \beta_0}{4\pi} \cdot \sin(\theta) \cdot \frac{e^{-j\beta_0 r}}{r} \quad (4.59)$$

$$\mathbf{H}_\theta(\omega t, r, \theta) = -\frac{\mathbf{m}_z \omega \mu_0 \beta_0}{4\pi Z_0} \cdot \sin(\theta) \cdot \frac{e^{-j\beta_0 r}}{r} \quad (4.60)$$

Total strength of electric and magnetic field in the far field zone of electric dipole, oriented as in Fig. 4.20 b), dependent on time and locus of point yields

$$E_\theta(\omega t, r, \theta) = \frac{p_z Z_0 \beta_0}{4\pi} \cdot \frac{\sin \theta}{r} \cdot \sin\left(\omega t + \frac{\pi}{2} - \beta_0 r\right) \quad (4.61)$$

$$H_\varphi(\omega t, r, \theta) = \frac{p_z \beta_0}{4\pi} \cdot \frac{\sin \theta}{r} \cdot \sin\left(\omega t + \frac{\pi}{2} - \beta_0 r\right) \quad (4.62)$$

Total strength of electric and magnetic field in the far field zone of magnetic dipole, oriented as in Fig. 4.20 c), dependent on time and locus of point yields

$$E_\varphi(\omega t, r, \theta) = \frac{m_z \omega \mu_0 \beta_0}{4\pi} \cdot \frac{\sin \theta}{r} \cdot \sin(\omega t - \beta_0 r) \quad (4.63)$$

$$H_\theta(\omega t, r, \theta) = -\frac{m_z \omega \mu_0 \beta_0}{4\pi Z_0} \cdot \frac{\sin \theta}{r} \cdot \sin(\omega t - \beta_0 r) \quad (4.64)$$

One of features of waves in the far field zone is the wavefront called also equiphase surface. It is the set of points at which field strength has the same phase at a given instant³. Evidently the equiphase surface of the isotropic antenna is the sphere.

The wavefront constraint of the electric dipole means constant phase in Eq. (4.61) and in (4.62)

$$\omega t + \frac{\pi}{2} - \beta_0 r = \text{const} \quad \text{and for magnetic dipole in Eq (4.63) and in (4.64)} \quad \omega t - \beta_0 r = \text{const} \quad .$$

Hence the wavefront of both dipoles must be also the sphere $r = \text{const}$. The wavefront constraint includes also information about movement direction of the wavefront. In order to fulfill the constraint, radius r must increase with passage of the time i.e. the wavefront moves outwards.

In arbitrary place of the space surrounding any antenna ratio of magnitudes of vectors of phasors of electric and magnetic field

$$\mathbf{Z}_w(r, \theta, \varphi) = \frac{|\vec{\mathbf{E}}(r, \theta, \varphi)|}{|\vec{\mathbf{H}}(r, \theta, \varphi)|} \quad (4.65)$$

is called wave impedance.

Even for the electric and magnetic dipole general formula for the wave impedance are complicated but its constrains to the symmetry plane $x0y$ is agreeable. In the formulas below the distance r is scaled with the wavelength λ transmitted or received by the dipole. r/λ can be seen as the “electrical distance” which is in line with definition of electrical size presented in chapter [EL_size]

$$\mathbf{Z}_w^{(e)}\left(\frac{r}{\lambda}, 90^\circ, \varphi\right) = Z_0 \frac{1 + j \frac{4\pi^2 \left(\frac{r}{\lambda}\right)^2 - 1}{2\pi \left(\frac{r}{\lambda}\right)}}{1 + j 2\pi \left(\frac{r}{\lambda}\right)} \quad (4.66)$$

$$\mathbf{Z}_w^{(m)}\left(\frac{r}{\lambda}, 90^\circ, \varphi\right) = Z_0 \frac{1 + j 2\pi \left(\frac{r}{\lambda}\right)}{1 + j \frac{4\pi^2 \left(\frac{r}{\lambda}\right)^2 - 1}{2\pi \left(\frac{r}{\lambda}\right)}} \quad (4.67)$$

Magnitude and phase angle of the wave impedances formulated in Eqs. (4.66) and (4.67) are shown in Fig. 4.21.

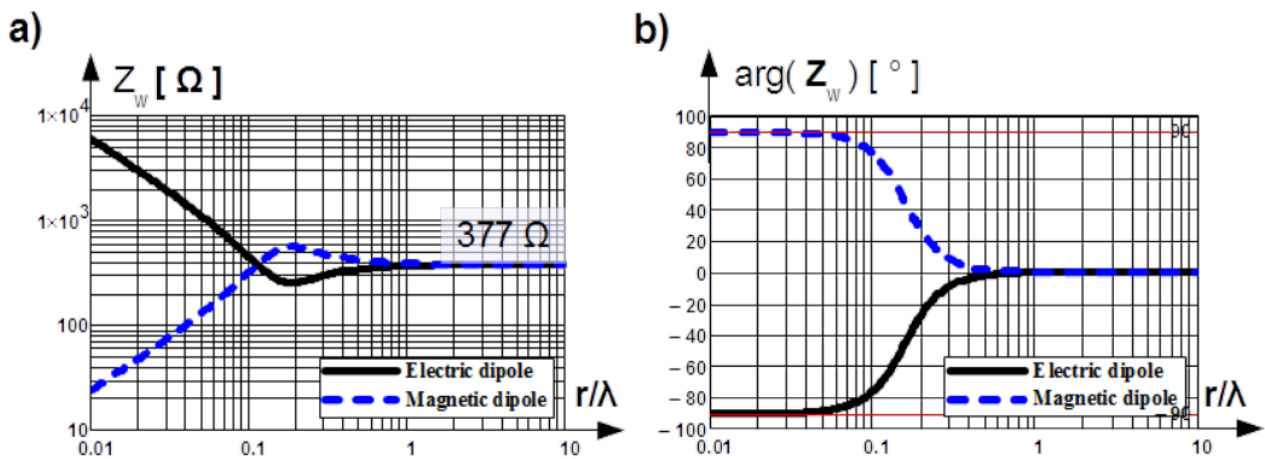


Figure 4.21: Magnitude and phase angle of the wave impedance \mathbf{Z}_w of the electric and magnetic dipole in the symmetry plane $x0y$ versus electrical distance r/λ from the dipole.

According to the rule of thumb it can be stated that the near field zone is within electrical distance $r/\lambda < 0.1$. By that distance the phase angle rises to -80° for electric dipole and decays to 80° for magnetic dipole. Within that distance field is practically pure electric or magnetic. The same rule of thumb

tells us to presume the far field zone in an electrical distance $r/\lambda > 1$. Memorize that the wave impedance in the far field zone regardless the direction approaches the intrinsic impedance Eq. (4.49)⁴, which for the vacuum and approximately for the air is $Z_0 = 120\pi \Omega \approx 377 \Omega$. The wave impedance in the far field zone has resistive character and it represents real radiated power.

It is evident why the zone between $0.1 < r/\lambda < 1$ is called reactive. The phase shifting between electric and magnetic field means reactive power commuting between the antenna and point of space under consideration. The real part of impedance in the reactive zone is responsible for real power to be radiated.

The far field zone by real antennas depend on their construction and is usually few times bigger than $r/\lambda = 1$.

Field probes

Probes are used for measurements of field strength in near and reactive zone. They should not distort incident field that's why they must be electrically small. This rationalizes their drawback namely moderate signal of response.

Construction of the sensor in the field probe imitate electric or magnetic dipole with finite dimensions. Equivalent circuits are shown in Fig. 4.22. C_S and L_S are capacitance and inductance of the electric and magnetic sensor respectively. R_L is resistance of the circuitry terminating the sensor.

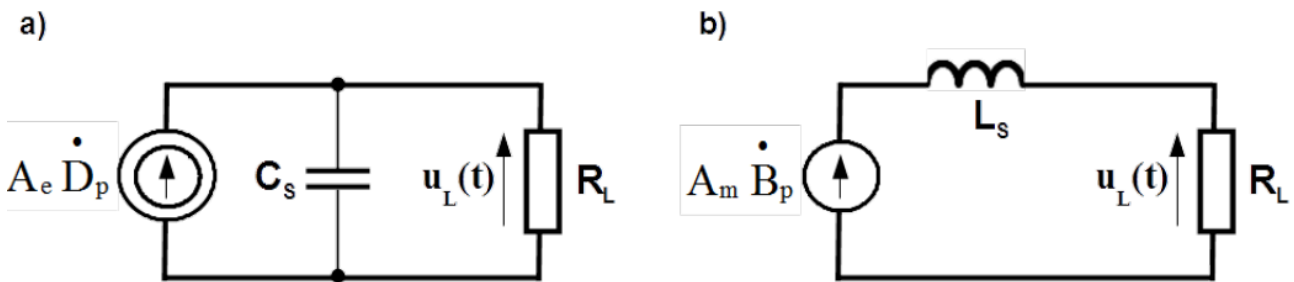


Figure 4.22: Equivalent circuits of electric sensor a), magnetic sensor b).

Output voltage $u_L(t)$ of the electric sensor is linked with the component of the density of the displacement current $\dot{D}_p(t)$ in the space point in which the sensor is placed and matched with the orientation of the probe, see Fig. 4.22a)

$$C_S \frac{du_L(t)}{dt} + \frac{u_L(t)}{R_L} = A_e \frac{dD_p(t)}{dt} = A_e \dot{D}_p(t) \quad (4.68)$$

A_e is parameter of the probe transferring the component of the density of the displacement current $\dot{D}_p(t)$ to the current source in the equivalent circuit in Fig. 4.22a), expressed in area units. It is called equivalent surface.

In the frequency band of applications current driven through the capacitance C_S is negligibly small and

can be omitted. Then response $u_L(t)$ of the sensor is proportional to the component of the density of the displacement current $\dot{D}_p(t)$. The sensor is a current source with magnetomotive force $A_e \dot{D}_p(t)$.

Current $i(t)$ in the mesh in Fig. 4.22b) is linked with the time derivative of the component of magnetic inductance $\dot{B}_p(t)$ in the space point in which the sensor is placed and matched with the orientation of the sensor

$$L_S \frac{di(t)}{dt} + R_L i(t) = A_m \frac{dB_p(t)}{dt} = A_m \dot{B}_p(t) \quad (4.69)$$

A_m is parameter of the probe transferring the time derivative of the component of magnetic inductance $\dot{B}_p(t)$ to the voltage source in the equivalent circuit in Fig. 4.22b), expressed in area units. It is called equivalent surface.

In the frequency band of applications voltage across the inductance L_S is negligibly small and can be omitted. Then response $u_L(t)$ of the sensor is proportional to the time derivative of the component of magnetic inductance $\dot{B}_p(t)$. The sensor is a voltage source with electromotive force $A_m \dot{B}_p(t)$.

On the market are available directive and isotropic probes. The first sense only field component matched with the probe orientation, the second sense three orthogonal components of field in space.

There is variety of probes capable of capturing amplitude in overall frequency band of application. Directly by the sensor they have RF detector, most frequently diode one. Thereafter there is A/C converter and the signal is delivered either to the display integrated with the sensor in case of autonomous probe or is converted to light and transmitted via the fiber glass to the computer interface. Increasingly the fiber glass is used simultaneously for powering electronic by the sensor.

Probes are able to measure faithfully only CW i.e. single frequency fields. They are inapplicable for any modulated or transient fields.

Example of autonomous isotropic probe for electric and magnetic field with the bandwidth from DC to 400 kHz is shown in Fig. 4.23a) and isotropic electric probe with optical transmission of signal and power applicable in the bandwidth from 10 kHz to 6 GHz in Fig. 4.23b).

a)



b)



Figure 4.23: Isotropic autonomous electric and magnetic field probe a), electric field probe with optical transmission of signal and power b).

There are other types of probes called in jargon D-dot and B-dot probes. They are applicable for measurements of pulsed fields. In such probes digital processing of the sensor response, which is proportional to the field derivative, see Eq. (4.68) and Eq. (4.69), is preceded with the time integration. They are exclusively directional probes.

Example of free space directional D-dot probe with the bandwidth from from 100 kHz to 3.5 GHz is

shown in Fig. 4.24a) and free space directional B-dot probe with the bandwidth from 100 kHz to 2 GHz in Fig. 4.24b).

a)



b)



Figure 4.24: Free space directional D-dot probe a), Free space directional B-dot probe b).

Antennas

In technical terminology terms electric and magnetic antenna are used. The first concerns antennas with the wave impedance in the near field zone bigger than intrinsic impedance.

Antennas are used for selective measurements of stationary fields in the far field zone. It can be assumed that they do not distort incident field. Analogue voltage signal induced in the antenna is transmitted from the antenna terminal to the spectrum analyzer or other radio frequency selective measurement receiver which records frequency spectrum of the measured field.

Antennas for the measurement of electric fields are variations of electric dipoles. Dipole can be interpreted as unloaded symmetrical transmission line with straightened out conductors. The tips of dipole's arms are nodes for current distribution and antinodes for voltage distribution. Current vanishes there and voltage varies from plus to minus amplitude due to open circuit condition.

By $\lambda/2$ dipole as shown in Fig. 4.25a) the current distribution, the blue area is half of the approximately cosine function⁵ with amplitude in the midpoint between the arms i.e. by antenna terminal. Voltage distribution, the orange needles is half of the sine function with fixed zero value by antenna terminal and varying between plus and minus amplitudes at the tips.

In Fig. 4.25 b) a half dipole antenna is shown. Such miniature antennas are used as grounded probes of electric fields or much bigger as monopole (rod) receiving antennas.

Dipole radiate efficiently if its length is matched with approximately multiple of the half of the wavelength $\lambda/2$. This efficiency is very sensitive on mismatching. In order to expand the frequency bandwidth rods in the ordinary dipole are replaced with conus (bi-conical antenna), triangle (bow-tie antenna) or more complex shapes by broad band antennas.

In Fig. 4.30 b) the bow-tie-log-periodic antenna is shown. Its frequency of operation extends from 30 MHz do 1500 MHz. The bow-tie section of the antenna, big triangles next to the feeding point covers frequency band from 30 MHz to about 300 MHz. It is connected parallelly with the Log-Periodic Dipole Antenna LPDA ahead. The LPDA is group of dipole antennas of varying sizes strung together. The dipole antennas diminish in size from the back to the front. The element at the back of the array which is the largest is tuned to frequency about 300 MHz and that at the front is a half wavelength at the highest frequency of operation i.e at 1500 MHz.

In the antenna boom between coaxial junction and bow-tie section a black box with the balun is mounted. Input of the dipole antenna is symmetric but the feeding point coaxial. The balun is a two port adapting symmetric to coaxial terminal. The name is a cluster of two words balanced-unbalanced.

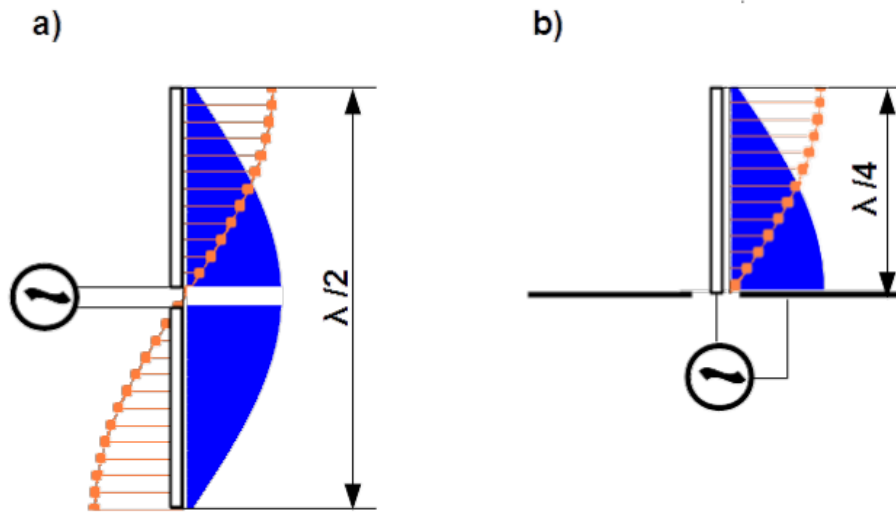


Figure 4.25: Electric dipole with the length matched to the $\lambda/2$ wavelength a) and monopole matched to the $\lambda/4$ wavelength.

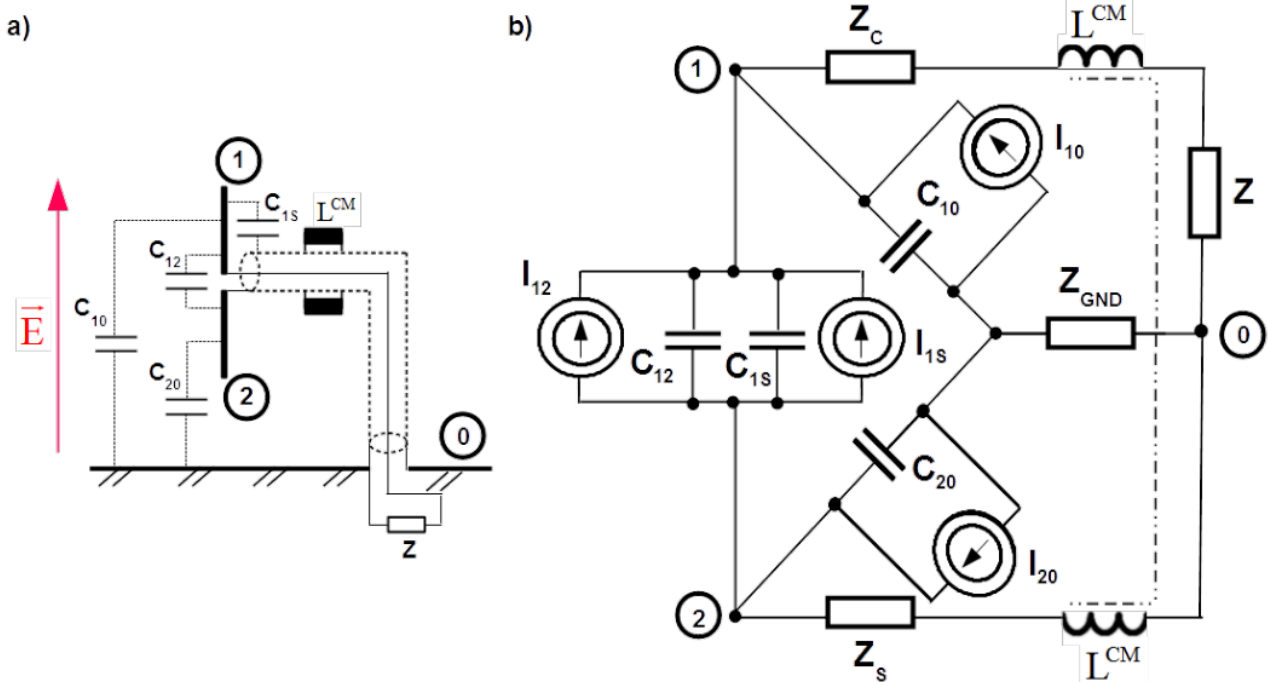


Figure 4.26: Illustration how the current balun operates.

Desired signal of electric dipole stems from capacitance between the arms. It is C_{12} in Fig.4.26 a). Additionally each arm has its own capacitance to the ground. They are C_{10} and C_{20} . There is still one more capacitance that must be taken into account. Namely between the arm connected to the core of the coaxial cable and the shield. It is arm 1 and capacitance C_{1s} in Fig.4.26 a). Capacitance between the arm 2 and the cable shield is short circuited. Z is the input impedance of the measurement receiver.

Equivalent circuit of the dipole is composed of parallel circuits of the current sources with their

capacitances as it was explained for the free space electric sensor shown in Fig.4.22 a)⁶. In Fig.4.26 b) branch with Z_C represents impedances of cable core, Z_S cable shield and Z_{GND} the ground reference. If capacitances C_{10} and C_{20} are different then they contribute to the differential current driven through the core, the measurement receiver and the shield. Moreover probable is also common mode current returning through the ground. Differential contribution of capacitances C_{10} and C_{20} cannot be eliminated. It overlays with desired signal I_{12} causing distortion.

The current balun is simply ferrite mounted on the coaxial cable direct by junction with symmetrical antenna output. The common mode choke⁷ L^{CM} shown in Fig. 4.26 suppresses common mode contribution of capacitances C_{10} and C_{20} but it does not eliminate it totally. Total elimination of differential and common mode distortion caused by capacitances C_{10} and C_{20} would happen if they were equal. Practically this condition is fulfilled by horizontal polarization of the antenna and very high above the ground reference, regardless polarization⁸.

There is still another parasitic capacitance C_{1S} which contributes differentially to the desired signal, see Fig.4.26 b) and cannot be eliminated. The only way is to keep the capacitance small and place the common mode choke L^{CM} as close as possible by antenna feeding.

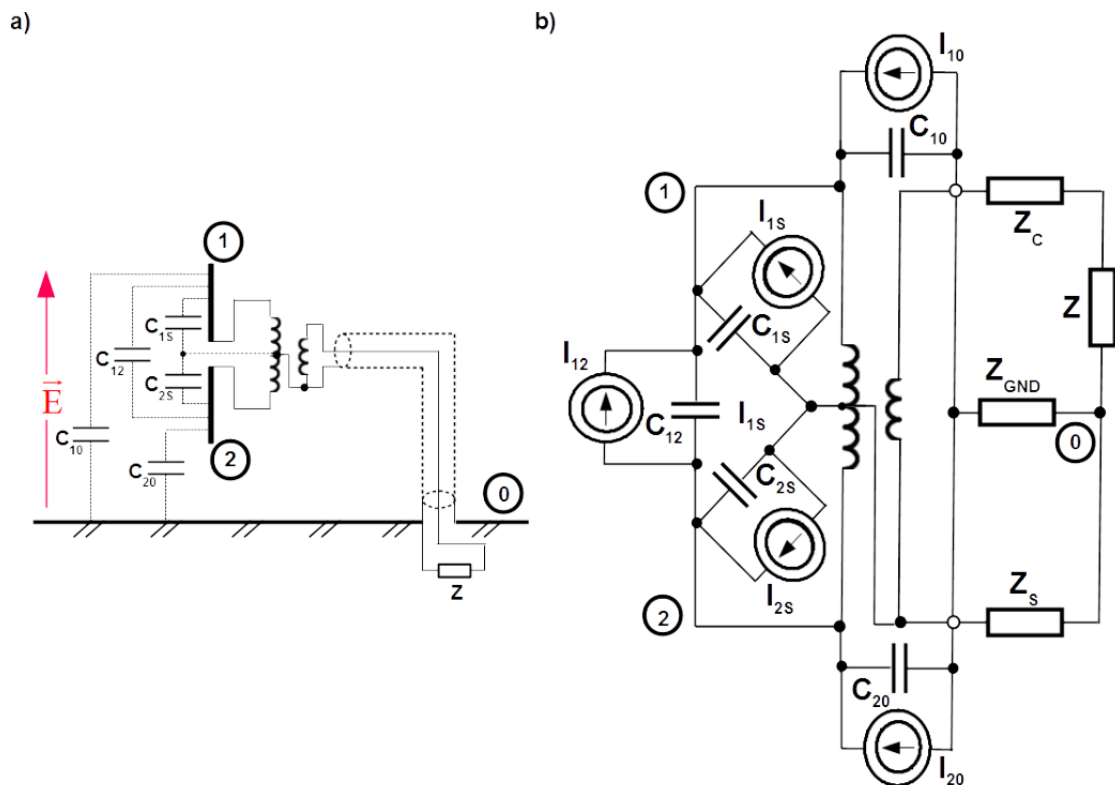


Figure 4.27: Illustration how the voltage balun operates.

More sophisticated are voltage baluns, based on transformers. Example of one of them is shown in Fig. 4.27. Transformer separates galvanically symmetrical terminal of the antenna from coaxial cable connector. Additionally cable shield tapes the centre of the transformer winding on the symmetrical side. It has triple advantage:

- cancellation of the common mode distortion due to capacitances C_{10} and C_{20} , thanks galvanic separation,

- both arms of the dipole are liberated from the potential of the cable shield, thanks galvanic separation,
- capacitances of both dipole arms to the cable shield C_{1S} and C_{2S} are equal one to another due to introducing the potential of the cable shield to the midpoint between the arms.

Contribution of the differential component in the distortion caused by unequal capacitances C_{10} and C_{20} is ruled in the same way same as by the current balun.

The balun in the antenna shown in Fig. 4.30 b) is necessary because of the bow-tie section. The LPDAs' antennas are not finished with them. The adjacent dipoles in a LPDA antenna are connected to the symmetrical line routed inside the antenna (red and blue lines in Fig. 4.28) alternately. Consequently averaged capacitances of upper and lower arms to the cable shield and to the ground reference are equalized, minimizing distortion of the measured signal.

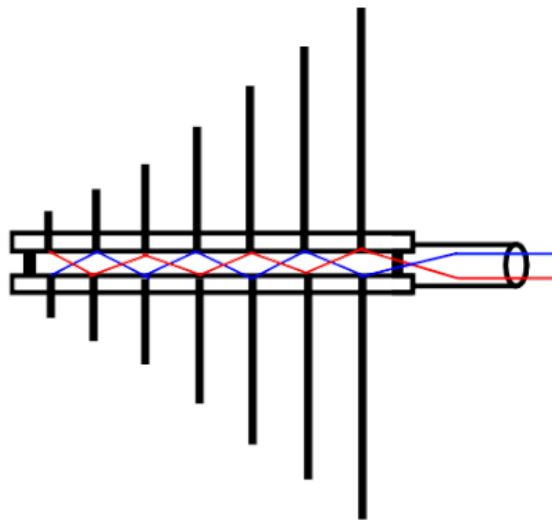


Figure 4.28: Alternately fed dipoles in the LPDA.

All precautions concerning symmetrization in the antenna can be spoiled with incorrect routing of the coaxial cable behind the antenna. In the document [CISPR-16-1-4] two recommendations are formulated:

- by EMC testing of radiated emission the coaxial cable behind the antenna should be maintained horizontal, i.e. parallel to the ground plane, for a distance of approximately 1 m or more to the rear of the antenna before dropping to the ground plane,
- by verification of the anechoic chambers the coaxial cable behind the antenna should be oriented horizontally behind the antenna for a distance as close to 2 m as physically possible.

The LPDA antennas available on the market have booms with about 1 m length.

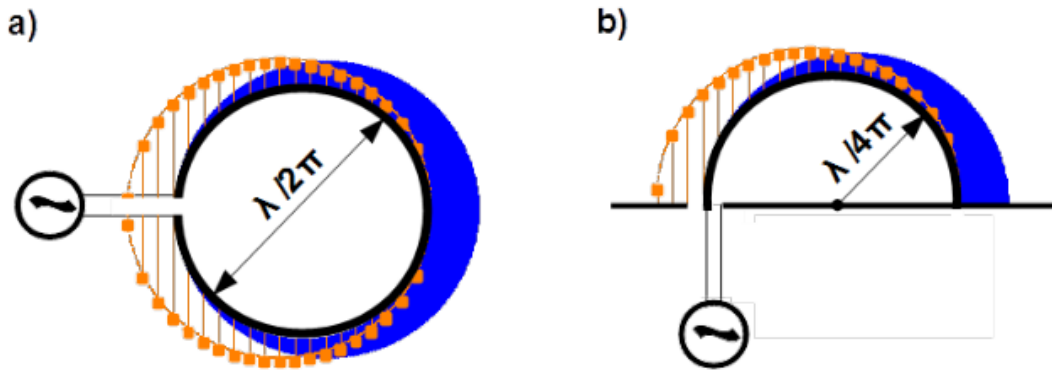


Figure 4.29: Magnetic dipole with the circumference matched to the $\lambda/2$ wavelength a) and half dipole with the circumference matched to the $\lambda/4$ wavelength.

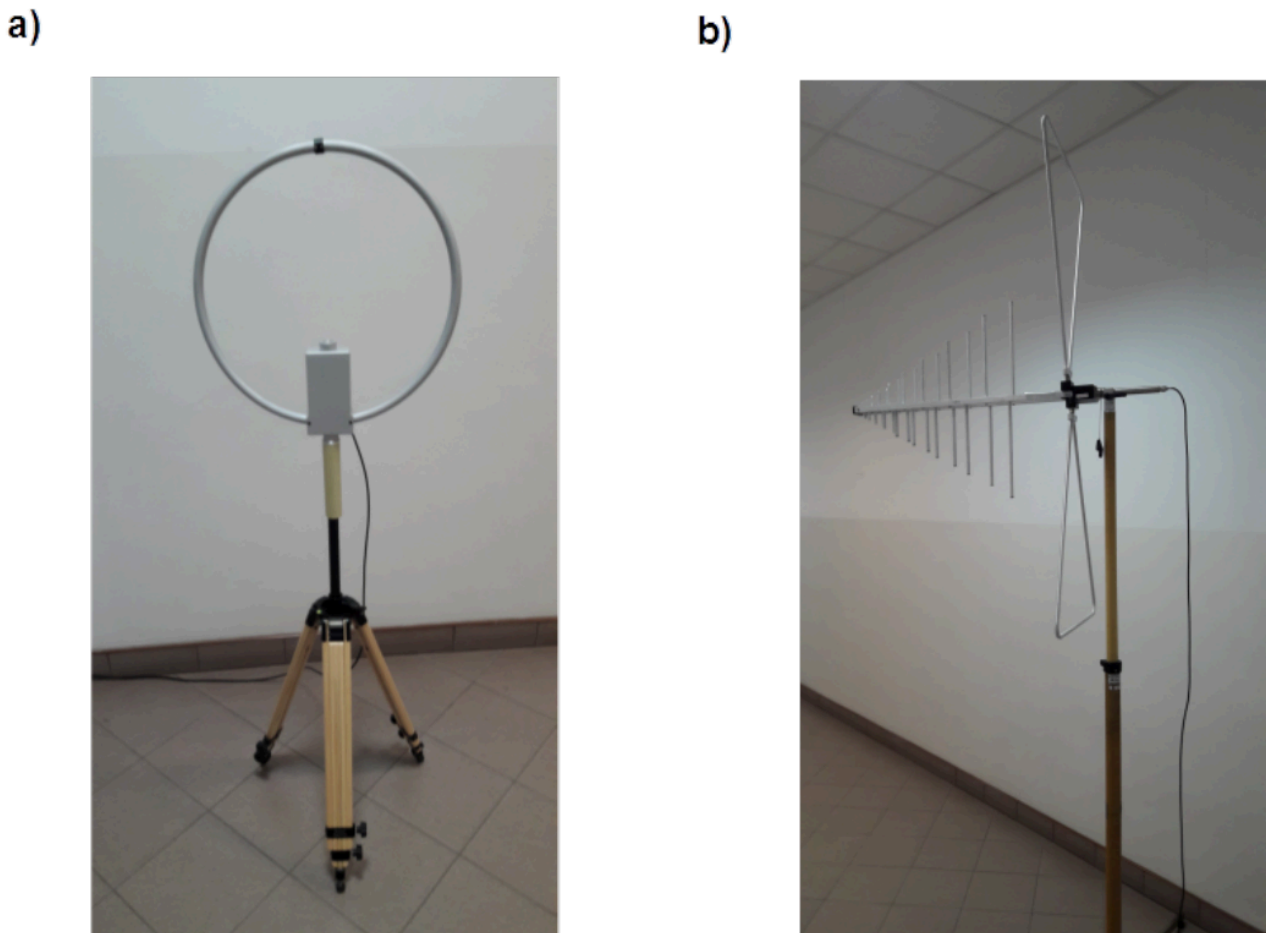


Figure 4.30: Broad band loop antenna for measurements of magnetic field a) and broad band bow-tie-log-periodic antenna for measurements of electric field.

Antennas for the measurement of magnetic fields are variations of magnetic dipoles. Magnetic dipole can be interpreted as short circuited symmetrical transmission line with the circle shape. The junction point

of upper and lower conductor is the node for voltage distribution and antinode for current distribution. Voltage vanishes there and current varies from plus to minus amplitude due to short circuit condition.

By $\lambda/2$ loop dipole⁹ as shown in Fig. 4.29 a) the current distribution, the blue area is half of the approximately cosine function with amplitude in the junction point of upper and lower conductor. Voltage distribution, the orange needles is half of the sine function with fixed zero value by the junction point of upper and lower conductor and varying between plus and minus amplitudes at the antenna feeding.

In Fig. 4.29 b) a half loop antenna is shown. Such loops with miniature size are used as grounded probes of magnetic fields.

Loop antennas are used in the frequency range up to 30 MHz. Their response is very weak. The bigger radius the stronger response due to its dependence on magnetic flux streaming through the loop area. However lower location sensitivity by the measurements of inhomogeneous fields due to averaging of the flux with the loop area. By the loop antennas signal sensitivity and averaging effect must be always compromised. By active loop antenna with built in amplifier size of the loop can be reduced.

In Fig. 4.30 a) the loop antenna with frequency of operation from 9 kHz to 30 MHz is shown. In the box by the tripod the amplifier is placed. At the top of the antenna a black ring is visible. Loop antennas have metal tube around, which plays a role of electric shield. Thanks the shield picking up unwanted responses steaming from electric fields can be avoided. This shield however must be broken to prevent the metal tube from acting like a shorted turn. The plastic ring positions the free ends of the broken metal tube.

Antenna factor.

By measurements of radiated disturbances with antennas it is necessary to recalculate the signal at the input of the measurement receiver to the field strength to which the antenna is exposed. The antenna factor facilitates this conversion.

If receiving antenna is exposed to the field, electromotive force EMF is induced in it. Antennas are not sensing the field module but the component matched with their orientation, E_z or H_x in Fig. 4.31. In other words induced EMF depends on the projection of the field vector on the E-plane for electric and H-plane for magnetic antenna. Z_s is the antenna impedance seen from its terminals.

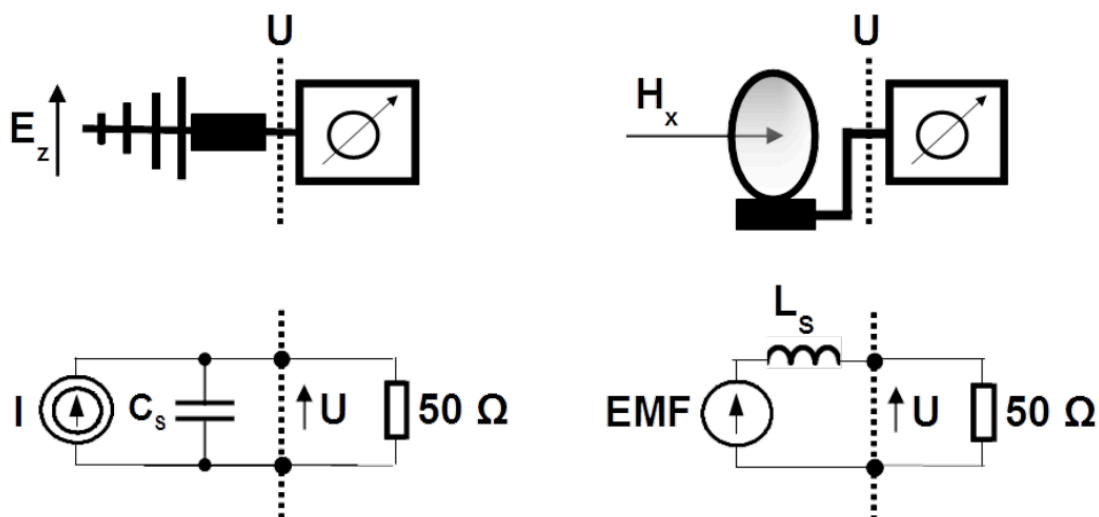


Figure 4.31: Definition of the antenna factor.

By determining the antenna factor the antenna is oriented to the plane matching the field with known strength E_z or H_x . The instrument with 50Ω input resistance capable of HF voltage measurements,

such as: power meter with insertion unit or power sensor, spectrum analyzer or measurement receiver, is connected to the terminals of the antenna. Ratio of field strength and voltage at the measuring instrument is the antenna factor.

$$AF^{(E)} \left[\frac{1}{m} \right] = \frac{E_z}{U} \qquad AF^{(H)} \left[\frac{1}{\Omega m} \right] = \frac{H_x}{U} \qquad (4.70)$$

In the dB scale the units are dB[1/m] and dB[1/(Ωm)] respectively. The antennas' factors are determined for the far field zone in the air where wave and intrinsic impedances are identical $E/H = Z_0 \approx 377 \ \Omega$. Alternatively manufacturers and calibration laboratories presents the factor for magnetic antennas as follows

$$AF^{(H)} \left[\frac{1}{m} \right] = AF^{(H)} \left[dB \left(\frac{1}{\Omega m} \right) \right] + 51.5[dB(\Omega)]$$

Surface power density.

Vector product of phasors of electric field strength and conjugate of magnetic field strength at arbitrary point in space builds the phasor of the Poynting's vector

$$\vec{S} = \vec{E} \times \vec{H}^* \qquad (4.72)$$

Surface integral of the phasor of the Poynting's vector over any closed surface s , oriented outwards versus solid enclosing some antennas gives the phasor of total apparent power \mathbf{P}_{app} on this surface [Hammond_2]

Formula does not parse

crucial is that \vec{ds} is the surface vector oriented outward versus the solid with antennas.

If phasors in Eq. (4.72) are scaled with RMS values then Poynting's vector \vec{S} gives density per surface unit of apparent power at the point of interest¹⁰. Sense of the Poynting's vector shows direction of power transportation in case of electric antennas and opposite direction in case of magnetic antennas. In the near and reactive field zone the imaginary part of the Poynting's vector represents density of reactive power traveling back and forth between the antenna and the point of interest and real part represents density of real power radiated out of the antenna.

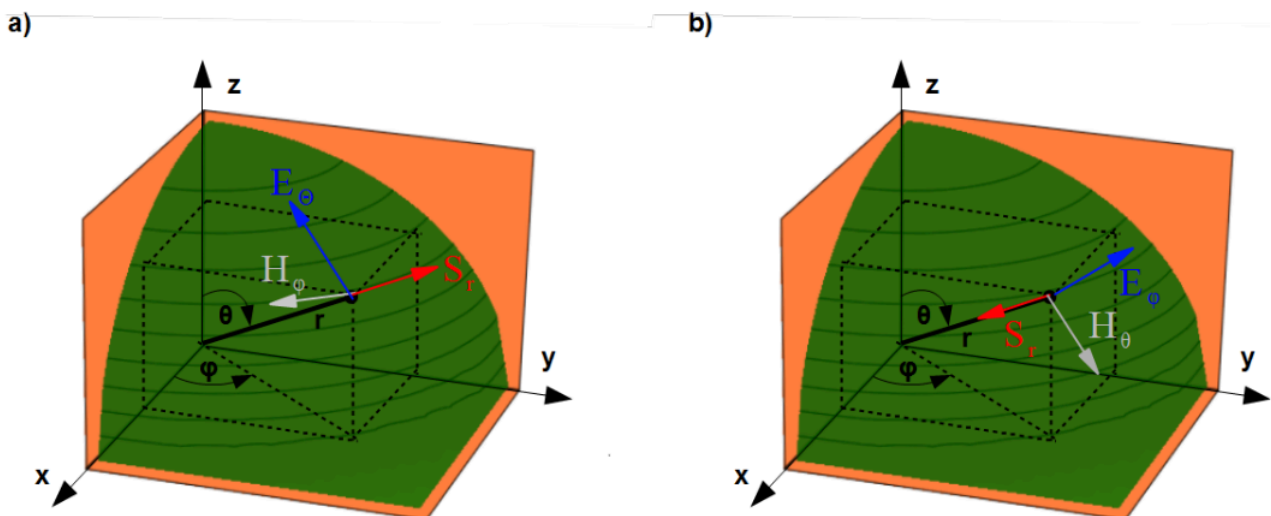


Figure 4.32: The triple field vectors on the equiphase surface by electric antenna a), by magnetic antenna b).

In the far field zone the imaginary part of the Poynting's vector decays. It is actually attribute of the far field zone. There is no phase shift between fields' strengths. Magnitude of the Poynting's vector represents solely density of radiated power.

Each antenna, even geometrically complex is seen, from the observation point located at the wavefront, as the point radiator. Therefore three features of the dipoles' fields in the far field zone can be extended to antennas with any shape. Two of them are listed below:

- the equiphase surface is the sphere,
- the field strength decreases in the far field zone reciprocally proportional to the distance.

For formulation of the third one, additional definition is necessary. It will be introduced later in this paragraph.

Let us imagine wavefront of an antenna with electric field strength polarized in the $\varphi = \text{const}$ plane and magnetic field strength polarized in the $z = \text{const}$ plane, green coloured in Fig. 4.32 a). The triple of the vectors can be oriented as shown there. The magnitude of the Poynting's vector yields

$$S_r(r, \theta) = E_\theta(r, \theta)H_\varphi(r, \theta) = \frac{E_\theta^2(r, \theta)}{Z_0} = Z_0 H_\varphi^2(r, \theta) \quad (4.74)$$

Let us imagine wavefront of an antenna with magnetic field strength polarized in the $\varphi = \text{const}$ plane and electric field strength polarized in the $z = \text{const}$ plane, green coloured in Fig. 4.32 b). The triple of the vectors can be oriented as shown there. The magnitude of the Poynting's vector yields

$$S_r(r, \theta) = E_\varphi(r, \theta)H_\theta(r, \theta) = \frac{E_\varphi^2(r, \theta)}{Z_0} = Z_0 H_\theta^2(r, \theta) \quad (4.75)$$

If the antenna in Fig. 4.32 a) is elementary electric dipole with strengths expressed with Eqs. (4.57) and (4.58) then

$$S_r^{(E)}(r, \theta) = \frac{p_z^2 \beta_0^2 Z_0}{16\pi^2} \cdot \frac{\sin^2 \theta}{r^2} \quad (4.76)$$

Total power radiated by the electric dipole is equal to the surface integral of the Poynting vector Eq. (4.73) and can be calculated over equiphase sphere with arbitrary radius r .

$$\begin{aligned} P_{rad}^{(E)} &= \int_s S_r^{(E)} \vec{1}_r \cdot \vec{ds} = \int_s S_r^{(E)} r^2 \sin \theta d\theta d\varphi = \\ &= \frac{p_z^2 \beta_0^2 Z_0}{16\pi^2} \int_{-\frac{\pi}{2}}^{\frac{\pi}{2}} \sin^3 \theta d\theta \int_0^{2\pi} d\varphi = \\ &= \frac{p_z^2 \beta_0^2 Z_0}{6\pi} \end{aligned} \quad (4.77)$$

If the antenna in Fig. 4.32 b) is elementary magnetic dipole with strengths expressed with Eqs. (4.59) and (4.60) then

$$S_r^{(H)}(r, \theta) = -\frac{m_z^2 \omega^2 \mu_0^2 \beta_0^2}{16\pi^2 Z_0} \cdot \frac{\sin^2 \theta}{r^2} \quad (4.78)$$

Total power radiated by the electric dipole is equal to the surface integral of the Poynting vector Eq. (4.73) and can be calculated over equiphase sphere with arbitrary radius r .

$$\begin{aligned} P_{rad}^{(H)} &= \int_s S_r^{(H)} \left(-\vec{1}_r \right) \cdot \vec{ds} = \int_s S_r^{(H)} r^2 \sin \theta d\theta d\varphi = \\ &= -\frac{m_z^2 \omega^2 \mu_0^2 \beta_0^2}{16\pi^2 Z_0} \int_{-\frac{\pi}{2}}^{\frac{\pi}{2}} \sin^3 \theta d\theta \int_0^{2\pi} d\varphi = \\ &= \frac{m_z^2 \omega^2 \mu_0^2 \beta_0^2}{6\pi Z_0} \end{aligned} \quad (4.79)$$

In Eqs. (4.76) and (4.78) is apparent that the surface power density in the far field zone of elementary radiators decreases reciprocally proportional to the distance r in square. This is the third feature valid also for realised antennas with any shape and size.

Radiation pattern.

Ability of antennas to radiate electromagnetic energy in different directions is portrayed with radiation pattern. It is defined for electric, magnetic field strength as well as for radiated power in far field zone. The radiation pattern is a function built over equiphase surface. Its value represents vector magnitude or power density. For electric/magnetic antenna oriented along z-axis, as shown in Fig. 4.20 b)/Fig. 4.20 c) electric/magnetic field has only θ component dependent on all co-ordinates r , θ and φ . Patterns normalized with maximal value are objective measures for comparison of antennas' performance. They are independent on distance r

$$F^{(E)}(\theta, \varphi) = \frac{E_\theta(r, \theta, \varphi)}{E_{\theta_{max}}} \quad F^{(H)}(\theta, \varphi) = \frac{H_\theta(r, \theta, \varphi)}{H_{\theta_{max}}} \quad (4.80)$$

Obviously normalized pattern of power radiation yields, see Eq. (4.74)

$$F_P^{(E)}(\theta, \varphi) = \frac{S_r^{(E)}(r, \theta, \varphi)}{S_{r_{max}}^{(E)}} = [F^{(E)}(\theta, \varphi)]^2$$

Formula does not parse

$$F_P^{(H)}(\theta, \varphi) = \frac{S_r^{(H)}(r, \theta, \varphi)}{S_{r_{max}}^{(H)}} = [F^{(H)}(\theta, \varphi)]^2 \quad (4.82)$$

Radiation pattern of field strength of the electric and magnetic dipole according to Eq. (4.57) and Eq. (4.60) are identical

$$F^{(E)}(\theta) = F^{(H)}(\theta) = F(\theta) = \sin(\theta) \quad (4.84)$$

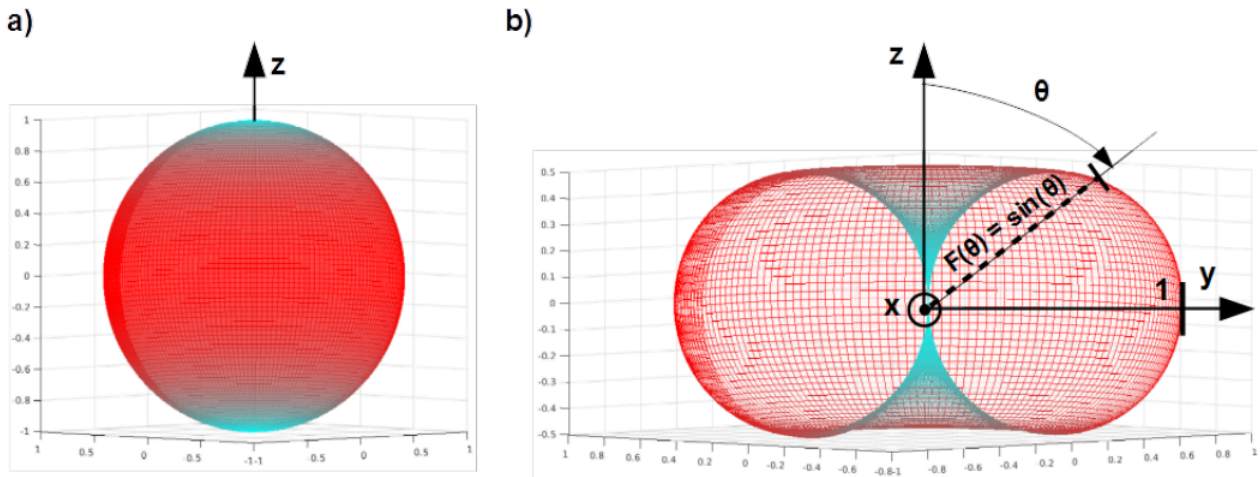


Figure 4.33: Radiation pattern of electric/magnetic field strength round the electric/magnetic dipole.

and of surface power density

$$F_P^{(E)}(\theta) = F_P^{(H)}(\theta) = F_P(\theta) = \sin^2(\theta) \quad (4.84)$$

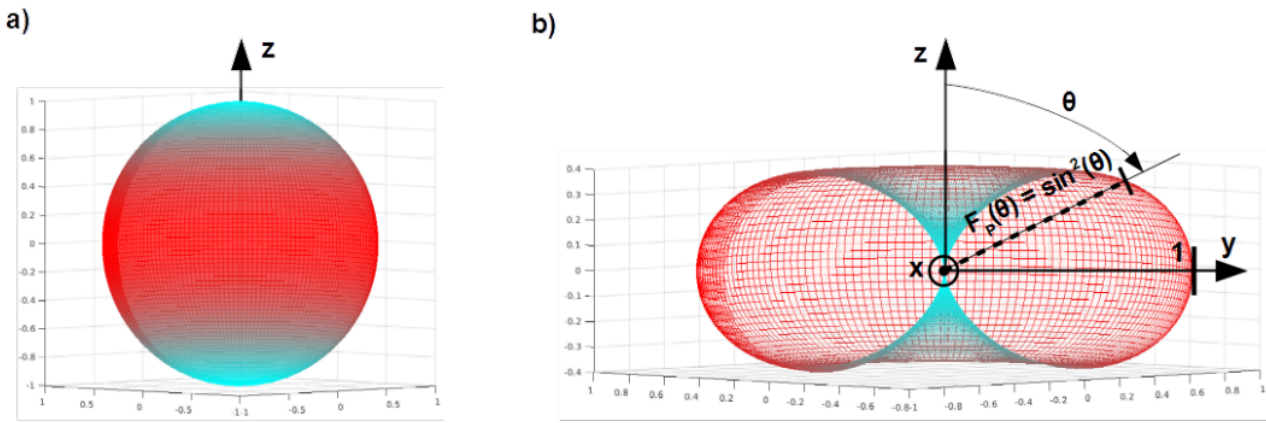


Figure 4.34: Radiation pattern of surface power density round the electric/magnetic dipole.

Radiation pattern of field strength of the electric and magnetic dipole in the spherical system of coordinates r, θ, φ is function of one variable θ . In the system of Cartesian coordinates x, y, z it is function of all variables and can be depicted as a map of colours on the surface of the sphere with radius $r = 1$, as shown in Fig. 4.33 a). From the engineer point of view such picture is useless.

Antennas' engineers are accustomed with mapping the one variable pattern $F(\theta)$ into the two variables pattern $F(r, \theta)$ in which $r = \sin(\theta)$. Such surface is the torus (doughnut) without hole in centre with circular cross-section in the plane $\theta = 90^\circ$ with radius $r = 1$ and two excentrically placed touching circles with radii equal 0.5 . Distance between the origin of the Cartesian system of coordinates and the point at the pattern's surface is equal to the value of the field strength by that elevation θ , see Fig. 4.33 b). From such portrait radiation ability can be directly determined quantitatively.

The same concerns the pattern of the surface power density which is identical for both dipoles. In the spherical system of coordinates r, θ, φ it is function of one variable θ . In the system of Cartesian coordinates x, y, z it is function of all variables and can be depicted as a map of colours on the surface of the sphere with radius $r = 1$, as shown in Fig. 4.34 a). Usually it is mapped into the two variables pattern $F(r, \theta)$ in which $r = \sin^2(\theta)$. Such surface is the vertically squeezed torus (doughnut) without hole in centre with circular cross-section in the plane $\theta = 90^\circ$ with radius $r = 1$ and two excentrically placed touching, deformed circles. Distance between the origin of the Cartesian system of coordinates and the point at the pattern's surface is equal to the value of the surface power density by that elevation θ , see Fig. 4.34 b).

Solid representing the two variables radiation pattern $F(r, \theta)$ is called the lobe. The electric as well as magnetic dipole has only one lobe which is the torus. The realized antennas have so called main lobe roundabout the desired radiation direction and usually more than one side lobe which is undesired, side effect causing waste of radiated power.

Dipoles and antennas presented up to now are oriented along z-axis of the global system of coordinates i.e. vertically. For presentation of radiation pattern at the plane, as it is usually the case in the antennas' data sheets, it is more convenient to use system of coordinates tied to the antenna. Then the cross-section including only electric field component or magnetic field component is called E-plane or H-plane respectively. For the dipole in Figs. 4.33 b) and 4.34 b), the presented cross-section is the E-plane if it is electric dipole and H-plane if it is magnetic dipole. The cross-section $\theta = 90^\circ$ would be H-plane for electric dipole and E-plane for magnetic dipole.

Directive gain and directivity.

Compared is antenna under interest with isotropic antenna radiating the same power. Directive gain $D(r, \theta)$ is ratio of the surface radiated power of the first and the second. Directivity is maximal value of the directive gain. Both parameters gives the measure of squeezing the power beam referred to the omnidirectional radiation.

Let us derive these parameters for the electric and magnetic dipole as shown in Fig. 4.20 b) and c). Division of total radiated power of the electric dipole Eq. (4.77) and magnetic dipole Eq. (4.79) by the solid angle of the sphere $4\pi r^2$ gives surface power density of the isotropic antenna

$$S_i(r) = \frac{p_z^2 \beta_0^2 Z_0}{24\pi^2 r^2} \quad S_i(r) = \frac{m_z^2 \omega^2 \mu_0^2 \beta_0^2}{24\pi^2 Z_0 r^2} \quad (4.85)$$

According to the definition, the directive gain is fraction of surface power density of the dipole and density of isotropic radiator Eq. (4.85). The numerator in this fraction is Eq. (4.76) by the electric dipole and Eq. (4.78) by the magnetic dipole

$$D(\theta) = \frac{3}{2} \sin^2 \theta \quad (4.86)$$

and directivity

$$D_{max} = D(90^\circ) = \frac{3}{2} \quad (4.87)$$

In the dB scale $D_{max} \approx 1.8 \text{ dB}_i$ ¹¹. In the direction of the maximal radiation, the dipole radiates 50% or 1.8 dB_i more power then isotropic radiator with the same totally radiated power.

(Energetic) gain,

usually named simply gain is the directivity diminished by energetic efficiency of the antenna η defined as ratio of total power radiated by the antenna P_{rad} and power at the antenna feeding port P_{in}

$$G_i = \eta D_{max} = \frac{P_{rad}}{P_{in}} D_{max} \quad (4.88)$$

By interpretation of power at the antenna feeding port P_{in} ambiguity can creep in. If net power¹² is introduced as the input power $P_{in} = P_{fwr} - P_{rev}$ then the gain is preceded with the adjective absolute. If forward power sent from the signal source is introduced as the input power $P_{in} = P_{fwr}$ then the gain is preceded with the adjective realised. By absolute gain, unlike by realised gain mismatching at the feeding point is taken into account. Be prudent by evaluation of catalogue data of an antenna in respect of its gain.

More practical meaning has the gain G_d referred to the half wave dipole. Since the gain of the half wave dipole referred to the isotropic antenna is 1.64 in the linear scale and 2.15 dB_i , see [Clayton]

$$G_d = \frac{1}{1.64} G_i$$

Formula does not parse

$$G_{dB_d} = G_{dB_i} - 2.15 \text{ dB}_i \quad (4.90)$$

Equivalent isotropically radiated power EIRP

is the input power at the terminal of the isotropic radiator necessary for radiation with the surface power density equal to the maximum of the magnitude of the surface power density $S(r)$ of the considered antenna in the far field zone. It is product of this value and solid angle of the sphere

$$EIRP = 4\pi r^2 |S(r)|_{max} \quad (4.91)$$

The EIRP does not depend on the distance r . Indeed the EIRP is explicitly proportional to the distance r in square but reciprocal proportionality to distance r in square is implied in the $|S(r)|_{max}$ due to attribute of the far field zone.

For the electric dipole calculation is based on Eq. (4.76) and for magnetic dipole on Eq. (4.78) with setting $\theta = 90^\circ$

$$EIRP^{(E)} = \frac{p_z^2 \beta_0^2 Z_0}{4\pi} \quad EIRP^{(H)} = \frac{m_z^2 \omega^2 \mu_0^2 \beta_0^2}{4\pi Z_0} \quad (4.92)$$

Let us derive the measurement procedure of the EIRP for an electric antenna. The set up is established in the full anechoic chamber in which walls, ceiling and floor are lined with the absorbers marked with pyramids in Fig. 4.35, simulating reflection free space. The investigated antenna T_x and receiving antenna R_x are placed at the same height above the floor in order to match their elevations with $\theta = 90^\circ$. The investigated antenna must be rotated about the vertical axis to the azimuth maximizing signal U_R in the measurement receiver and fixed in this position.

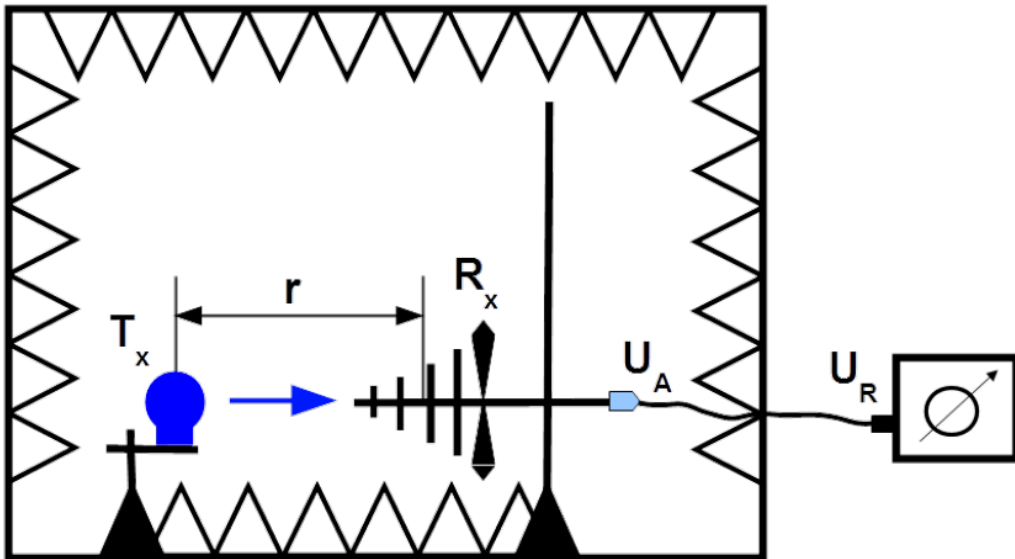


Figure 4.35: Ascertainment of the EIRP in the full anechoic chamber.

Applied must be Eq. (4.74) for surface power density in the direction of maximal radiation i.e. by elevation $\theta = 90^\circ$ and Eq. (4.31) for antenna factor of an electric antenna

$$S_r(r, 90^\circ) = \frac{E_\theta^2(r, 90^\circ)}{Z_0} = \frac{(AF^{(E)})^2}{Z_0} U_A^2(r) \quad (4.93)$$

For EIRP this formula must be multiplied by the solid angle of the sphere

$$EIRP = \frac{4\pi r^2}{Z_0} (AF^{(E)})^2 U_A^2(r) \quad (4.94)$$

Requested unit for the EIRP is mW and for voltage at the antenna terminal μV . Suitable formula yields

$$EIRP [mW] = \frac{4\pi r^2 [m^2]}{377[\Omega]} (AF^{(E)})^2 \left[\frac{1}{m^2} \right] U_A^2(r) [(\mu V)^2] 10^{-9} \quad (4.95)$$

Both sides of equation are logarithmised and multiplied by 10

$$EIRP_{dB(mW)}(r) = 10 \log \left(\frac{4\pi r^2 [m^2]}{377[\Omega]} \right) - 90_{dB} + 20 \log \left\{ AF^{(E)} \left[\frac{1}{m} \right] \right\} +$$

Formula does not parse

Formula does not parse

Voltage at the feeding terminal of the receiving antenna $U_{AdB(\mu V)}$ is greater than voltage measured by the receiver $U_{RdB(\mu V)}$ about attenuation A_{CdB} of the measurement path (cables, feed through)

$$U_{AdB(\mu V)}(r) = A_{CdB} + U_{RdB(\mu V)}(r)$$

$$EIRP_{dB(mW)}(r) = \left[10 \log \left(\frac{4\pi r^2}{377} \right) - 90_{dB} \right] + AF_{dB(1/m)}^{(E)} +$$

Formula does not parse

Formula does not parse

The EIRP is independent on distance r . Indeed there is radius in square in the numerator in Eqs. from (4.94) to (4.98) but measurement is done in the far field zone in which surface power density decreases reciprocally proportional to the distance in square. Consequently the same concerns the voltage at the antenna terminal. By increasing distance e.g. three times the term in square bracket in Eq. (4.98) increases about 9.5 dB but in the same time the voltage at the antenna terminal $U_{AdB(\mu V)}$ and consequently at the receiver input $U_{RdB(\mu V)}$ decreases about the same amount.

Typical distance for performing the measurements of the EIRP is ($r = 3 \text{ m}$). By doing so correction factor in the square brackets is -95.2_{dB} .

Radiation resistance

Total radiated power is represented in the equivalent circuit of the antenna with radiation resistance R_{rad} through which current I from the source feeding antenna is driven $R_{rad}I^2$.

Let us calculate this resistance for the electric dipole. Total radiated power is ruled with Eq. (4.77). Replacing the magnitude of dipole moment with the product of current magnitude I and infinitesimal segment l Eq. (4.41), moreover with implementing the wavelength λ_0 instead of the phase constant β_0 , according to Eq. (4.50) yields

$$R_{rad}^{(E)} = \frac{2\pi Z_0}{3} \left(\frac{l}{\lambda_0} \right)^2 \quad (4.99)$$

In vacuum and approximately in air this resistance is $R_{rad}^{(E)} \approx 789.57 \left(\frac{l}{\lambda_0} \right)^2 [\Omega]$ if the dipole length

l and the wavelength λ_0 have the same units.

In feasible short dipole relation l/λ_0 and consequently radiation resistance is very small. Therefore radiation ability is very weak¹³.

For example, for a length ($l = 1 \text{ cm}$) and a frequency of 300 MHz ($\lambda_0 = 1 \text{ m}$), the radiation resistance is $R_{rad}^{(E)} \approx 79[m\Omega]$ In order to radiate 1 W of power, required is current of 3.6 A!

If the frequency is changed to 3 MHz ($\lambda_0 = 100 \text{ m}$), the radiation resistance is $R_{rad}^{(E)} \approx 7.9 [\mu\Omega]$ and the current required to radiate 1 W is 356 A!

Moreover resistance R_{rad} is serially circuited with the element representing antenna outlet to the lossless space. Depending on electrical length of the dipole l/λ_0 it can be capacitance, shortcircuit or

inductance but for a short dipole it is huge capacitance limiting current driven through radiation resistance. It is the second factor contributing to very small radiation efficiency of the Hertzian as well as short dipole.

Let us proceed now to the radiation resistance of magnetic dipole. Total radiated power is ruled with Eq. (4.79). Replacing the magnitude of dipole moment with the product of current magnitude I and infinitesimal loop area πa^2 Eq. (4.42), moreover with implementing the wavelength λ_0 instead of the phase constant β_0 , according to Eq. (4.50) and relation $\omega = 2\pi v/\lambda_0$ between angular frequency, wave

velocity v and wavelength yields $\omega\beta_0 = \frac{4\pi^2}{\lambda_0^2}v$

Finally

$$R_{rad}^{(H)} = \frac{8\pi^3\mu_0^2v^2}{3Z_0} \left(\frac{\pi a^2}{\lambda_0^2}\right)^2 \quad (4.104)$$

Value of the wave speed in vacuum is given in Eq.([v_0]) therefore this resistance in air is approximately

$$R_{rad}^{(H)} \approx 31'170.91 \left(\frac{\pi a^2}{\lambda_0^2}\right)^2 [\Omega]$$

if radius a and wavelength λ_0 have the same units.

Consider a loop of radius ($a = 1$ cm). At 300 MHz the wavelength ($\lambda_0 = 1$ m) and the radiation resistance is $R_{rad}^{(H)} \approx 3.08\mu\Omega$ In order to radiate 1 W, the loop requires a current of 18 A!

At 3 MHz the wavelength ($\lambda_0 = 100$ m) and the radiation resistance is $R_{rad}^{(H)} \approx 30.8p\Omega$ and current required to radiate 1 W is 180 kA!

Both elementary dipoles radiate very weakly but their comparison shows that magnetic dipole is overwhelmingly worse radiator than electric. In practice they are scarcely met as unintentional antennas.

Half power beamWidth HPBW

called also 3 dB beamwidth is an angle span, either in azimuth or in elevation between two directions encompassing set of directions with the surface power density decaying not more then to the half of the maximum. In other words not reduced about more then 3 dB.

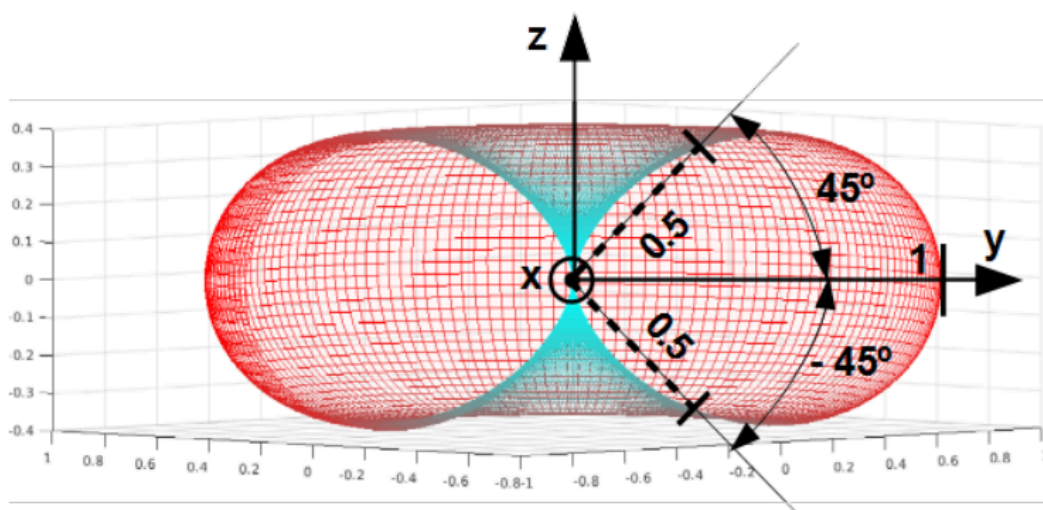


Figure 4.36: Illustration of the half power beamwidth of electric and magnetic dipole.

The electrical dipole is omnidirectional in respect to azimuth φ , therefore determining the HPBW on the plane $\theta = 0^\circ$ is groundless. For the elevation¹⁴ the upper bound is $\theta = 45^\circ$ and lower bound $\theta = 135^\circ$ therefore $HPBW = 90^\circ$, see Fig. (4.36).

HPBW expresses spreading of the power beam. The narrower HPBW, the better concentration of radiated power roundabout desired direction.

Unintentional antennas

It is mentioned frequently, that any cable can be either transmitting or receiving antenna.

By the measurement of radiated emission of the table top equipments in the Semi Anechoic Chamber SAC, the EUT must be placed on the table with 80 cm height. The mains cord should be stretched towards the table edge, dropped down towards the floor and plugged in the supply socket under the metal floor. Typical arrangement of the mains cord is shown in Fig. 4.37 a). Such cable is a monopole antenna while the EUT case is its ground reference. If the common mode current is driven in the cord and the cord length is matched with the wavelength, then the cable radiate and it is very often the case.

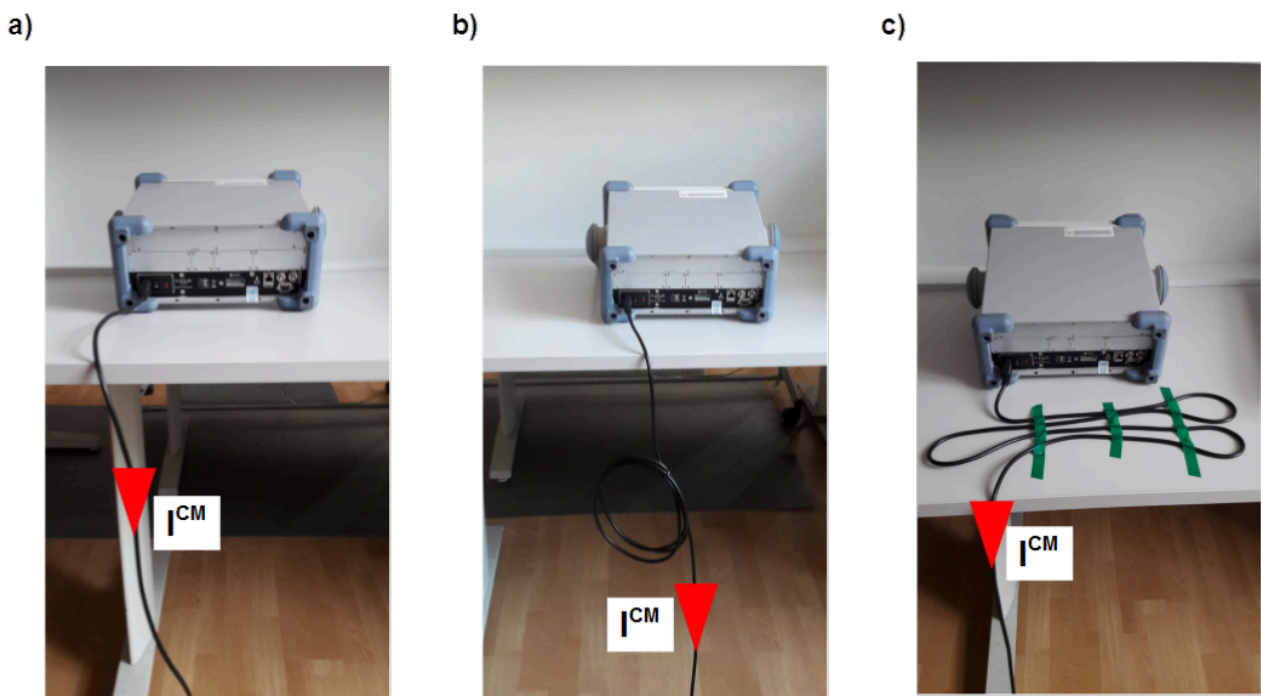


Figure 4.37: Examples of the mains cable as an unintentional antenna: monopole antenna a), loop antenna b) excess cable folded to and forth c).

In Fig. 4.37 b) excess cable is arranged as it should not be. It is wound in few turns building the loop antenna. If the common mode current is driven in the cord and the loop diameter is matched with the wavelength, then it can radiate. Excess cable should be folded to and forth in order to form a low inductive bundle as shown in Fig. 4.37 c).

Let's consider the metal case with the primary plane wave inside, propagating towards the wall with vector's orientation of: electric field \vec{E}_p , magnetic field \vec{H}_p and Poynting vector \vec{S}_p as shown in the side projection in Fig. 4.38 b). By continuous metal wall of the case, surface current would be induced on the internal surface of the wall. The slot enables the current to leak outside. It flows on the external surface of the wall, in surrounding of the slot as shown with reddish region in Fig. 4.38 a). Black arrows on the edges

of the slot shows direction of the driven current. It is accompanied with electric field in the vicinity of the slot oriented as vector \vec{E} in Fig. 4.38 b). Imagine that the edges of the slot build two dipoles shortcircuited at the top of the arms. Such entity can hardly radiate due to cancellation in the far field zone. But as shown with the reddish region in Fig. 4.38 a) current is driven also on the external surface around the edges.

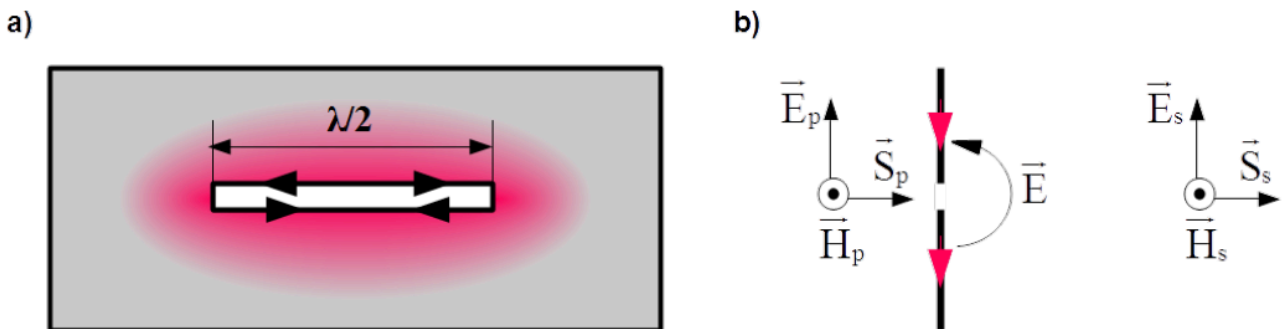


Figure 4.38: Half wavelength slot antenna.

Therefore the secondary wave oriented as shown with the vectors of: electric field \vec{E}_s , magnetic field \vec{H}_s and Poynting vector \vec{S}_s in the side projection in Fig. 4.38 b) propagates from the case, particularly by matching the slot length. Example is $\lambda/2$ matching shown in Fig. 4.38 a). Memorize that orientation of the propagated field is dual to the electric dipole. Horizontally oriented slot propagates vertically oriented electric field.

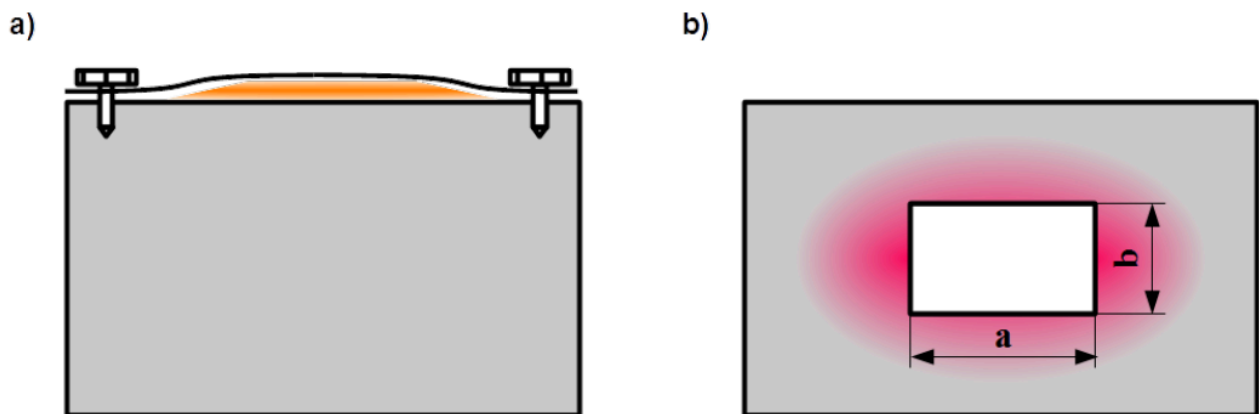


Figure 4.39: Gap by point wise fixing of two pieces of the case a), window in a case as the aperture antenna b).

By point wise techniques of joining parts of the metal cases with screws, nuts or spot welding, gaps between places tied together, marked with yellowish area in Fig. 4.39 a) are formed. Things like incertitude of joined edges and deformations caused by excessed contact pressing force are contribution factors of it. In order to reduce effect of secondary radiation from such gaps distances between fixed spots must ensure length mismatching or/and EMC gaskets obstructing electromagnetically the gaps must be applied.

Windows and openings in cases are indispensable. They serves for mounting displays, cameras, switches, buttons, as sight hole or for ventilation and manipulation of the arrangement. Due to the same rules as by the gaps in the metal case the surface currents flow on the external surface of the wall as shown with the

reddish area in Fig. 4.39 b). The window can build aperture antenna enabling the secondary wave to radiate out of the case.

There is always maximal frequency called cut off, up to which the window is not capable to radiate. It is associated with the biggest wavelength which can be radiated. Above the cut off frequency the wavelength for the rectangular window with sides ab and the circular window with the radius r are approximately ruled with following inequalities

Formula does not parse

Inequality for the circular window is convergent with matching of the circumference of the magnetic dipole to the $\lambda/2$ wavelength $\lambda \approx 12.57r$ as illustrated in Fig. 4.29. It is also in line with condition of not being electrically small i.e. bigger than 0.1λ , see subsection [El_size].

Guided waves

So far in the chapter 4.4 we have been discussing conveying energy, signals and disturbances with radiation. By this art of transportation both field vectors \vec{E} as well as \vec{H} are perpendicular to the direction of propagation. This type of waves is called TEM (transverse electric magnetic) mode. The same TEM mode is present in transmission lines elaborated by galvanic coupling in chapter 4.2 as well as by electric and magnetic coupling in chapter 4.3. Transportation passed along the line and fields are perpendicular to it¹⁵. Therefore TEM mode is often referred to as the transmission line mode.

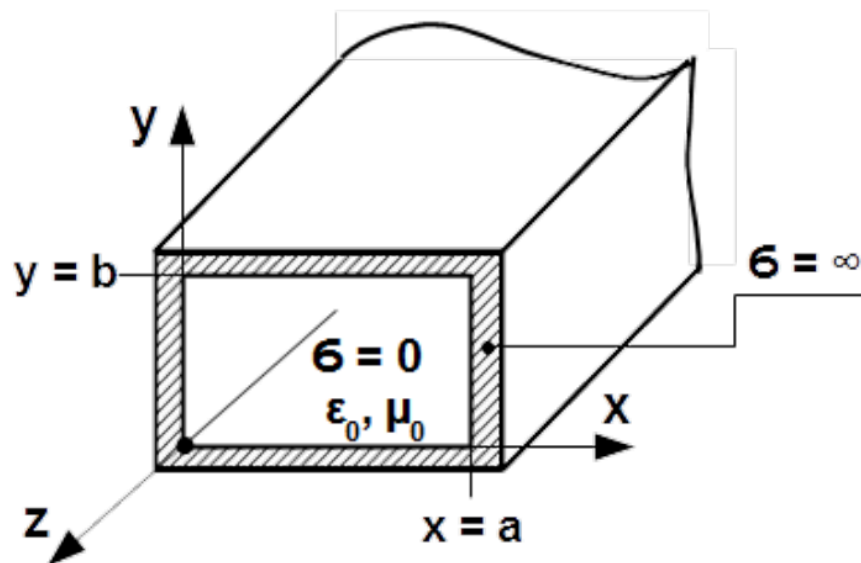


Figure 4.40: A rectangle waveguide.

Let us consider tubular structure with rectangular cross-section, built of perfectly conducting material $\sigma = \infty$ filled with lossless dielectric $\sigma = 0$ with dielectric permittivity ϵ_0 and magnetic permeability μ_0 as shown in Fig. 4.40. Since \vec{E} must be always perpendicular and \vec{H} always tangential to the boundary, it is not possible to excite TEM in such structure.

Let us assume that in such structure propagates wave with three component of phasor's electric field: two cross-sectional $\mathbf{E}_x(x, y, z)$, $\mathbf{E}_y(x, y, z)$ and longitudinal $\mathbf{E}_z(x, y, z)$. The last is governed with the partial differential equation called the wave equation

$$\nabla^2 \mathbf{E}_z + \omega^2 \mu_0 \epsilon_0 \mathbf{E}_z = 0 \quad (4.109)$$

This equation can be solved by the method of separation of variables

$$\mathbf{E}_z(x, y, z) = \mathbf{X}(x)\mathbf{Y}(y)\mathbf{Z}(z)$$

$$\frac{\mathbf{X}''}{\mathbf{X}} + \frac{\mathbf{Y}''}{\mathbf{Y}} + \frac{\mathbf{Z}''}{\mathbf{Z}} + \beta_0^2 = 0 \quad (4.110)$$

where β_0 is phase constant as defined in Eq. (4.50).

Eq. (4.110) can be split into three independent ordinary differential equations

$$\mathbf{X}'' - \gamma_x^2 \mathbf{X} = 0 \quad (4.111)$$

$$\mathbf{Y}'' - \gamma_y^2 \mathbf{Y} = 0 \quad (4.112)$$

$$\mathbf{Z}'' - \gamma_z^2 \mathbf{Z} = 0 \quad (4.113)$$

along with dispersion equation

$$\gamma_x^2 + \gamma_y^2 + \gamma_z^2 + \beta_0^2 = 0 \quad (4.114)$$

where γ_x , γ_y and γ_z are separations' constants.

Solution of Eq. (4.111) is following linear combination of waves $\mathbf{X}(x) = Ae^{\gamma_x x} + Be^{-\gamma_x x}$ traveling forth and back along x axis. $\gamma_x x = \alpha_x + j\beta_x$ can be a complex quantity. As \mathbf{E}_z is tangential to the walls of the waveguide but tangential component of electric field must be zero on perfectly conducting metal wall, $\mathbf{X}(x)$ must disappear by $x = 0$ and $x = a$. This is possible only if $\alpha_x = 0$. Consequently magnitude $X(x)$ is a standing wave with the nodes on walls

$$X_m(x) = (A_m - B_m) \sin(\beta_{x,m} x) = X_{0,m} \sin(\beta_{x,m} x) \\ \beta_{x,m} = m \frac{\pi}{a} \quad (4.117)$$

where m is integer number.

Identical procedure applied to Eq. (4.112) yields $Y_n(y) = Y_{0,n} \sin(\beta_{y,n} y)$ along with

$$\beta_{y,n} = n \frac{\pi}{b} \quad (4.119)$$

where n is integer number.

Solution of Eq. (4.113) is following linear combination of waves $\mathbf{Z}(z) = Ce^{j\gamma_z z} + De^{-j\gamma_z z}$ traveling back $Ce^{j\gamma_z z}$ and forth $De^{-j\gamma_z z}$ along the z-axis. The waveguide is infinite in respect to z-axis. Therefore physical meaning has only one wave.

The source of field is placed somewhere in the waveguide. From that location on, two waves propagate: one forwards another backwards in respect to z-axis. Assuming that source of field is placed by $z < 0$ so that by $z = 0$ regular propagation takes place, then by $z \geq 0$ propagates only

$$\mathbf{Z}_{mn}(z) = D_{mn} e^{-\gamma_{z,mn} z} \quad (4.121)$$

where

$$\gamma_{z,mn}^2 = -\beta_0^2 - (\gamma_{x,mn}^2 + \gamma_{y,mn}^2) = \beta_{x,mn}^2 + \beta_{y,mn}^2 - \beta_0^2 \quad (4.125)$$

$\gamma_{z,mn}$ can be real, imaginary or can have zero value by the break point which corresponds to the cut-off frequency $f_{c,mn}$

$$f_{c,mn} = \frac{v_0}{2} \sqrt{\left(\frac{m}{a}\right)^2 + \left(\frac{n}{b}\right)^2} \quad (4.123)$$

where v_0 is wave velocity in vacuum and indexes mn corresponds to Eqs. (4.117) and (4.119).

Finally separation constant $\gamma_{z,mn}$ which is identical with propagation constant in z direction is

$$\gamma_{z,mn} = \begin{cases} \frac{\omega}{v_0} \sqrt{\left(\frac{f_{c,mn}}{f}\right)^2 - 1} & \text{for } f < f_{c,mn} \\ j \frac{\omega}{v_0} \sqrt{1 - \left(\frac{f_{c,mn}}{f}\right)^2} & \text{for } f > f_{c,mn} \end{cases} \quad (4.124)$$

and z component of the phasor of electric field

$$\mathbf{E}_{z,mn}(x, y, z) = E_{z,mn}(0) \sin\left(\frac{m\pi}{a}x\right) \sin\left(\frac{n\pi}{b}y\right) e^{-\gamma_{z,mn}z} \quad (4.125)$$

$E_{z,mn}(0)$ is product of $X_m(0)$, $Y_n(0)$ and D_{mn} . For unique solution the value $E_{z,mn}(0)$ must be known.

Derivation of remaining field components can be found for instance in [Hammond_2].

Eq. (4.125) can be rearranged with introduction of phase constant by propagation in free space with cut-off frequency $\beta_0(f_{c,mn})$

$$\gamma_{z,mn} = \begin{cases} \beta_0(f_{c,mn}) \sqrt{1 - \left(\frac{f}{f_{c,mn}}\right)^2} & \text{for } \frac{f}{f_{c,mn}} < 1 \\ j\beta_0(f_{c,mn}) \sqrt{\left(\frac{f}{f_{c,mn}}\right)^2 - 1} & \text{for } \frac{f}{f_{c,mn}} > 1 \end{cases} \quad (4.126)$$

Dependence of the module of the propagation constant $|\gamma_z|$ versus frequency related to the cut-off frequency $f/f_{c,mn}$ is shown in Fig.4.41.

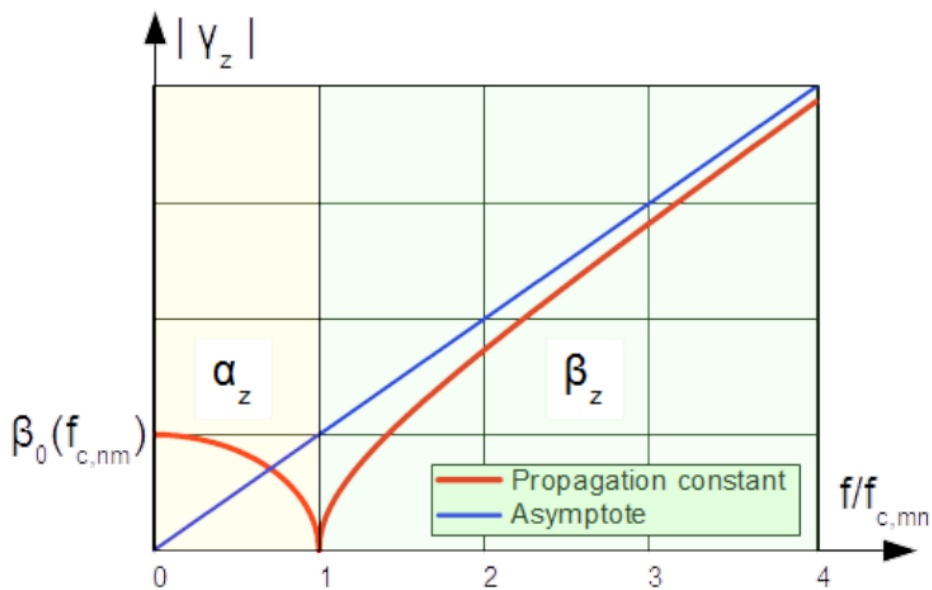


Figure 4.41: Frequency dependence of the module of the propagation constant $|\gamma_z|$.

Below the cut-off frequency (yellowish region) the propagation constant is real $\gamma_z = \alpha_z$. The wave is attenuated. Above the cut-off frequency (greenish region) the propagation constant is imaginary $\gamma_z = j\beta_z$. The wave is able to propagate. The propagation constant in this region approaches asymptote

$$\beta_{z,mn} = \beta_0 (f_{c,mn}) \frac{f}{f_{c,mn}}$$

It is blue straight line in Fig.4.41.

The type of fields discussed up to now are so called E-mode named equivalently TM-mode. Notice that the lowest mode of this type of fields can be E_{11} (TM_{11}) due to constraint on tangential component of E field on the walls.

Similarly H_z component for the H mode (TE) mode can be derived

$$\mathbf{H}_{z,mn}(x, y, z) = H_{z,mn}(0) \cos\left(\frac{m\pi}{a}x\right) \cos\left(\frac{n\pi}{b}y\right) e^{-\gamma_{z,mn}z} \quad (4.128)$$

Dependence in x and y direction is cosinusoidal since H field must be tangential on the metal walls i.e.

$$\frac{\partial H_z}{\partial n} = 0. \text{ Consequently the lowest mode that can be propagated can have one number equal zero i.e.}$$

$$H_{10}, H_{01} \text{ (} TE_{10}, TE_{01} \text{)}.$$

1. Proximity effect between strains makes the exact analysis of the problem more complex but the tendency is unambiguous.↵
2. $w \gg t$ ↵
3. If in a given instant the field strength at one point of the equiphase surface has e.g. positive magnitude, then it also has at all remaining points.↵
4. \mathbf{E}_r component by electric dipole Eq. (4.43) and \mathbf{H}_r component by magnetic dipole Eq. (4.54) disappears due to lack of summand with the first power of radius r .↵
5. Exactly cosinusoidal distribution is valid for lossless symmetrical transmission line with parallelly layouted forward and return conductors. Per unit length parameter LC of such line are constant. By straightened out conductors LC parameters depend on position along the arms.↵
6. By field probes the parasitic capacitances can be neglected due to small electrical size. It is not the case by antennas.↵
7. Common mode chokes are covered in chapter [Filters]↵
8. By EMC measurements of radiated emission, antenna height must be scanned from 1 m to 4 m. Up to the height 2 m the capacitances are hardly equal.↵
9. It is a circle with the radius $r = \lambda/(4\pi)$.↵
10. By scaling with the magnitudes, power density is $\frac{1}{2}(\vec{\mathbf{E}} \times \vec{\mathbf{H}}^*)$.↵
11. Index i points out the isotropic radiator as the reference.↵
12. Difference of power sent from the source and power reflected at the antenna feeding terminal by mismatching.↵
13. Notice that it is in line with definition of electrical dimension and with the rule about radiation inability of electrically small objects, see chapter [El_size].↵
14. Introduce $F_P(\theta) = 1/2$ into equation on power radiation pattern of the dipole Eq. (4.84).↵
15. It is apart from small region next to the conductors' surfaces where the Poynting's vector is leant toward the inside of conductors where the wave energy is converted into heat.↵

5. Protection from disturbances

LF/RF filtering

Overlying the useful voltage with disturbances

From the point of view of the victim the wave coupling is not the third art of hazard. Waves can interfere either by means of electric or magnetic coupling, depending on coupling impedance.

Electric coupling can be represented with magnetomotive force MMF depending on displacement current as shown in Fig. [DB_circuits] a) in chapter [sssec:Field_probes]. It is justified because coupling capacitance like capacitance C_S of the \dot{D} probe is usually negligibly small. Magnetic coupling can be represented with electromotive force EMF depending on time derivative of magnetic inductance as shown in Fig. [DB_circuits] b) in chapter [sssec:Field_probes]. It is justified because coupling inductance like inductance L_S of the \dot{B} probe is usually negligibly small.

There are two contributions of symmetrical coupling with symmetrical line as shown in Fig. 5.1.

- External magnetic field of disturbance can couple with the loop built with forth and return line, between nodes 1, 3, 4 and 2. This coupling is represented with EMF_{13}^{DM} and EMF_{42}^{DM} . They drive current I_{sm}^{DM} (symmetrical-magnetic) in the forth and return line.
- External electric field of disturbance can energise capacitances C_{12} and C_{34} between forth and return lines. This coupling is represented with MMF_{12}^{DM} and MMF_{34}^{DM} . They drive current I_{se}^{DM} (symmetrical-electric) in the forth and return line.

Currents I_{sm}^{DM} as well as I_{se}^{DM} causes voltage drop across the load U_{34} , which overlaps the useful voltage.

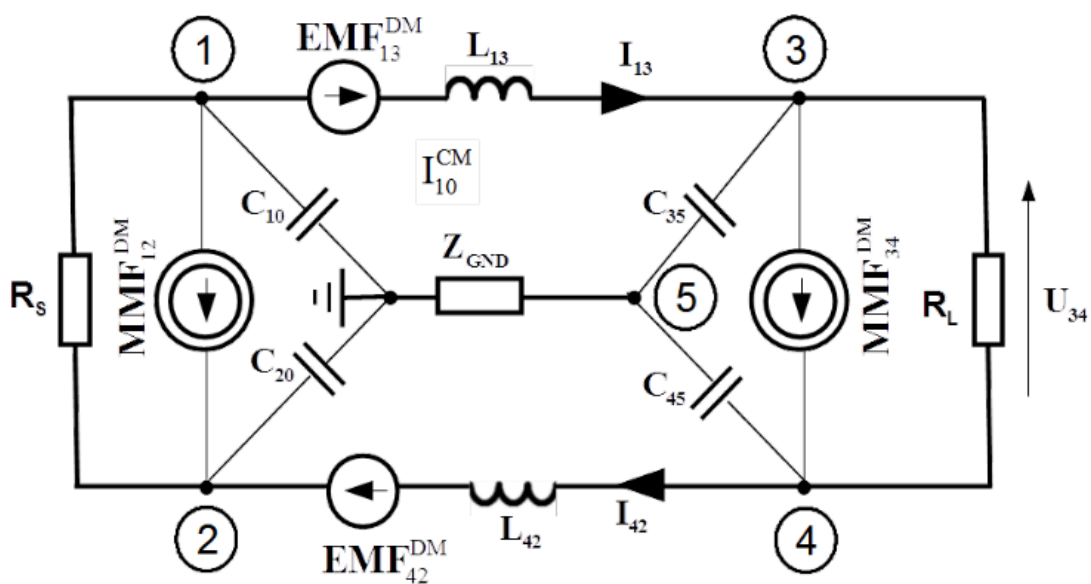


Figure 5.1: Symmetrical coupling of disturbances with symmetrical line.

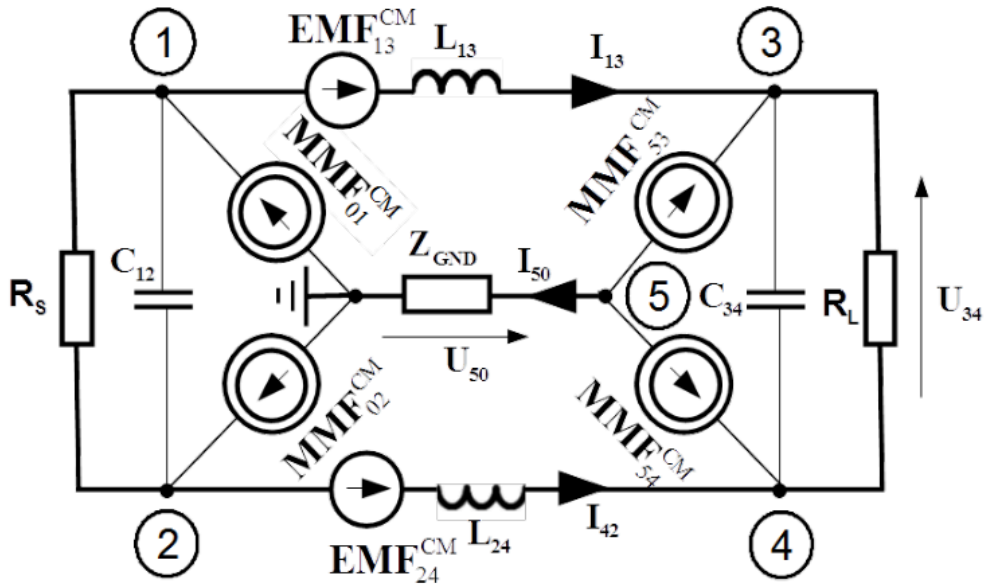


Figure 5.2: Asymmetrical coupling of disturbances with symmetrical line.

Two contributions of asymmetrical coupling with symmetrical line are possible, as shown in Fig. 5.2.

- External magnetic field of disturbance can couple with the loops built with forth line and ground reference, the first one between nodes: 1, 3, 5 and 0, the second one between nodes: 2, 4, 5 and 0. They are represented with EMF_{13}^{CM} and EMF_{24}^{CM} .
- External electric field of disturbance can energise capacitances C_{10} , C_{20} , C_{35} and C_{45} , each between line under consideration and the ground reference. They are represented with MMF_{10}^{CM} , MMF_{20}^{CM} , MMF_{53}^{CM} , and MMF_{54}^{CM} .

Contributions of asymmetrical coupling are harmless as long as the transmission line is perfectly balanced, in the same sense as in chapter [TCL_chapter]. Lack of balance there caused conversion of symmetrical signal to asymmetrical disturbance polluting the surrounding. Here lack of balance makes the symmetrical line sensitive to asymmetrical disturbance in which the line is immersed.

By deviation from symmetry, common mode current I_{50} is driven in the ground reference causing longitudinal voltage drop U_{50} across impedance Z_{GND} . It contributes in symmetrical (transverse) voltage U_{34} across the load.

Ratio of longitudinal voltage U_{50} to transverse voltage U_{34}

$$L_{LC} = \frac{U_{50}}{U_{34}} \quad L_{LC(dB)} = 20 \log \left(\frac{U_{50}}{U_{34}} \right) \quad (5.1)$$

is called loss of longitudinal (to transverse) conversion, alternatively Longitudinal Conversion Loss LCL. It is used for rating deviation from the ideal balance by symmetrical transmission. By approaching perfect equilibrium, L_{LC} tends to infinity.

The LCL is reciprocal to TCL introduced in chapter [TCL_chapter]. TCL quantifies lack of perfection of symmetry provoking the asymmetrical disturbance, LCL vulnerability to pick them up.

By unsymmetrical transmission any decomposition of disturbance and any protection barriers against them exist. The whole disturbance couples with them.

In order to protect the victim from the magnetomotive force appearing by electrical coupling, reasonably big capacitors mounted in parallel to the MMF must be applied. Such capacitor shortcircuits the MMF,

avoiding penetration of remaining parts of the circuit. However protection from the electromotive force appearing by magnetic coupling can be realised with reasonably big inductance mounted serially to the EMF. Such inductance reduces the disturbance current in the mesh with the EMF.

Ingredients of filters

Let us consider multiconductor line as shown in Fig. 5.3 transmitting power from source to load or signal from transmitter to receiver. Occasionally this line can be a medium for disturbance propagation from source to victim. Disturbance current in each line I_i can be decomposed into differential I_i^{DM} and common I_i^{CM} mode.

$$I_i = I_i^{DM} + I_i^{CM}$$

Attribute of the components are:

- nullifying the differential mode,
- cumulation of common mode in the return path.

$$\sum_{i=1}^N I_i^{DM} = 0 \quad I^{CM} = I_{N+1} = \sum_{i=1}^N I_i^{CM} \quad (5.3)$$

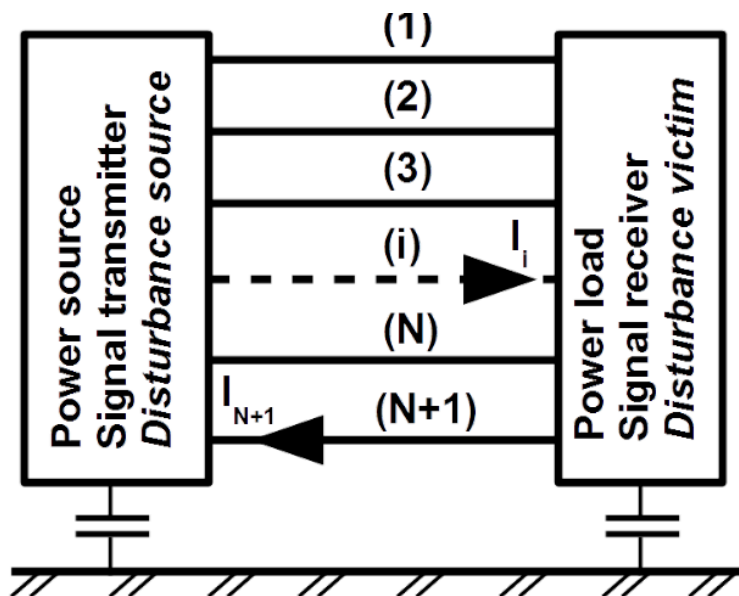


Figure 5.3: Multiconductor transmission line.

Return path can be for instance PE line by power cord or cable shield by signal transmission. However arrangements connected with the line always have some capacitances to the ground reference, as shown in Fig. 5.3. With increased frequency impedance of the return path becomes bigger than that of the return path via ground capacitances and the ground impedance, due to magnetic inductance. By such frequencies the nominal return line (N+1) must be viewed as ordinary forth lines ($i = 1, 2, \dots, N$). The multilines gains one conductor.

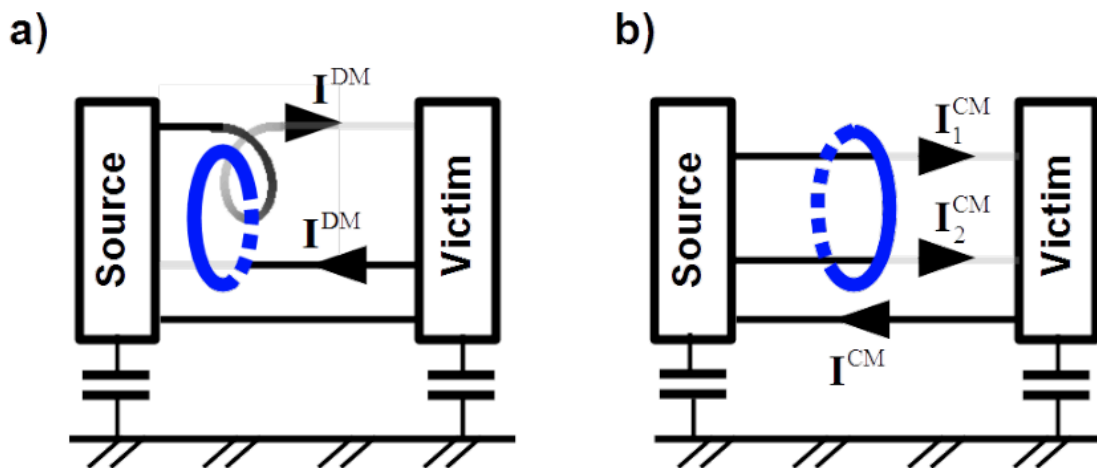


Figure 5.4: Separation of differential and common mode in two conductor line.

It is straightforward to separate modes one from another in two-conductors line. The target can be either individual suppression of them or quantification. As the blue ellipse in Fig. 5.4 a suppressing magnetic core or a measurement clamp can be imagined. If conductors are passed reversely through the hole in the core, as in Fig. 5.4 a) then magnetic flux excited in the core is due only to differential mode current¹. In contrast to accordant passage, as in Fig. 5.4 b) which causes excitation of magnetic flux only due to common mode current.

Separation of the common mode is valid also for any multiconductor line. However separation of differential mode is ambiguous because the differential modes build a set with number of elements depending on total number of conductors (N).

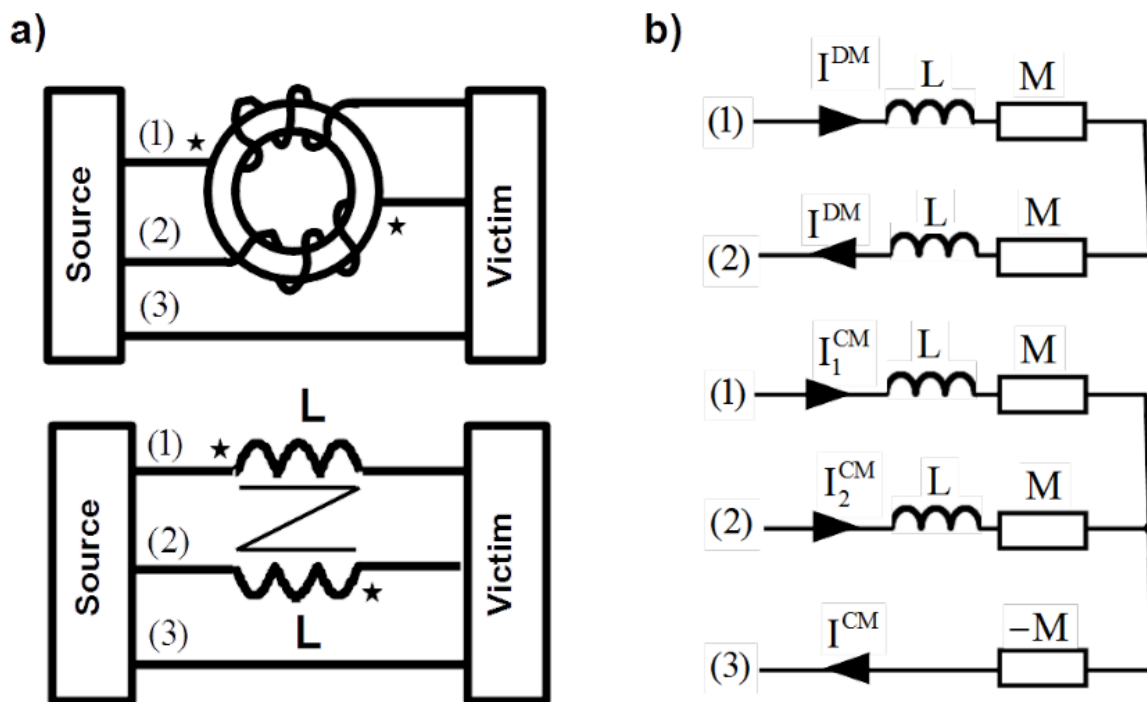


Figure 5.5: Two conductors DM choke.

In Fig. 5.5 a) differential mode choke with three turns is presented². As the circuit symbol either zig-zag or stars marking beginnings of the windings are used. Equivalent circuits of the choke for DM and CM currents are shown in Fig. 5.5 b). Symbol M represents coupling inductance ($M = kL$) where k is coupling factor. By lack of leakage field ($k = 1$), the DM choke has inductance equal to four-tuple of the self inductance L for the DM current and it is transparent for the CM current.

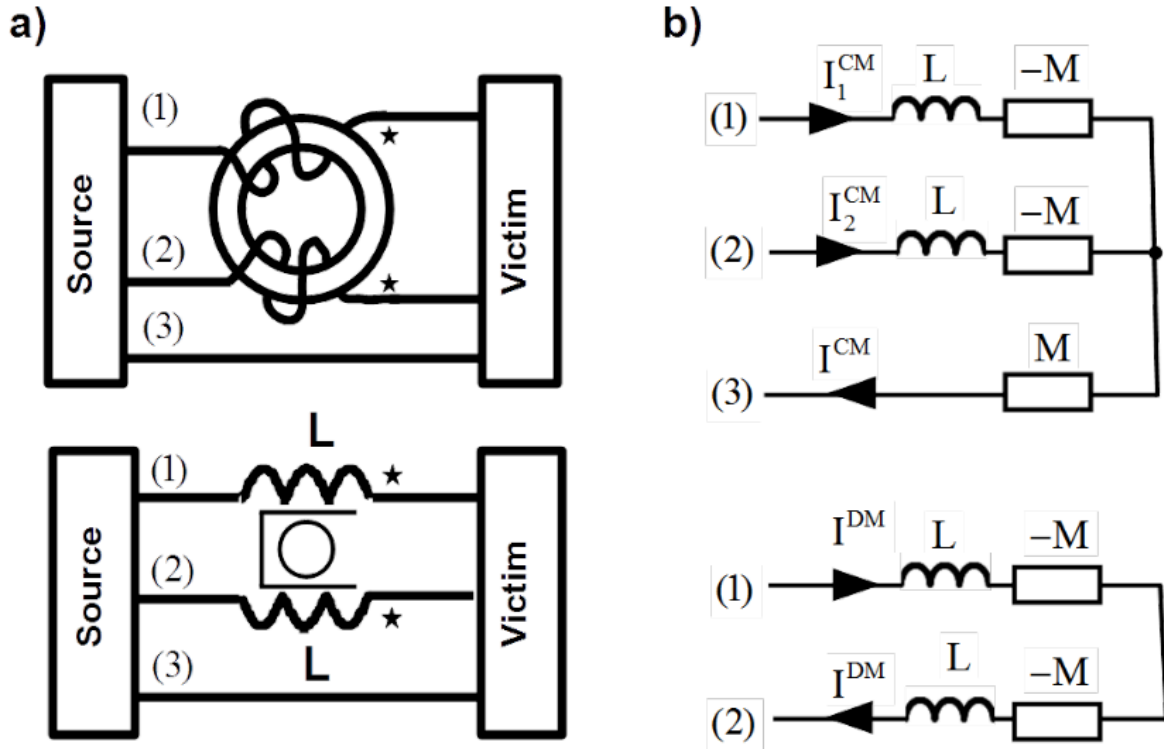


Figure 5.6: Two conductors CM choke.

In Fig. 5.6 a) common mode choke with two turns is presented. As the circuit symbol either U-shape, circle or stars marking beginnings of the windings are used. Equivalent circuits of the choke for CM and DM currents are shown in Fig. 5.6 b). By lack of leakage field ($k = 1$), the CM choke has inductance equal to M for the CM current and it is transparent for the DM current.

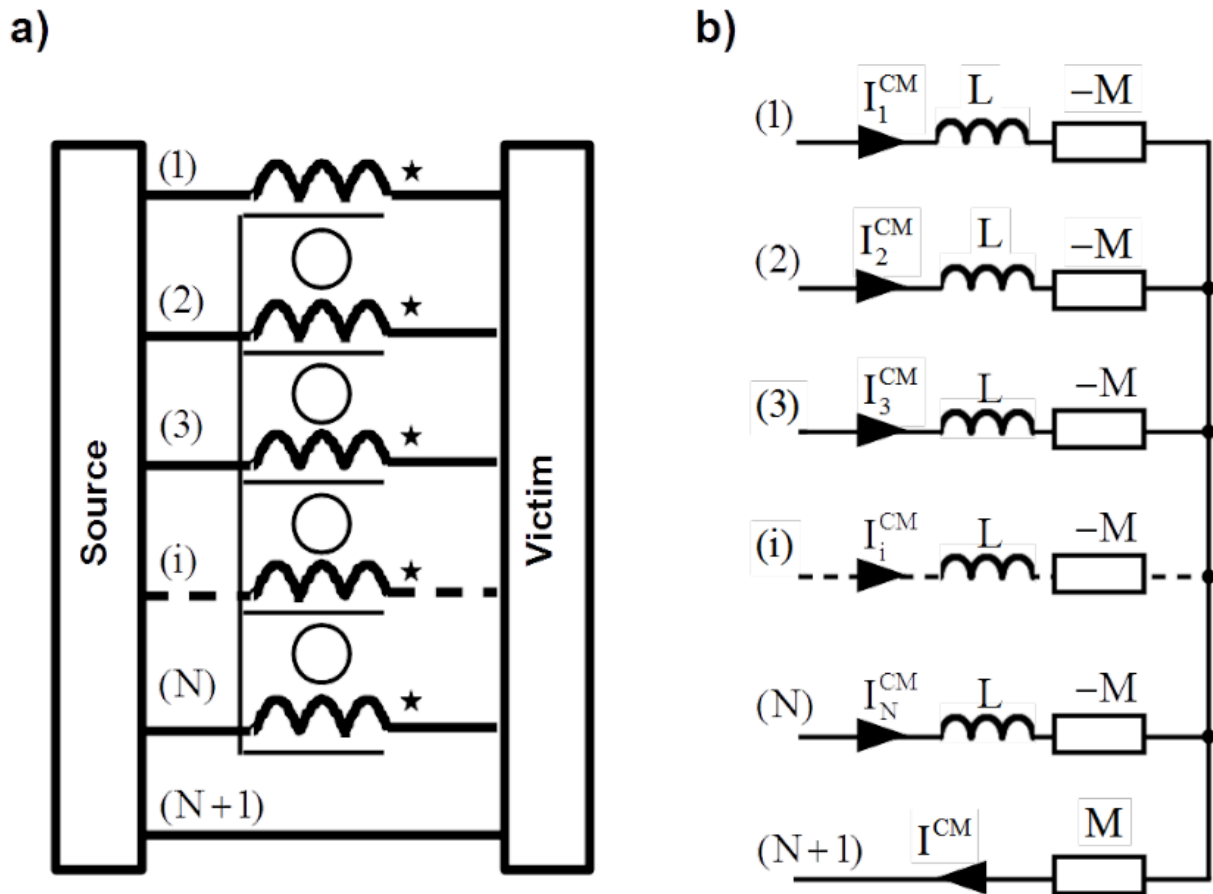


Figure 5.7: CM choke built of multiconductor line.

Resulting common mode inductance equal to M is also valid for multiconductor line with arbitrary number of conductors, as shown in Fig. 5.7.

Notice that, residual current devices (RCD) commonly used in the LV electric installations as protection against electric shock are nothing else but common mode chokes mounted at all supply lines excluding PE line. They sense the residual current i.e. common mode current driven through the PE line. It is leakage current occurring only by fault. There are different sensitivity groups of RCDs depending on the broken residual current:

- high sensitivity (HS): 5 – 10 – 30 mA (for direct-contact / life injury protection),
- medium sensitivity (MS): 100 – 300 – 500 – 1000 mA (for fire protection),
- low sensitivity (LS): 3 – 10 – 30 A (typically for protection of machine).

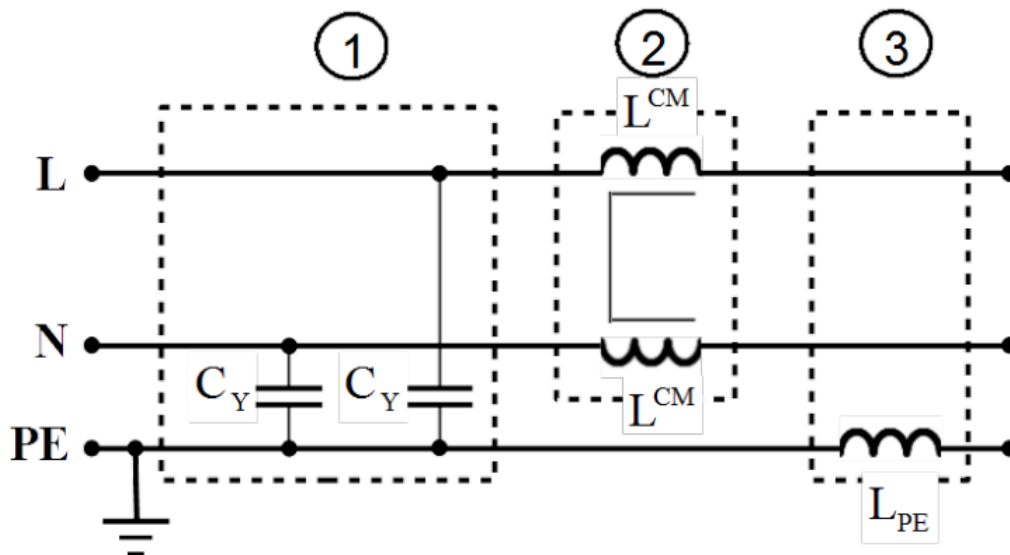


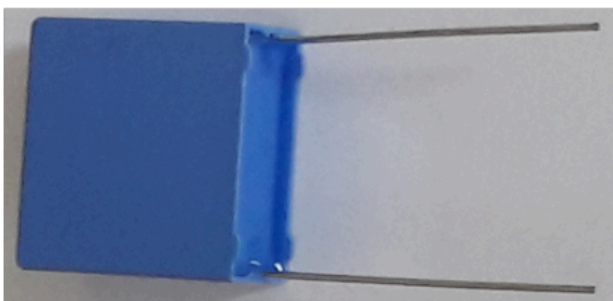
Figure 5.8: CM suppression elements in mains filter.

Common mode disturbance can be suppressed in the mains filter in three manners as shown exemplarily for one phase filter in Fig. 5.8, with:

1. so called C_Y capacitors mounted between each live and PE conductor,
2. common mode choke built on all live conductors,
3. choke in the PE conductor.

As presented in chapter [Film_cap] capacitors realised in THD technology have inductive character starting from specific frequency. From this frequency on they lose ability to shortcircuit the MMF. It is due to leads inductances, see Fig. 5.9 a). In special, costly application the feedthrough condensers are used. They do not have leads and their body has tubular or disk shape. One electrode is fed along the axis as shown in Fig. 5.9 b). Another electrode is metal cylinder with mounting collar at one end. Condenser is inserted into the hole in the metal wall between filter compartments. The collar ensures round about contact with the wall. The threaded nut screwed on the other side of the wall fixes the condenser.

a)



b)



Figure 5.9: Example of the THD a) and feedthrough b) C_Y condenser.

In the same way CM disturbance can be suppressed in the signal lines. Examples are gathered in Fig. 5.10.

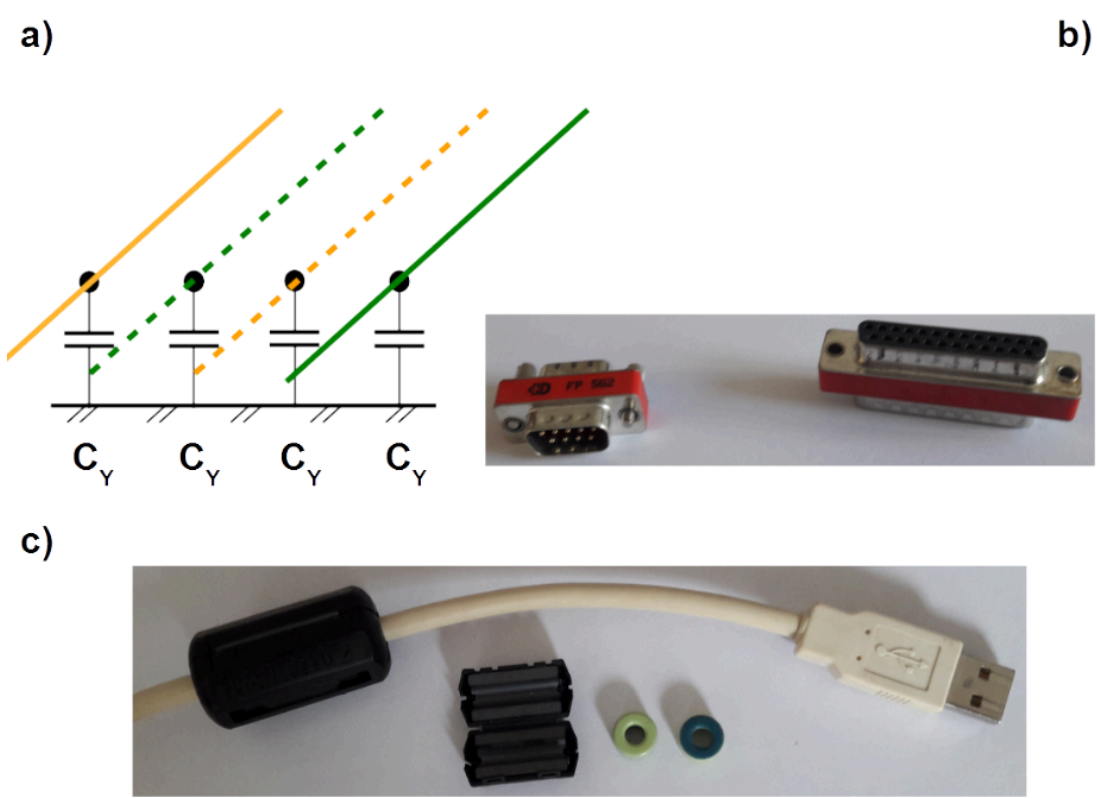


Figure 5.10: C_Y capacitors in the multiconductor line a), $C_Y = 100 \text{ pF}$ condensers built in the D-sub adapter b), CM choke as the snap ferrite or ferrite bead for mounting on the multiconductor line c).

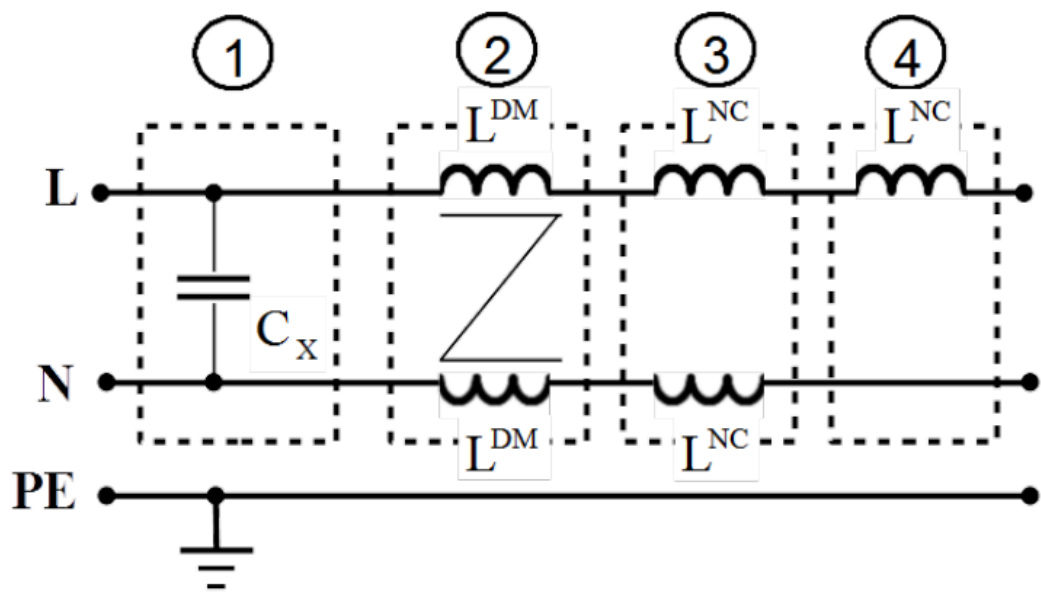


Figure 5.11: DM suppression elements in mains filter.

Differential mode disturbance can be suppressed in the mains filter in four manners as shown exemplarily for one phase filter in Fig. 5.11, with:

1. so called C_X capacitors mounted across the phase and neutral line,
2. differential mode choke built on the phase and neutral line,
3. (not coupled) chokes mounted in the phase and neutral line,
4. choke mounted in either the phase or neutral line.

Measures 2 and 4 cannot be realised in the three phase filter. Moreover measure 4 is not recommended. Indeed double inductance mounted in one line can suppress differential mode alike by dividing it in both lines but this change influences in the same time relation between common and differential mode currents. Possibly it can worsen suppression of common mode.

Notice that measures for suppressing the common and differential mode support mutually one another:

1. C_Y capacitors in Fig. 5.8 build capacitance $C_Y/2$ across phase and neutral line thus suppresses the differential mode disturbance,
2. the leakage flux of the common mode choke in Fig. 5.8 suppresses the differential mode disturbance,
3. the leakage flux of the differential mode choke in Fig. 5.11 suppresses the common mode disturbance,
4. (not coupled) chokes mounted in the phase and neutral line suppress as well as the common mode disturbance.

Few words are necessary about mysterious C_X and C_Y capacitors. Class – X and Class – Y capacitors are safety certified, whereupon the first are designed to “fail short” and the second to “fail open”. C_X are allowed to be mounted only across the live lines because “failing short” between live line and PE could cause electrical shock hazard. Only C_Y are allowed to be mounted between any live line and PE. Since they “fail open”, electric shock hazard is excluded. Of course C_Y capacitors can be applied across the live lines but it is not practiced because they are more expensive then C_X and have smaller maximal values in series. There are three subclasses of C_X capacitors: X1, X2 and X3 and four subclasses of C_Y : Y1, Y2, Y3 and Y4. Most common are C_{X2} and C_{Y2} .

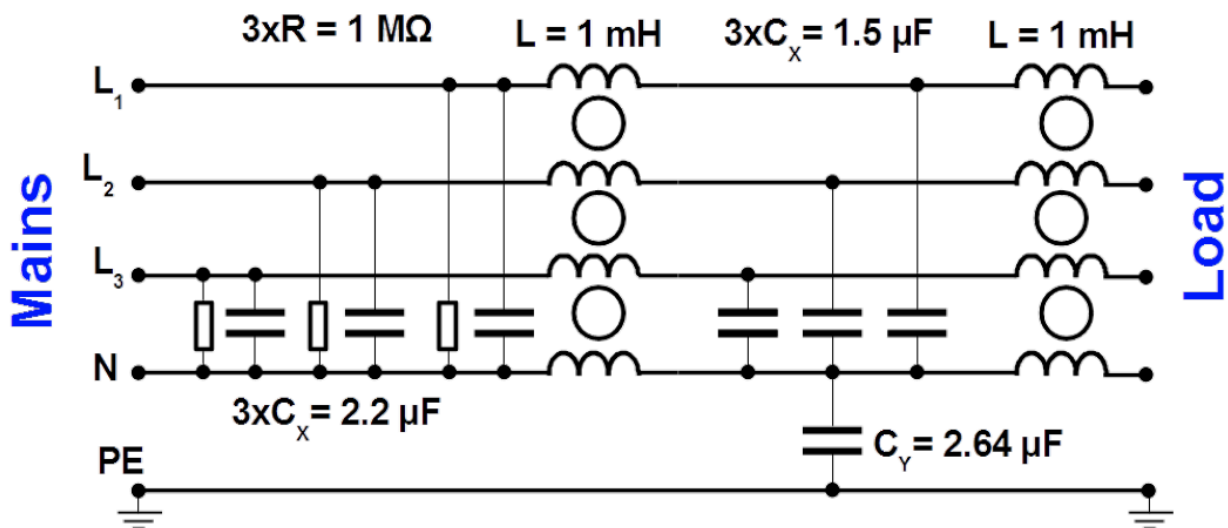


Figure 5.12: Three phase four line filter.

Why C_X capacitors in filter shown in Fig. 5.12 are not mounted across the live lines?

Rated voltage of C_X condensers available in the market are about $310 V_{RMS}$. They do not withstand $400 V_{RMS}$ line to line voltage of the European mains. Therefore they are circuited in the star connected to Neutral line. Of course their attenuation is worse but alternative does not exist.

Rated voltage of C_Y condensers available in the market are about $250 V_{RMS}$. They withstand line to PE voltage of the European mains by symmetry i.e. $230 V_{RMS}$. However its designed value must be raised due to unsymmetry of the load and tolerance of the mains voltage ($+10\%$). Therefore they are circuited between the star point of C_X condensers and PE line. Again their attenuation is worse but alternative does not exist.

Resistances in parallel to the C_X condensers on the mains side of the filter accelerate discharge of C_X by disconnecting the appliance from the mains. According to standard [IEC-61010-1] after disconnecting the mains, voltage must decay below the active danger level within 5 s at the mains terminal and within 10 s at the remaining terminals. The active danger level is equal to $33 V_{RMS}$ or 46.7 V peak value by AC voltage and 70 V DC. In humid environment these values are: $16 V_{RMS}$, 22.6 V and 35 V respectively.

For value estimation of the discharge R resistance following relations should be applied

$$U_{Save} < U_{Max} \cdot e^{-\frac{5s}{RC}} \quad R < \frac{5s}{C \cdot \ln\left(\frac{U_{Max}}{U_{Save}}\right)}$$

By the European mains voltage discharge resistance $R = 1 M\Omega$ mounted in filter in Fig. 5.12 is much smaller than the threshold value by the worst case.

Non linear suppressors

Non linear suppressors protect victims from surges described in chapter [Thunderstorm], hence the name surge protection devices SPD. They are mounted in parallel at the protected port of the device (victim)³, as shown in Fig. 5.13. Two types of protectors are used: *crowbar* shortcircuiting (almost) the poles of the port and *clamp* limiting the voltage of the pulse and sucking the surge current. The SPDs have very big impedance by normal circumstances at the port, falling to very low values by triggering i.e. when the transient exceeds the threshold.

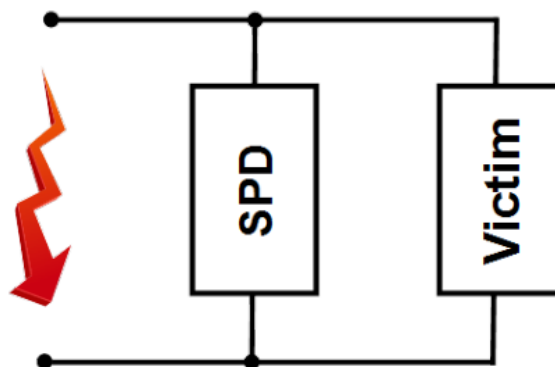


Figure 5.13: Principle of protection against surges.

Presentation of the SPDs here is concentrated on protection of the power AC mains ports because of importance of safety and reliability requirements.

The crowbar devices are based on encapsulated gas arresters, known in abbreviation as Gas Discharge Tubes GDTs. Its $I(U)$ approximated characteristic is shown in Fig. 5.14. Notice that it is identical as presented in Fig. [Gas_discharge] with interchanged axes⁴. In normal operating conditions, called the OFF state the GDTs are very good insulators and do not contribute the leakage current. They do not shortcircuits

the poles totally by ignition of the arc, called ON state because as it was demonstrated in Tab. [vapor-arc] there is little voltage across the arc, between 12 V and 17.5 V, depending on electrodes' material. Anyway dissipation in the GDT is minimal. Therefore they can handle transients with very big energy.

Their drawback, compared with the clamp devices is longer reaction time and sustaining the arc after regress of the transient. The normal AC power conditions inhibit self-extinction of once ignited arc.

The background of clamp devices is reversely polarised semiconductor junction. Therefore clamp devices exhibits some capacitance contributing the leakage current in the OFF state. There are two types of the clamp devices: the Metal Oxide Varistors (MOVs) and Transient Voltage Suppression Diodes (TVSDs). In the ON state, they limit the voltage transient to a specific level by varying its internal resistance, see Fig. 5.15 and 5.16. They absorb the transient's energy and therefore, cannot withstand transients with as big energy as the GDTs do. Big disadvantage of the MOVs is the "Upturn region" shown in Fig. 5.15. By very high currents their resistance increases rapidly.

The clamp devices "faults short" therefore they cannot be mounted between live lines and PE line.

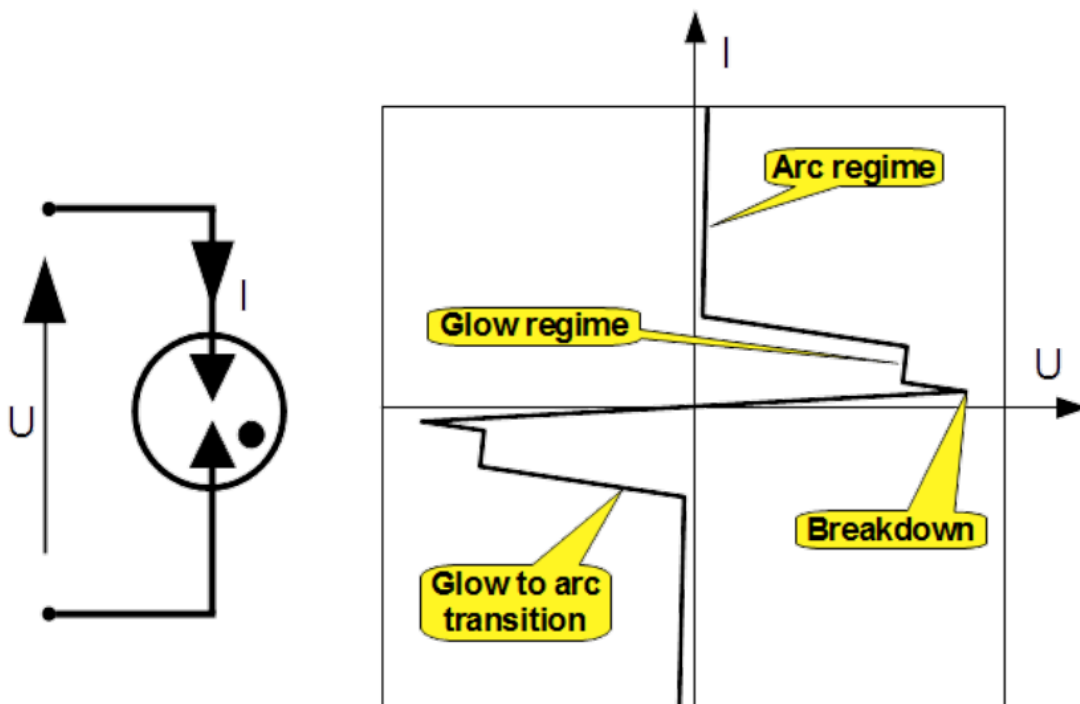


Figure 5.14: Gas Discharge Tube.

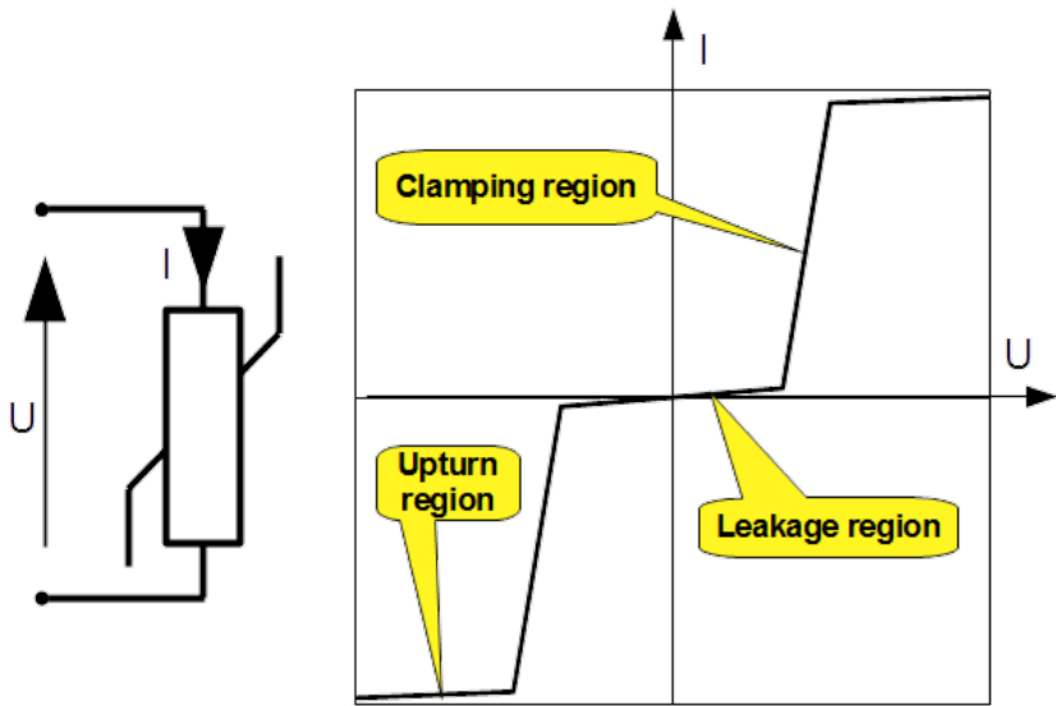


Figure 5.15: Metal Oxide Varistor.

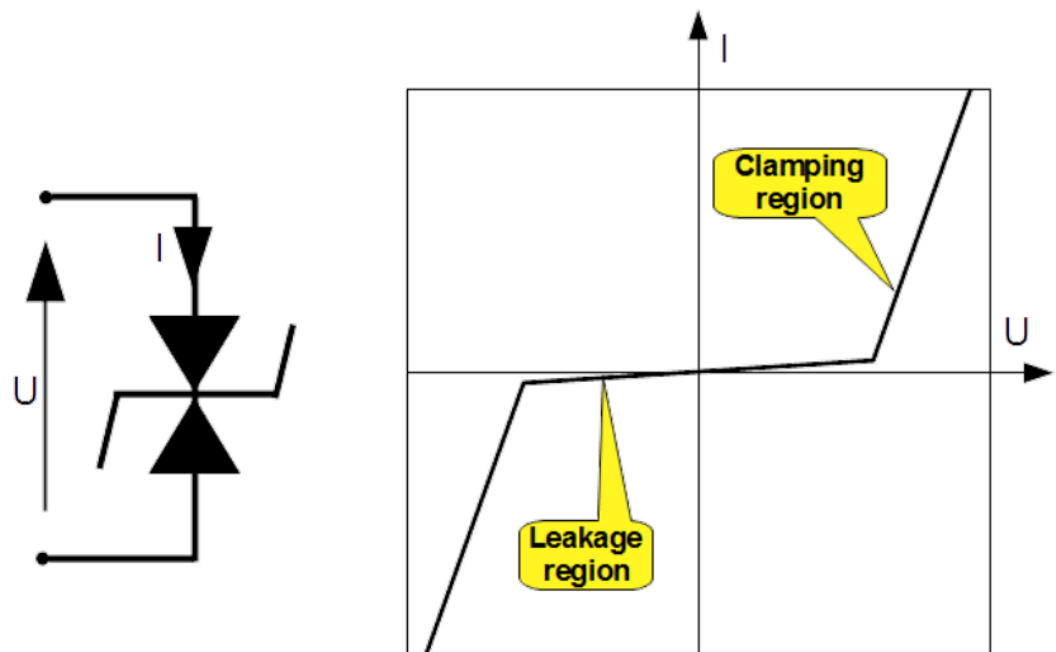


Figure 5.16: Transient Voltage Suppression Diode.

Table 5.1: Comparison of typical SPDs parameters applicable at the AC mains port.

	GDT	MOV	TVSD
Response time	$< 1 \mu s$	$< 100 ns$	$< 1 ns$
Capacitance in OFF state	$< 1.5 pF$	$180 pF - 1.7 nF$	$1 nF - 11 nF$
Resistance in OFF state	$10 G\Omega$	$180 k\Omega - 900 k\Omega$	$1.5 M\Omega - 22 M\Omega$
Trigger voltage	$280 V - 7.5 kV$	$130 V - 650 V$	$90 V - 625 V$
Maximal surge current	$10 kA$	$10 kA$	$6 kA$

[SPD_parameters]

In Tab. 5.1 parameters of typical SPDs applicable at the AC mains port are gathered. As to time of reaction and swallowed transient energy, they decrease from left to right. GDTs and MOVs can handle merely surges while TVSDs as well BURST (5 ns rise time) and even ESD (800 ps rise time). The best insulation and hence the smallest leakage current ensure GDTs. At the opposite pole are TVSDs.

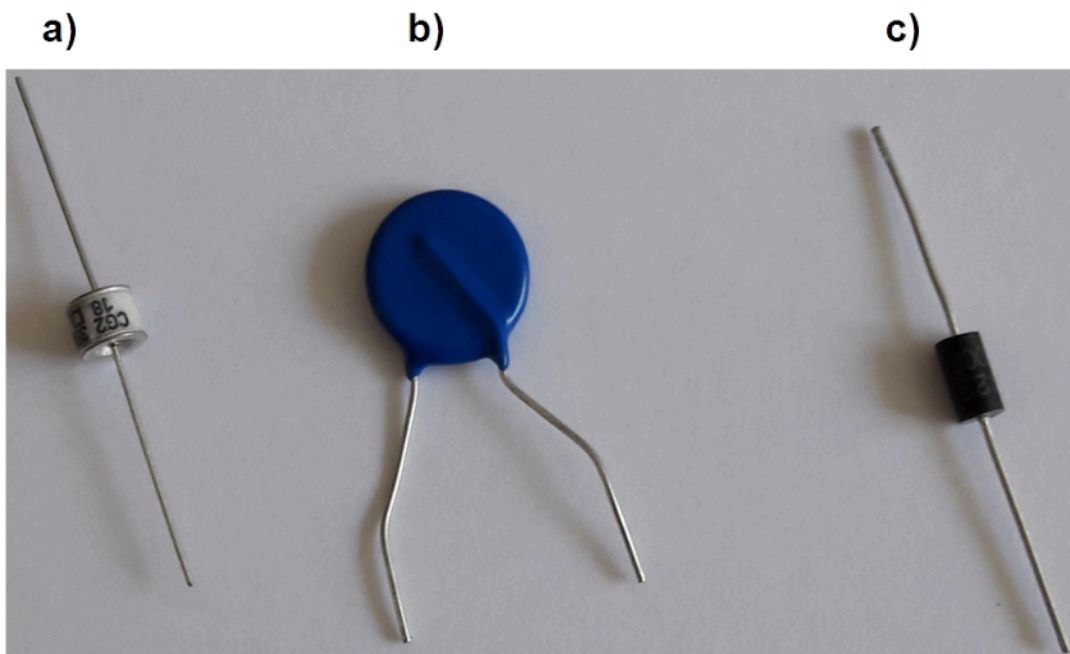


Figure 5.17: Examples of the SPDs in the THD technology: GDT a), MOV b), TVSD c).

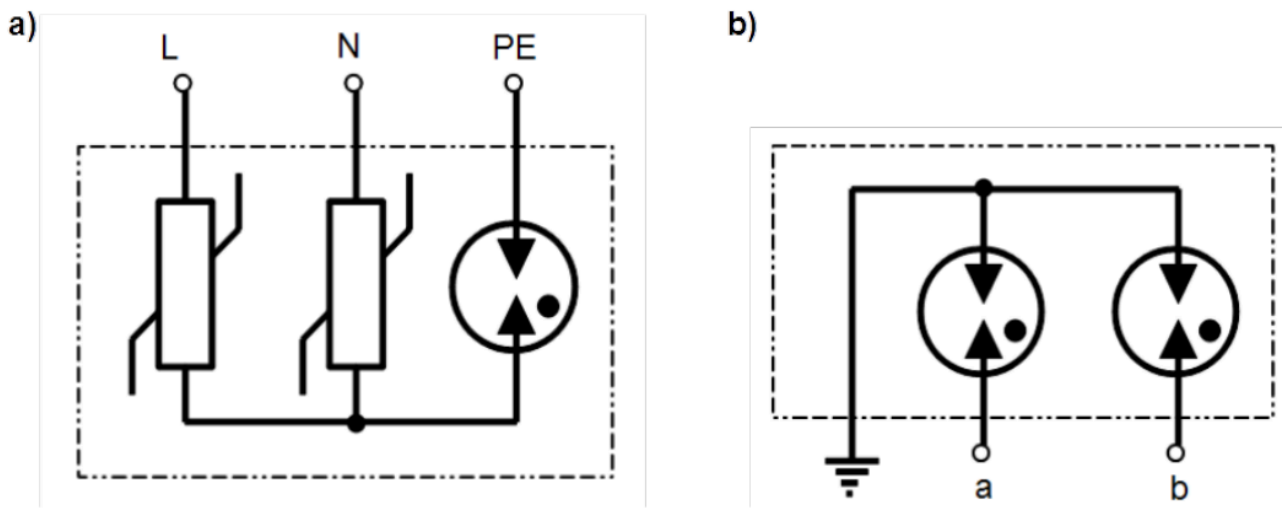


Figure 5.18: Combined SPDs at the AC mains port a), at the telecom port b).

Combined SPDs for the one phase AC mains is presented in Fig. 5.18 a). Neither GDT is mounted between live lines nor MOVs are mounted between live lines and PE. In this way protection against electric shock is not violated.

The GDT can be mounted directly to the ground in case of telecom line, as shown in Fig. 5.18 b). 48 VDC is not capable of sustaining the arc. It extinguishes with vanishing the transient.

Shielding

The task of a shield is to mitigate the field in the desired region. Two scenarios are possible: embracing protected region, as shown in Fig. 5.19 a) or surrounding the source of undesirable field, as shown in Fig. 5.19 b).

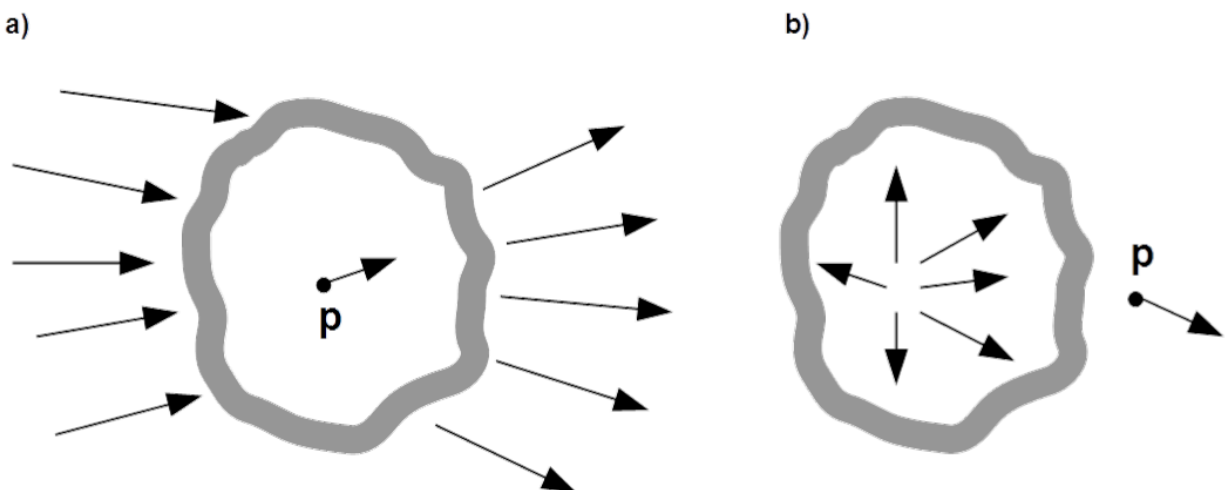


Figure 5.19: Shielding embracing victim a), embracing sinner b).

Constitutive formulas of shielding effectiveness are as follows

$$\begin{aligned}
 SE^E(p) &= \frac{|\vec{E}_0(p)|}{|\vec{E}_S(p)|} & SE_{dB}^E(p) &= 20 \log \left(\frac{|\vec{E}_0(p)|}{|\vec{E}_S(p)|} \right) \\
 SE^H(p) &= \frac{|\vec{H}_0(p)|}{|\vec{H}_S(p)|} & SE_{dB}^H(p) &= 20 \log \left(\frac{|\vec{H}_0(p)|}{|\vec{H}_S(p)|} \right)
 \end{aligned}
 \tag{5.5}$$

These formulas are the ratios of absolute values of the fields $E_0(p)$ or $H_0(p)$ in point p of interest without the shield and fields $E_S(p)$ or $H_S(p)$ in the same point p after immersing the shield.

Mind that shielding effectiveness is defined in the same way as attenuation of a two-port described in chapter [Attenuation]. Field strength in the point of interest is determined in two situation: by direct exposition to the sinner and by inserting in-between the shield. Later it will be shown that shielding effectiveness is also referred to some medium quantity like attenuation to the reference impedance.

Static and quasi-static fields

Metal shields

If separated, source charge e.g. $+Q$, as shown in Fig. 5.20 is enclosed in the metallic compartment⁵, then surrounding is not free of its electric field, unless the enclosure is grounded. Free electrons in metal are attracted by the free source charge inside, causing excess of positive charges at the outer surface of the enclosure. It does not matter whether the free source charge is placed centrally or eccentrically as shown in Fig. 5.20 a) and b) respectively. Electric flux over arbitrary closed surface S is related to the net free charges $\sum Q$ enclosed in the integration surface with the Gauss's theorem

$$\oint_S \vec{D} \cdot d\vec{S} = \sum Q$$

where \vec{D} is vector of electric flux density.

In both cases the net charge is equal to the source $+Q$ charge. Consequently $SE_{E_{dB}}(p) = 0$ dB.

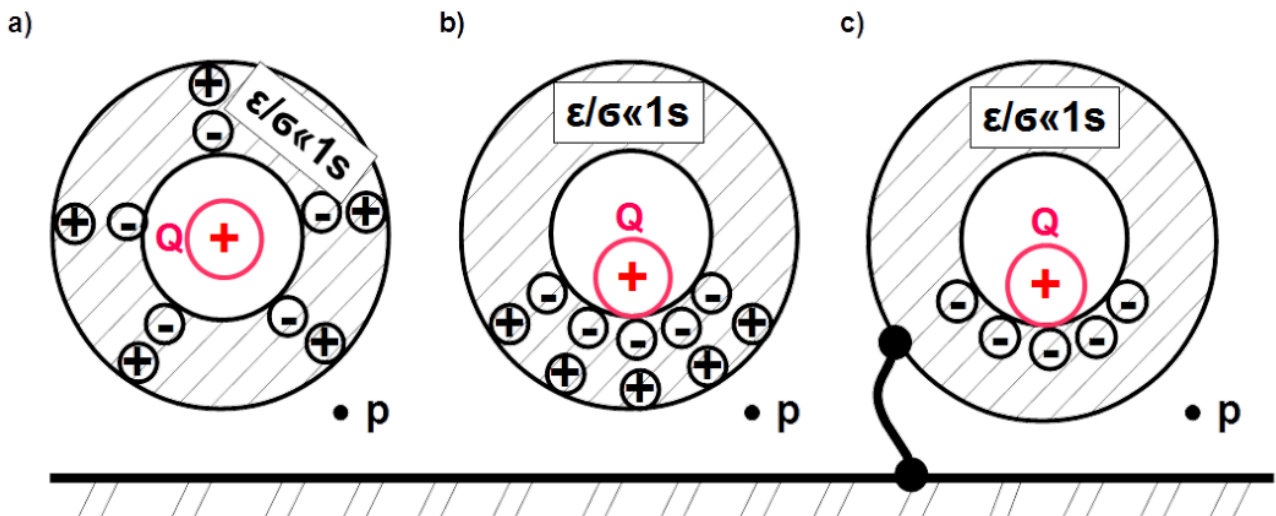


Figure 5.20: Shielding of surrounding from the free charge in metal enclosure.

By grounding the enclosure, as shown in n Fig. 5.20 c) free electrons are brought from the most distant region of the ground, leaving free of charge the outer surface of the enclosure and causing $SE_{dB}^E(p) \rightarrow \infty$ dB . Free charges in conductor seek to get away from each other as far as possible leaving the inside free of electric field.

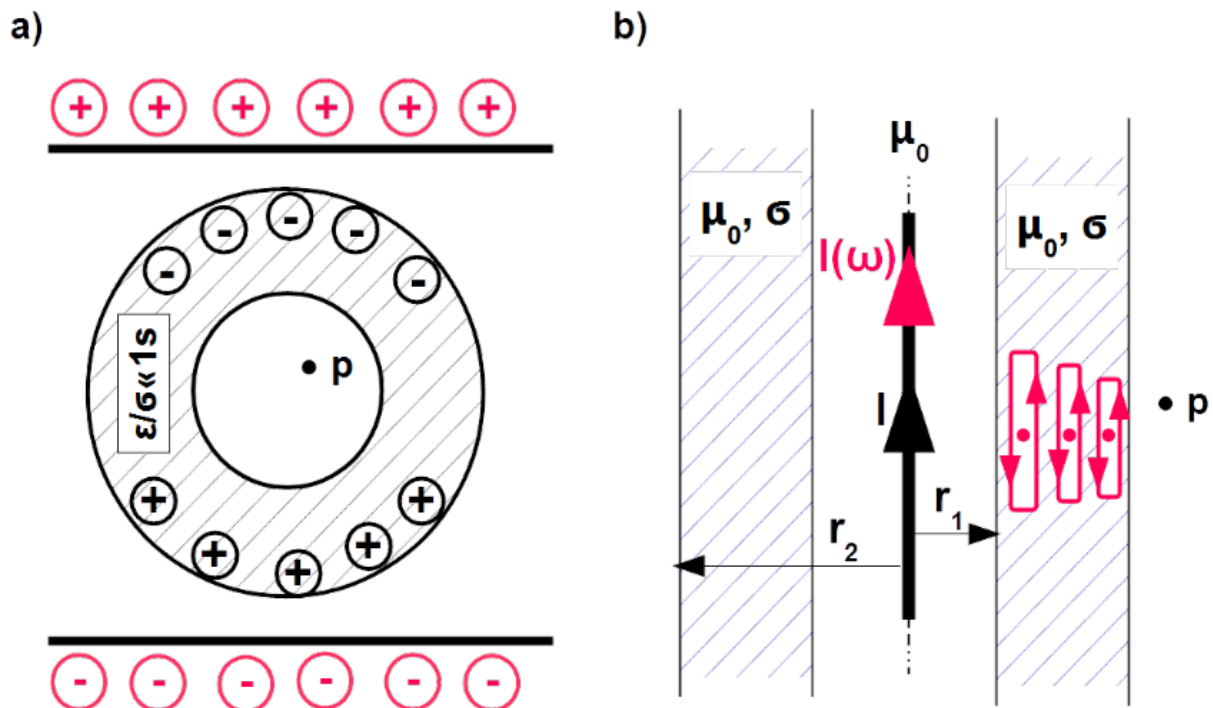


Figure 5.21: Space shielded from the external electrostatic field with the metal enclosure a), transparency of the metal enclosure by magnetostatic field and shielding mechanism by quasi-stationary magnetic field b).

In the same way the case shown in Fig. 5.21 a) can be rationalised. Voltage is maintained between two horizontal metal plates. This results in charging one plate positively and another negatively with the same quantity of charge. Free electrons are attracted by the positive charges concentrated at the upper metal plate from the most remote regions of enclosure. Consequently the same quantity of positive and negative charges are concentrated only at the outer surface of the enclosure liberating the inside from the field.

Rules valid for electrostatic fields are in force in case of extremely low or quasi-static electric fields.

As to magnetic properties of materials there are two origins of it. Atoms have magnetic moment quantified with Eq.([m_dipole]), due to circular movement of electrons around nucleus. Moreover, electrons besides electric charge have the property of spin about their own axes. In other words, electrons possess an intrinsic magnetic dipole moment⁶ [Hammond_2]. In most materials these magnetic moments almost cancels each other. Their relative permeability μ_r is almost equal one, whereat $\mu_r < 1$ by diamagnetics and $\mu_r > 1$ by paramagnetics. Diamagnetics subjected to an external magnetic field reduces resulting field whereat magnetic moments in paramagnetic materials turn in direction to strengthen the incident field. Ferromagnetics are paramagnetics with very strong amplification attribute.

Magnetic field of conducted currents is ruled with the Ampère's circular theorem which couples strength of magnetic field \vec{H} with net conducted current I embraced with the integration perimeter l

$$\oint_l \vec{H} \cdot d\vec{l} = \sum I$$

In Fig. 5.21 b) infinitely long cylindrical structure is shown. Conductor driving constant current I is laid out along the axis. It is source of azimuthal magnetic field according to the Ampère's circular theorem. Nothing changes if conductor is immersed in the paramagnetic or diamagnetic metal cylinder ($\mu_r = 1$) with inner and outer radius r_1 and r_2 respectively. The net conducted current remains unchanged i.e. shield effectiveness is zero.

Situation changes if the current is alternated $I(\omega)$ as presented with the red arrow in Fig. 5.21 b). Magnetic induction $\vec{B}(\omega)$ is source of eddy currents in the shield material. Nature of eddy currents is conduction. They can be depicted with small loops distributed in the whole cross section of the shield (red contours). Overlapping of current's loops results with inhomogeneous distribution of the longitudinal current density in the shield. This reduces net current present in the Ampère's theorem.

The inhomogeneous current distribution and in consequence shielding effectiveness depends on relation between skin depth defined with formula Eq. (5.21) and thickness of the shield. The smaller this relation, the bigger shielding effectiveness. In extreme case skin depth tends to zero, volume current becomes surface current on the inner surface of the shield liberating the shield material and space outside the shield from magnetic field.

On the opposite pole is situation by very thin shield compared to the skin depth. Then the sense of the current density at the outer surface of the shield is opposite to that at the inner surface. Resulting induced current, applied in the Ampère's circular theorem is almost zero and shield effectiveness is minimal.

Skin depth by 50 Hz in copper, aluminium and brass are $\delta_{Cu} \approx 9 \text{ mm}$, $\delta_{Al} \approx 1.2 \text{ cm}$ and $\delta_{Brass} \approx 1.8 \text{ cm}$. By iron with $\mu_r = 1000$ it is $\delta_{Fe} \approx 0.7 \text{ mm}$. The engineer's rule of thumb i.e. 1/10 suggests effective shielding by 50 Hz with shield thickness between 10 cm and 20 cm applying copper, aluminium or brass respectively and 7 cm by iron shield.

One example of such shielding is copper foil or tape wrapped over the pulse transformer of Switched Mode Power Supplier. Such transformers operate with frequencies from tenth of kHz up to over 100 kHz. Wrapping is the only measure protecting the surrounding on the PCB from direct magnetic coupling.

Computer era of monitors based on electron guns in which electron beam is deflected with low frequency magnetic field is over. At that time operation of monitors for example in offices located by railway stations with electrical traction was possible only with placing monitors in mu-metal or permalloy covers. Their relative permeability μ_r by 1 kHz are 30'000 and 80'000 respectively. The same concerned TV sets and oscilloscopes with electron guns.

Shielding of alternated magnetic field due to eddy currents can be interpreted with energy conservation. Energy of the source current $I(\omega)$ is dissipated in the conducting material, decreasing energy bound in magnetic field. The reference quantity for shielding effectiveness is the skin depth. Memorise, that grounding of the shield, unlike by static electric field has any influence on the effectiveness.

Shielding with diamagnetics and ferromagnetics

If separated, source charge e.g. $+Q$, as shown in Fig. 5.22 is enclosed in the dielectric compartment, then surrounding is not free of its electric field. Electric dipoles inside the enclosure, either induced or permanent turns in the direction to weaken the source field inside the dielectric. In consequence negative charge appears at the internal surface of dielectric and positive at the external surface. Anyway the net charge remains unchanged $+Q$ causing zero effectiveness of shielding. It is independent on the shape of the enclosure as shown in Fig. 5.22 a) and b).

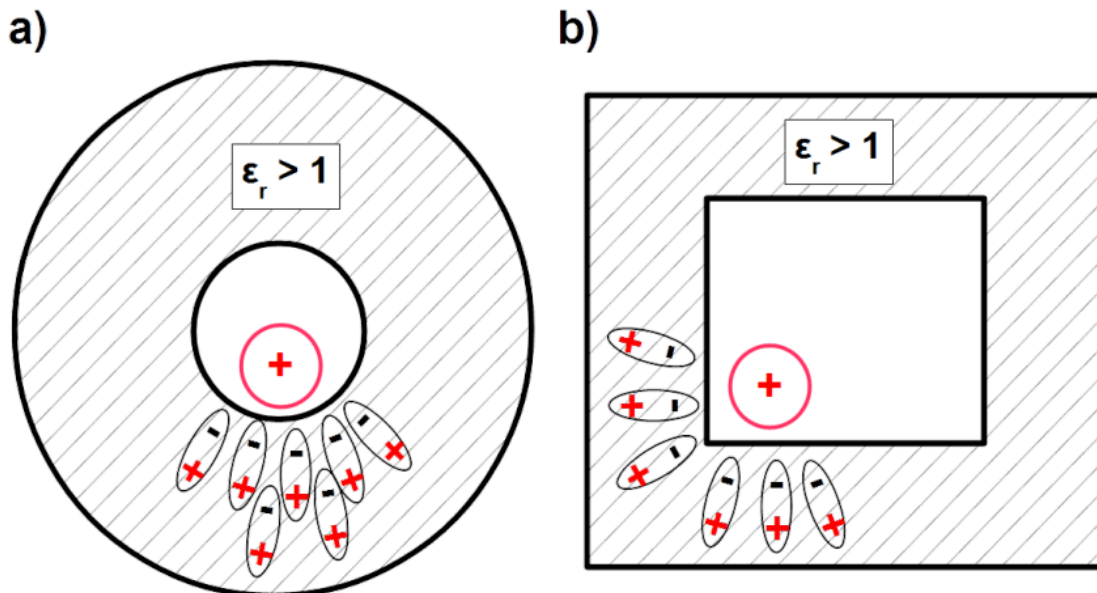


Figure 5.22: Lack of shielding of surrounding from the free charge in dielectric enclosure.

If between two charged metal plates oriented horizontally as shown in Fig. 5.21 a) dielectric cylinder is inserted as shown in Fig. 5.23 a) then electric field inside cylinder is mitigated. There is twofold representation of field strength vector \vec{E} in the figure⁷. One is set of streamlines, another is colours' visualization of the vector magnitude.

Dielectric material which weakens the incident field of free charges "expels" the field from the inside. The strongest field depicted with bright tones is around the cylinder. Cylinder itself and its interior are dark. Presented example is calculated by $\epsilon_r = 10$. Shielding effectiveness inside was $SE_E(p) \approx 7.5 \text{ dB}$. Noticeable is dielectric permittivity ϵ as reference by shielding effectiveness of electric field.

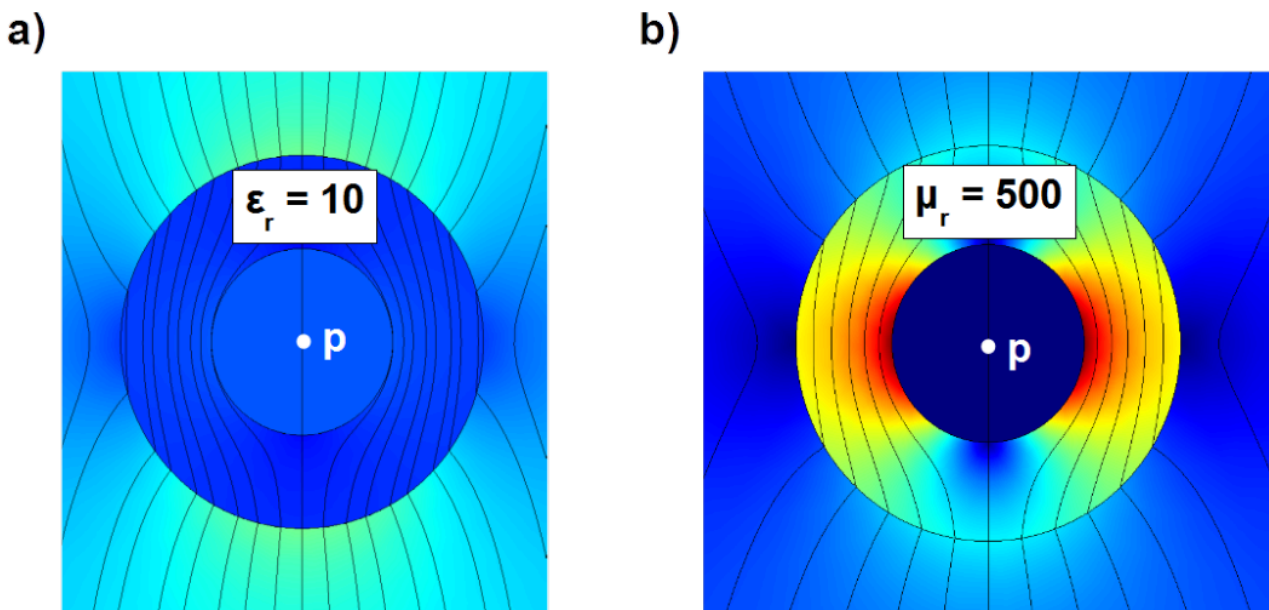


Figure 5.23: Shielding from static electric field with diamagnetic material a), from static magnetic field with ferromagnetic material b).

Imagine two metal bars oriented vertically, driving constant current one forth, another back. Between the bars homogeneous magnetic field is established. If between the bars ferromagnetic cylinder is inserted as shown in Fig. 5.23 b) then magnetic field inside cylinder is mitigated. There is twofold representation of vector of magnetic flux density \vec{B} in the figure⁸. One is set of streamlines, another is colours' visualization of the vector magnitude.

Ferromagnetic material which strengthens the incident field of conducted currents in the bars "attracts" the field to the inside. The strongest field depicted with bright tones is inside the cylinder. Cylinder exterior and interior are dark. Presented example is calculated by $\mu_r = 500$. Shielding effectiveness inside was $SE^H(p) \approx 40 \text{ dB}$.

Measurement of static magnetic fields with probes is always preceded with compensation (calibration) procedure. It consists in simulating conditions liberating from any static magnetic field. For this, the field sensor is placed in the ferromagnetic cylinder with bottom in order to eliminate influence of the Earth magnetic field.

Noticeable is magnetic permeability μ as reference by shielding effectiveness of magnetic field.

RF shielding in the far field zone

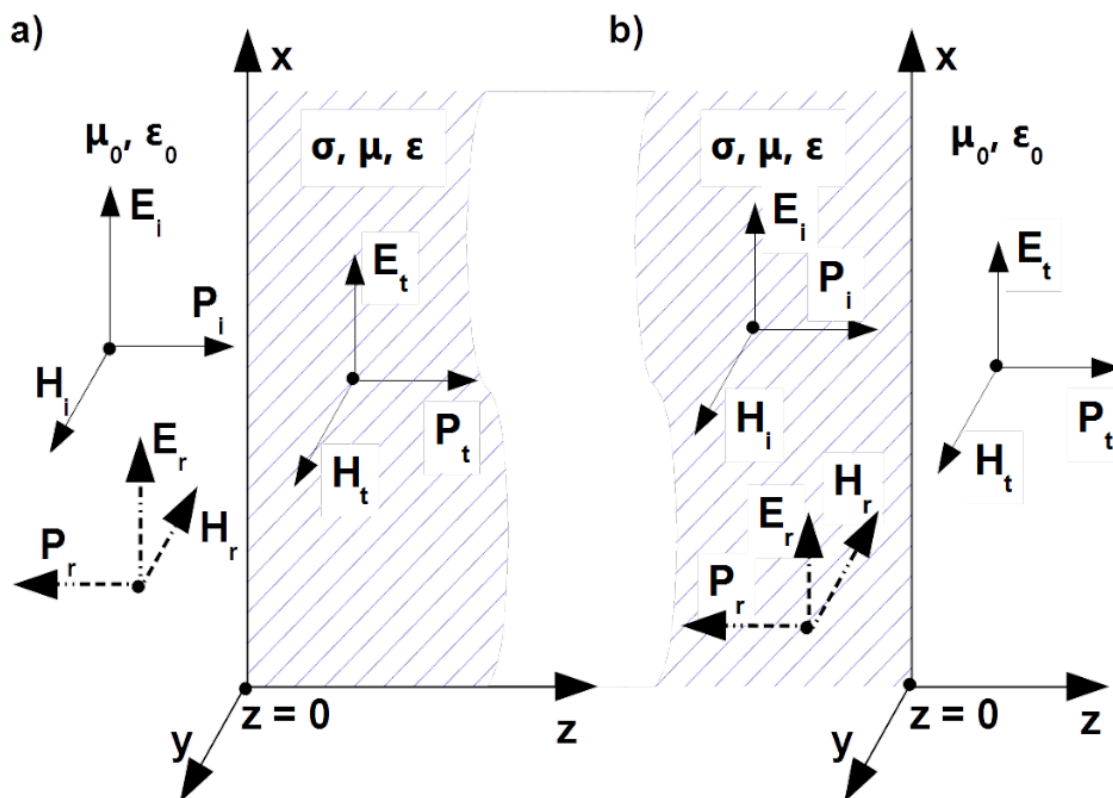


Figure 5.24: Passage of electromagnetic plane TEM wave from lossless half infinite space to lossy half infinite medium a) and from lossy half infinite medium to lossless half infinite space.

If the incident plane (TEM) wave \vec{E}_i, \vec{H}_i propagates in z-direction in the lossless medium μ_0, ϵ_0 as shown in Fig. 5.24 a) then

$$\begin{aligned}\vec{\mathbf{E}}_i(z) &= \mathbf{E}_m e^{-j\beta_0 z} \cdot \vec{\mathbf{1}}_x = Z_0 \mathbf{H}_m e^{-j\beta_0 z} \cdot \vec{\mathbf{1}}_x \\ \vec{\mathbf{H}}_i(z) &= \frac{\mathbf{E}_m}{Z_0} e^{-j\beta_0 z} \cdot \vec{\mathbf{1}}_y = \mathbf{H}_m e^{-j\beta_0 z} \cdot \vec{\mathbf{1}}_y\end{aligned}\quad (5.24)$$

where Z_0 is intrinsic impedance defined in Eq. ([Z_0]) and β_0 is phase constant defined in Eq. ([beta]).

Vector product of these vectors gives the Poynting vector $\vec{\mathbf{P}}_i(z)$ oriented along the z-axis.

$$\vec{\mathbf{P}}_i(z) = \vec{\mathbf{E}}_i(z) \times \vec{\mathbf{H}}_i(z) \quad (5.9)$$

If such plane (TEM) wave impinges on a lossy medium σ , μ , ϵ tangential to the wavefront, by $z = 0$ as shown in Fig. 5.24 a) then part of the field is reflected and travels backwards. These fields have subscripts r . Analogue to the voltage and current reflection coefficients in the circuit theory, presented in chapter [impedance matching], Eq. ([GAMMA_2]) and Eq. ([GAMMA_4]) respectively, reflection coefficients Γ^E and Γ^H for electric and magnetic field at the boundary are introduced

$$\Gamma^E = \left| \frac{\vec{\mathbf{E}}_r}{\vec{\mathbf{E}}_i} \right| \quad \Gamma^H = - \left| \frac{\vec{\mathbf{H}}_r}{\vec{\mathbf{H}}_i} \right| \quad (5.18a)$$

along with transmission coefficients \mathbf{T}^E and \mathbf{T}^H

$$\mathbf{T}^E = \left| \frac{\vec{\mathbf{E}}_t}{\vec{\mathbf{E}}_i} \right| \quad \mathbf{T}^H = \left| \frac{\vec{\mathbf{H}}_t}{\vec{\mathbf{H}}_i} \right| \quad (5.18b)$$

These coefficients concerns phasors \mathbf{E} and \mathbf{H} for vector's senses according to Fig. 5.24 a).

$$\begin{aligned}\vec{\mathbf{E}}_r(z) &= \Gamma^E \mathbf{E}_m e^{j\beta_0 z} \cdot \vec{\mathbf{1}}_x = -Z_0 \Gamma^H \mathbf{H}_m e^{j\beta_0 z} \cdot \vec{\mathbf{1}}_x \\ \vec{\mathbf{H}}_r(z) &= -\frac{\Gamma^E \mathbf{E}_m}{Z_0} e^{j\beta_0 z} \cdot \vec{\mathbf{1}}_y = \Gamma^H \mathbf{H}_m e^{j\beta_0 z} \cdot \vec{\mathbf{1}}_y\end{aligned}\quad (5.12)$$

The rest is transmitted to the lossy medium. These fields have subscripts t . Transmission coefficients \mathbf{T}^E and \mathbf{T}^H denotes amount of transmitted fields

$$\begin{aligned}\vec{\mathbf{E}}_t(z) &= \mathbf{T}^E \mathbf{E}_m e^{-\gamma z} \cdot \vec{\mathbf{1}}_x = \mathbf{Z} \mathbf{T}^H \mathbf{H}_m e^{-\gamma z} \cdot \vec{\mathbf{1}}_x \\ \vec{\mathbf{H}}_t(z) &= \frac{\mathbf{T}^E \mathbf{E}_m}{\mathbf{Z}} e^{-\gamma z} \cdot \vec{\mathbf{1}}_y = \mathbf{T}^H \mathbf{H}_m e^{-\gamma z} \cdot \vec{\mathbf{1}}_y\end{aligned}\quad (5.25)$$

where

$$\gamma = \sqrt{j\omega\mu(\sigma + j\omega\epsilon)} = \alpha + j\beta \quad (5.14)$$

is propagation constant in the lossy medium which is composed of attenuation coefficient α and phase constant β .

\mathbf{Z} is intrinsic impedance of the lossy medium

$$\mathbf{Z} = \sqrt{\frac{j\omega\mu}{\sigma + j\omega\epsilon}} \quad (5.15)$$

Continuity of tangential component of the electric field at the interface $z = 0$

$$1 + \Gamma^E = \mathbf{T}^E \quad Z_0 (1 - \Gamma^H) = \mathbf{Z} \mathbf{T}^H \quad (5.16)$$

along with continuity of tangential component of the magnetic field at the interface $z = 0$ yields

$$\mathbf{Z} (1 - \Gamma^E) = Z_0 \mathbf{T}^E \quad 1 + \Gamma^H = \mathbf{T}^H \quad (5.17)$$

yields

$$\Gamma^E = \frac{\mathbf{Z} - Z_0}{\mathbf{Z} + Z_0} \quad \Gamma^H = \frac{Z_0 - \mathbf{Z}}{Z_0 + \mathbf{Z}} \quad (5.18)$$

For the sake of convenience only $\mathbf{\Gamma}^E$ will be used with omitted superscript

$$\mathbf{\Gamma} = \mathbf{\Gamma}^E = -\mathbf{\Gamma}^H = \frac{\mathbf{Z} - Z_0}{\mathbf{Z} + Z_0} \quad (5.19)$$

Transmission coefficients are as follows

$$\mathbf{T}^E = 2 \frac{\mathbf{Z}}{\mathbf{Z} + Z_0} \quad \mathbf{T}^H = 2 \frac{Z_0}{\mathbf{Z} + Z_0} \quad Z_0 \mathbf{T}^E = \mathbf{Z} \mathbf{T}^H \quad (5.20)$$

In most cases shields are constructed from materials in which density of displacement current is negligible small compared to conducted current by frequency of interest⁹ ($\sigma \gg \omega\epsilon$) then propagation constant, defined with Eq. (5.14) simplifies

$$\gamma = \alpha + j\beta = (1 + j) \sqrt{\frac{\omega\mu\sigma}{2}} = (1 + j) \frac{1}{\delta} \quad (5.21)$$

Compare with Eq. ([delta]).

Intrinsic impedance defined with Eq. (5.15) simplifies as follows

$$\mathbf{Z} = (1 + j) \sqrt{\frac{\omega\mu}{2\sigma}} = (1 + j) \frac{1}{\sigma\delta} = \sqrt{\frac{\omega\mu}{\sigma}} e^{j\frac{\pi}{4}} \quad (5.22)$$

Notice that propagation constant γ as well as intrinsic impedance \mathbf{Z} increases proportionally to square root of frequency.

Remarkable is very small value of intrinsic impedance by well conducting metals. For aluminium and copper its module is smaller than $70 \text{ m}\Omega$ and $60 \text{ m}\Omega$ respectively by 40 GHz .

If the lossless medium is vacuum with intrinsic impedance $Z_0 = 377 \text{ }\Omega$ and lossy medium is well conducting metal, then $\mathbf{Z} \ll Z_0$ and $\mathbf{\Gamma} \approx -1$. It mean that electric field is almost totally reflected because $\vec{\mathbf{E}}_r \approx -\vec{\mathbf{E}}_i$ but magnetic field is nearly doubled since $\mathbf{T}^H = 1 - \mathbf{\Gamma} \approx 2$. Analogy to line with distributed parameters, terminated with the shortcircuit is obvious.

If the incident plane (TEM) wave $\vec{\mathbf{E}}_i, \vec{\mathbf{H}}_i$ propagates in z-direction in the lossy medium σ, μ, ϵ as shown in Fig. 5.24 b) then

$$\begin{aligned} \vec{\mathbf{E}}_i(z) &= \mathbf{E}_m e^{-\gamma z} \cdot \vec{\mathbf{1}}_x = \mathbf{Z} \mathbf{H}_m e^{-\gamma z} \cdot \vec{\mathbf{1}}_x \\ \vec{\mathbf{H}}_i(z) &= \frac{\mathbf{E}_m}{\mathbf{Z}} e^{-\gamma z} \cdot \vec{\mathbf{1}}_y = \mathbf{H}_m e^{-\gamma z} \cdot \vec{\mathbf{1}}_y \end{aligned} \quad (5.24)$$

By reaching the outlet surface to the lossless medium tangential to the wavefront by $z = 0$ as shown in Fig. 5.24 b), part of the field is reflected and travels backwards. These fields have subscripts r .

$$\begin{aligned} \vec{\mathbf{E}}_r(z) &= \mathbf{\Gamma}^E \mathbf{E}_m e^{\gamma z} \cdot \vec{\mathbf{1}}_x = -\mathbf{Z} \mathbf{\Gamma}^H \mathbf{H}_m e^{\gamma z} \cdot \vec{\mathbf{1}}_x \\ \vec{\mathbf{H}}_r(z) &= -\frac{\mathbf{\Gamma}^E \mathbf{E}_m}{\mathbf{Z}} e^{\gamma z} \cdot \vec{\mathbf{1}}_y = \mathbf{\Gamma}^H \mathbf{H}_m e^{\gamma z} \cdot \vec{\mathbf{1}}_y \end{aligned} \quad (5.24)$$

The rest is transmitted to the lossless half infinite medium

$$\begin{aligned} \vec{\mathbf{E}}_t(z) &= \mathbf{T}^E \mathbf{E}_m e^{-j\beta_0 z} \cdot \vec{\mathbf{1}}_x = Z_0 \mathbf{T}^H \mathbf{H}_m e^{-j\beta_0 z} \cdot \vec{\mathbf{1}}_x \\ \vec{\mathbf{H}}_t(z) &= \frac{\mathbf{T}^E \mathbf{E}_m}{Z_0} e^{-j\beta_0 z} \cdot \vec{\mathbf{1}}_y = \mathbf{T}^H \mathbf{H}_m e^{-j\beta_0 z} \cdot \vec{\mathbf{1}}_y \end{aligned} \quad (5.25)$$

Proceeding in the same manner as in case shown in Fig. 5.24 a) following relations can be derived

$$\mathbf{\Gamma} = \mathbf{\Gamma}^E = -\mathbf{\Gamma}^H = \frac{Z_0 - \mathbf{Z}}{Z_0 + \mathbf{Z}} \quad (5.26)$$

Transmission coefficients are as follows

$$\mathbf{T}^E = 2 \frac{Z_0}{Z_0 + \mathbf{Z}} \quad \mathbf{T}^H = 2 \frac{\mathbf{Z}}{Z_0 + \mathbf{Z}} \quad \mathbf{Z} \mathbf{T}^E = Z_0 \mathbf{T}^H \quad (5.27)$$

Noticeable is the case when the lossy medium is well conducting metal with much smaller intrinsic

impedance Z then intrinsic impedance of the lossless vacuum $Z \ll Z_0 = 377 \Omega$. Then $\Gamma \approx 1$. It mean that electric field is nearly doubled $T^E = 1 + \Gamma \approx 2$ but magnetic field is nearly extinguished $\vec{H}_r \approx -\vec{H}_i$. Similar as by the line with distributed parameters terminated with the opencircuit.

If shielding barrier has finite thickness d then inside the shield two waves are traveling: forwards $\vec{E}_{12}(z)$, $\vec{H}_{12}(z)$ from boundary 1 to 2 and backwards $\vec{E}_{21}(z)$, $\vec{H}_{21}(z)$ from boundary 2 to 1 as shown in Fig. 5.25. Behind the shield the rest of field $\vec{E}_t(z)$, $\vec{H}_t(z)$ propagates reflection free

$$\begin{aligned} \vec{E}_{12}(z) &= \mathbf{E}_{12}(0)e^{-\gamma z} \vec{1}_x & \vec{E}_{21}(z) &= \mathbf{E}_{12}(0)e^{\gamma z} \vec{1}_x \\ \vec{H}_{12}(z) &= \frac{\mathbf{E}_{12}(0)}{Z} e^{-\gamma z} \vec{1}_y & \vec{H}_{21}(z) &= -\frac{\mathbf{E}_{21}(0)}{Z} e^{\gamma z} \vec{1}_y \\ \vec{E}_t(z) &= \mathbf{E}_t(d)e^{-j\beta_0(z-d)} \vec{1}_x & \vec{H}_t(z) &= \frac{\mathbf{E}_t(d)}{Z_0} e^{-j\beta_0(z-d)} \vec{1}_y \end{aligned}$$

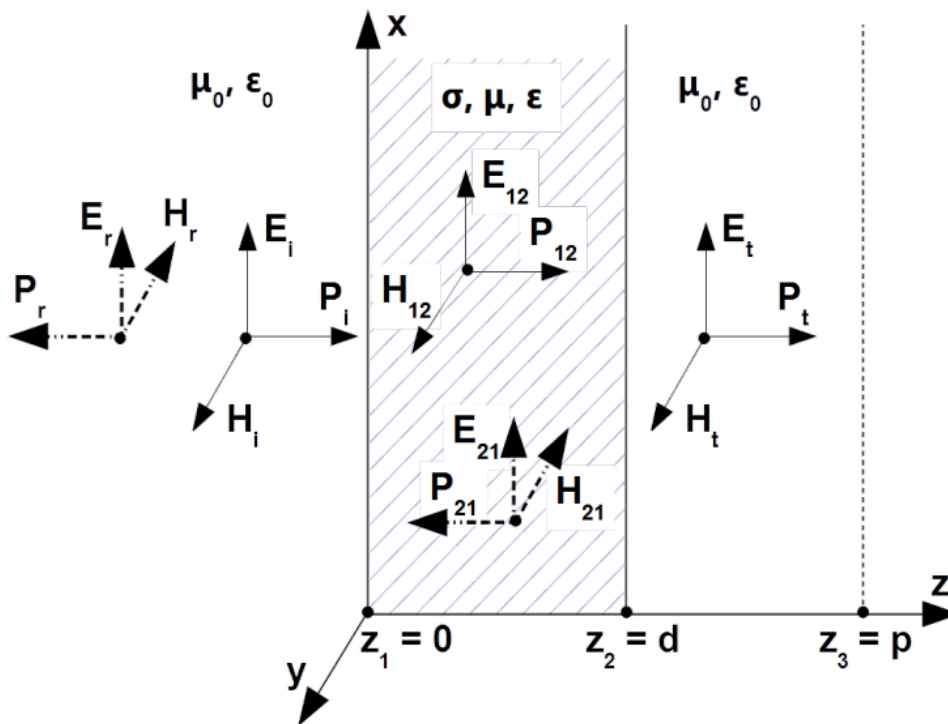


Figure 5.25: Electromagnetic plane TEM wave impinged on a shielded barrier with finite thickness d .

Continuity of tangential component of the electric field at the boundary $z = 0$ and $z = d$

$$\mathbf{E}_i(0) + \mathbf{E}_r(0) = \mathbf{E}_{12}(0) + \mathbf{E}_{21}(0)$$

Formula does not parse

$$\mathbf{E}_{12}(0)e^{-\gamma d} + \mathbf{E}_{21}(0)e^{\gamma d} = \mathbf{E}_t(d) \quad (5.30)$$

along with continuity of tangential component of the magnetic field at the boundary $z = 0$ and $z = d$

$$\frac{\mathbf{E}_i(0)}{Z_0} - \frac{\mathbf{E}_r(0)}{Z_0} = \frac{\mathbf{E}_{12}(0)}{\mathbf{Z}} - \frac{\mathbf{E}_{21}(0)}{\mathbf{Z}}$$

Formula does not parse

$$\frac{\mathbf{E}_{12}(0)}{\mathbf{Z}} e^{-\gamma d} - \frac{\mathbf{E}_{21}(0)}{\mathbf{Z}} e^{\gamma d} = \frac{\mathbf{E}_t(d)}{Z_0} \quad (5.32)$$

gives the ratio of incident wave at the interface $z_1 = 0$ and transmitted wave at the interface $z_2 = d$ [Clayton]

$$\frac{\mathbf{E}_i(0)}{\mathbf{E}_t(d)} = \frac{(Z_0 + \mathbf{Z})^2}{4Z_0\mathbf{Z}} \left[1 - \left(\frac{Z_0 - \mathbf{Z}}{Z_0 + \mathbf{Z}} \right)^2 e^{-2\gamma d} \right] e^{\gamma d} \quad (5.33)$$

Shielding effectiveness of electric field due to Eq.(5.21) yields¹⁰

$$SE^E(p) = \left| \frac{\mathbf{E}_i(p)}{\mathbf{E}_t(p)} \right| = \left| \frac{\mathbf{E}_i(0)}{\mathbf{E}_t(d)} \right| = \left| \frac{(Z_0 + \mathbf{Z})^2}{4Z_0\mathbf{Z}} \right| \cdot \left| 1 - \left(\frac{Z_0 - \mathbf{Z}}{Z_0 + \mathbf{Z}} \right)^2 e^{-2\gamma d} \right| e^{\frac{d}{\delta}} \quad (5.34)$$

Let's derive transmitted field due to single forward passage through barrier. By impinging the barrier by $z_1 = 0$ transmitted is part of the incident field $\mathbf{E}_i(0)$ according to transmission coefficient \mathbf{T}^E presented in Eq. (5.20)

$$\mathbf{E}_{121}(0) = \mathbf{T}^E \mathbf{E}_i(0) = \frac{2\mathbf{Z}}{Z_0 + \mathbf{Z}} \mathbf{E}_i(0) \quad (5.35)$$

This field by reaching the interface of the barrier by $z_2 = d$ is attenuated by the exponential function $e^{-\gamma d}$

$$\mathbf{E}_{121}(d) = \frac{2\mathbf{Z}}{Z_0 + \mathbf{Z}} e^{-\gamma d} \mathbf{E}_i(0) \quad (5.36)$$

Part of the field according to transmission coefficient \mathbf{T}^E presented in Eq. (5.27) leaves the barrier

$$\mathbf{E}_{t1}(d) = \mathbf{T}^E \mathbf{E}_{121}(d) = \frac{2Z_0}{Z_0 + \mathbf{Z}} \cdot \frac{2\mathbf{Z}}{Z_0 + \mathbf{Z}} \mathbf{E}_i(0) e^{-\gamma d} = \frac{4\mathbf{Z}Z_0}{(Z_0 + \mathbf{Z})^2} \mathbf{E}_i(0) e^{-\gamma d} \quad (5.37)$$

Shielding effectiveness defined with Eq. (5.34) is product of three terms. The first one R represents reflection loss caused at the left and the right interface. If barrier is constructed from a well conducting metal then

$$R = \left| \frac{(Z_0 + \mathbf{Z})^2}{4Z_0\mathbf{Z}} \right| \approx \left| \frac{Z_0}{4\mathbf{Z}} \right| \quad (5.38)$$

The second term

$$A = e^{\frac{d}{\delta}} \quad (5.39)$$

represents the absorption loss of the wave as it proceeds through the barrier.

Eqs. (5.38) and (5.39) are the terms of Eq. (5.34). This manifests responsibility of the the third term

$$M = \left| 1 - \left(\frac{Z_0 - \mathbf{Z}}{Z_0 + \mathbf{Z}} \right)^2 e^{-2\gamma d} \right|$$

for additional effects of multiple reflections and transmissions. This is called the correction term.

For good conducting metal $\frac{Z_0 - \mathbf{Z}}{Z_0 + \mathbf{Z}} \approx 1e^{j0}$

$$M \approx \left| 1 - e^{-\frac{2d}{\delta}} e^{-j\frac{2d}{\delta}} \right| \quad (5.41)$$

If moreover the shield thickness d is much bigger then the skin depth δ ($d \gg \delta$), then $e^{-\frac{2d}{\delta}} \ll 1$ and $M \approx 1$. However for barrier thicknesses that are comparable with a skin depth δ ($d \sim \delta$) the coefficient

M is smaller than 1 reducing shielding effectiveness. Correction term M can be negative for thin and bad conducting materials. In this way effectiveness is deteriorated. For good conducting materials it is about 0 dB. Maximal value of M is about 3 dB.

The correction term M can be derived with summation of repetitive forth and back passages, as illustrated in Fig. 5.26. In this figure propagation direction is shown as tilted to the shield surface only for clarity of presentation. Actually meant is the plane wave with the wave front tangential to the shield surface.

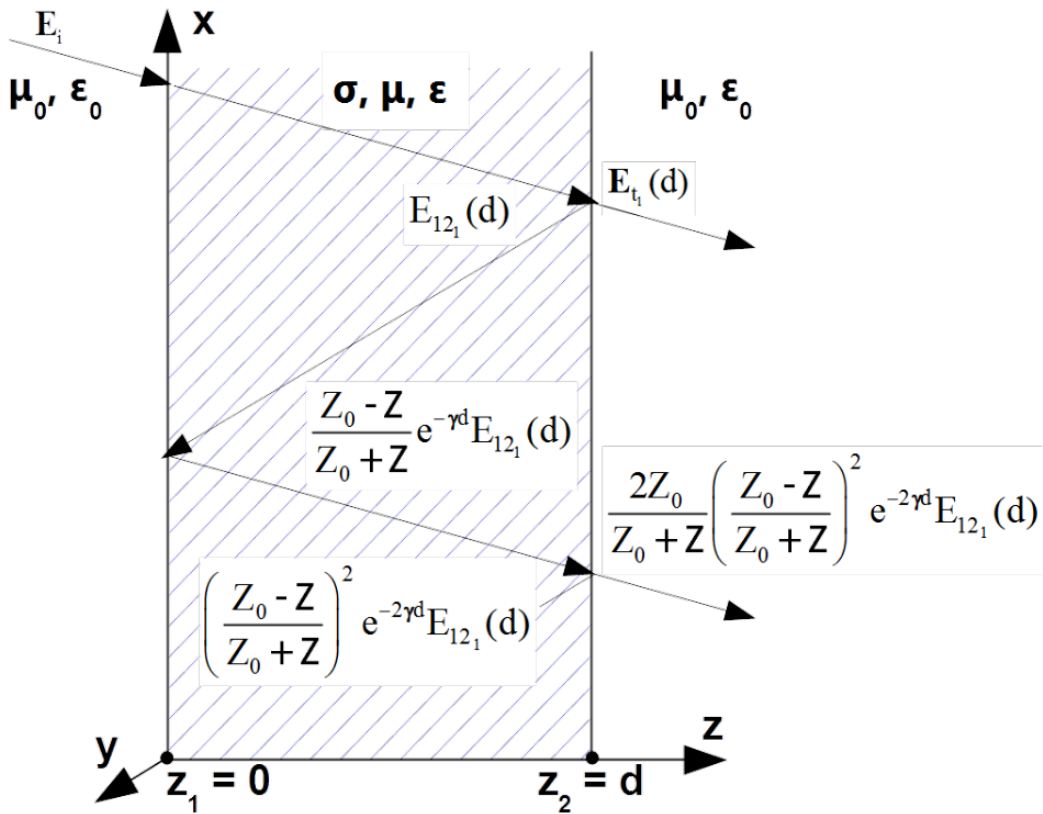


Figure 5.26: Multiple reflections and transmissions between barrier interfaces.

The incident wave $E_{12_1}(z)$ by passage for the first time to the interface $z_2 = d$ is determined with Eq. (5.36). One part of this field $E_{t_1}(d)$ is transmitted outside the shield according to Eq. (5.37). The rest is reflected according to the reflection coefficient Γ^E determined with Eq. ([Gamma]). This field propagating backwards to the left interface suffers attenuation and phase shift

$$\frac{Z_0 - Z}{Z_0 + Z} e^{\gamma(z-d)} E_{12_1}(d)$$

This field by reaching the left barrier by $z = 0$ reflects again according to the reflection coefficient Γ^E determined with Eq. ([Gamma]) and propagates forward suffering attenuation and phase shift

$$\left(\frac{Z_0 - Z}{Z_0 + Z} \right)^2 e^{-\gamma d} e^{-\gamma z} E_{12_1}(d)$$

Part of the field according to transmission coefficient \mathbf{T}^E presented in Eq. (5.27) leaves the barrier

$$E_{t_2}(d) = \frac{2Z_0}{Z_0 + Z} \left(\frac{Z_0 - Z}{Z_0 + Z} \right)^2 e^{-2\gamma d} E_{12_1}(d) \quad (5.44)$$

The rest is reflected for the third time. This process repeats infinitely.

By introduction of the term

$$\Delta = \frac{Z_0 - Z}{Z_0 + Z} \cdot e^{-\gamma d}$$

transmitted fields is following sum

$$\mathbf{E}_t(d) = \frac{4Z_0 Z}{(Z_0 + Z)^2} \cdot e^{-\gamma d} \cdot (1 + \Delta^2 + \Delta^4 + \dots) \cdot \mathbf{E}_i(0)$$

For $|\Delta| < 1$ following relation is valid $1 + \Delta^2 + \Delta^4 + \dots = \frac{1}{1 - \Delta^2}$

Finally, relation $\mathbf{E}_i(0)/\mathbf{E}_t(d)$ is identical as presented with Eq. (5.33) (q.e.d.)!

Derivation of the shield effectiveness for magnetic field $SE^H(p)$ gives the same results.

Memorise that, shield effectiveness of electric and magnetic field in the far field zone is identical regardless thickness d of the shielding barrier, although sequence of stages is different.

In case of electric field majority of shielding effectiveness stems from reflection at the left surface $z_1 = 0$. Reflection coefficient Γ^E there is ruled with Eq. (5.19)¹¹. Contrariwise there is rather amplification instead of reflection of magnetic field at this surface, since according to Eq. (5.19) $\Gamma^H \approx 1$. In consequence magnetic field transmitted to the shield material is almost doubled, see \mathbf{T}^H in Eq. (5.20). By passage from the left to the right interface electric and magnetic fields are attenuated in the same way according to attenuation coefficient γ . At the right interface roles of electric and magnetic fields swap. Electric field is barely reflected and almost double field is transmitted outside. On the contrary magnetic field is almost totally reflected.

Another situation is if the shield is situated in the near field zone of electric or magnetic radiator. Reflection coefficient Γ^E and Γ^H and transmission coefficients \mathbf{T}^E and \mathbf{T}^H at the left interface of the shield, $z_1 = 0$ are ruled with Eq. (5.19) and Eq. (5.20) respectively. At the right interface, by $z_2 = d$ they obey Eq. (5.26) and Eq. (5.27) respectively.

In case of near field zone intrinsic impedance Z_0 in above mentioned formulas must be replaced with the wave impedance Z_w , defined with Eq. ([Zw]). In case of electrical radiator the wave impedance in the near field zone is much bigger than intrinsic impedance Z_0 of the medium and in case of magnetic radiator much smaller, as can be drawn from Fig.[Zw_em_Fig].

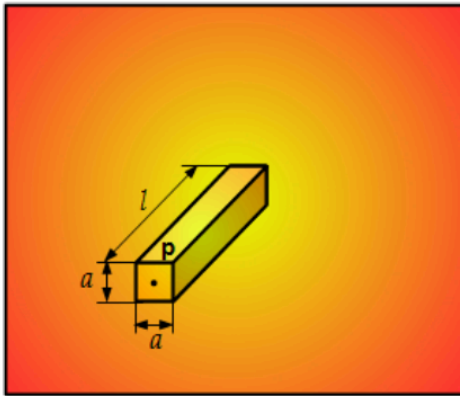
By electrical radiator replacement of Z_0 with Z_w only slightly increases shielding effectiveness because already by $Z_0 = 377 \Omega$ Γ^E is practically equal -1 and \mathbf{T}^E equal 0 at the interface $z_1 = 0$ ¹². Thickness d of shielding material is irrelevant.

There is another scenario by magnetic radiator. Z_w is comparable with intrinsic impedance Z of shielding material. In consequence there is good impedance matching at the interface $z_1 = 0$ as well at the interface $z_2 = d$, compare explanation in chapter [impedance matching]. Relatively much field is transferred to the shield at the interface $z_1 = 0$ and from the shield at the interface $z_2 = d$. Shielding effect is mainly due to attenuation in the shielding material. Therefore thickness d of shield material is crucial.

Feed-throughs and apertures in RF shields

Shielding enclosures must have in many applications possibility of transferring optical signals with glass fibre and media such as gas, compressed air, water supply, waste water. In order not to deteriorate shielding effectiveness feed-throughs are indispensable. Feed-through is simply a wave guide as presented in chapter [wave-guides]. It can have square, circular as shown in Fig. 5.27 or polygonal cross-section.

a)



b)

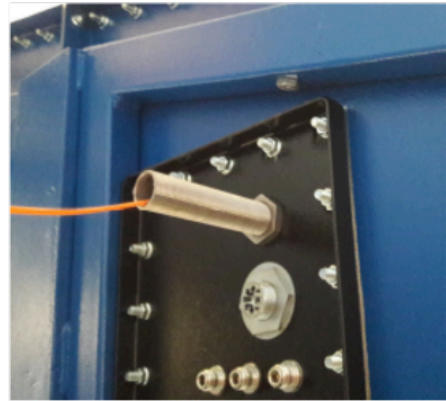


Figure 5.27: Feed-through with square a) and circular cross-section with the pulled through glass fibre b).

\mathbf{E}_z component is defined with Eq. ([gamma_z]). For frequencies below cut-off attenuation coefficient $\gamma_{z,mn}$ defined with the first row of Eq. ([gamma_z2]) is real and is noted here with $\alpha_{z,mn}$

$$\alpha_{z,mn} = \frac{\omega}{v_0} \sqrt{\left(\frac{f_{c,mn}}{f}\right)^2 - 1} \quad (5.48)$$

Assuming that the frequency is much less than the cutoff frequency for the mode, $\alpha_{z,mn}$ simplifies to

$$\alpha_{z,mn} \approx \frac{2\pi f_{c,mn}}{v_0} \quad (5.49)$$

Substituting the relation for the cut-off frequency for the lowest-order TE_{10} mode given in Eq. ([gamma_zz]) $f_{c,10} = v_0/2a$ gives $\alpha_{z,10} \approx \pi/a$. Finally shielding effectiveness in dB yields

$$SE_{dB}^E(p) = 20 \cdot \log[e^{\alpha_{z,10}l}] = 20 \cdot \pi \cdot \log[e] \cdot \frac{l}{a} \approx 27.3 \cdot \frac{l}{a} \quad (5.50)$$

Concluding: in order to ensure attenuation of the feed-through bigger than 100 dB , relation of its length l to cross-sectional dimension a should be bigger than 4.



Figure 5.28: Aperture in shielding enclosure mantled with honeycomb barrier.

Ventilation apertures are usually mantled with honeycomb grid as shown in Fig. 5.28. It is just a matrix of feed-throughs with hexagonal cross-section.

1. By neglecting the leakage field.↔
2. Number of turns is determined with the number of conductor passages through the hole.↔
3. Protected are ports of any network like: power mains, ethernet, telecommunication, cable TV etc..↔
4. Proportionality in the plot is deformed in order to make visible all discharge regimes.↔
5. According to [Hammond] for good conducting materials (metals) holds inequality $\epsilon/\sigma \ll 1s$.↔
6. This explains why magnetic monopoles do not exist.↔
7. Mind that \vec{E} represents total field i.e. due to all charges: free charges at the metal plates and polarization charges of dipoles in material.↔
8. Mind that \vec{B} represents total field i.e. due to all currents: conducted current driven in the metal bars and magnetisation current in material.↔
9. The second Maxwell's equation rules magnetic field originating from current

$$\text{rot } \vec{H} = \sigma \vec{E} + j\omega\epsilon \vec{E}$$
 . Current can be conducted or can be due to dielectric attribute of material named the displacement current.↔
10. Any exponential function with imaginary operator j in exponent such as $e^{j\frac{d}{\delta}}$ has constant module equal 1 and is responsible only for phase shifting.↔
11. $\Gamma^E \approx -1$ because $Z \ll Z_0$ ↔
12. Remind that in case of static field shielding would happen totally at the interface $z_1 = 0$ and other side of the shield would be free of any electric field.↔

Bibliography

- [1] 2014/30/UE: DIRECTIVE OF THE EUROPEAN PARLIAMENT AND OF THE COUNCIL on the harmonisation of laws of the Member States relating to electromagnetic compatibility. , 2014. Official Journal of the European Union L 96/79
- [2] 2014/53/UE: DIRECTIVE OF THE EUROPEAN PARLIAMENT AND OF THE COUNCIL on the harmonisation of laws of the Member States relating to the making available on the market of radio equipment and repealing Directive 1999/5/EC., 2014. Official Journal of the European Union L 153/62
- [3] 2014/35/UE: DIRECTIVE OF THE EUROPEAN PARLIAMENT AND OF THE COUNCIL on the harmonisation of laws of the Member States relating to the making available on the market of electrical equipment designed for use within certain voltage limits., 2014. Official Journal of the European Union L 96/357
- [4] EURAMET e.V.: Guidelines on the Evaluation of Vector Network Analysers (VNA)., 2018. EURAMET Calibration Guide No.12 Ver. 3.0
- [5] Percy Hammond: Electromagnetism for engineers, an introductory course., Oxford, 1997. Oxford University Press Pergamon Press, 2001. Electromagnetic compatibility. Prentice Hall ,
- [6] Percy Hammond: Applied Electromagnetism.
- [7] Jasper J. Goedbloed: New York, 1992.
- [8] Mark I. Montrose: EMC Made Simple, Board and System Design. www.montrosecompliance.com, 2014. Printed Circuit, Montrose Compliance Service, Inc.
- [9] J. Dobrowolski: Matrix. Microwave Network Design Using the Scattering, Boston, London 2010. Artech House
- [10] EN 50160: Voltage characteristics of electricity supplied by public electricity networks., 2010. CENELEC
- [11] IEC 60364-1: Low-voltage electrical installations Part 1: Fundamental principles, assessment of general characteristics, definitions., 2005. IEC
- [12] IEC 61010-1: Safety requirements for electrical equipment for measurement, control, and laboratory use Part 1: General requirements., 2010/AMD1:2016/COR1:2019. IEC
- [13] CISPR 16-1-4: Specification for radio disturbance and immunity measuring apparatus and methods – Part 1-4: Radio disturbance and immunity measuring apparatus – Antennas and test sites for radiated disturbance measurements., 2019. IEC
- [14] EN 61000-4-20: Electromagnetic compatibility (EMC) – Part 4-20: Testing and measurement techniques – Emission and immunity testing in transverse electromagnetic (TEM) waveguides., 2010. CENELEC
- [15] EN 61000-4-2: Electromagnetic compatibility (EMC) – Part 4-2: Testing and measurement techniques – Electrostatic discharge immunity test, 2009. CENELEC
- [16] EN 61643-11:2013/A11:2018: Low-voltage surge protective devices – Part 11: Surge protective devices connected to low-voltage power systems – Requirements and test methods, 2018. CENELEC
- [17] EN 61000-4-5: Electromagnetic compatibility (EMC) – Part 4-5: Testing and measurement techniques – Surge immunity test, 2019. CENELEC
- [18] IEC 61000-2-9: Electromagnetic compatibility (EMC) – Part 2: Environment – Section 9: Description of HEMP environment – Radiated disturbance. Basic EMC publication, 1996. IEC
- [19] H. W. Ott: Noise reduction techniques in electronic systems., 1988. Wiley & Sons John, John Wiley & Sons, Inc. , 1986.
- [21] C. R. Paul: Introduction to electromagnetic compatibility. John Wiley & Sons, Inc. , 1992.
- [20] D. Halliday, R. Resnick: Physics.
- [22] C. R. Paul: Analysis of multiconductor transmission lines., 2008. John Wiley & Sons, Inc.
- [23] G. M. Kunkel: Shielding of Electromagnetic Waves, Theory and Practice., Print ISBN: 978-3-030-19237-2, 2020. Springer Nature Switzerland AG
- [24] Ch. Hafner: The Generalized Multipole Technique for Computational Electromagnetics., 1990. Artech House, Inc.
- [25] D. M. Kerns, R. W. Beatty: Basic theory of waveguide junctions and introductory microwave network analysis., 1967. Pergamon Press Inc.

- [26] F. L. Warner: Microwave attenuation measurements. IEE Monography Series 19 Peter Pergamon Ltd , 1977.
- [27] H. Johnson, M. Graham: High-Speed Digital Design a Handbook of Black Magic., 1993. Prentice Hall
- [28] W. Schnorrenberg: Spektrumanalyse Theorie und Praxis., 1990. Vogel Fachbuch Messtechnik
- [29] F. Dittmann, M. Kahmann: Geschichte der elektrischen Messtechnik, Messen mit und von Elektrizität., ISBN: 9783800738557, Berlin 2014. VDE Verlag
- [30] J. Baran, J. Sroka: Distortion of ESD Generator Pulse Due to Limited Bandwidth of Verication Path., Vol. 52, No. 4, str. 797-803, Nov. 2010. Trans. on EMC
- [31] DEHN+SÖHNE: www.dehn.de, 2018. Überspannungsschutz. Haupkatalog ,
- [32] Wind power and human health, icker, noise and air quality issue brief # 2., 2010. West Michigan Wind Assessment www.gvsu.edu/wind.
- [33] Eye Anatomy. <https://www.glaucoma.org/glaucoma/anatomy-of-the-eye.php>.
- [34] NASA <https://www.jpl.nasa.gov/infographics/uploads/infographics/full/11469.jpg>